NASA Contractor Report 195423

Investigation and Feasibility Assessment of TOPAZ-II Derivations for Space Power Applications

Alexander G. Parlos and Kenneth L. Peddicord
Texas A&M University, College Station, Texas

Prepared under Grant NAG3–1235

National Aeronautics and
Space Administration

Lewis Research Center

May 1998

Available from

NASA Center for Aerospace Information
800 Elkridge Landing Road
Linthicum Heights, MD 21090-2934
Price Code: A10

National Technical Information Service
5287 Port Royal Road
Springfield, VA 22100
Price Code: A10

Executive Summary

Investigation and Feasibility Assessment of TOPAZ-II Derivative
for
Space Power Applications
Using a Gain Scheduled Controller Design

The use of shunt regulators for load-following of proposed static space nuclear power systems (SNPSs) such as TOPAZ raises a number of concerns, such as the possibility of a failure in the shunt regulators requiring reactor shutdown, or the possible need to deliver somewhat higher power level to the load than originally expected. Therefore, a back-up system is needed in TOPAZ to eliminate the possibility of a single-point failure in the shunt regulators, and to increase the overall system reliability despite changing mission needs and deteriorating equipment.

The objective of this research is to develop a controller for the voltage regulation in static SNPSs, which is capable of overcoming system variations resulting from operation at different power levels. This is accomplished by developing several linearized models of TOPAZ using a simplified, validated reference model of an integrated nonlinear SNPS model, covering its entire operating envelope. A dynamic compensator is designed using each of the linearized models based on the Linear Quadratic Gaussian with Loop Transfer Recovery (LQG/LTR) method. The LQG/LTR method is a systematic multivariable control system technique with several desirable properties such as a nominal stability and performance, as well as stability robustness to unmodeled dynamics. The various compensators matrices, including the gain and system matrices, are fitted to a scheduling variable, namely the SNPS electric power produced, to obtain a nonlinear gain-scheduled compensator.

The performance of the gain-scheduled compensator is systematically investigated via transient and steady-state simulations using the integrated nonlinear SNPS model. The

simulations, which include sensor noise at the plant output, demonstrate the effects of variations in the fuel temperature reactivity feedback coefficient on the load-following capabilities of the SNPS. Robustness analysis results of the gain-scheduled compensator demonstrate that the proposed control concept exhibits a significant degree of operational flexibility, and it is primarily intended for long-term space mission requiring significant levels of power system autonomy.

TABLE OF CONTENTS

CHAPTER Page

CHAPTER I

INTRODUCTION

The objective of this research is to develop a gain-scheduled adaptive control system that achieves voltage stability in a proposed static energy conversion space nuclear power system (SNPS), while generating different levels of electric power. The SNPS being analyzed in this research uses a fast, lithium-cooled nuclear reactor with thermal power output of 6.8 MW_{th}, and which has been proposed for use in future space mission by various researchers [1], [3]. This SNPS, capable of providing 300 kW_e electric power output, is based on the General Electric (GE) Company thermoelectric power conversion design for the SP-100 system [1].

The systematic controller design is based on linearized models of the SNPS valid at different equilibrium points. The linear models are generated from a more detailed nonlinear SNPS model, which has been previously utilized in the design of a model reference adaptive control algorithm. This controller enabled an integrated SNPS model to follow the predictable and desired response of the nonlinear reference model used in designing it, despite changes in the SNPS operating parameters throughout its entire lifetime [2].

Linear controllers are designed using the relatively new method of control system design for Multiple Input-Multiple Output (MIMO) systems known as the Linear Quadratic Gaussian with Loop Transfer Recovery (LQG/LTR). The linear controllers

This report follows a style based on the *IEEE Transactions on Automatic Control.*

are then scheduled (fitted) to arrive at a nonlinear controller with adaptive gains. The nonlinear controller is tested using the integrated nonlinear SNPS model throughout its operating regime.

In this chapter, the motivation for the voltage controller design is discussed. A brief survey of previous work done on output voltage regulation of the proposed SNPSs is followed by the research objectives and contributions of this thesis. Finally, the organization of the remainder of this thesis is outlined.

I.1 Motivation

SNPSs have been under investigation as an alternative for both commercial and military space missions since the 1950's [1]. Such systems have a projected longevity of 7 to 10 years of continuous operation without the need for maintainance, they can supply a wide range of power (tens of kW_e to thousands of MW_e), and in certain power ranges they have significant mass advantage over other space power sources.

In static SNPSs, the conventional approach for regulating the electric load demand has been the use of banks of shunt resistors (regulators). However, designs based on this approach raise a number of concerns, such as the possibility of a failure in the shunt regulators requiring reactor shutdown, or the possible need to deliver somewhat higher power level to the load than originally expected, because of changing mission needs or deteriorating equipment. Furthermore, operating the nuclear reactor at its nominal power level at all times, regardless of the load output of the system, results in the rejection of the excess load demand into space in the form of thermal

energy. This heat rejection increases the cooling requirements and consequently the total mass of the spacecraft. Results of parametric studies investigating the effects of multiple failures of the thermoelectric-electromagnetic (TE-EM) pumps and partial degradation of the waste heat rejection capability on the electric power output show that the system's power output is affected only slightly [13]. However, a failure in the shunt regulators has been pointed out to be a single-point failure. Hence, the use of shunt resistors in thermoelectric SNPSs calls for a back-up system. Such a back-up system could certainly improve the overall system reliability and eliminate a possible single-point failure.

I.2 Literature Review

Principal space reactor programs were terminated in the early 1970s, and only very limited activity took place during the remainder of the decade [1]. Around 1979, the Department of Energy (DOE) initiated a modestly funded development program, focused on the heat-pipe-cooled reactor concept at the Los Alamos National Laboratory. By 1982, in view of the advent of a number of potential missions that would need nuclear systems, the DOE, the National Aeronautics and Space Administration (NASA), and the Department of Defense (DOD) had embarked on the development of a more active space reactor program [1]. Accordingly, in February of 1983, the SP-100 Program was initiated by NASA, DOE and the Defence Advanced Research Projects Agency (DARPA). The initial focus was on design of a 100 kW_e system scalable from tens to hundreds of kW_e.

Energy conversion in static SNPSs has been accomplished through thermoelectric or thermionic converters [6], [7], [8], [9], [10]. In SNPSs which employ thermionic energy conversion, control issues are similar to those using thermoelectric energy conversion [8]. Therefore a number of findings from this study are equally applicable to thermionic SNPSs. Thermionic energy conversion concepts have been applied to various space nuclear power systems under investigation, as alternatives to thermoelectric concepts [7], [8], [9], [10].

The U.S. Air Force (USAF) has had a long standing interest in thermionic space power dating back to the early 1960s, when a heat-pipe-cooled thermionic converter was demonstrated through work at the predecessor to the Wright Laboratory (WL) [7]. The STAR-C thermionic SNPS is a 40 kW_e reactor system designed in response to evolving USAF space power requirements, which has eliminated the possibility of a single point failure resulting from a single converter failure [8]. The Idaho National Engineering Laboratory (INEL) has developed the Small Ex-core Heat Pipe Thermionic Reactor (SEHPTR) concep' to meet the safety and reliability requirements identified by the USAF [9]. The SEHPTR concept has also eliminated the possibility of a single point failure resulting from a single converter failure. These studies indicate that converter failures can be tolerated in thermionic systems, because the converters can be interconnected in a series-parallel electrical network so that the current can flow around the failed cells through the remaining operational ones. Furthermore, the large number of independent power converters employed increases the network reliability with a small amount of additional redundancy [8], [9], [11]. Thus, high overall system reliability of the thermionic system has been achieved with

only modest converter reliability. Nevertheless, a potential single point failure due to shunt regulators is still present.

The Advanced Thermionics Initiative (ATI) program was organized to integrate thermionic technology advances into a converter suitable for in-core reactor applications in the 10 to 40 kW_e power range [7]. The ATI program organization and its participating contractors have stated their goal for the development of a robust, long-life, high efficiency, simplified thermionic converter which can be incorporated into other space nuclear power reactor programs, and they have demonstrated their interaction during the annual program reviews.

Since SNPSs, such as the thermoelectric-based SP-100, will frequently experience changes in the external load demand, in 1985, a system simulation model, SNPSAM (Space Nuclear Power System Analysis Model), was developed at the University of New Mexico's Institute for Space Nuclear Power Studies, to investigate the load-following characteristics of an integrated SP-100 system without a shunt regulator for the electric load [4]. The results of this study showed that, although the nuclear reactor is always load-following, the integrated system is only load following up to a critical value of the external load demand; beyond this point, the system is nonload-following, requiring an external controller.

In research investigating thermoelectric systems, the conventional approach for regulating the electric load demand has been to employ a shunt resistor (regulator) between the system and the payload [3], [4], [6], [12], [13], [14]. This approach, however, requires operating the nuclear reactor at its nominal power level at all times, regardless of the load output of the system, and the excess load demand is

rejected into space in the form of thermal energy [3]. This heat rejection, increases the cooling requirements and consequently the total mass of the spacecraft. In the reliability and vulnerability studies of the SP-100 system [13], parametric analyses using SNPSAM-Mode-3 have been performed to investigate the effects of degradation of the system's waste heat rejection, due to a partial loss of surface area and/or the emissivity of the radiator panels, on the SP-100 operating parameters. The results of the parametric analyses assessing the effects of multiple failures of the TE-EM pumps and partial degradation of the waste heat rejection capability on the electric power output demonstrate that the system's electric output is affected only slightly [13]. However, a failure in the shunt regulators has been pointed out to be a single-point failure in these systems, and it has been concluded that the use of shunt regulators in thermoelectric, or even in thermionic, systems calls for a back-up load-following control system [3], [4], [13].

A more recent study has made use of an adaptive controller to demonstrate that a model reference adaptive controller could cause a selected system state variable to track the transient trajectory of the corresponding state variable of a reference model with local stability in the SNPS [2], [5]. Although these results of the application of the adaptive controller suggest that a SNPS can operate in a load-following mode without the use of a shunt regulator, the particular application by Metzger et al. [2], [5] does not address all of the questions that may arise from replacing a shunt regulator with a more automated, less hardware-intensive, load-following control system for a SNPS [3]. Such issues are, however, addressed in this study.

I.3 Objectives of the Research

The original objectives of this research are stated in the following sections.

I.3.1 Linearized Model Development

A number of linearized models will be generated by analytically linearizing a simplified nonlinear reference model of an integrated nonlinear SNPS model at various equilibrium points in an operating range of 50% and 150% of full power. along with numerically perturbing the latter model to obtain certain linearized reference model parameters at these equilibrium points. The linearized reference models generated are expected to be valid only for a finite range about the equilibrium points and will be validated with the integrated nonlinear SNPS model [17]. The number of linearized reference models to be generated will be determined by investigating the validity range of each linearized reference model and by assessing whether the entire operating range of the static SNPS has been covered.

I.3.2 External Controller Design (Outer Loop)

The external controller (compensator) designs for various operating power levels will be based on the corresponding linearized reference models of the plant and the LQG/LTR design methodology [16], [15]. The LQG/LTR controllers are a subclass of the MBCs, which explicity incorporate the SNPS model dynamics into the design process. Hence. an accurate linearized reference model is required to design a high-performance external controller.

I.3.3 Gain-Scheduling of the Linear Compensators (Outer Loop)

The linear controllers designed using the LQG/LTR design methodology are expected to be valid for operation within only a certain range about their respective equilibrium points. A single nonlinear controller (external controller) is therefore required, in order to continuously control the reactor in a range of 50% to 150% of the nominal power level. Gain-scheduling of the linear controllers, as well as of the linearized reference models, will be done by fitting each of the linear controller and linearized reference model parameters to a variable which is indicative of the system changing operating conditions.

I.3.4 Design and Testing of the Adaptive Controller (Inner Loop)

Model reference adaptive control is well developed for linear systems [2], hence the linearized reference models of the SNPS will be used in the design of the adaptive controller. The constant gains in the reference adaptive control algorithm will be determined at various equilibrium points within the operating regime of the reactor. These gains will then be scheduled, to arrive at a single nonlinear adaptive controller that can cause the output (load voltage) of the SNPS to track the transient trajectory of the output of a reference model. The model reference adaptive controller will be tested with and without the external nonlinear controller, for the load-following of the integrated nonlinear SNPS model. As it turned out, the last objective was never implemented, because the outer loop of the dual-loop controller had satisfactory performance without the presence of an inner loop.

I.4 Contributions of the Research

Following are the main contributions of this work :

1) As opposed to current practice for load-following in proposed static SNPSs, a more automated, less hardware-intensive control system is proposed. This control system is intended as a back-up to shunt regulators, and is capable of effective control during variations in the power system response resulting from long-duration missions and component degradation.

2) The designed linear controllers have certain guaranteed properties. Nonlinear transient response simulations indicate that to some extent these properties carry-over to the nonlinear gain-scheduled controller proposed in this study.

3) The structure of an originally proposed dual-loop controller, comprising of an internal model reference adaptive controller and an external nonlinear controller, is proposed to be significantly modified. As a result of the performance indicators of the external nonlinear controller proposed in this study, there appears to be no need to still include the internal loop, i.e. the model reference adaptive controller, in the dual-loop controller for the type of parameter variations study in this thesis.

I.5 Organization of the Thesis

In Chapter II, the static SNPS under consideration is briefly described. The control problem in this particular system is stated. A dual-loop control mechanism is proposed as a solution for this problem, and current methods used to resolve the problem are presented.

In Chapter III, the various SNPS models used in this thesis are described. The generation of the linearized reference models from an integrated, nonlinear SNPS model is also described. The scheduling of the linear models is explained and evaluation of the scheduled model with respect to the integrated, nonlinear SNPS model is presented via simulation at various operating power levels.

In Chapter IV, the linear control system design method used in this research is described and the mathematical preliminaries regarding this method are presented.

In Chapter V, the design and gain-scheduling of the linear controllers proposed in this thesis is explained, and satisfaction of the design specifications by the linear controllers is verified.

In Chapter VI, the performance of the linear and the gain-scheduled external controllers is analyzed at various operating power levels. The performance limits of the various controllers are determined, and a robustness study of the gain-scheduled controller is performed.

In Chapter VII, the summary, the conclusions and some topics for further research are discussed.

CHAPTER II

VOLTAGE CONTROL IN STATIC SPACE NUCLEAR POWER SYSTEMS

II.1 Introduction

In this chapter, the voltage regulation problem in static SNPSs is stated. A brief description of the static SNPS being analyzed is presented. The need for a back-up system for eliminating the possibility of a single-point failure in the shunt regulators of static SNPSs using thermoelectric, or even thermionic, power conversion is pointed out. A dual-loop control mechanism originally proposed to correct this problem is described. Furthermore, the conventional approach for regulating the electric load demand in static SNPSs and the studies of various researchers are briefly described.

II.2 Description of the Static Space Nuclear Power System

The static SNPS under consideration uses a uranium nitride (UN)-fueled and lithium-cooled fast nuclear reactor with thermal power output of 6.8 MW_{th}. This reactor system has been proposed for use in future space mission by previous researchers [1], [3]. The particular system considered is capable of generating 300 kW_e and is based on the General Electric (GE) Company thermoelectric power conversion design for the SP-100 system [1]. In this SNPS, energy conversion is accomplished through direct conversion of thermal energy to electric energy via thermoelectric

converters. The system's major components are the nuclear reactor, the primary coolant loop, the primary heat exchanger, the thermoelectric-electromagnetic (TE-EM) pump, and the thermoelectric converter.

In the design presented by the GE Company [5], the lithium coolant exits the reactor's outlet plenum from six outlet lines. Each of the six outlet lines divides into two branches, and each of these twelve branches contains a TE-EM pump and a thermoelectric Power Conversion Assembly (PCA). After the lithium coolant exits the PCA, the twelve braches recombine into six reactor inlets. Each of the twelve primary heat transport branches is thermally coupled to a secondary coolant branch in the TE-EM pump and in the PCA where the thermoelectric elements are sandwiched between the primary and the secondary lithium coolant ducts. Each secondary lithium coolant branch is accompanied by a separate heat pipe radiator panel that radiates the waste thermal energy into space. Figure 1 is a drawing of the GE 100 kW_e SP-100 system depicting the system's key features [4].

II.3 Statement of the Control Problem

A major concern in the design of SNPSs is to ensure that these systems will operate safely and respond in a predictable and desired manner. Because of the design requirements of SNPSs and the stringent conditions under which they will have to operate, it is essential that the effects of an unanticipated system response be minimized. An unexpected system response may be due to degradation of the performance of the radiator heat pipes, loss of radiator heat pipes as a result of collisions with space debris, degradation of the performance of the thermoelectric

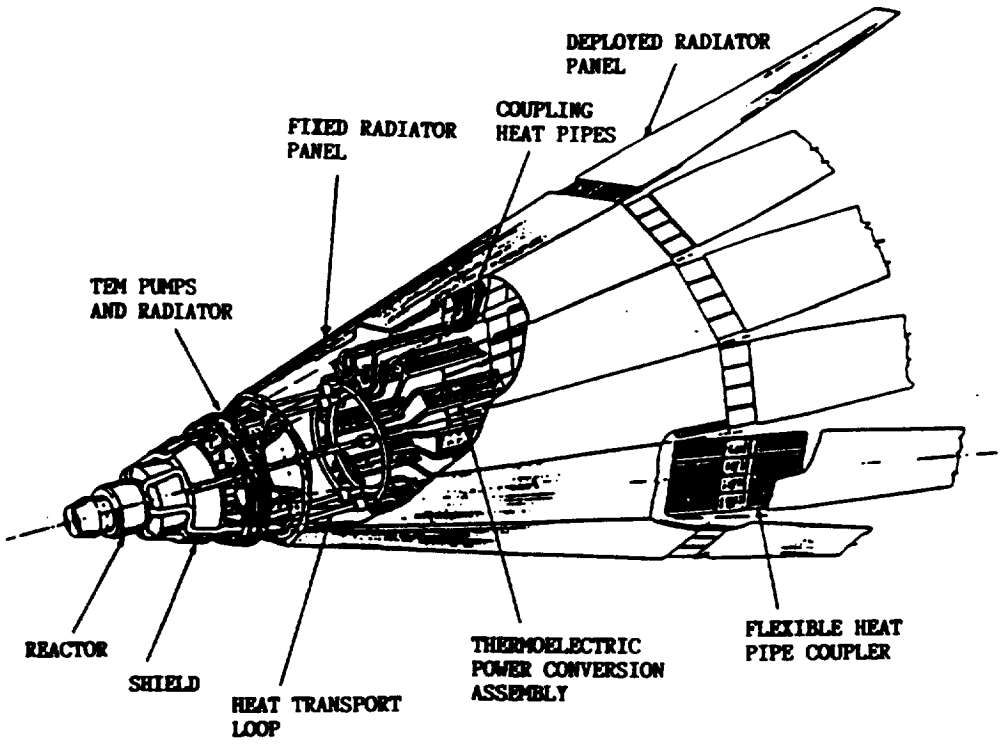

Figure 1. A Drawing of the General Electric SP-100 Thermoelectric Power System Design Depicting Its Key Features (Adapted from [6]).

elements in the pumps and power conversion elements, fouling of the heat transport system, loss of a thermoelectric-electromagnetic (TE-EM) pump, sticking of the reactor control elements, and changes in the nuclear fuel characteristics due to fuel burnup, which might be reflected reflected in changes in the fuel temperature feedback coefficient.

Current designs of proposed static SNPSs require the use of banks of resistors (shunt regulators) to regulate the electric power delivered to the payload. Both thermoelectric and thermionic systems, employ a shunt regulator to reduce the power delivered to the load. In such systems, a failure in the shunt regulators could lead to reactor shutdown. Because of changing mission needs or deteriorating equipment, use of shunt regulators could also result in not delivering the expected electric power level, when the reactor operates below nominal thermal power. Furthermore, because the excessive load demand is rejected into space by radiation in the form of waste thermal energy, such an operation of the power system would increase the cooling requirements and hence the total mass of the spacecraft. In various studies by previous researchers, it has been demonstrated that a failure in the shunt resistors can not be tolerated [3], [4], [13]. Additionally, the results of studies investigating the load-following characteristics of static SNPSs without a shunt regulator show that although the nuclear reactor is always load-following, the integrated power system becomes nonload-following beyond a critical value of the load demand [4]. Therefore, a controller is needed in static SNPSs, to compensate for the possible reliability deficiencies resulting from the use of shunt regulators for the load-following of the power system. Such a controller could increase the overall system reliability, and it could improve the safe operation of both thermionic and thermoelectric SNPSs throughout their lifetime.

II.4 Description of the Proposed Dual-Loop Controller

A dual-loop control mechanism was initially proposed to eliminate the possibility of a single-point failure in the shunt regulators of the static SNPSs. The

dual-loop controller, which combines the advantages of an adaptive controller (inner loop), with those of an external controller (outer loop) is expected to demonstrate the load-following capability of a 300 kWe thermoelectric SNPS during its lifetime, by appropriately manipulating the neutronic, and thus the thermal power produced by the nuclear reactor. The controlled variable is the load voltage, regulated at 100 V, whereas the manipulated variable is the core external reactivity, altered through the control drum motion. The dual-loop controller anticipates readings from sensors measuring the load voltage, the neutronic power, the primary coolant mass flow rate, the primary coolant temperature at the core inlet and exit, and the control drum position. Though in the final implementation of the external controller only the load voltage sensor reading is utilized. The controller generates a command for the new control drum position in order to meet the demanded electric power, while regulating the load voltage at the desired level. A block diagram of the dual-loop controller is depicted in Figure 2.

II.4.1 Adaptive Control Loop (Inner Loop) of the Static Space Nuclear Power System

The adaptive controller uses a model reference adaptive algorithm, which tends to minimize the difference between the output of a reference model and that of the actual system. The adaptive controller, which is activated only when the power system exhibits significant variations from nominal operating conditions, ensures that such variations do not hinder the performance of the external controller. The inner loop accomplishes this by causing the actual system response to match the expected response of the reference model, regardless of the complexity of the reference model

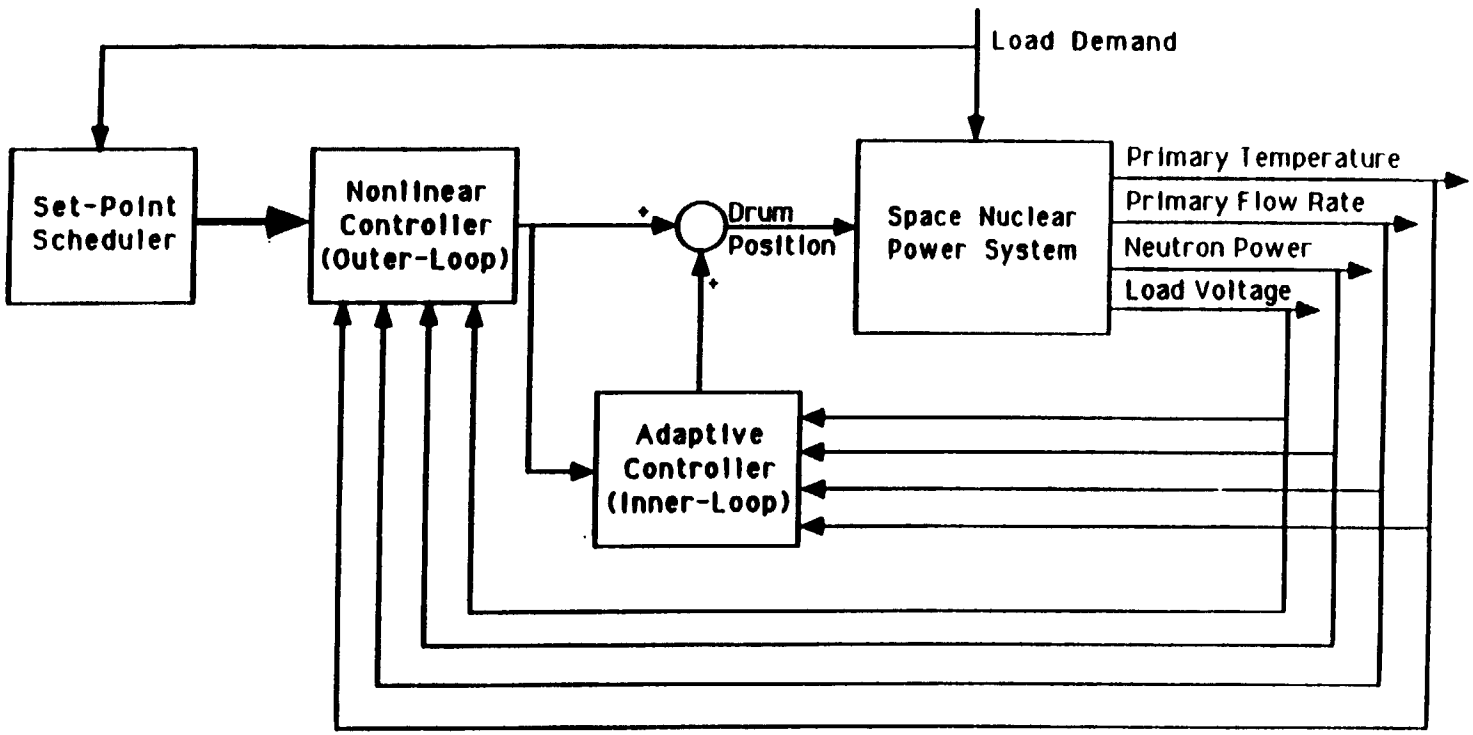

Figure 2. A Block Diagram of the Dual-Loop Controller

which embodies the physics of the plant. The design of this controller is fully described in Metzger et al. [5].

II.4.2 Nonlinear External Control Loop (Outer Loop) of the Static Space Nuclear Power System

The nonlinear external controller forms the outer loop of the dual-loop controller, and is designed to operate when the power system responds as anticipated. The external controller is designed by gain-scheduling the linear controllers which are based on the reference model of the plant, and are obtained by using the LQG/LTR method. The outer loop, which is active at all times is anticipated to exhibit limited robustness, and it is anticipated to be capable of overcoming system variations resulting from operation at different power levels.

II.5 Current Practice

The voltage regulation problem in static SNPSs has not yet been solved. As explained earlier, the current designs of the proposed static SNPSs using thermoelectric or thermionic energy conversion employ a shunt regulator (resistors) to reduce the power delivered to the load when the reactor is operating below its nominal thermal power level. The results of the studies investigating the load-following capabilities of the TE power systems have demonstrated that :

1.) A failure in the shunt regulator of the power system is a single-point failure,

2.) The use of a shunt regulator for the load-following of the power system cannot be eliminated since the integrated power system operating without a shunt regulator becomes nonload-following beyond a critical value of the load resistance (when the

load resistance is equal to the internal resistance of the PCA), even though the nuclear reactor is always load-following, and,

3.) Using an adaptive control algorithm with selective state-variable weighting allows the power system to respond in a predictable, desirable and stable manner despite changes in the system's operating parameters.

Even though reliability and vulnerability studies of static SNPSs have achieved a good understanding of the operating characteristics and the overall performance of the integrated system, they do not propose an effective control mechanism which could eliminate the possibility of a single-point failure resulting from failed shunt regulators.

CHAPTER III

STATIC SPACE NUCLEAR POWER SYSTEM MODELING

III.1 Introduction

The performance of the model-based controller proposed in this research depends particularly on the accuracy of the SNPS model used to desing it. Therefore, it is of great importance to obtain a model that embodies the physics of the SNPS under consideration. In this chapter, the description of an integrated, nonlinear model of the SNPS is presented along with a simplified, though nonlinear, reference model derived from it. The inputs, the outputs and the states of these models are described. The differences between the equations of the reference model and of the integrated SNPS model are pointed out. The linearization of the nonlinear reference model to obtain the linearized reference models about different equilibrium points is explained, and the range for which each linearized model is valid is determined. Then the linearized models which cover the entire operating regime (50% to 150% of the nominal electric power level) of the power system are scheduled (fitted) as a function of the electric power produced by the system. An analysis of the linearized reference models and the scheduled reference model is presented and their validity is investigated via transient and steady-state response comparisons with the integrated, nonlinear SNPS model. A FORTRAN computer program which incorporates the integrated, nonlinear SNPS model and the nonlinear reference model is used for these simulations.

III.2 Description of the Integrated Nonlinear Space Nuclear Power System Model

The integrated nonlinear SNPS model used in this research, was developed for analyzing integrated thermoelectric systems [4]. This coupled model is capable of predicting the performance of an integrated thermoelectric SNPS during both steady-state and transient operations, as well as predicting the system's load-following characteristics and the integration of the power system with the payload. Additionally, this power system model can be used to analyze the system response to various external perturbations, the effect of system parameter changes on the transient system response, and the effectiveness of a power system controller.

The major components of this system model are the nuclear reactor core, the primary coolant loop, the TE energy converter, the TE-EM pumps, the primary heat exchangers, and the main radiator. These components are listed in Table 1. A schematic diagram of the integrated, nonlinear SNPS model is depicted in Figure 3.

The integrated nonlinear SNPS model has 16 states as shown in Table 2. The states of the model are coupled through a set of time varying, first order, nonlinear differential equations which represent the individual models that describe the integrated model. The equations that describe the neutronic power, the delayed neutron precursor concentrations, and the energy equations of the fuel, clad and the reactor coolant are solved at each simulation time step using a stiff differential equation solver. The remainder of the state equations are solved separately for each branch at each time step also using a stiff differential equation solver.

Table 1. Major Components of the Integrated Nonlinear SNPS Model

Components	Model	Model Descripuon
Nuclear Reactor	Neutron Kinetics and Reactivity Control Model	* Point kinetics model with six delayed neutron groups. * Calculates the thermal power generated in the core due to fission for a step, ramp, or any arbitrary reactivity insertion function.
	Reactivity Feedback Model	* Calculates reactivity feedback due to Doppler effect, fuel expansion, and coolant expansion.
	Reactor Thermal Model	* A lumped parameter model. * Calculates the fuel and cladding average temperatures. * Calculates the core coolant average and exit temperatures.
	Reactor Hydraulic Model	* Calculates the pressure drop in the reactor core region and in the annulus between the core baffle and the reactor vessel.
Primary Coolant Loop	TE-EM Pump Model	* Couples the EM pump model to both the TE model and a 2-D thermal analysis model for the pump magnet. * Calculates the pumping head and the overall pump efficiency.
	Piping Hydraulic Model	* Calculates the pressure drop in the primary coolant loop pipings.
	Heat Exchanger Thermal Model	* The energy balance model of the HX coolant channels is coupled to the main TE converter model. * Calculates the temperatures of the coolant and the wall in the HX coolant channels. * Calculates the total thermal energy extracted from the heat exchanger and the exit coolant temperature from the heat exchanger.
Energy Conversion	TE Model	* A Transient 1-D finite element model. * Uses temperature dependent material properties. * Handles any combinations of boundary conditions. * Calculates the electric power output, conversion efficiency, and the waste heat rejection.
Radiator	Waste Heat Rejection Model	* Direct radiation model from the cold shoes of the TE generators into space. * Takes into account the effect of the sonic limit of the radiator's potassium heat pipes.

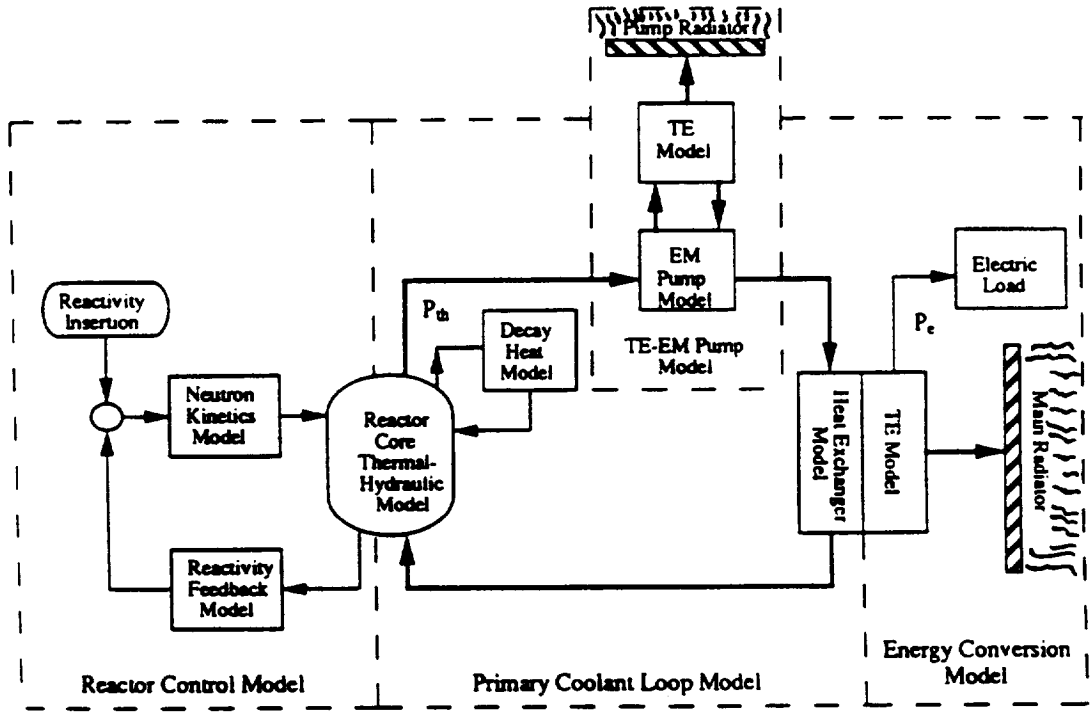

Figure 3. A Schematic Diagram of the Integrated, Nonlinear Space Nuclear Power System Model (Adapted from [6]).

III.2.1 The Nuclear Reactor Model

The neutron kinetics model solves the point kinetics equations using six delayed neutron groups. It calculates the time derivative of the reactor thermal power generated by fission, and the time derivative of the delayed neutron precursors. In this model, the total reactivity input is the sum of the feedback reactivity caused by temperature variations (fuel expansion, Doppler, and coolant feedback effects), and the external reactivity inserted into the core.

Table 2. States, Input, Output and Disturbance of the Integrated Nonlinear SNPS Model

States	Description
Primary	Neutronic power, MW_{th}
	Delayed-neutron precursor concentration I, MW_{th}
	Delayed-neutron precursor concentration II, MW_{th}
	Delayed-neutron precursor concentration III, MW_{th}
	Delayed-neutron precursor concentration IV, MW_{th}
	Delayed-neutron precursor concentration V, MW_{th}
	Delayed-neutron precursor concentration VI, MW_{th}
	Fuel temperature, K
	Average core coolant temperature, K
	Average primary branch coolant temperature, K
	Primary coolant mass flow rate, kg/s
Secondary	Thermoelectric temperature of the PCA, K
	Thermoelectric temperature of the TE-EM pump, K
	Secondary coolant temperature, K
	Secondary coolant mass flow rate, kg/s
	Radiator surface temperature, K

Input	External reactivity, $\Delta k/k$
Controlled Output	Load voltage, V
Disturbance	Load demand, MW_e

The reactor core thermal model calculates the fuel and the average cladding temperatures, and the average core coolant and core exit temperatures using a lumped parameter approach. The model determines a centerline fuel temperature at each simulation time step, using the steady-state, one-dimensional heat conduction equation, assuming a flat radial power profile throughout the core. The average fuel temperature is calculated by averaging the clad temperature and the centerline temperature. The model calculates the core coolant exit and inlet temperatures as

the sum of the average core coolant temperature and the thermal energy added to or removed from the core coolant divided by the coolant mass flow rate through the core and the coolant specific heat, respectively.

The core hydraulic model calculates the pressure drop in the reactor core as the sum of the pressure losses in the flow channels in the annulus between the reactor vessel and core baffle, and in the flow channels of the reactor core using the equivalent hydraulic diameter concept.

III.2.2 The Primary Coolant Loop Model

As shown in Figure 4, the primary coolant loop of the integrated nonlinear SNPS model consists of three flow paths and twelve heat exchangers with common inlet and exit headers. The coolant flows out of the core through three coolant flow paths, each equipped with a TE-EM pump. The coolant flowing out of the pumps is combined in the hot header and fed to the primary heat exchangers; the flow exiting the heat exchangers then combines in the cold header and returns to the reactor core. The TE-EM pumps are located in the hot leg of the primary coolant loop to maximize the TE converter's efficiency and, consequently, the overall pump efficiency [4].

The TE-EM pump is a self-induced, direct current electromagnetic pump equipped with a hiperco-27 magnet and a SiGe/GaP TE converter. Each pump has two coolant ducts; the electric current provided by the pump's TE converter flows through the ducts in a perpendicular direction to both the magnetic field and the coolant flow. Figure 5 depicts a cross sectional view of the TE-EM pump, and Figure shows a line diagram describing the pump operation. The TE-EM pump model

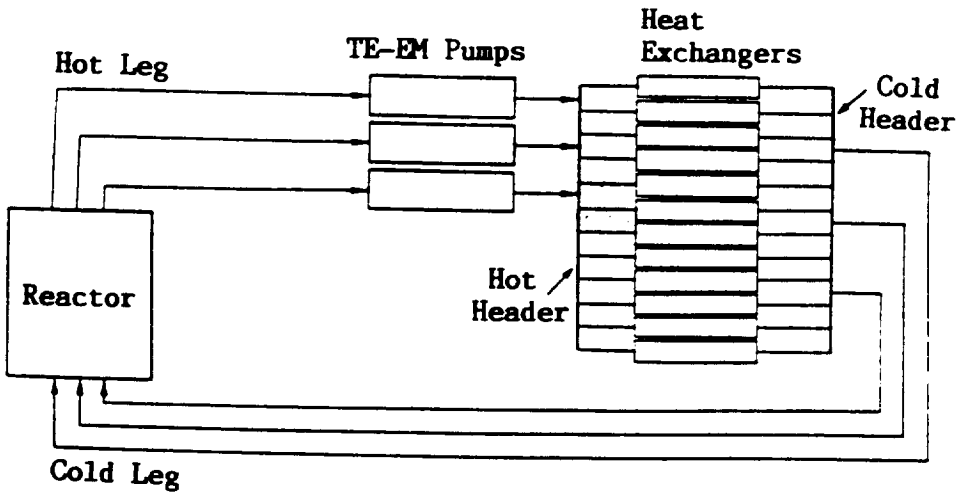

Figure 4. A Line Diagram of the Primary Coolant Loop (Adapted from [6]).

assumes a constant coolant flow area and a uniform magnetic flux density through the coolant ducts. The model also assumes that the TE converter cold shoe temperature is equal to the pump radiator surface temperature. Thus, the model neglects the temperature drop between the evaporator and the condenser of the radiator's heat pipes. Using these assumptions, the model determines the pressure rise across the pump duct, the electromagnetic (EM) pump efficiency, and the overall efficiency of the TE-EM pump.

The piping hydraulic model calculates the pressure drop in the primary coolant loop piping system. The model assumes the heat losses to be negligible, because

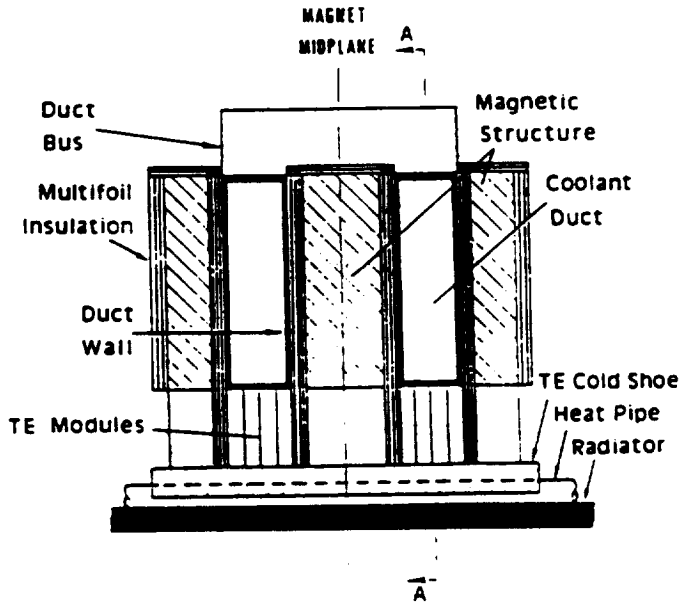

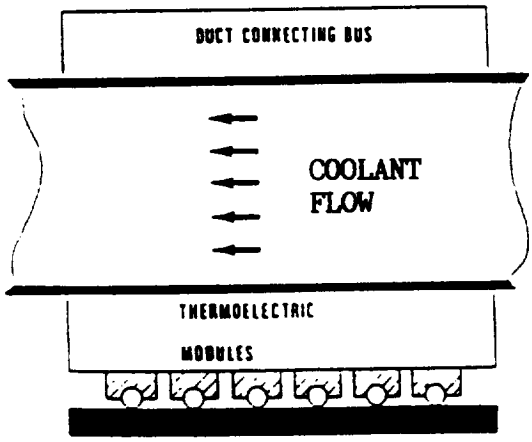

LONGITUDINAL CROSS SECTION A–A

Figure 5 Cross Sectional Views of the Self-Induced Thermoelectric- Electromagnetic (TE-EM) Pump (Adapted from [6]).

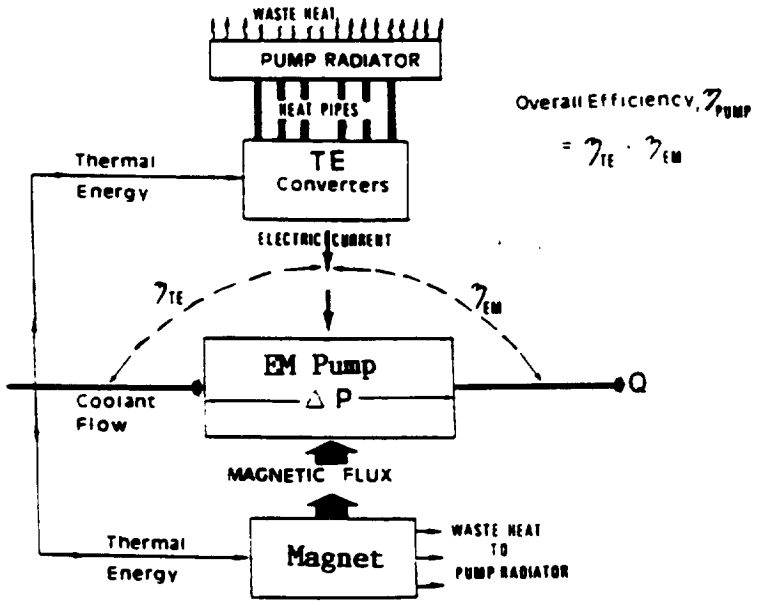

Figure 6. A Schematic Representation of the TE-EM Pump Model (Adapted from [6]).

the primary coolant piping system is thermally insulated by insulation multifoils. Consequently, the coolant temperature at the core exit can be assumed to equal that of the coolant inlet temperature to the TE-EM pumps. Additionally, the coolant inlet and outlet temperatures of the heat exchangers can also be considered equal to the temperatures at the pump exit and at the reactor core inlet, respectively.

The heat exchanger hydraulic model calculates the coolant flow rate in each coolant channel and the total pressure drop in the heat exchanger by ensuring that

the difference in friction pressure loss between any two consecutive channels equal the sum of the pressure losses in the hot and cold headers between the centers of the two channels. The model interpolates the friction factor as a function of Reynolds number. Such a function enables the integrated nonlinear SNPS model to respond to any changes in the reactor power and, consequently, to changes in the coolant flow from laminar to turbulent conditions, or vice versa.

The heat exchanger model calculates the coolant and wall temperature distributions in the coolant channels in the direction of the coolant flow. These temperatures are calculated through the coupling of the heat exchanger thermal model to the main TE converter model.

III.2.3 The TE Converter Model

The TE converter model allows the TE material properties such as the Seebeck coefficient, the thermal conductivity and the electrical resistivity to vary with temperature. The model calculates the electric voltage generated across the external load of the power system, the conversion efficiency of the TE generator and the electric power output of the system.

III.3 Description of the Nonlinear Reference Space Nuclear Power System Model

The reference model used in the design of the voltage controller is a simplified version of the integrated nonlinear SNPS model presented in the previous section, and it includes the physics that defines the system. The major differences between the nonlinear reference model and the integrated nonlinear SNPS model are the following [2]:

1.) The nonlinear reference model has two delayed neutron precursor groups compared to the six groups of the integrated nonlinear SNPS model. The two-group delayed neutron precursor constants are obtained from the six-group delayed neutron precursor constants by using the method described by Skinner and Cohen [4].

2.) The integrated nonlinear SNPS model provides for energy deposition in the nuclear fuel with a fuel clad, whereas the nonlinear reference model does not provide for a fuel clad.

3.) There are no momentum equations in the primary and secondary coolants loops of the nonlinear reference model.

4.) Values that can fluctuate in the integrated nonlinear SNPS model, such as the mass flow rate, remain constant in the nonlinear reference model for each operating power level.

5.) The heat transfer loop is modeled as a single lumped loop in the nonlinear reference model, and not as 12 separate branches as in the integrated nonlinear SNPS model.

6.) The secondary heat transfer loop and the radiator are lumped in one energy equation in the nonlinear reference model, while the integrated nonlinear SNPS model has a separate energy equation for each of the secondary coolant branches and each of the radiator panels.

7.) The nonlinear reference model does not have a separate set of energy equations for the TE-EM pumps as does the integrated nonlinear SNPS model, because the coolant flow rates are considered constant for each operating power level.

Table 3. States, Input, Output and Disturbance of the Nonlinear Reference Model

States	Description
Primary	Neutronic power, MW_{th}
	Delayed-neutron precursor concentration I, MW_{th}
	Delayed-neutron precursor concentration II, MW_{th}
	Fuel temperature, K
	Coolant core exit temperature, K
	Heat exchanger exit temperature, K
	Coolant core inlet temperature, K
Secondary	Thermoelectric temperature, K
	Secondary coolant temperature, K

Input	External reactivity, $\Delta k/k$
Controlled Output	Load voltage, V
Disturbance	Load demand, MW_e

The nonlinear reference model has nine states, one input, four measured outputs and one disturbance, as shown in Table 3, and it is described by the following nine, first-order differential equations:

1.) The reactor kinetics equations :

$$\frac{dP_n(t)}{dt} = \frac{\rho_t(t) - \beta_t}{\Lambda} P_n(t) + \lambda^{(1)} C^{(1)}(t) + \lambda^{(2)} C^{(2)}(t), \qquad (1)$$

where,

$P_n(t)$: the reactor neutron power (the neutronic power),

$C^{(i)}(t)$: the delayed neutron precursor concentration for the i^{th} group,

$\rho_t(t)$: the total core reactivity,

β_t : the total delayed neutron fraction,

Λ : the neutron generation time, and,

$\lambda^{(i)}$: the delayed neutron precursor constant for the i^{th} group,

where the delayed neutron precursor concentrations are determined from :

$$\frac{dC^{(1)}(t)}{dt} = \frac{\beta^{(1)}}{\Lambda} P_n(t) - \lambda^{(1)} C^{(1)}(t), \tag{2}$$

and

$$\frac{dC^{(2)}(t)}{dt} = \frac{\beta^{(2)}}{\Lambda} P_n(t) - \lambda^{(2)} C^{(2)}(t), \tag{3}$$

where,

$\beta^{(i)}$: the delayed neutron fraction for the i^{th} group,

and, where the total core reactivity used in the reactor kinetics equations is given by

$$\rho_t(t) = \rho_{ex}(t) + \alpha_D ln\left[\frac{T_f(t)}{T_f(t=0)}\right] + \alpha_{fuel}[T_f(t) - T_f(t=0)] + \alpha_{cr}[T_{cr}(t) - T_{cr}(t=0)], \tag{4}$$

where,

$\rho_{ex}(t)$: the external reactivity,

α_D : the Doppler reactivity feedback coefficient,

$T_f(t)$: the average fuel temperature,

α_{fuel} : the fuel temperature reactivity feedback coefficient,

α_{cr} : the coolant temperature reactivity feedback coefficient,

$T_{cr}(t)$: the average core coolant temperature.

The nuclear fuel energy equation :

$$\frac{dT_f(t)}{dt} = \frac{P_n(t)}{M_f c_{pf}} - \frac{(T_f(t) - 0.5\,T_{cro}(t) - 0.5\,T_{in}(t))}{\tau_f}, \tag{5}$$

where,

M_f : the mass of the nuclear fuel,

c_{pf} : the specific heat of the nuclear fuel,

$T_{cro}(t)$: the core coolant exit temperature,

$T_{in}(t)$: the core coolant inlet temperature, and where τ_f is defined in the following paragraphs.

3.) The cold-leg energy equation

$$\frac{dT_{in}(t)}{dt} = \frac{(T_{hxo}(t) - T_{in}(t))}{\tau_{in}}. \tag{6}$$

where,

$T_{hxo}(t)$: the heat exchanger coolant exit temperature, and where τ_{in} is defined in the following paragraphs.

4.) The reactor coolant energy equation

$$\frac{dT_{cro}(t)}{dt} = \frac{(T_f(t) - 0.5\,T_{cro}(t) - 0.5\,T_{in}(t))}{\tau_{cr}} - \frac{\dot{m}_{tot}}{M_{cr}}(T_{cro}(t) - T_{in}(t)), \tag{7}$$

where,

M_{cr} : the core coolant mass,

$\dot{m}_{tot}$: the total core coolant mass flow rate, and where, τ_{cr} is defined in the following paragraphs.

5.) The primary loop coolant energy equation :

$$\frac{dT_{hxo}(t)}{dt} = \frac{\dot{m}_{tot}}{M_c}(T_{cro}(t) - T_{hxo}(t)) - \frac{(0.5\,T_{cro}(t) - 0.5\,T_{hxo}(t) - T_{te}(t))}{\tau_{cp}}, \tag{8}$$

where,

M_c : the coolant mass in the primary heat transfer branches.

$T_{te}(t)$: the thermoelectric temperature, and where τ_{cp} is defined in the following paragraphs.

6.) The PCA thermoelectric energy equation :

$$\frac{dT_{te}(t)}{dt} = \frac{(0.5\,T_{cro}(t) + 0.5\,T_{hxo}(t) - T_{te}(t))}{\tau_{hx}} - \frac{(T_{te}(t) - T_s(t))}{\tau_{shx}} - \frac{I_{tot}(t)V_{load}(t)}{M_{te}c_{pte}}. \tag{9}$$

where,

$I_{tot}(t)$: the current drawn by the load,

$V_{load}(t)$: the voltage drop across the load,

M_{te} : the mass of the thermoelectrics,

c_{pte} : the specific heat of the PCA thermoelectrics, and where τ_{hx} and τ_{shx} are defined in the following paragraphs.

7.) The secondary coolant energy equation :

$$\frac{dT_s(t)}{dt} = \frac{(T_{te}(t) - T_s(t))}{\tau_{sr}} - \frac{(T_s(t) - T_{sink})}{\tau_r}, \tag{10}$$

where,

$T_s(t)$ = secondary coolant temperature,

T_{sink} = effective sink temperature, and where, τ_{sr} and τ_r are defined in the following paragraphs.

The τ's in the energy equations (Eqs. (5) through (10)) are time constants that are initially calculated for each operating power level, from the physical properties of the system such that the equations satisfy steady-state conditions. The τ's are defined as follows:

$$\tau_f = (T_f(t) - 0.5\,T_{cro}(t) - 0.5\,T_{in}(t))\frac{M_f c_{pf}}{P_n(t)}, \tag{11}$$

$$\tau_{cr} = \frac{(T_f(t) - 0.5\,T_{cro}(t) - 0.5\,T_{in}(t))M_{cr}}{(T_{cro}(t) - T_{in}(t))\dot{m}_{tot}}. \tag{12}$$

$$\tau_{cp} = \frac{(0.5\,T_{cro}(t) + 0.5\,T_{hxo}(t) - T_{te}(t))M_c}{(T_{cro}(t) - T_{hxo}(t))\dot{m}_{tot}}, \tag{13}$$

$$\tau_{hx} = \frac{\tau_{cp} M_{te} c_{pte}}{M_c c_{pc}}, \tag{14}$$

$$\tau_{shx} = \frac{(T_{te}(t) - T_s(t))}{\frac{1}{\tau_{hx}}(0.5\,T_{cro}(t) + 0.5\,T_{hxo}(t) - T_{te}(t)) - \frac{I_{tot}(t)V_{load}(t)}{M_{te}c_{pte}}}, \tag{15}$$

$$\tau_{sr} = \frac{\tau_{shx} M_s c_{ps}}{M_{te} c_{pte}}, \tag{16}$$

and

$$\tau_r = \frac{\tau_{sr}(T_s(t) - T_{sink}(t))}{(T_{te}(t) - T_s(t))}, \tag{17}$$

where

c_{pc} : the primary coolant specific heat,

M_s : the coolant mass in the secondary coolant branches,

c_{ps} : the secondary coolant specific heat.

Equations (1) through (10) can be placed in the following state-space variable form:

$$\dot{\mathbf{x}}(t) = \mathbf{f}(\mathbf{x}(t), u(t), w(t)), \tag{18}$$

whereas the output equation can be defined by

$$\mathbf{y}(t) = \mathbf{g}(\mathbf{x}(t), u(t), w(t)), \tag{19}$$

where **f**(.) and **g**(.) are vectors of nonlinear functions of the system states, input, and disturbance. The state vector **x**(t) is defined by

$$\mathbf{x}(t) = \left[P_n(t) \quad C^{(1)}(t) \quad C^{(2)}(t) \quad T_f(t) \quad T_{cro}(t) \quad T_{hxo}(t) \quad T_{in}(t) \quad T_{te}(t) \quad T_s(t) \right]^T, \tag{20}$$

and,

$u(t)$ is the system input (external reactivity, $\rho_{ex}(t)$),

$w(t)$ is the system disturbance (the electric load demand, $I_{tot}(t)\, V_{load}(t)$), and,

$\mathbf{y}(t)$ is the measured system output (5×1).

The measurable outputs of the system are as follows :

1.) The neutronic power, $P_n(t)$,

2.) The core coolant exit temperature, $T_{cro}(t)$,

3.) The core coolant inlet temperature, $T_{in}(t)$,

4.) The total core coolant mass flow rate, $\dot{m}(t)$, and,

5.) The load voltage, $V_{load}(t)$.

Equations (18) and (19) are solved at each time step during the simulation using a stiff differential equation solver, as it is done when simulating the integrated nonlinear SNPS model.

III 4 Linearized Reference Models

III 4 1 Development of the Linearized Reference Model

The linearized reference models are obtained for each operating power level by analytically and numerically linearizing the nonlinear reference model. Analytical

linearization is performed on the nonlinear reference model of the SNPS using a Taylor series expansion about the stead-state values of the states, input and disturbance ($\mathbf{x_o}$, u_o, w_o). These steady-state values are obtained from operating the integrated nonlinear SNPS model at various power levels. Applying the Taylor's expansion to Equation (18), and neglecting higher order terms, the following is obtained:

$$\dot{\mathbf{x}}_0(t) + \delta\dot{\mathbf{x}}(t) \cong \mathbf{f}\,[\mathbf{x_0}(t), u_0(t), w_0(t)] + (\frac{\partial \mathbf{f}}{\partial \mathbf{x}})\,|_{(\mathbf{x_0},u_0,w_0)}\,\delta\mathbf{x}(t) + (\frac{\partial \mathbf{f}}{\partial u})\,|_{(\mathbf{x_0},u_0,w_0)}\,\delta u(t) + (\frac{\partial \mathbf{f}}{\partial w})\,|_{(\mathbf{x_0},u_0,w_0)}\delta w(t) \qquad (21)$$

where $\delta(.)$ is the perturbation from the equilibrium point and where all the derivatives are calculated at each operating power level. Because the system is at equilibrium at ($\mathbf{x_0}$, u_0, w_0), Equation (21) can be rewritten as :

$$\delta\dot{\mathbf{x}}(t) \cong (\frac{\partial \mathbf{f}}{\partial \mathbf{x}})\,|_{(\mathbf{x_0},u_0,w_0)}\,\delta\mathbf{x}(t) + (\frac{\partial \mathbf{f}}{\partial u})\,|_{(\mathbf{x_0},u_0,w_0)}\,\delta u(t) + (\frac{\partial \mathbf{f}}{\partial w})\,|_{(\mathbf{x_0},u_0,w_0)}\delta w(t). \qquad (22)$$

As a result of the hard nonlinearities present, the output Equation, (19), is numerically linearized by perturbing the system states, input variable and disturbance variable about an equilibrium point (steady-state conditions corresponding to a particular power level) and the rates of change of the system states and the output variables are determined. Expanding Equation (19) in a Taylor series about the equilibrium values of the states, input and disturbance, the following is obtained:

$$y_0 - \delta y(t) \cong \mathbf{g}(\mathbf{x_0}(t), u_0(t), w_0(t)) - \left(\frac{\partial \mathbf{g}}{\partial \mathbf{x}}\right)_{(\mathbf{x_0}, u_0, w_0)} \delta\mathbf{x}(t) - \left(\frac{\partial \mathbf{g}}{\partial u}\right)_{(\mathbf{x_0}, u_0, w_0)} \delta\mathbf{u}(t) - \left(\frac{\partial \mathbf{g}}{\partial w}\right)_{(\mathbf{x_0}, u_0, w_0)} \delta\mathbf{w}(t) \quad (23)$$

where $\delta(.)$ is the perturbation from the equilibrium point, and where all of the derivatives are evaluated at $(\mathbf{x_0}, u_0, w_0)$. In Equation (23), the output refers to the load voltage alone, because only one output can be independently controlled by the single input control.

From Equations (21) and (23), the following linearized reference system model is obtained which is valid about the equilibrium point ($\mathbf{x} = \mathbf{x_0}$, $u = u_0$, $w = w_0$) :

$$\delta\dot{\mathbf{x}}(t) = \mathbf{A}\,\delta\mathbf{x}(t) + \mathbf{B}\,\delta u(t) + \mathbf{L}\,\delta w(t) \quad (24)$$

$$\delta y(t) = \mathbf{C}\,\delta\mathbf{x}(t) + \mathbf{D}\,\delta u(t) + \mathbf{F}\,\delta w(t) \quad (25)$$

where $\delta\mathbf{x}(t)$, $\delta u(t)$, $\delta w(t)$, and $\delta y(t)$ are the vectors perturbed about their equilibrium values. Figure 7 depicts a block diagram of the linearized reference model.

The system matrices are given by the following expressions:

$$\mathbf{A} = \left(\frac{\partial \mathbf{f}}{\partial \mathbf{x}}\right)_{(\mathbf{x_0}, u_0, w_0)} \text{, State matrix } (9\times9) \quad (26)$$

$$\mathbf{B} = \left(\frac{\partial \mathbf{f}}{\partial u}\right)_{(\mathbf{x_0}, u_0, w_0)} \text{, State Input vector } (9\times1) \quad (27)$$

$$\mathbf{L} = \left(\frac{\partial \mathbf{f}}{\partial w}\right)_{(\mathbf{x_0}, u_0, w_0)} \text{, State Disturbance vector } (9\times1) \quad (28)$$

$$\mathbf{C} = \left(\frac{\partial \mathbf{g}}{\partial \mathbf{x}}\right)_{(\mathbf{x_0}, u_0, w_0)} \text{, Output vector } (1\times9) \quad (29)$$

$$\mathbf{D} = \left(\frac{\partial \mathbf{g}}{\partial u}\right)_{(\mathbf{x_0}, u_0, w_0)} \text{, Feedforward scalar term} \quad (30)$$

$$\mathbf{F} = \left(\frac{\partial \mathbf{g}}{\partial w}\right)_{(\mathbf{x_0}, u_0, w_0)} \text{, Output disturbance scalar term} \quad (31)$$

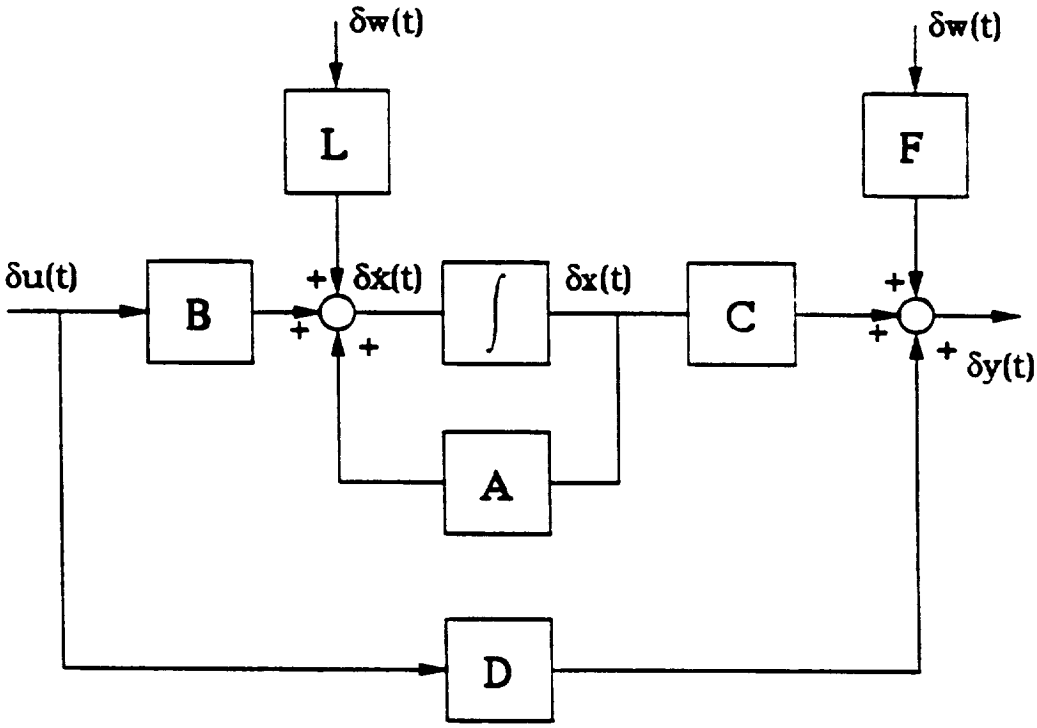

δx(t) : State Vector

δu(t) : Input Vector

δy(t) : Output Vector

δw(t) : Disturbance Vector

Figure 7. Block Diagram of the Linearized Reference Model

The elements of the linearized reference model are as follows :

$$A_{11} = \frac{-\beta_t}{\Lambda},$$

$$A_{12} = \lambda_1,$$

$$A_{13} = \lambda_2,$$

$$A_{14} = \frac{\alpha_{ex}}{\Lambda},$$

$$A_{21} = \frac{\beta_1}{\Lambda},$$

$$A_{22} = -\lambda_1,$$

$$A_{31} = \frac{\beta_2}{\Lambda},$$

$$A_{32} = -\lambda_2,$$

$$A_{41} = \frac{P_n(t=0)}{M_f c_{pf}},$$

$$A_{44} = \frac{-1}{\tau_f},$$

$$A_{45} = \frac{0.5}{\tau_f},$$

$$A_{47} = \frac{0.5}{\tau_f},$$

$$A_{54} = \frac{1}{\tau_{cr}},$$

$$A_{55} = \frac{-0.5}{\tau_{cr}} - \frac{\dot{m}_{tot}}{M_c},$$

$$A_{57} = \frac{-0.5}{\tau_{cr}} + \frac{\dot{m}_{tot}}{M_c},$$

$$A_{66} = -\frac{\dot{m}_{tot}}{M_c} - \frac{0.5}{\tau_{cp}},$$

$$A_{67} = \frac{\dot{m}_{tot}}{M_c} - \frac{0.5}{\tau_{cp}},$$

$$A_{68} = \frac{1}{\tau_{cp}},$$

$$A_{76} = \frac{1}{\tau_{cp}},$$

$$A_{77} = -\frac{1}{\tau_{cp}},$$

$$A_{85} = \frac{0.5}{\tau_{hx}},$$

$$A_{86} = \frac{0.5}{\tau_{hx}},$$

$$A_{88} = \frac{-1}{\tau_{hx}} - \frac{1}{\tau_{shx}},$$

$$A_{89} = \frac{1}{\tau_{shx}},$$

$$A_{98} = \frac{1}{\tau_{sr}},$$

$$A_{99} = \frac{-1}{\tau_{sr}} - \frac{1}{\tau_{r}},$$

$$B_{11} = \frac{1}{\Lambda},$$

$$L_{81} = -\frac{1}{M_{te}c_{pte}},$$

where, **A** is a (9×9) matrix, and **B** and **L** are (9×1) column vectors.

The numerical values of the elements of **A**, **B**, **C**, **L**, and **F** for various equilibrium points are given in Appendix A. All other elements not listed above or in Appendix A are identically zero.

III.4.2 Linearization Error Analysis

The linearized reference model obtained by linearizing the nonlinear reference model at a particular operating point is valid only for a small perturbation around this operating point. Therefore, a linearization error analysis is required to determine the magnitute of the perturbation about the equilibrium point for which the linearized model is valid. This range of validity is determined by comparing the state and output (load voltage) responses of the linearized reference model with those of the integrated nonlinear SNPS model for various perturbations in the external reactivity, corresponding to equivalent changes in the load demand. The percentage relative error (ϵ) in the states of the linearized reference model is defined as :

$$\epsilon = \max_{t \le t_{max}} \frac{\left(\delta x^{i}{}_{nl}(t) - \delta x^{i}{}_{l}(t)\right)}{x^{i}{}_{nl}(t)} \quad i = 1, \ldots, 9 \tag{32}$$

where $\delta x^{t}{}_{nl}(t)$ and $\delta x^{t}{}_{l}(t)$ are the state perturbations of the nonlinear integrated SNPS model and linearized reference models from the equilibrium point, respectively, and $x^{t}{}_{nl}(t)$ is the *absolute* state of the integrated nonlinear SNPS model. In this analysis, t_{max} is assumed to be 400 seconds since this covers the majority of the transient and steady state responses of the system. Step perturbations of the external reactivity from equilibrium, both in the positive and negative directions, are applied until the maximum percentage relative error, ϵ, of *any* of the states and the load voltage reaches about 10%. The maximum power level perturbation (positive or negative) for which this value of ϵ is reached is chosen as the validity range for the linearized reference model.

To obtain the models that cover the entire operating regime of the SNPS (from 50% to 150% of the full power), a linearized reference model of the SNPS is obtained at 100% of full power level. A linearization analysis is performed for this model and its validity range in the positive and negative directions is determined. The next operating point about which a linearized reference model is obtained is determined by considering the validity range of the previous model, and the extent to which two consecutive models will overlap. Because the validity range of the next model is not known apriori, this process is iterative in nature. The iterations are terminated when satisfactory overlapping is achieved. The linearization process is repeated about each selected operating point both above and below the full power level using the above procedure until the entire operating regime of the power system is covered.

Table 4. Validity Ranges of the Linearized Reference Models for Positive and Negative Step Perturbations in the Electric Power Output

Equilibrium Power Level	Maximum Positive Perturbation	Maximum Negative Perturbation
50%	5%	5%
55%	5%	5%
60%	5%	5%
65%	8%	6%
70%	10%	8%
75%	15%	12%
80%	18%	15%
85%	19%	15%
90%	23%	20%
95%	29%	26%
100%	38%	24%
105%	38%	23%
110%	37%	21%
115%*	35%	19%
120%*	30%	17%
125%*	25%	17%
130%*	20%	15%
135%*	15%	10%
140%*	10%	6%
145%*	5%	5%
150%*	5%	5%

* shows the models are valid at and beyond 150%

Table 4 depicts the validity ranges for the linearized reference models at different equilibrium points. It is observed that the validity ranges of the linearized reference models are quite large and the amount of the perturbations for models above 100% of full power are larger than those for the models designed for operating levels below full power. This can be explained by the fact that when the reactor operates above full

power. the responses of the system states and the output are varying less from the nominal power level than when the system operates below the nominal power level, due to a higher efficiency of the TE-EM pumps at power levels above the full power level. Therefore a smaller change in the external reactivity is required to bring the system at full power to a higher equilibrium point than to bring it to an operating level below the full power level.

III.5 Validation of Linearized Reference Models

In this section, a comparison of the state and output (load voltage) responses of various linearized reference models and the integrated nonlinear SNPS model to certain step changes in the external reactivity are presented. Figures 8 through 15 depict the open-loop responses of the load voltage and of the states of both the 110% of full power linearized reference model and the integrated nonlinear SNPS model to a step increase in the external reactivity, corresponding to a step load level increase from 100% to 110% of full power.

Similarly, Figures 16 through 23 depict the open-loop responses of the load voltage and of the states of both the 80% of full power linearized reference model and the integrated nonlinear SNPS model to a step load level decrease from 100% to 80% of full power.

Figures 24 and 25 show the responses of the neutronic power and the load voltage of the 110% of full power linearized reference model and the integrated nonlinear SNPS model to a step increase in the external reactivity, corresponding to a 35% of full power increase in the load level of the system, respectively. It is observed that

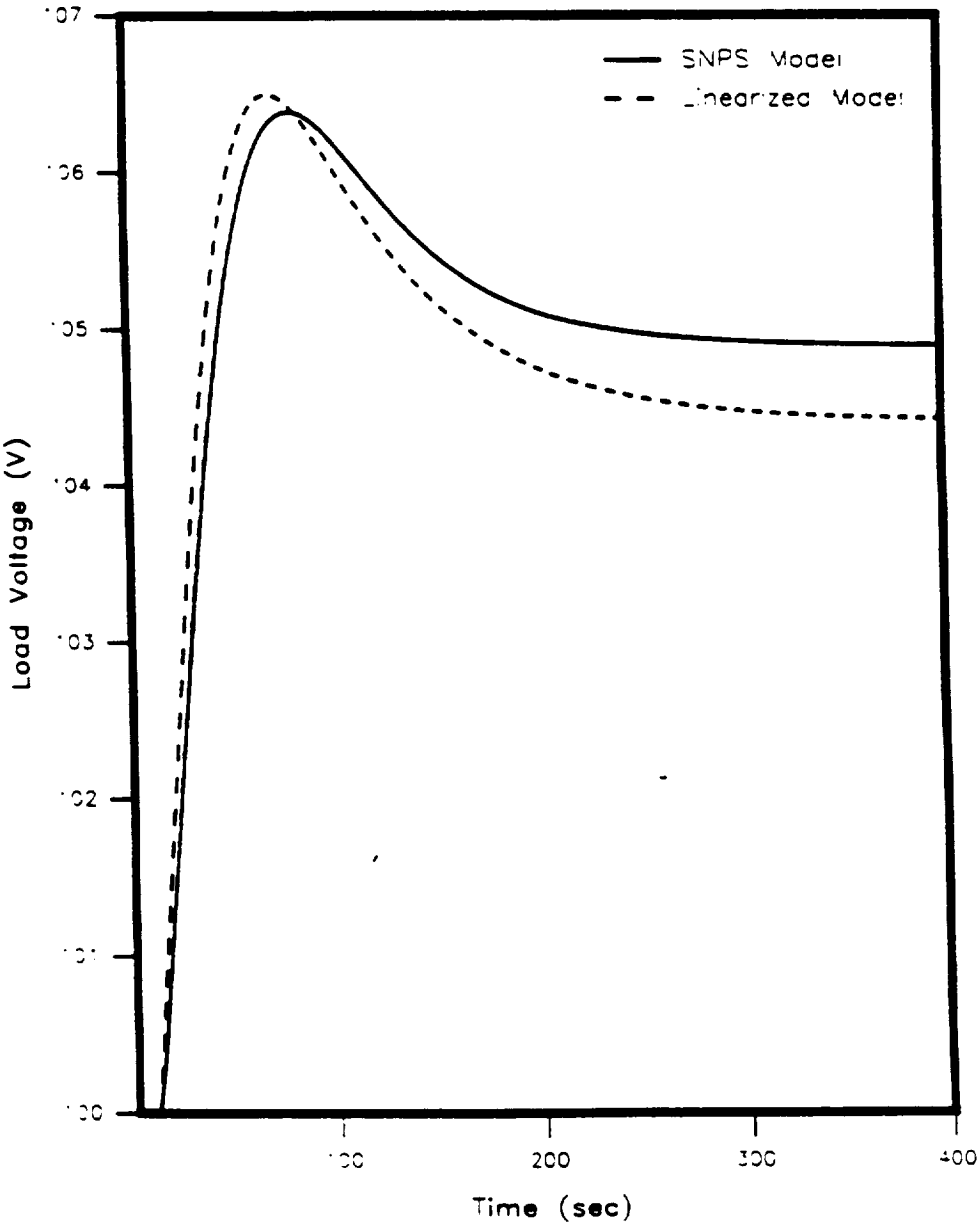

Figure 8. Load Voltage Responses for a Step Change in External Reactivity Corresponding to a Load Change from 100% to 110% of Full Power.

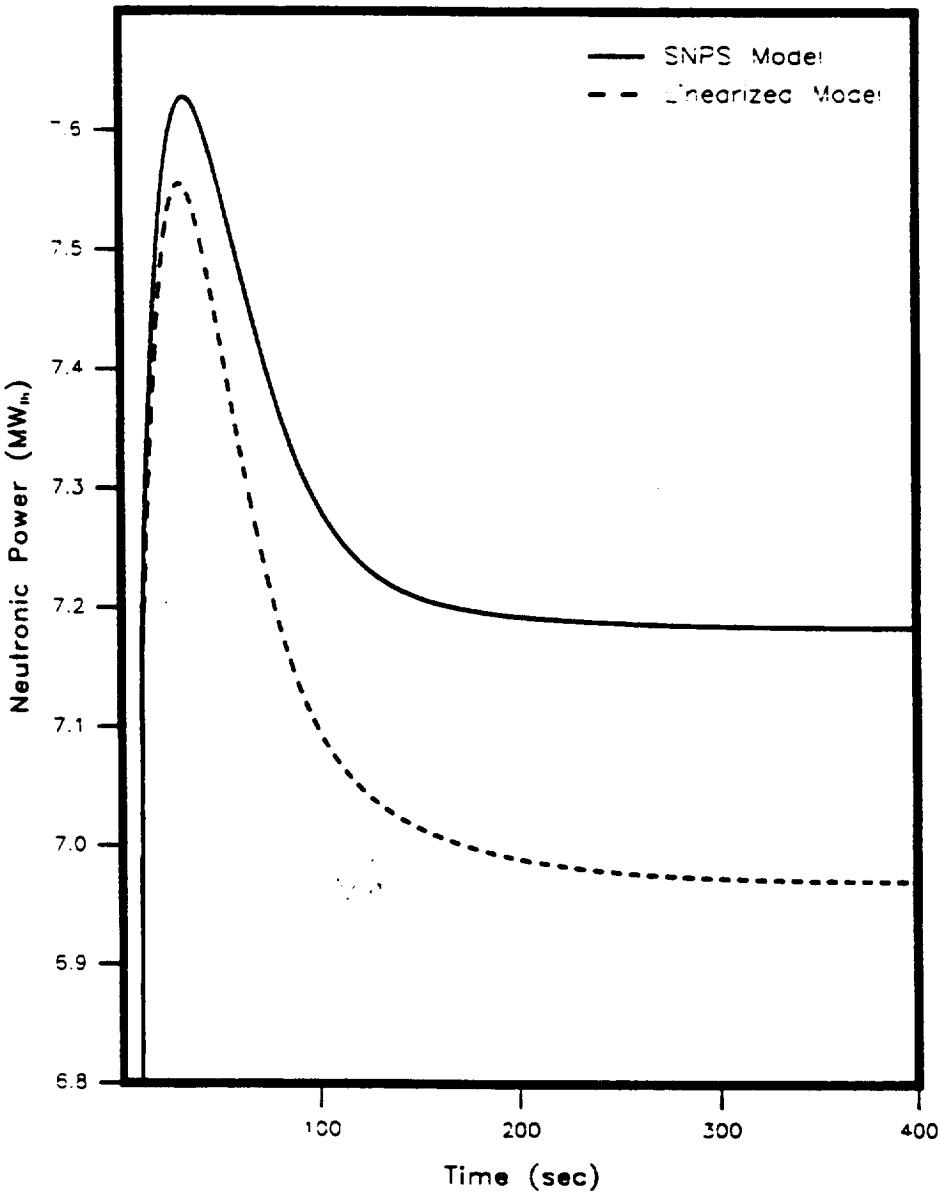

Figure 9. Neutronic Power Responses for a Step Change in External Reactivity Corresponding to a Load Change from 100% to 110% of Full Power.

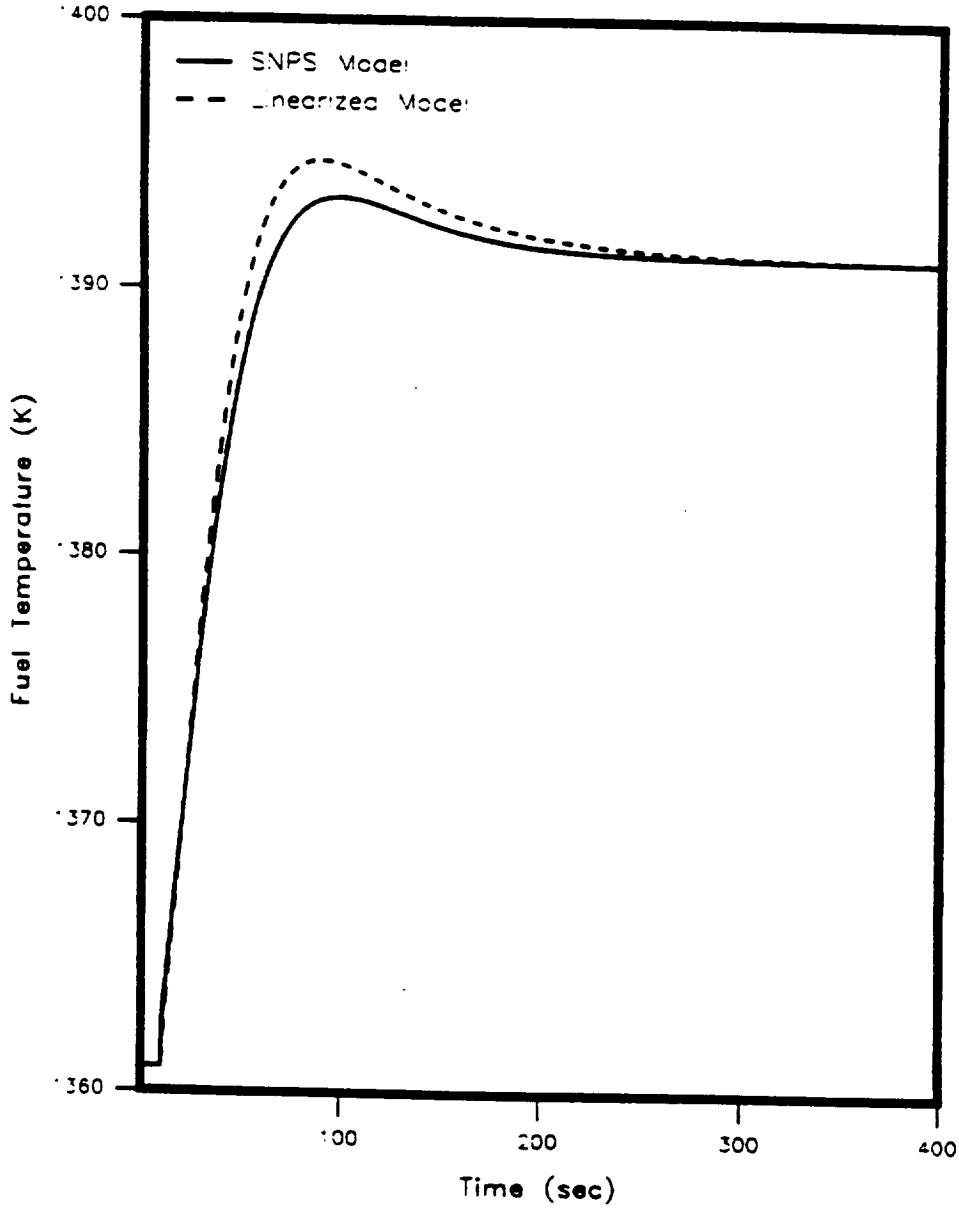

Figure 10. Fuel Temperature Responses for a Step Change in Reactivity Corresponding to a Load Change from 100% to 110% of Full Power.

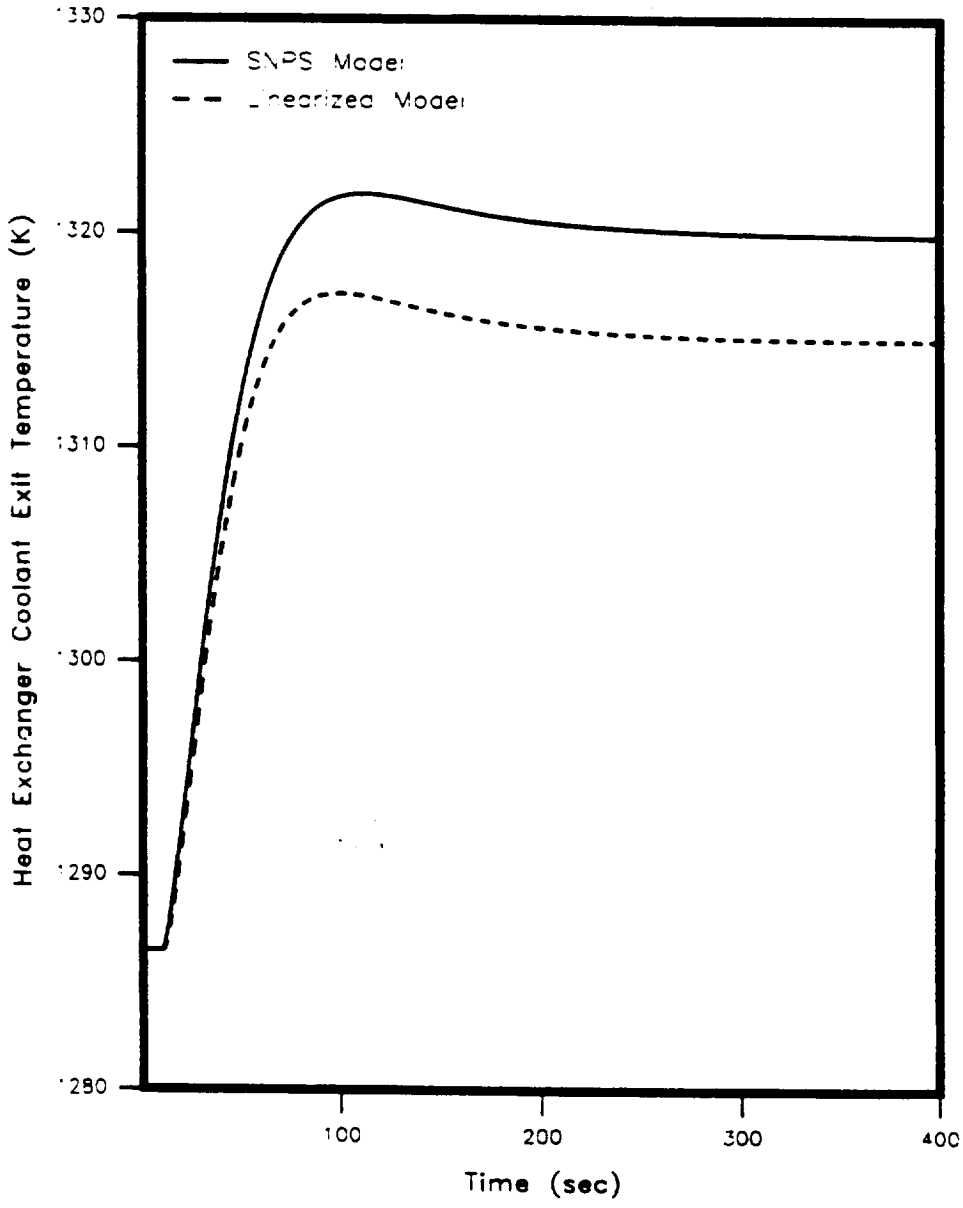

Figure 11. Core Coolant Exit Temperature Responses for a Step Change in External Reactivity Corresponding to a Load Change from 100% to 110% of Full Power.

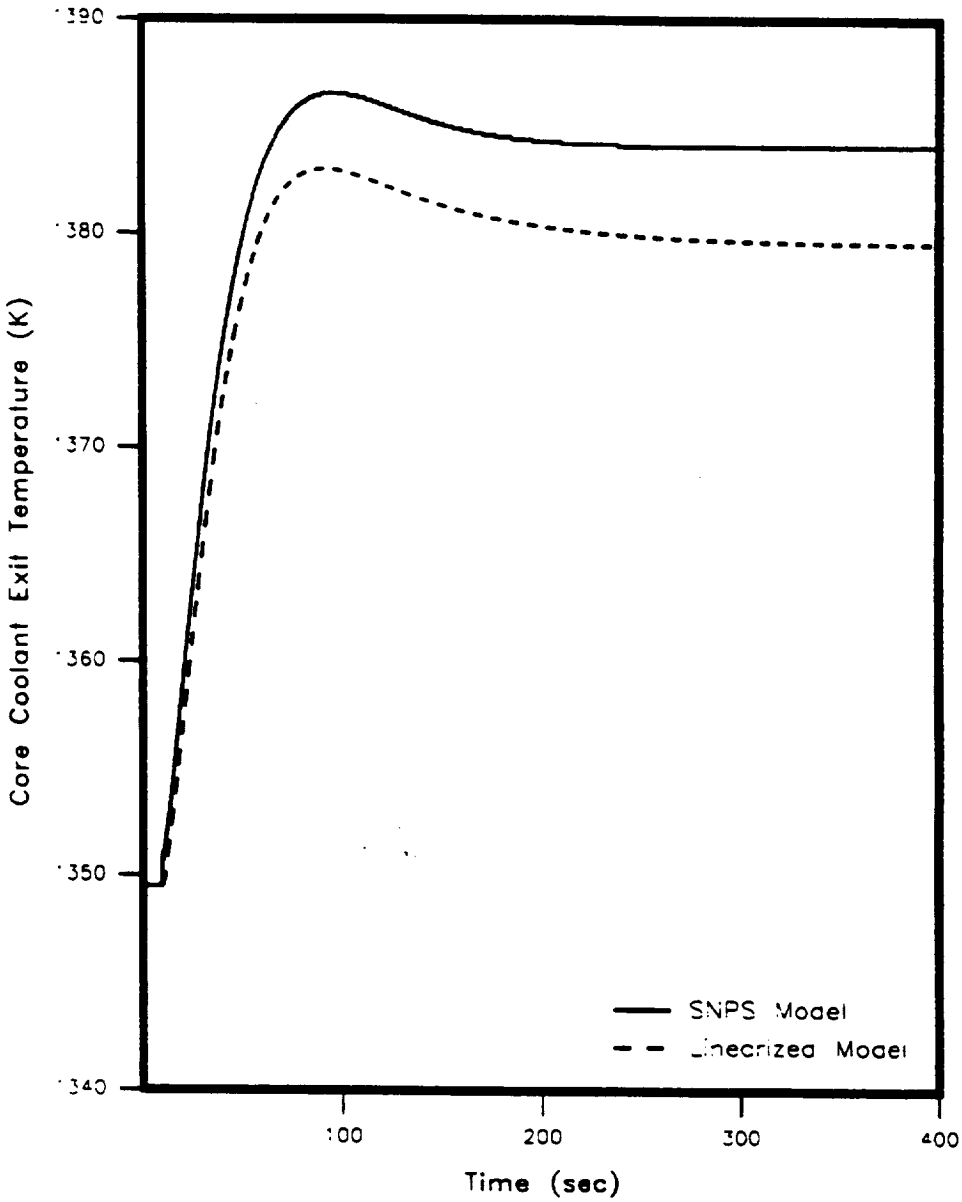

Figure 12. Heat Exchanger Coolant Exit Temperature Responses for a Step Change in External Reactivity Corresponding to a Load Change from 100% to 110% of Full Power.

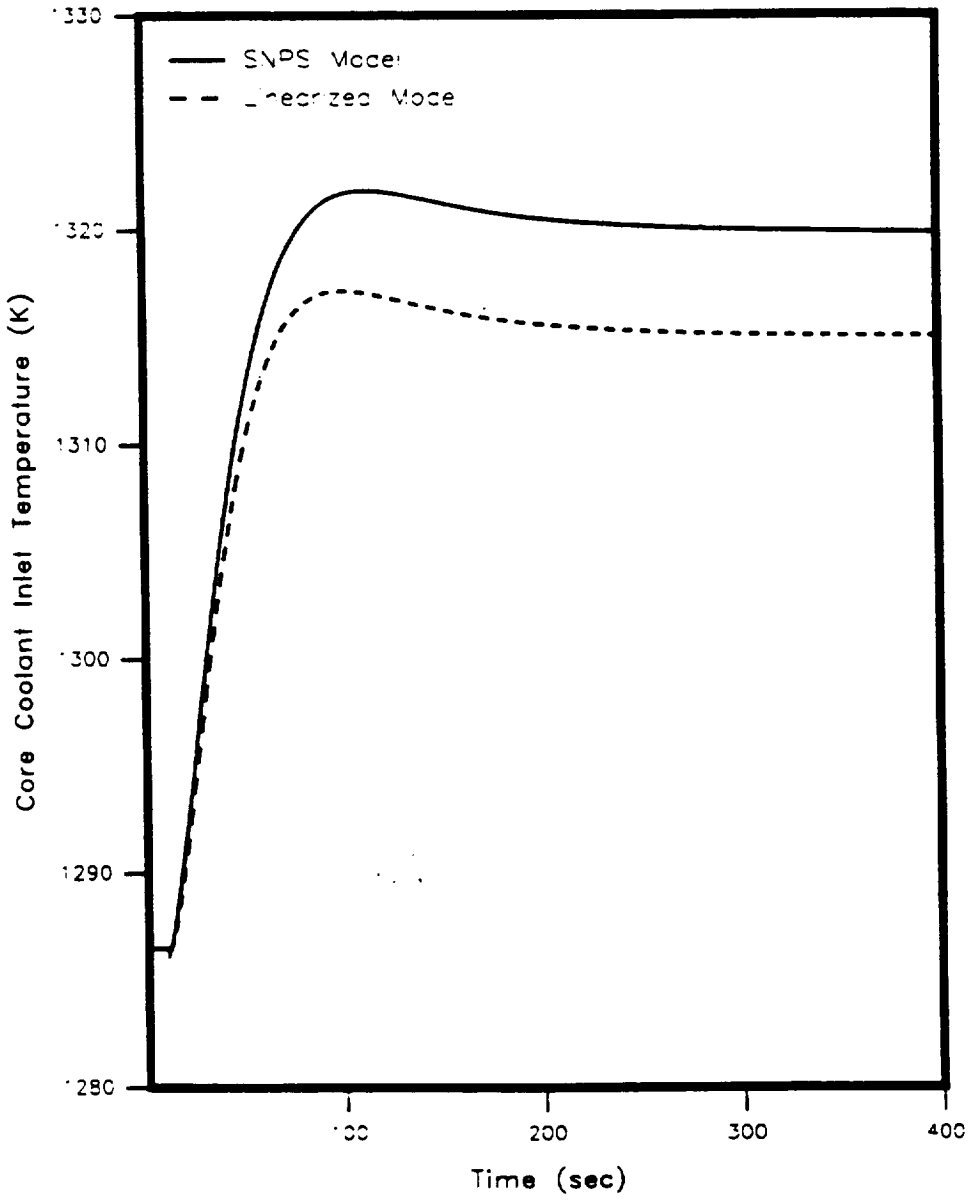

Figure 13. Core Coolant Inlet Temperature Responses for a Step Change in External Reactivity Corresponding to a Load Change from 100% to 110% of Full Power.

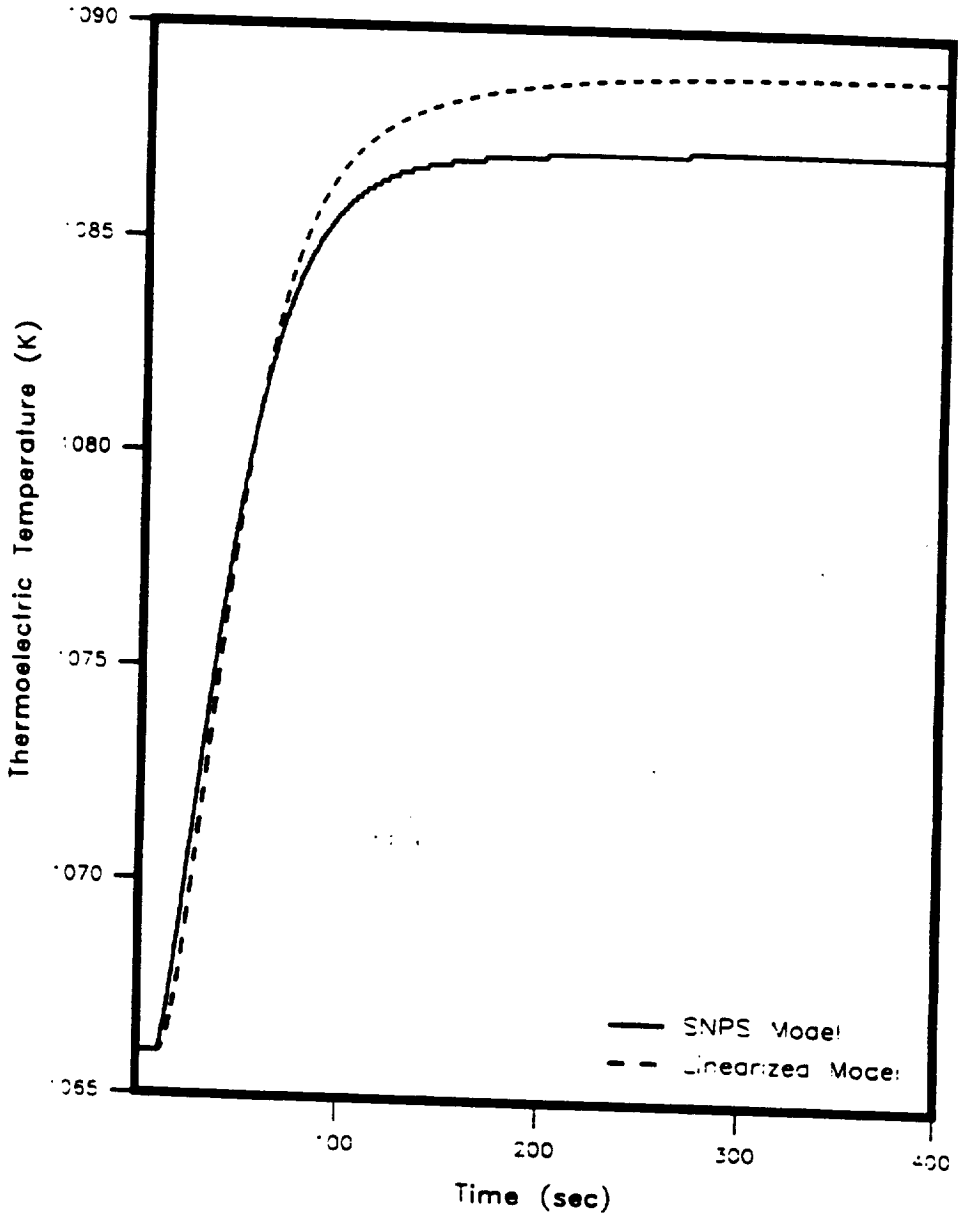

Figure 14. Thermoelectric Temperature Responses for a Step Change in External Reactivity Corresponding to a Load Change from 100% to 110% of Full Power.

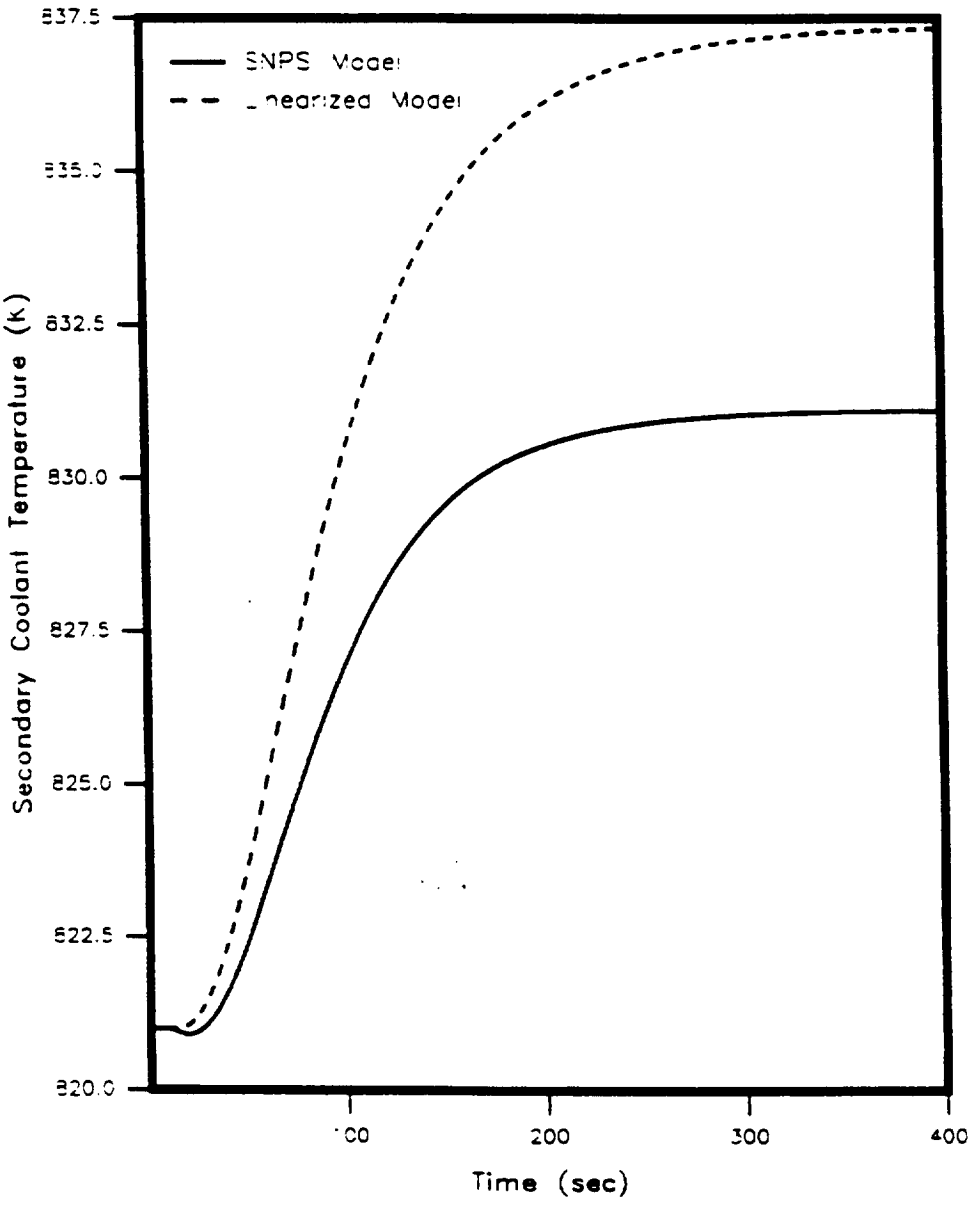

Figure 15. Secondary Coolant Temperature Responses for a Step Change in External Reactivity Corresponding to a Load Change from 100% to 110% of Full Power.

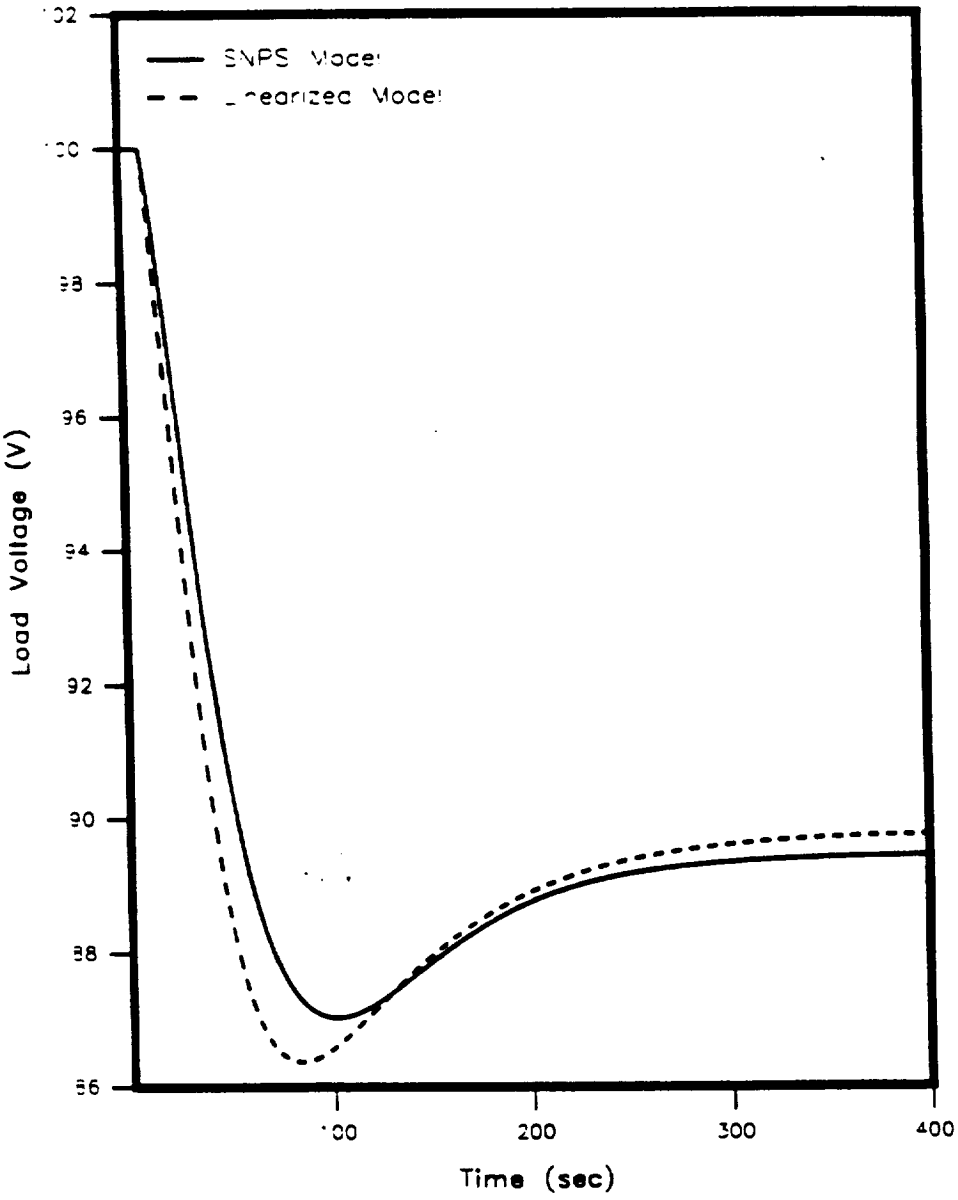

Figure 16. Load Voltage Responses for a Step Change in External Reactivity Corresponding to a Load Change from 100% to 80% of Full Power.

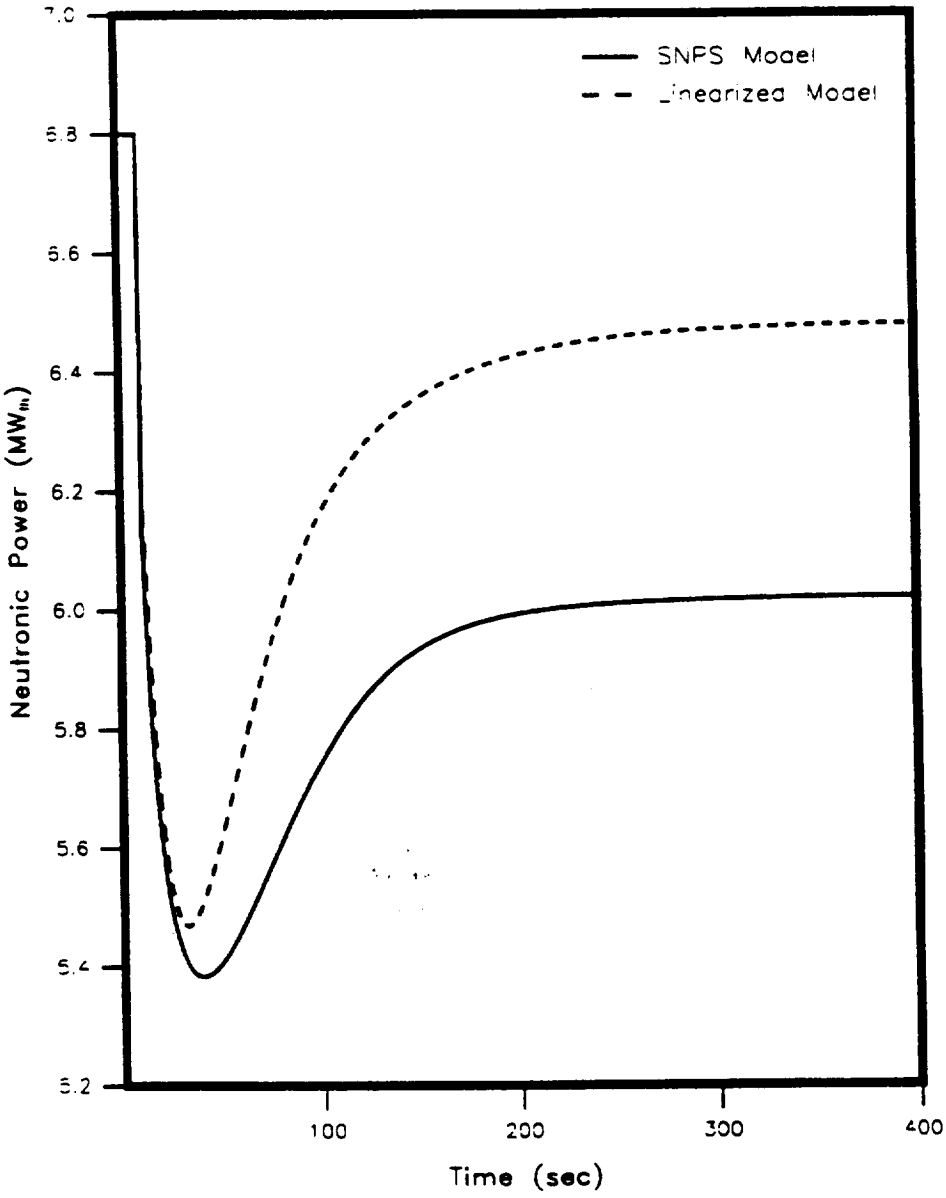

Figure 17. Neutronic Power Responses for a Step Change in External Reactivity Corresponding to a Load Change from 100% to 80% of Full Power.

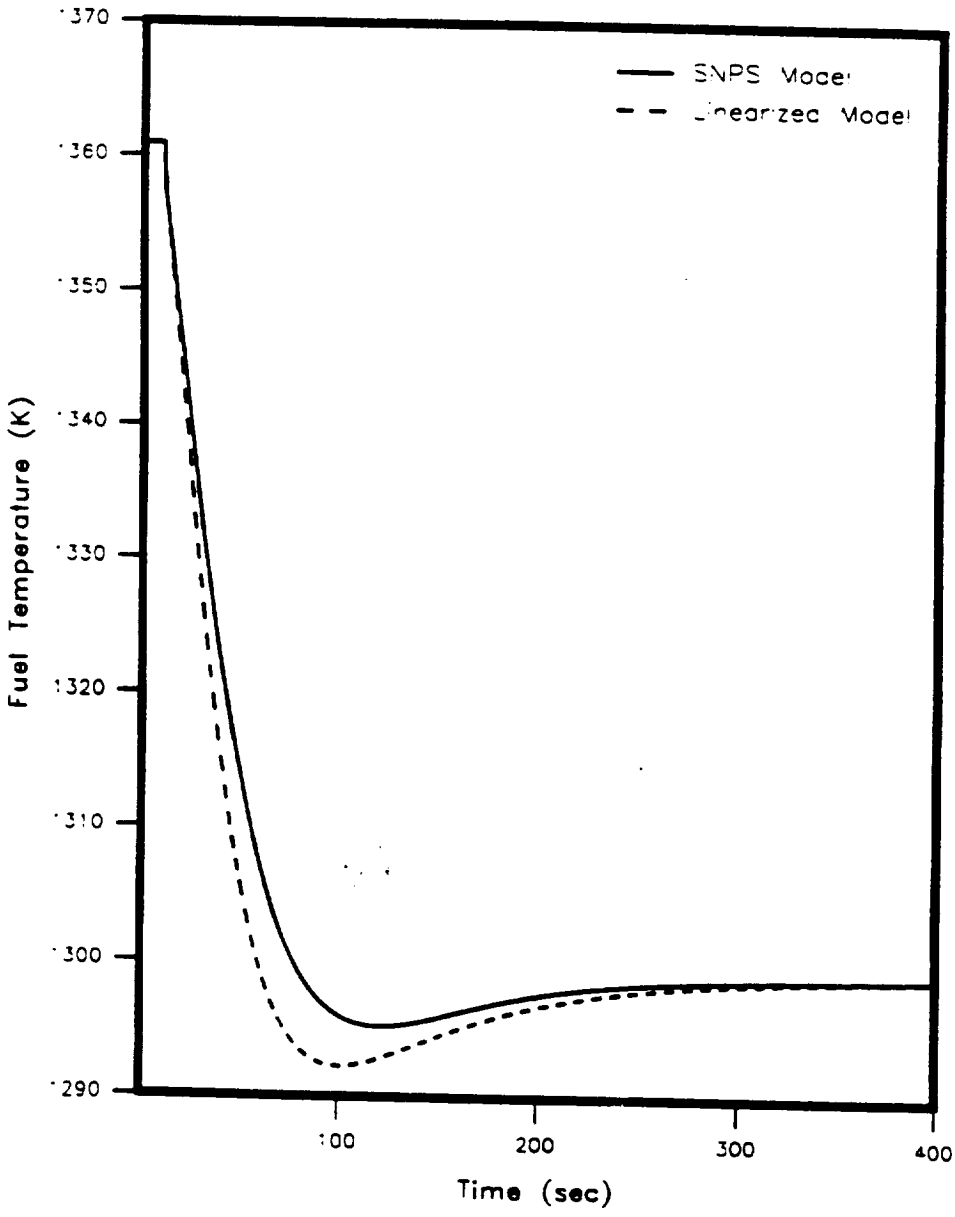

Figure 18. Fuel Temperature Responses for a Step Change in External Reactivity Corresponding to a Load Change from 100% to 80% of Full Power.

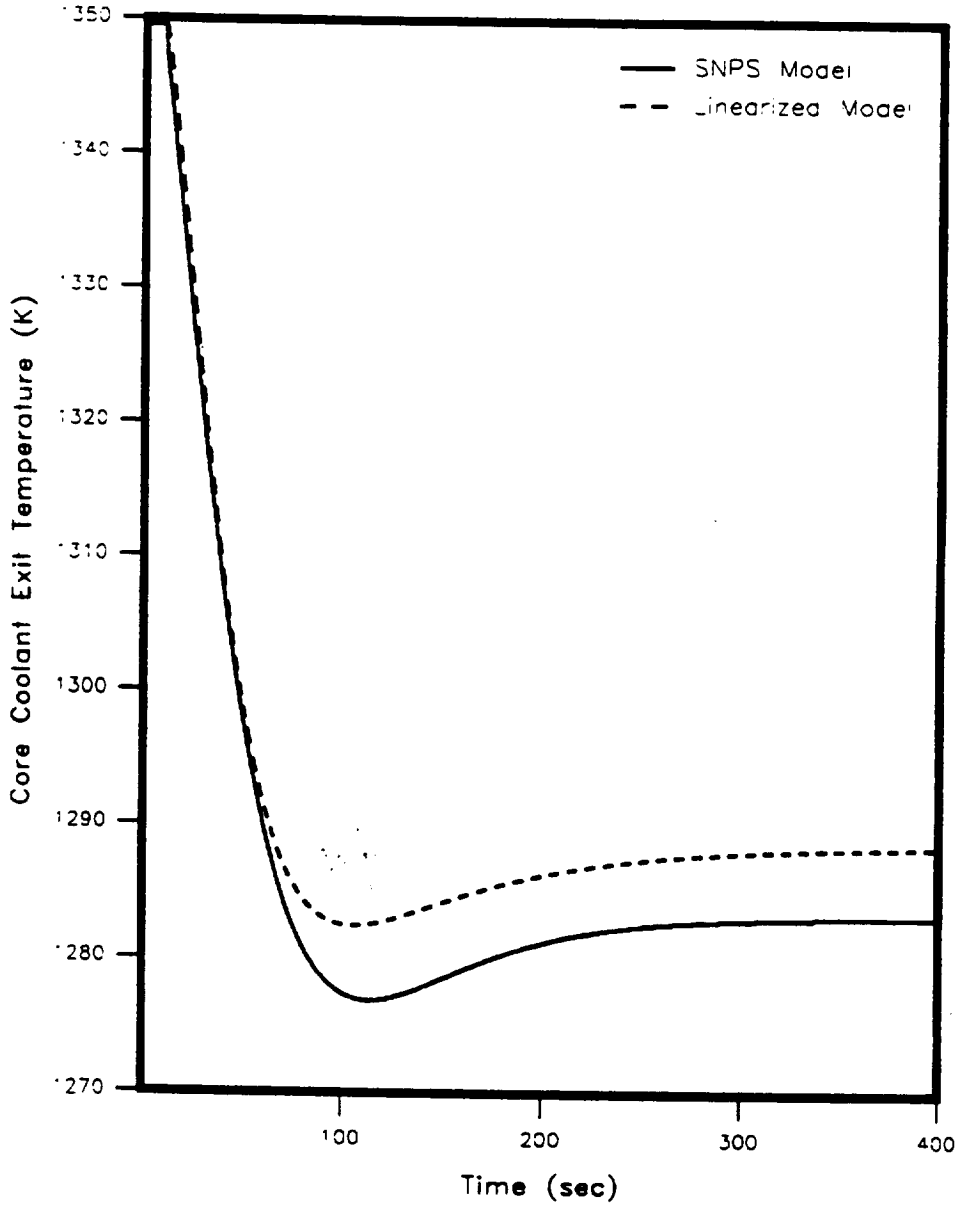

Figure 19. Core Coolant Exit Temperature Responses for a Step Change in External Reactivity Corresponding to a Load Change from 100% to 80% of Full Power.

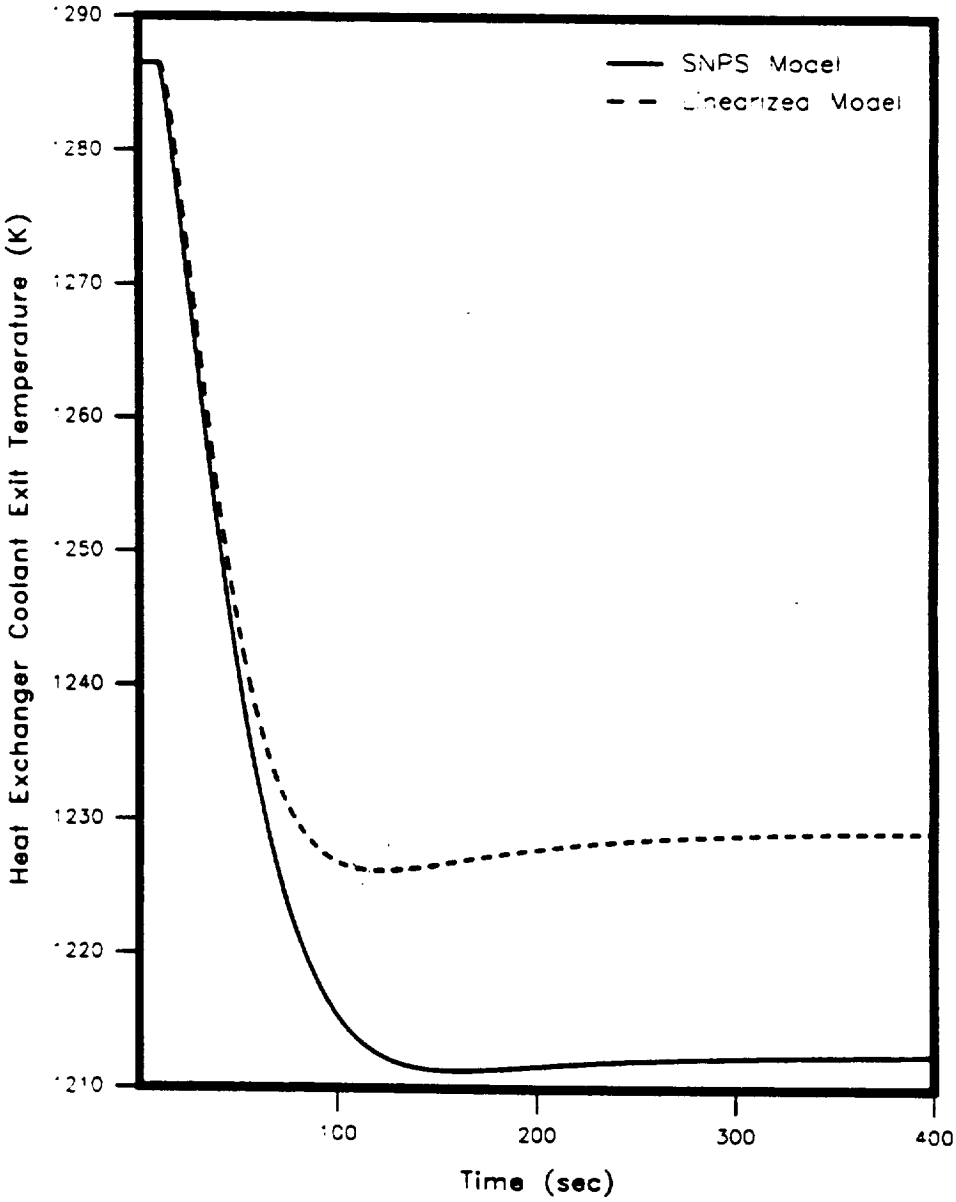

Figure 20. Heat Exchanger Coolant Exit Temperature Responses for a Step Change in External Reactivity Corresponding to a Load Change from 100% to 80% of Full Power.

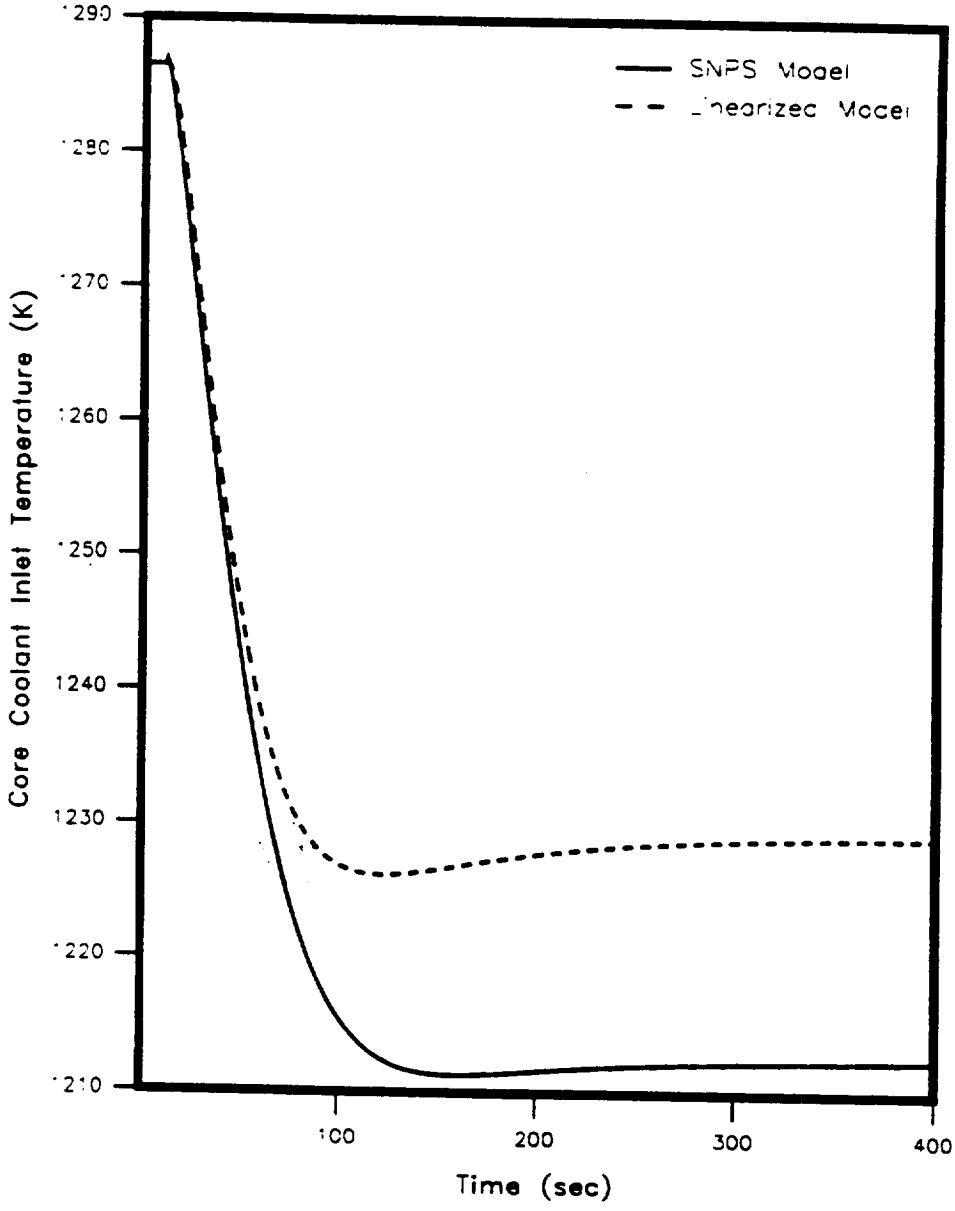

Figure 21. Core Coolant Inlet Temperature Responses for a Step Change in External Reactivity Corresponding to a Load Change from 100% to 80% of Full Power.

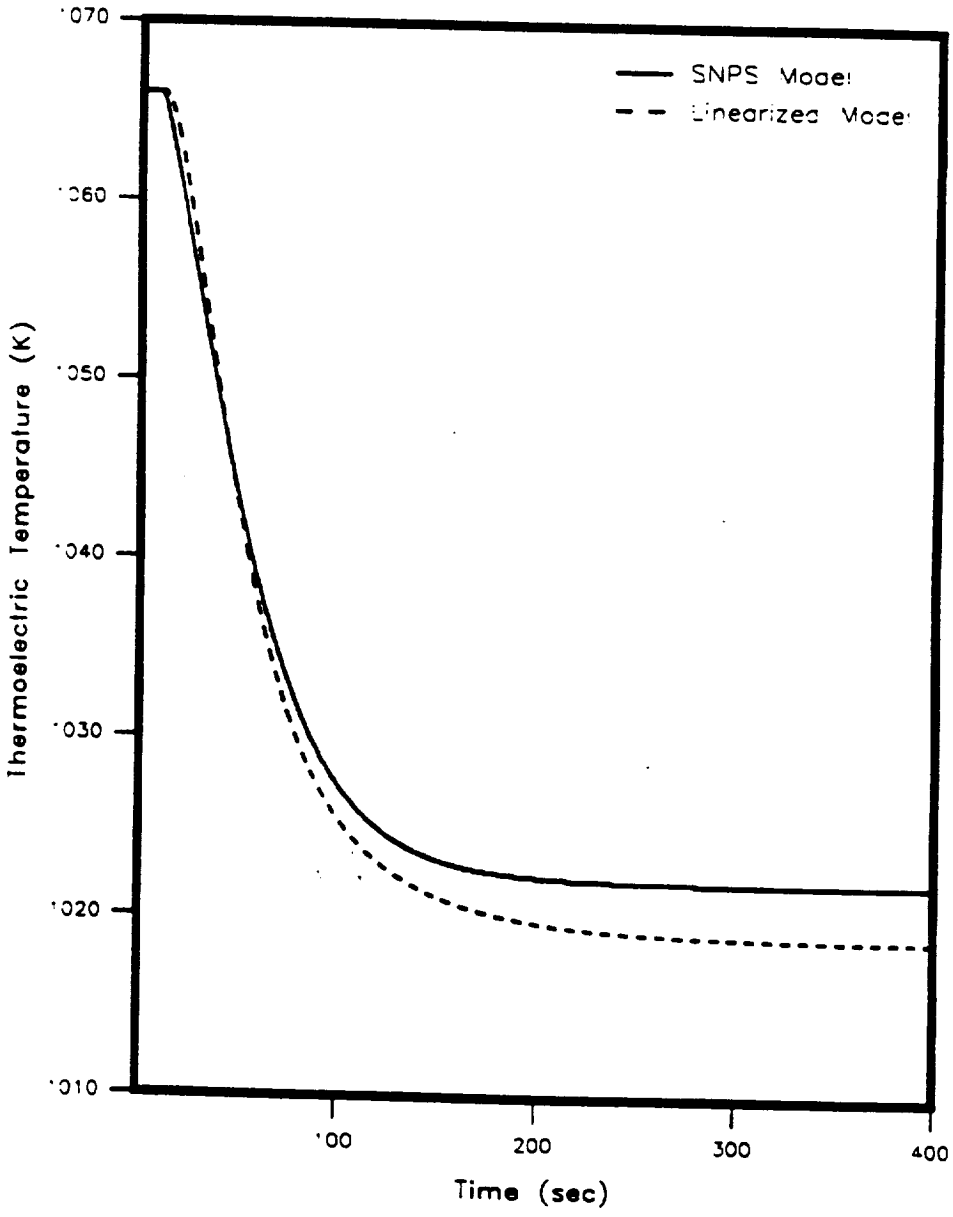

Figure 22. Thermoelectric Temperature Responses for a Step Change in External Reactivity Corresponding to a Load Change from 100% to 80% of Full Power.

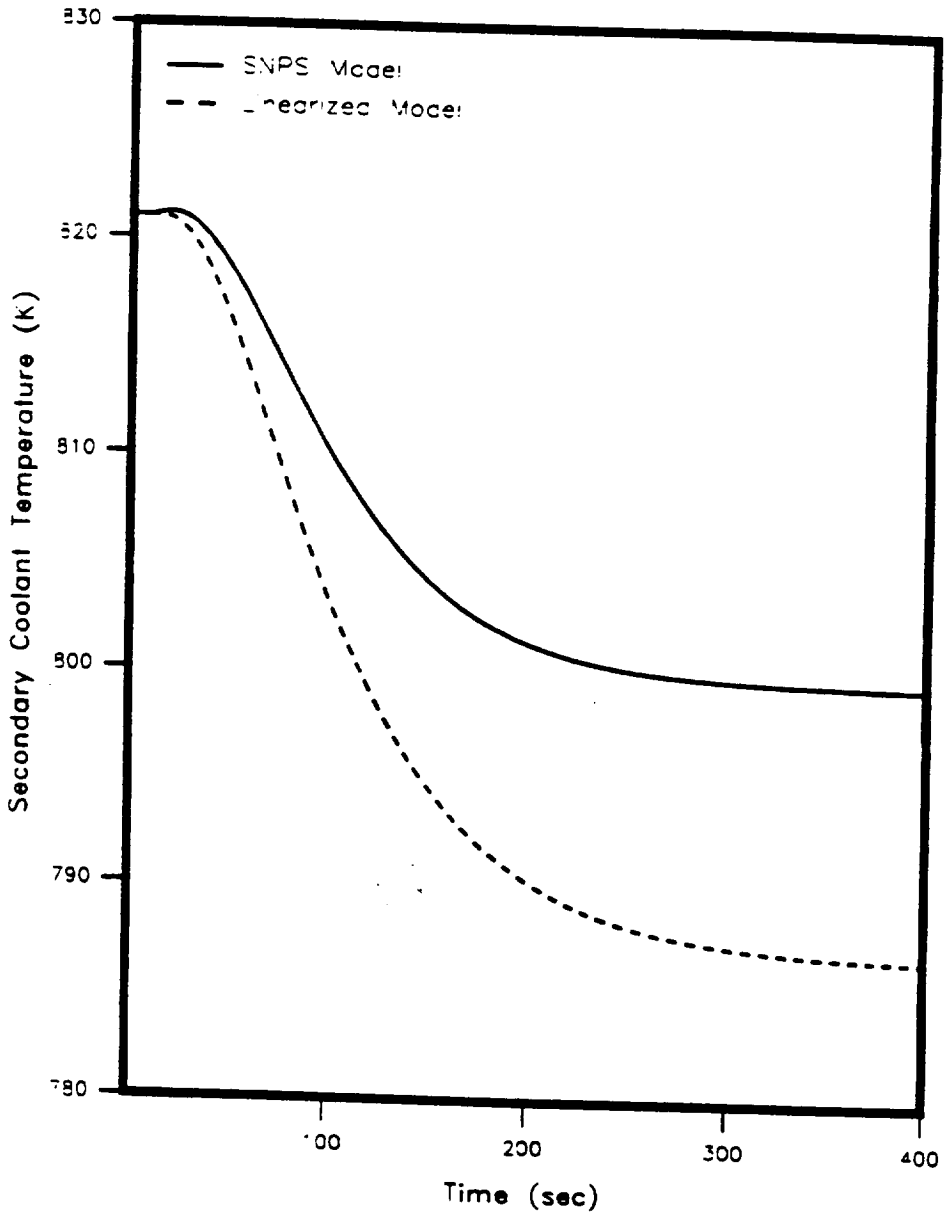

Figure 23. Secondary Coolant Temperature Responses for a Step Change in External Reactivity Corresponding to a Load Change from 100% to 80% of Full Power.

the output and state responses of the linearized reference model match the integrated nonlinear SNPS model responses quite closely.

III.6 Scheduling of Linearized Reference Models

Scheduling refers to the fitting of the linearized reference models to a variable which is indicative of the system changing operating conditions. In this case, the variable chosen is the electrical power (P_e) generated by the system. The scheduled plant dynamics can be represented as:

$$\delta\dot{\mathbf{x}}(t) = \mathbf{A}(P_e)\,\delta\mathbf{x}(t) + \mathbf{B}(P_e)\,\delta u(t) + \mathbf{L}(P_e)\,\delta w(t), \tag{33}$$

$$\delta y(t) = \mathbf{C}(P_e)\,\delta\mathbf{x}(t) + \mathbf{D}(P_e)\,\delta u(t) + \mathbf{F}(P_e)\,\delta w(t), \tag{34}$$

where $\delta y(t)$, $\delta\mathbf{x}(t)$, $\delta u(t)$, $\delta w(t)$ are the output, states, input and disturbance vectors of the scheduled reference model, respectively. **A**, **B**, **F**, **C**, **D**, and **L** are the scheduled model system matrices with elements that are functions of P_e. It is anticipated that the scheduled model reference will be more accurate than any single linearized reference model in the entire operating range of the SNPS.

III.7 Evaluation of the Scheduled Reference Model

Figures 26 through 33 show the responses of the load voltage and of the states of the 80% linearized reference model, the scheduled reference model and the integrated nonlinear SNPS model to an external step reactivity insertion of -9.51, cents which corresponds to a load level change from 100% to 80% of full power. Similarly, Figures 34 through 41 compare the responses of the load voltage and the states of

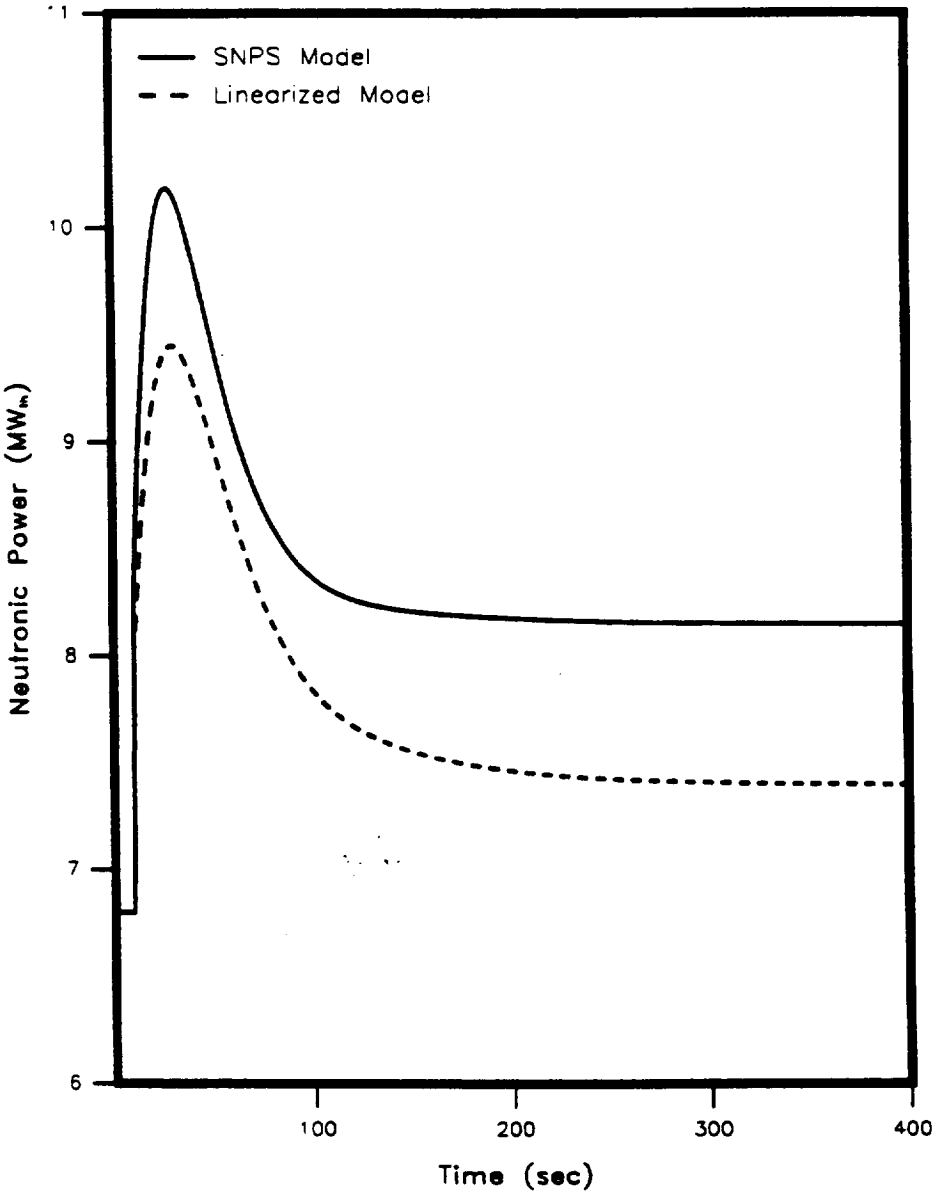

Figure 24. Neutronic Power Responses for a Step Change in External Reactivity Corresponding to a Load Change from 100% to 135% of Full Power.

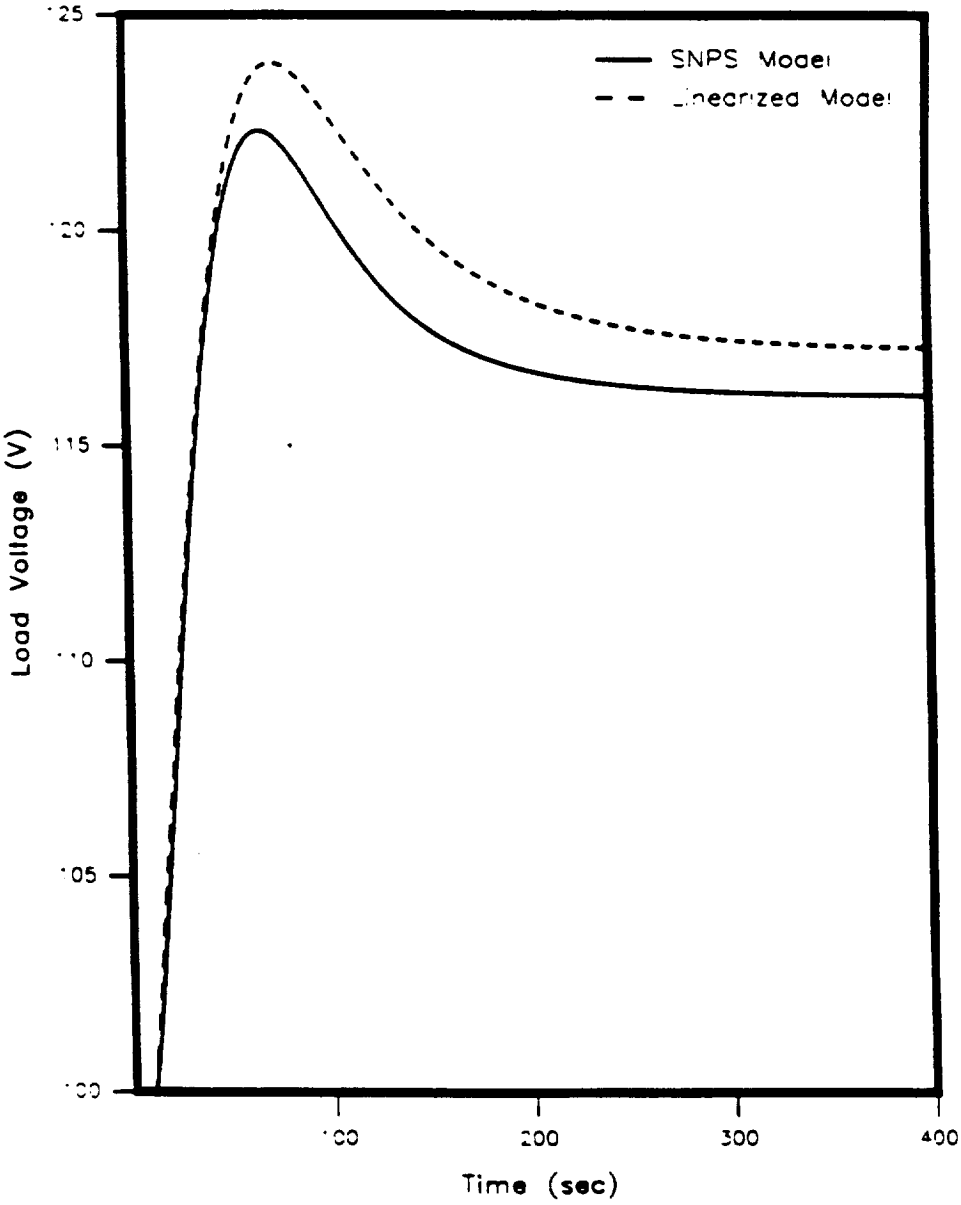

Figure 25. Load Voltage Responses for a Step Change in External Reactivity Corresponding to a Load Change from 100% to 135% of Full Power.

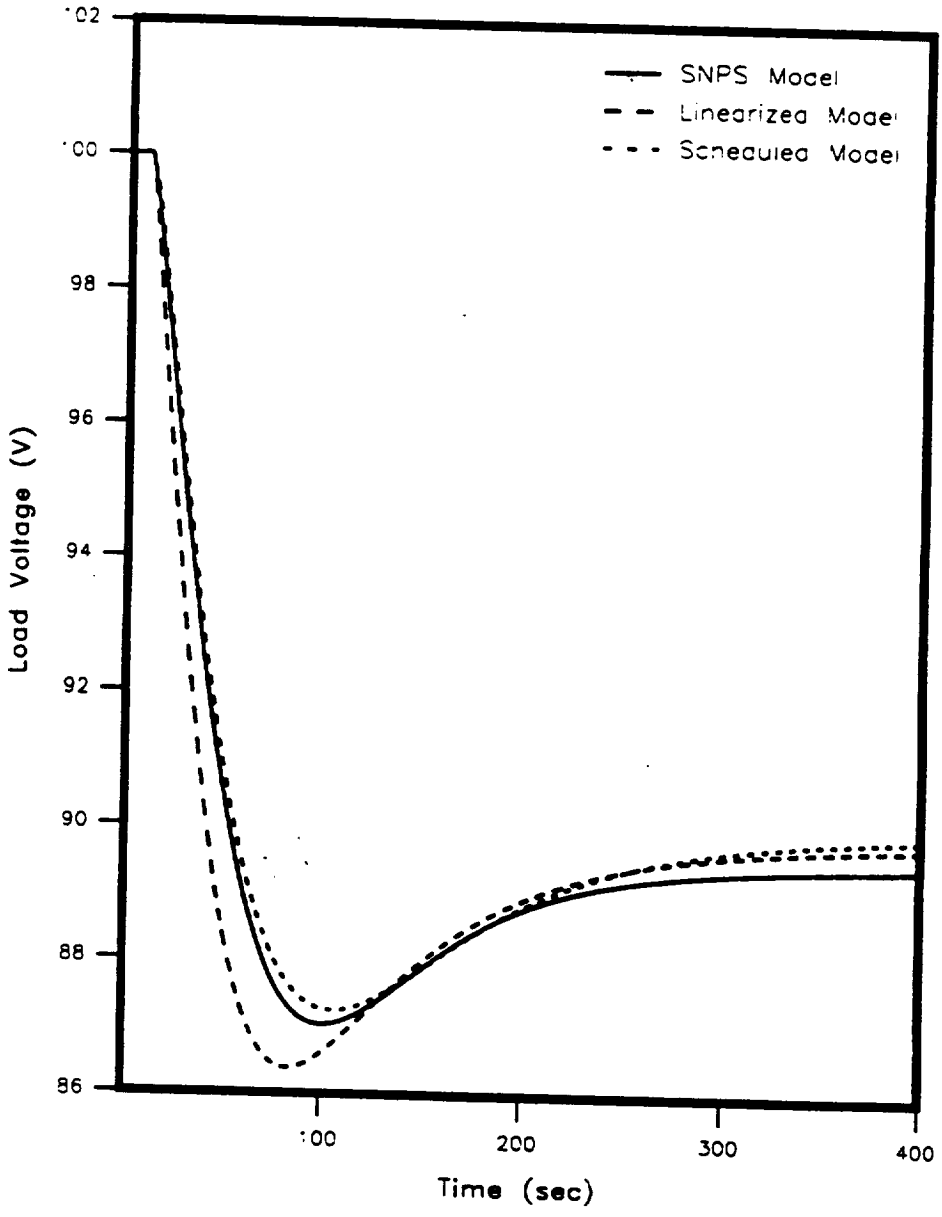

Figure 26. Load Voltage Responses for a Step Change in External Reactivity Corresponding to a Load Change from 100% to 80% of Full Power.

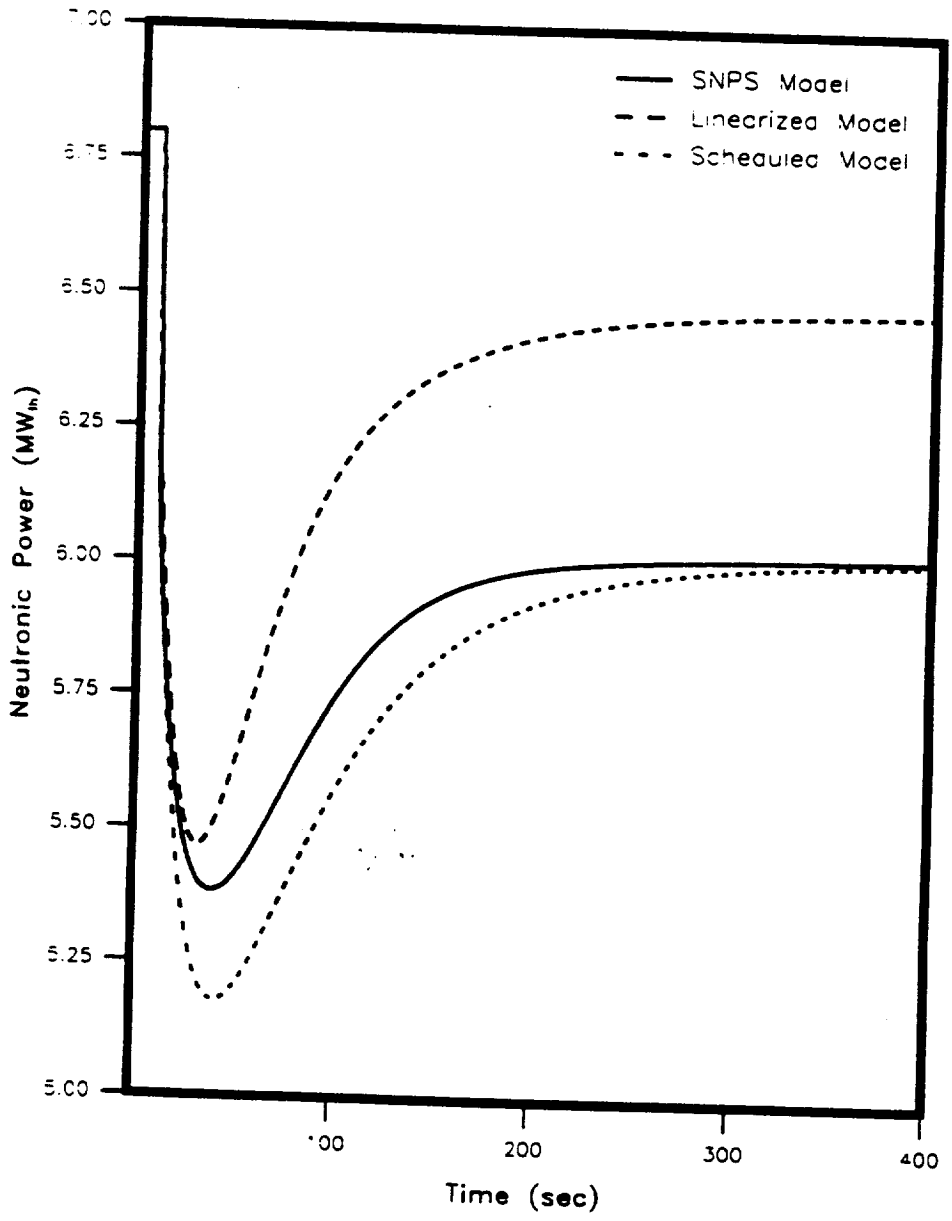

Figure 27. Neutronic Power Responses for a Step Change in External Reactivity Corresponding to a Load Change from 100% to 80% of Full Power.

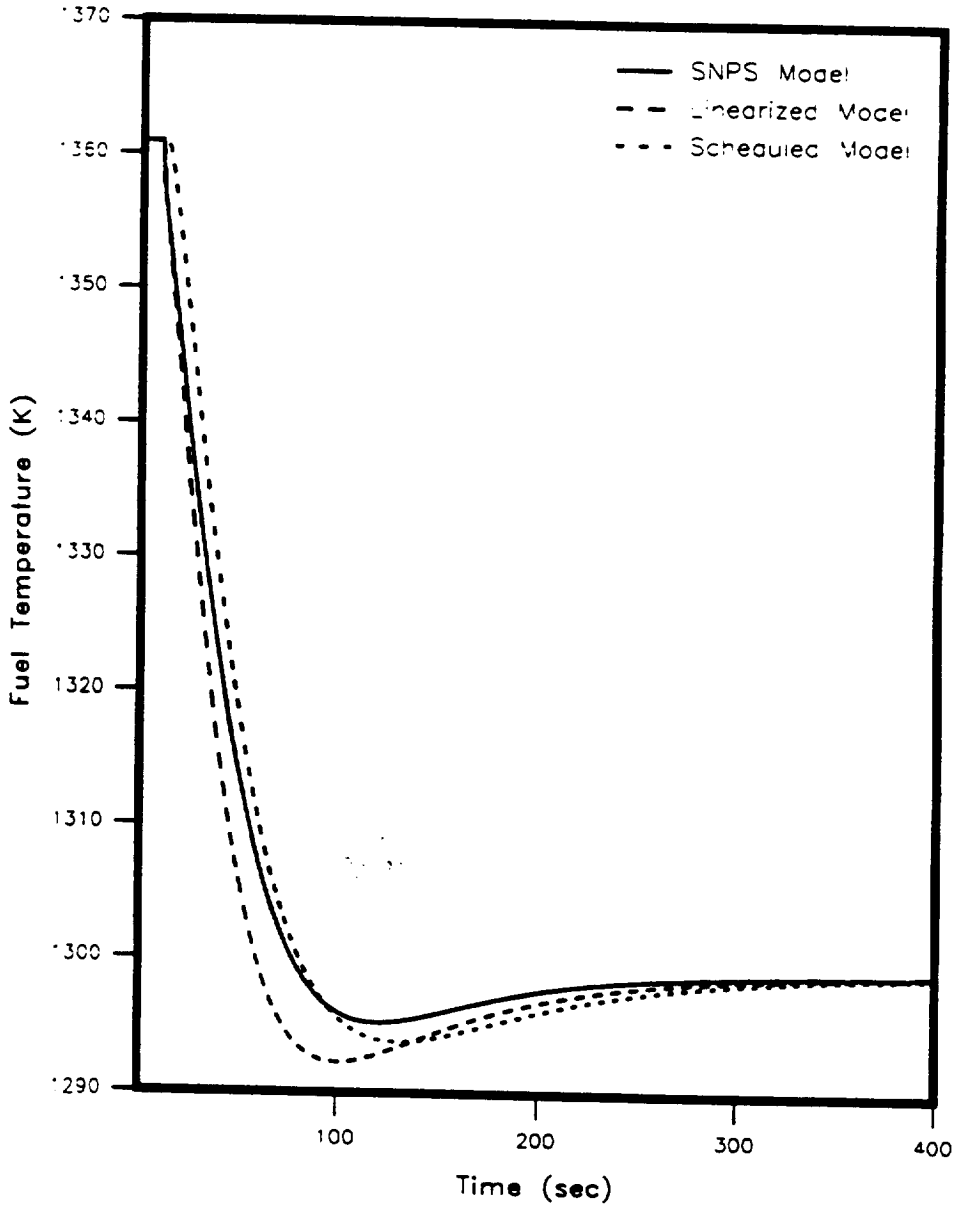

Figure 28. Fuel Temperature Responses for a Step Change in External Reactivity Corresponding to a Load Change from 100% to 80% of Full Power.

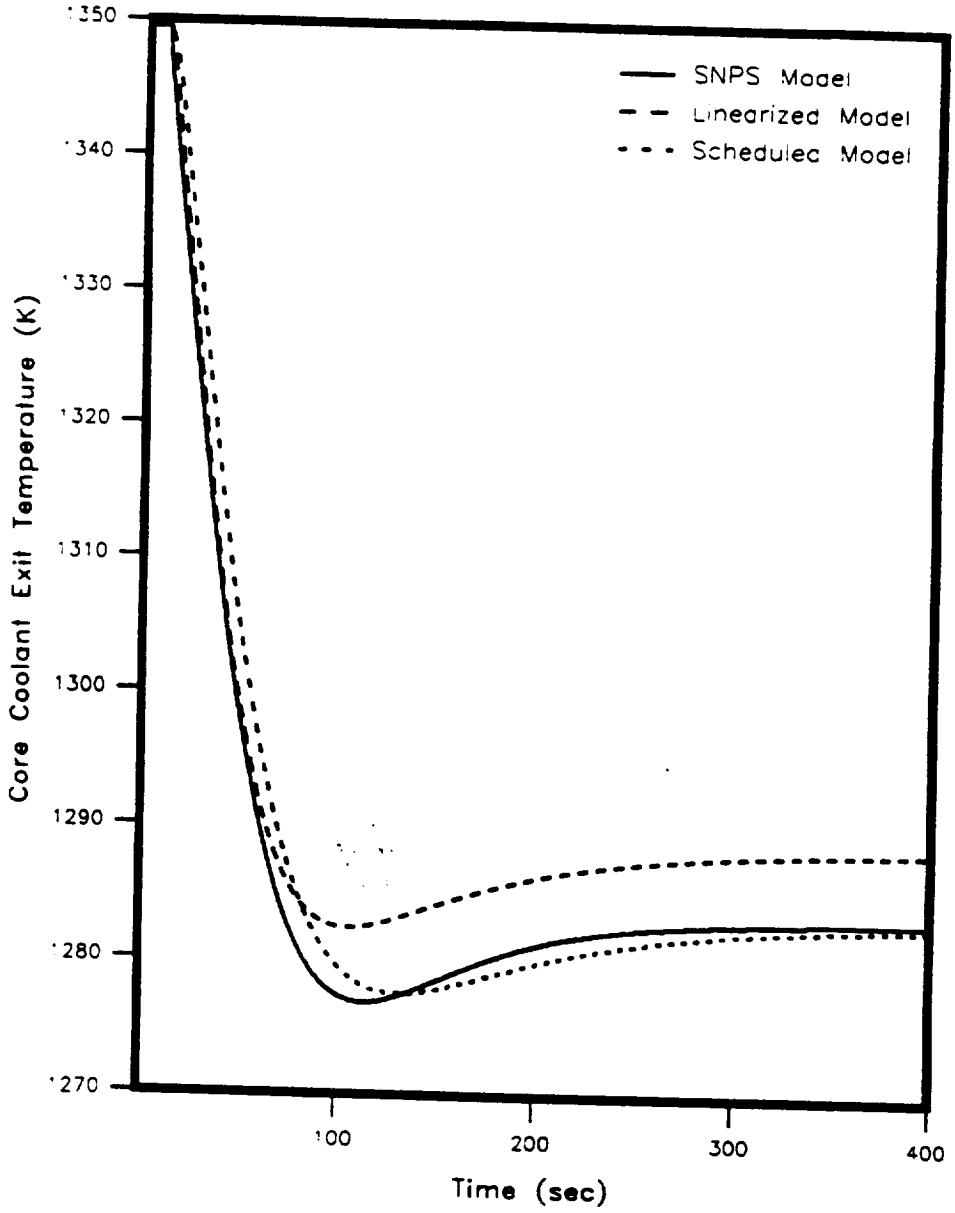

Figure 29. Core Coolant Exit Temperature Responses for a Step Change in External Reactivity Corresponding to a Load Change from 100% to 80% of Full Power.

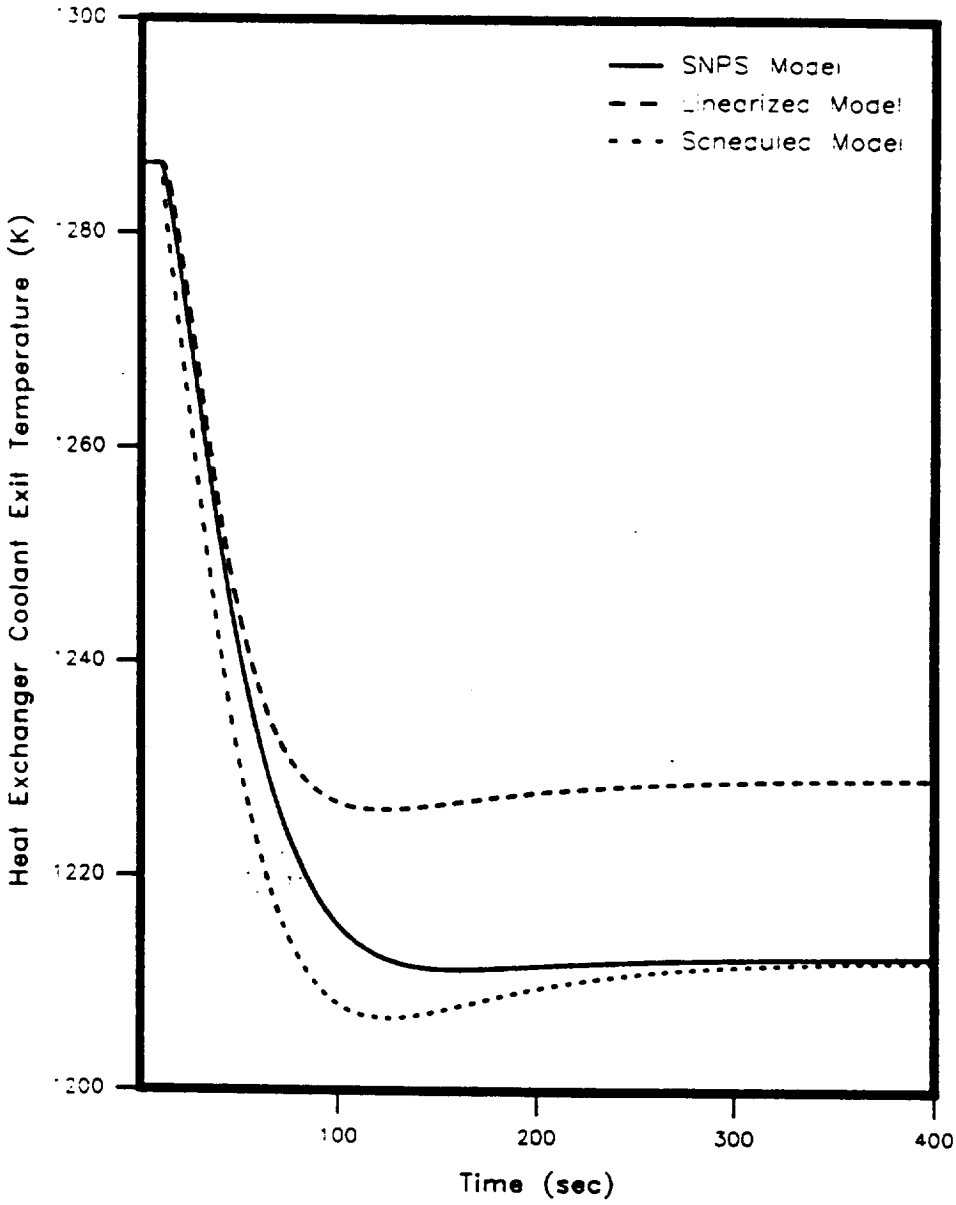

Figure 30. Heat Exchanger Coolant Exit Temperature Responses for a Step Change in External Reactivity Corresponding to a Load Change from 100% to 80% of Full Power.

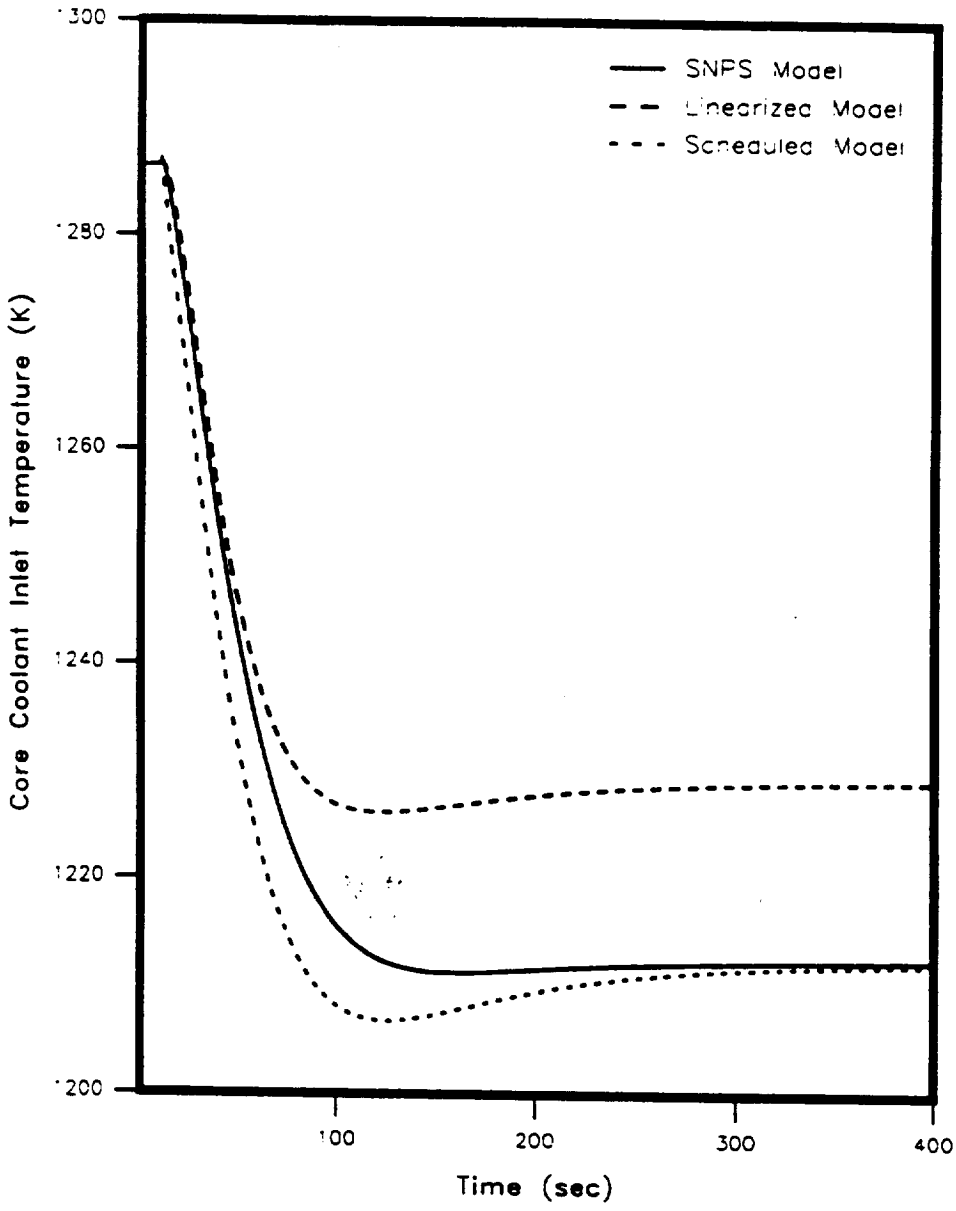

Figure 31. Core Coolant Inlet Temperature Responses for a Step Change in External Reactivity Corresponding to a Load Change from 100% to 80% of Full Power.

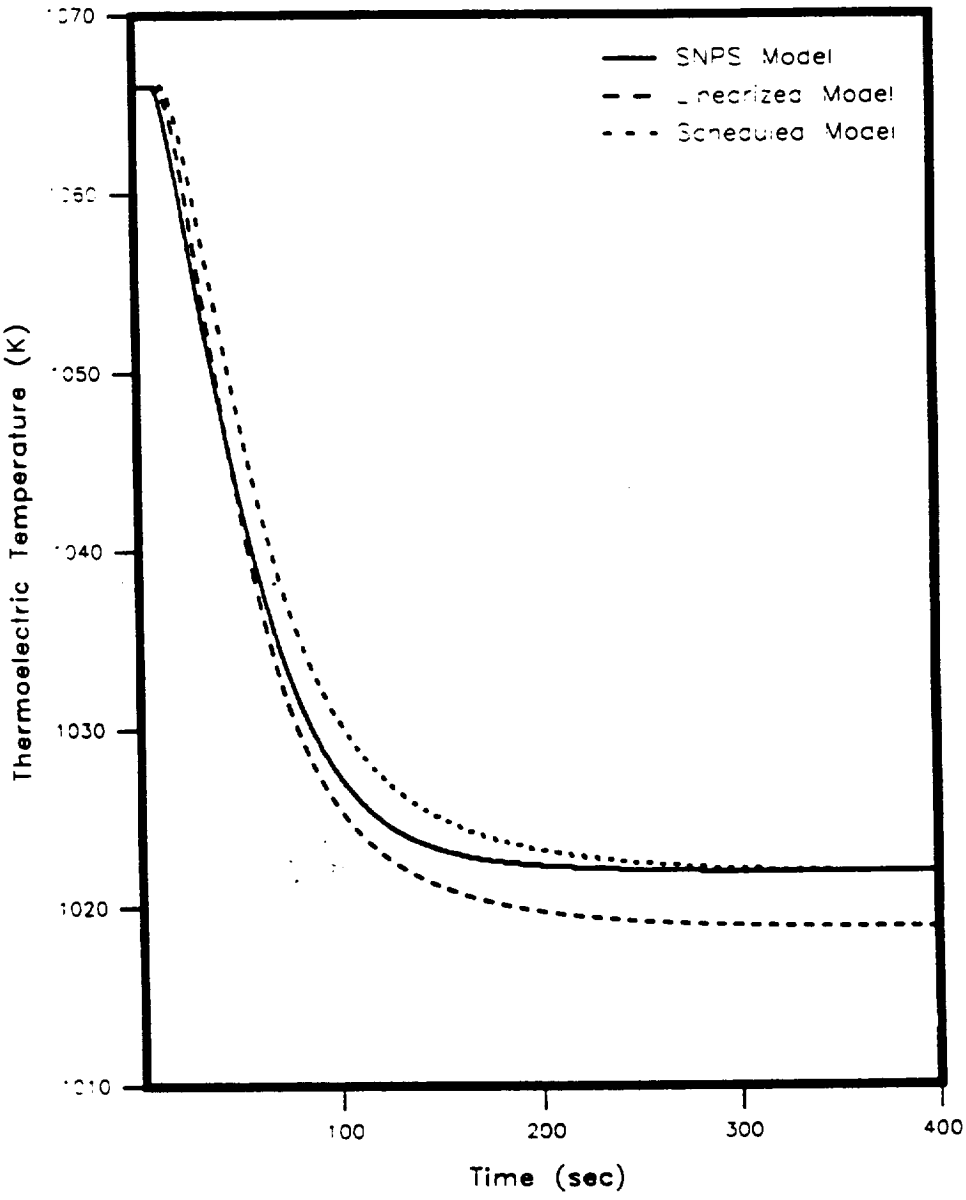

Figure 32. Thermoelectric Temperature Responses for a Step Change in External Reactivity Corresponding to a Load Change from 100% to 80% of Full Power.

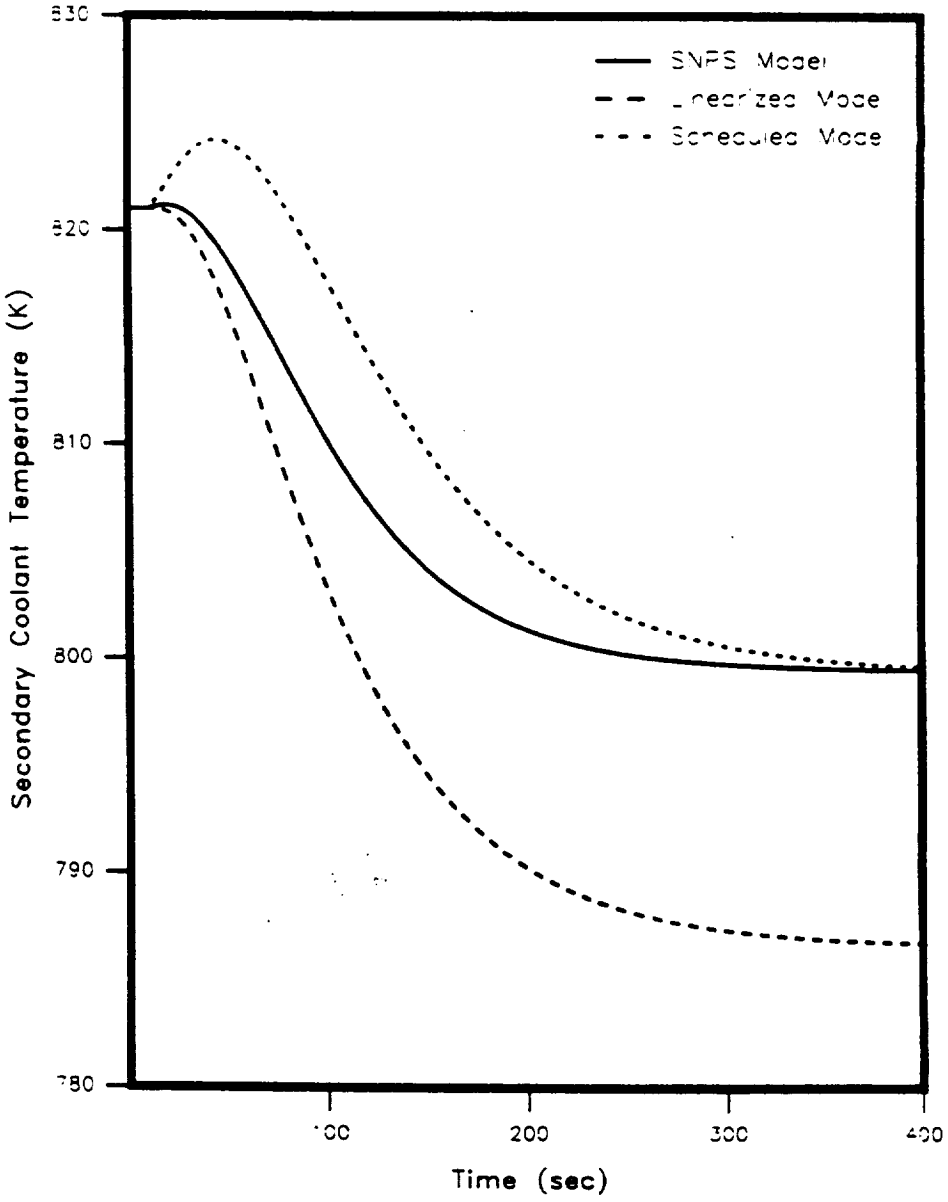

Figure 33. Secondary Coolant Temperature Responses for a Step Change in External Reactivity Corresponding to a Load Change from 100% to 80% of Full Power.

the 150% of full power linearized reference model, the scheduled reference model and the integrated nonlinear SNPS model to +23.73 cents of reactivity insertion, which corresponds to a load level change from 100% to 150% of full power.

The response of the secondary coolant temperature of the linearized reference model shows variations from that of the scheduled reference model; the scheduled reference model improves the steady state behaviour of this state in the expense of causing a non-minimum phase behaviour in the transient response of the state, even though the integrated nonlinear SNPS model is minimum phase. The deviation of the secondary coolant temperature response of the scheduled reference model from the integrated nonlinear SNPS model response has been determined to be less than 0.01%, therefore this non-minimum phase behaviour can be attributed to modeling error. By examining the aforementioned figures, it is observed that the scheduled reference model matches the integrated nonlinear SNPS model states better than a linearized reference model.

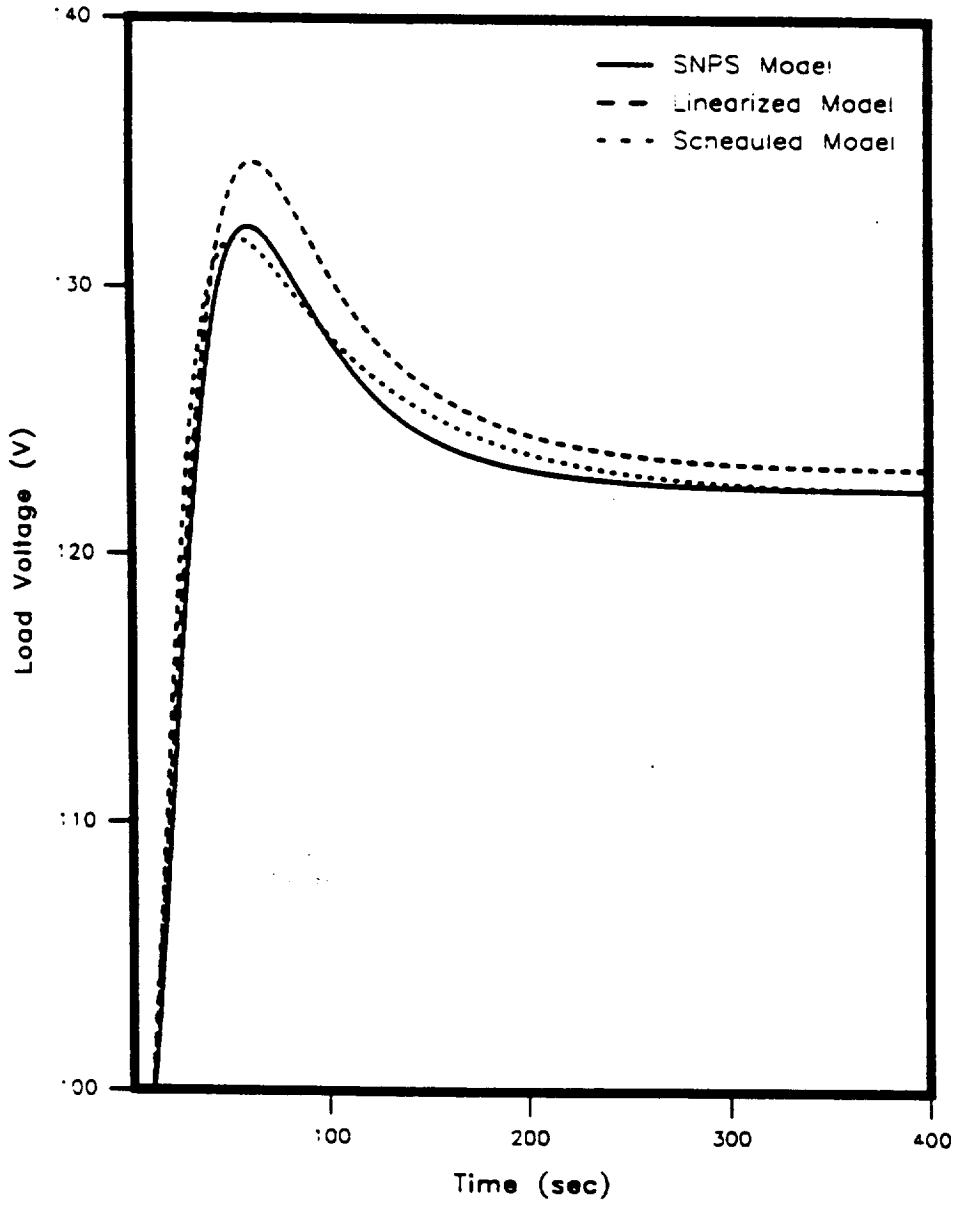

Figure 34. Load Voltage Responses for a Step Change in External Reactivity Corresponding to a Load Change from 100% to 150% of Full Power.

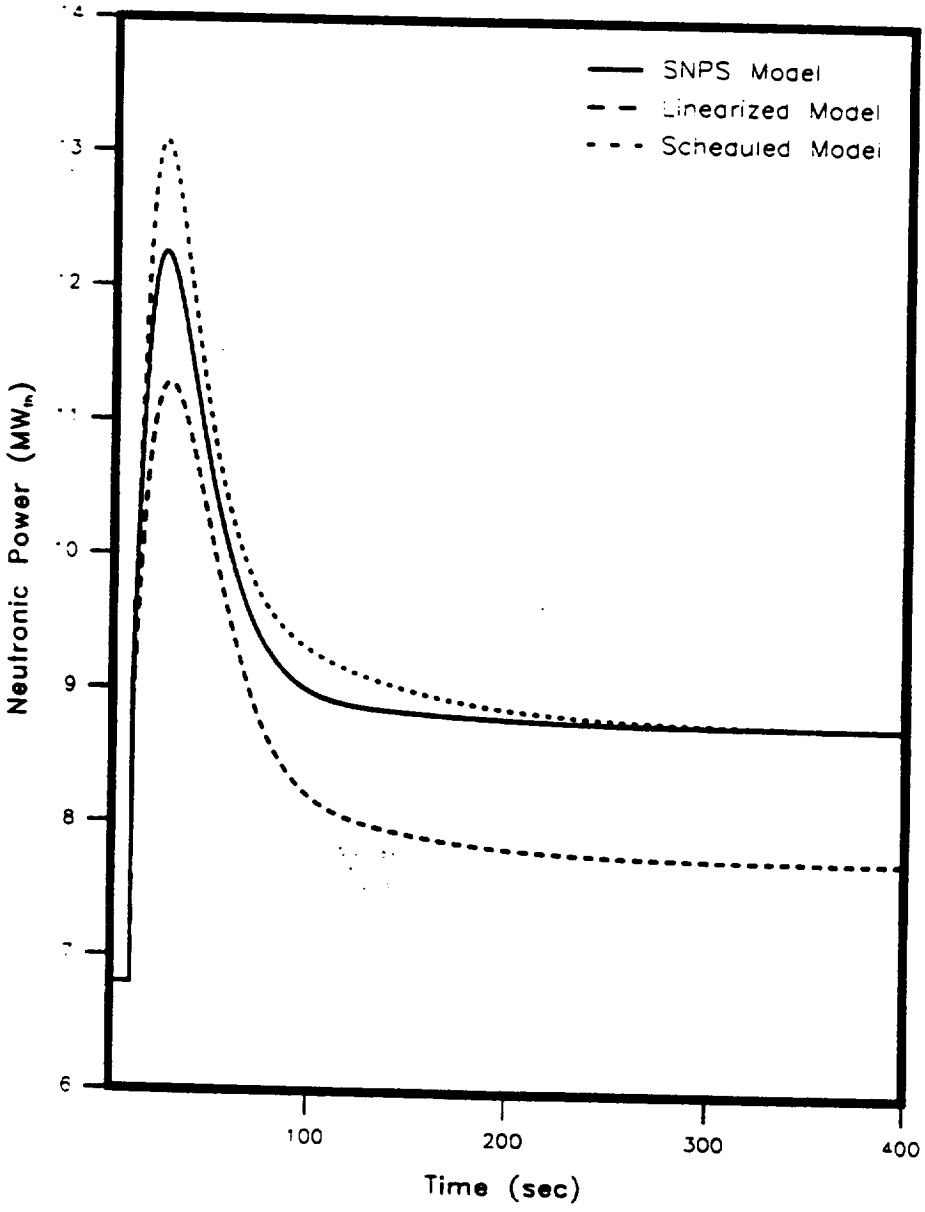

Figure 35. Neutronic Power Responses for a Step Change in Negative Reactivity Corresponding to a Load Change from 100% to 150% of Full Power.

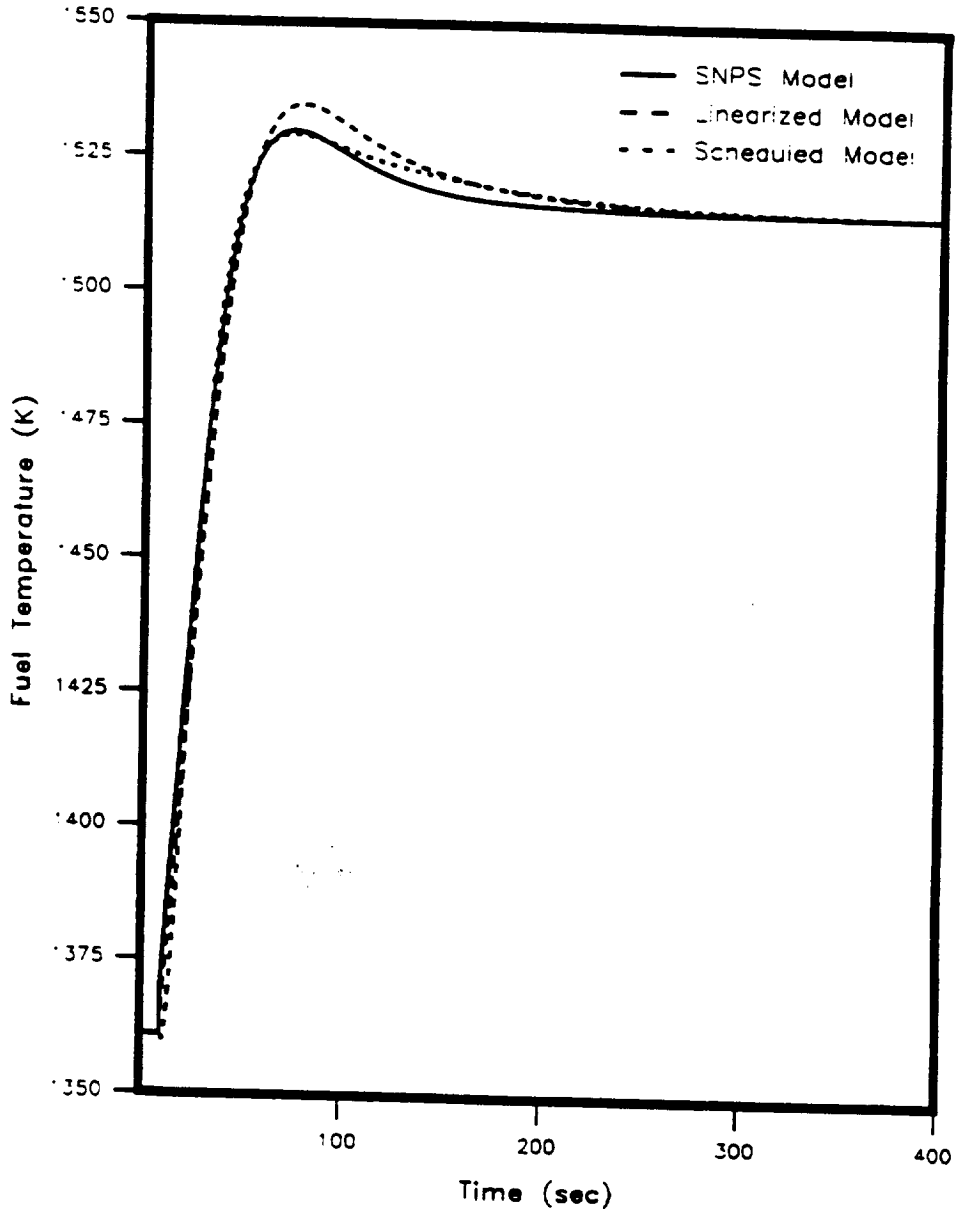

Figure 36. Fuel Temperature Responses for a Step Change in External Reactivity Corresponding to a Load Change from 100% to 150% of Full Power.

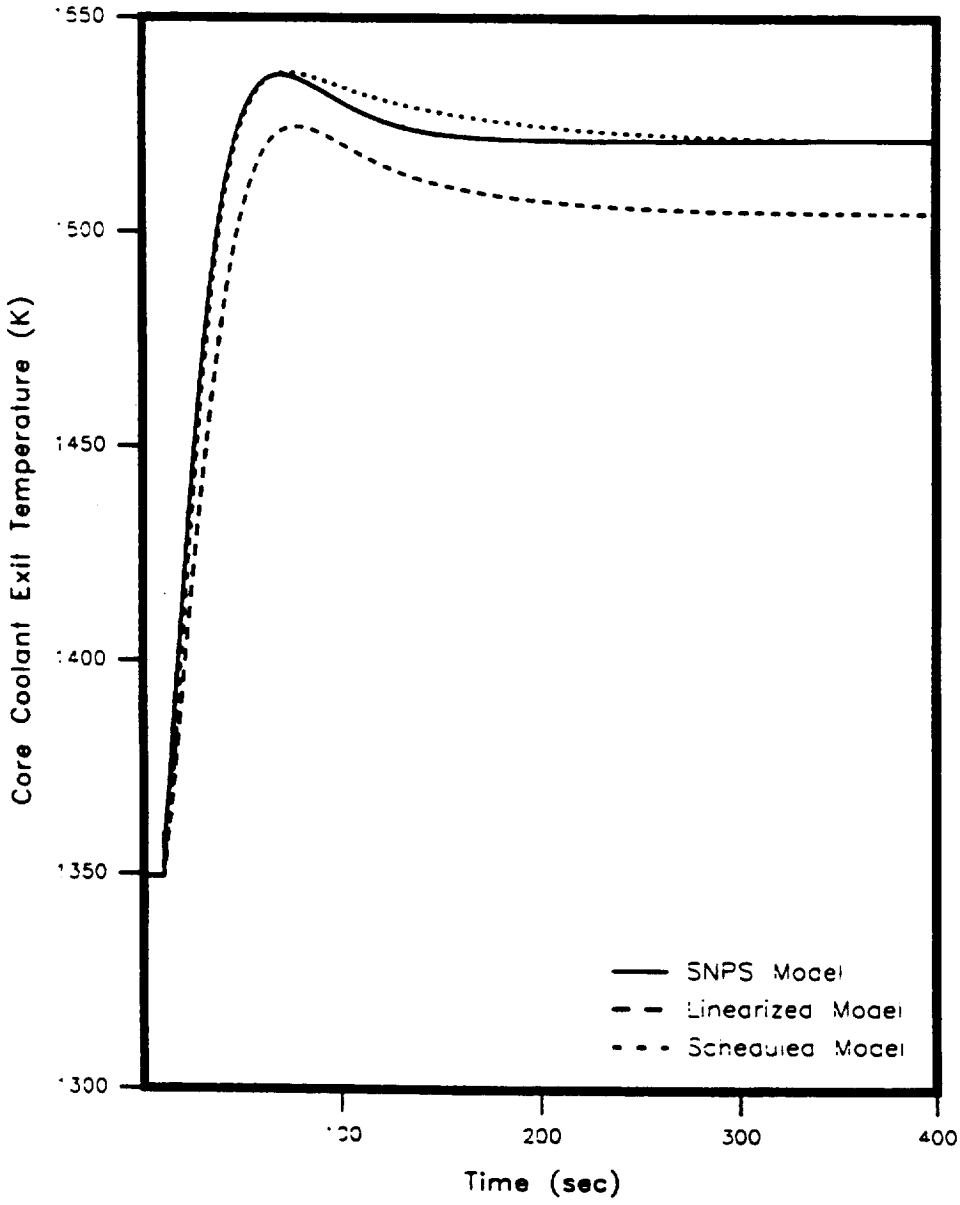

Figure 37. Core Coolant Exit Temperature Responses for a Step Change in External Reactivity Corresponding to a Load Change from 100% to 150% of Full Power.

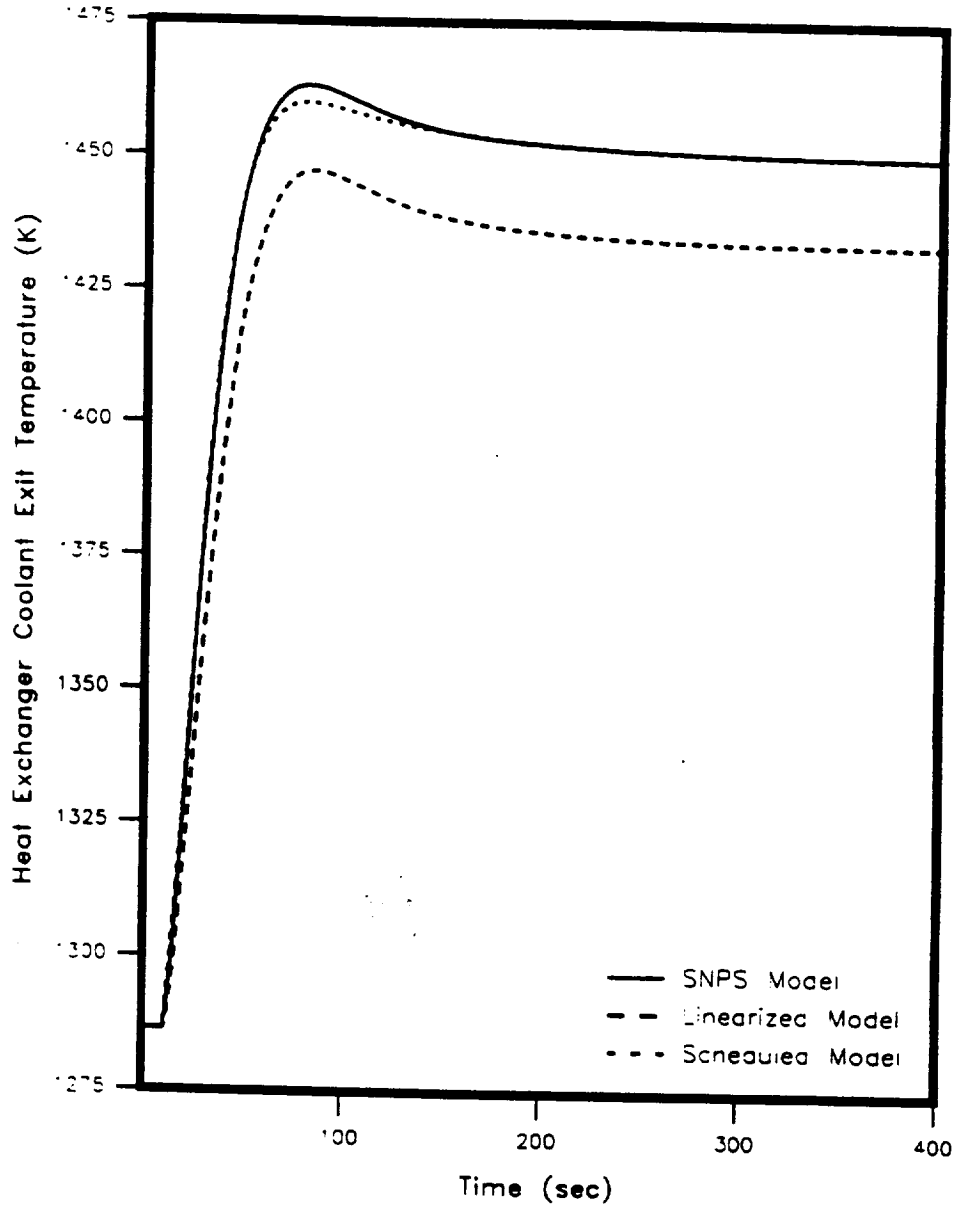

Figure 38. Heat Exchanger Coolant Exit Temperature Responses for a Step Change in External Reactivity Corresponding to a Load Change from 100% to 150% of Full Power.

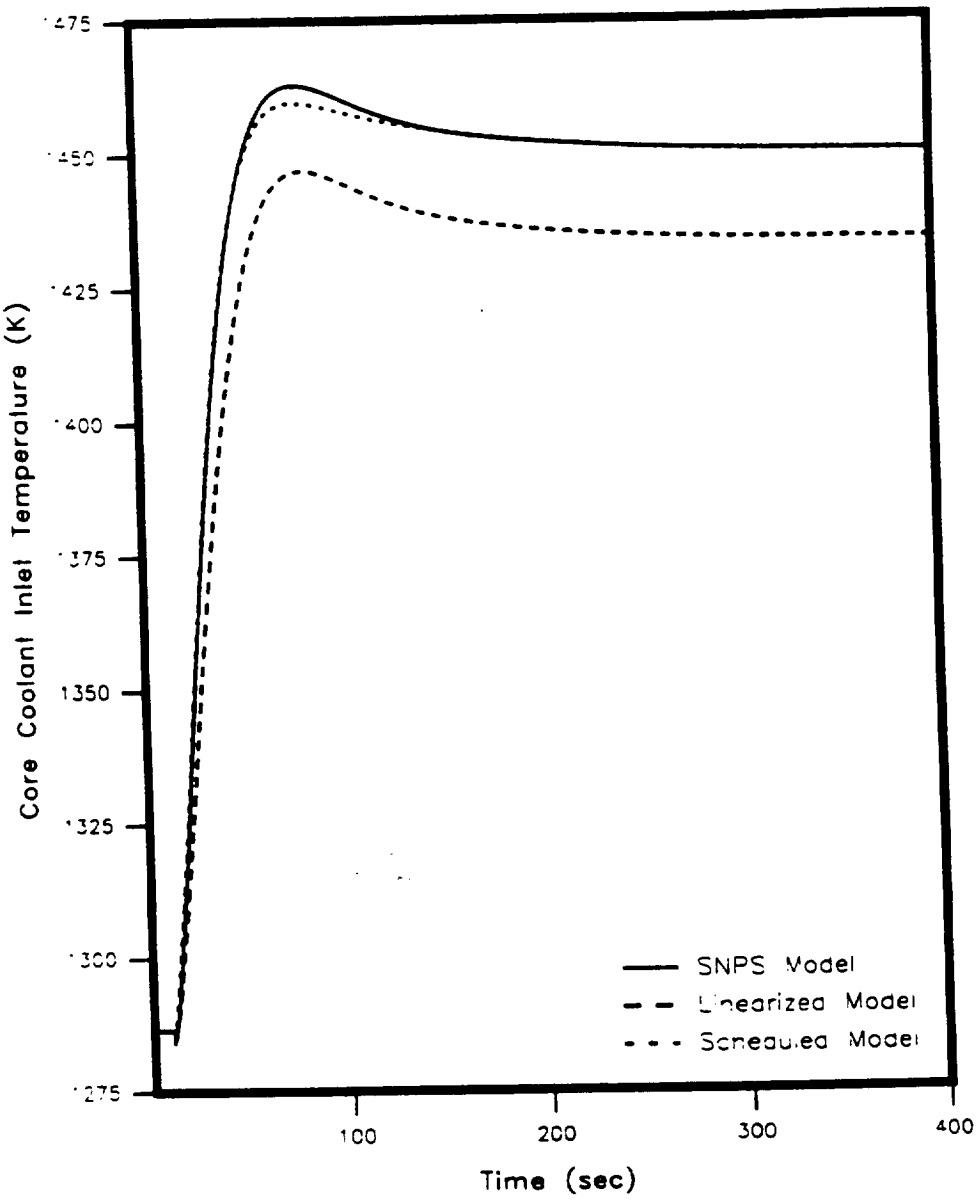

Figure 39. Core Coolant Inlet Temperature Responses for a Step Change in External Reactivity Corresponding to a Load Change from 100% to 150% of Full Power.

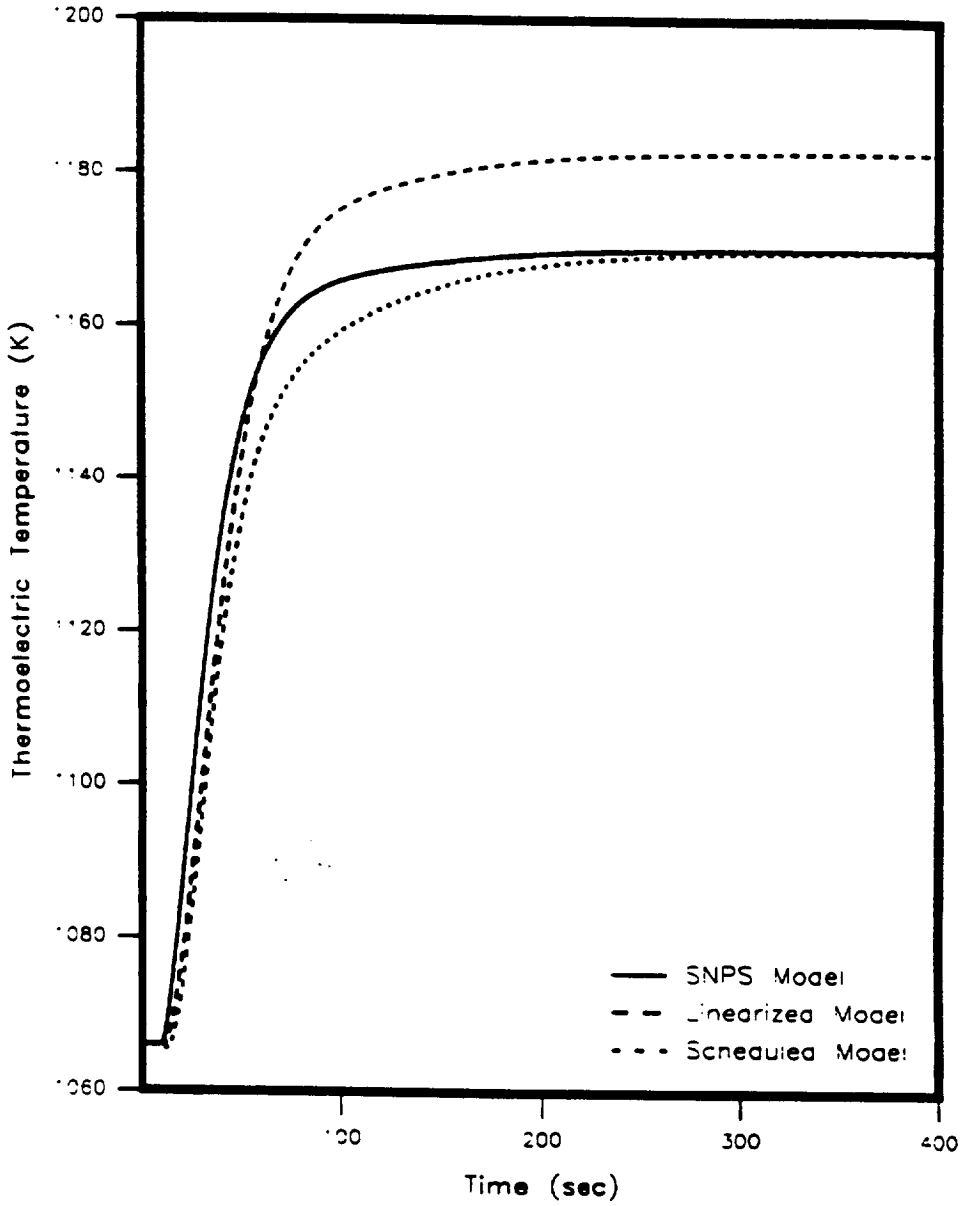

Figure 40. Thermoelectric Temperature Responses for a Step Change in External Reactivity Corresponding to a Load Change from 100% to 150% of Full Power.

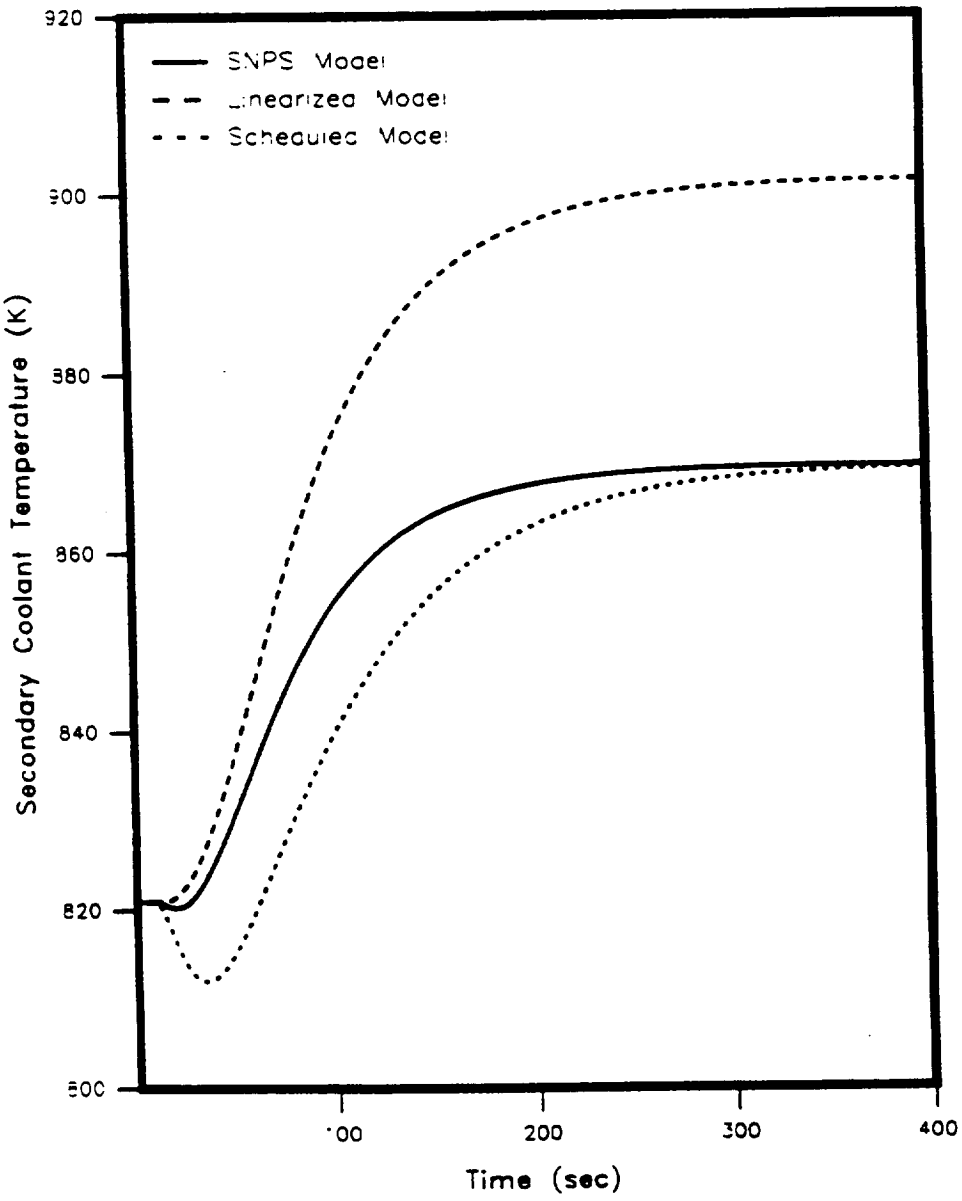

Figure 41. Secondary Coolant Temperature Responses for a Step Change in External Reactivity Corresponding to a Load Change from 100% to 150% of Full Power.

CHAPTER IV

LINEAR CONTROL SYSTEM DESIGN AND ANALYSIS TOOLS

IV.1 Introduction

The linearized reference models of the SNPS were found to be open-loop stable, yet load voltage responses of the linearized referencemodels have very short rise times. Thus, it is desired to design a compensator that :

1.) Slows down the load voltage response of the system, allowing more time for the insertion or removal of reactivity by the control drums.

2.) Achieves desirable performance such as command-following, disturbance rejection, sensor/actuator noise insensitivity at high frequencies, and,

3.) Exhibits stability robustness to system parameter variations, unmodeled dynamics, etc. .

In this chapter, some of the mathematical preliminaries, such as the definition and some properties of singular values, are discussed. Also, some loop shaping concepts are described in relation to the singular values of system transfer function matrices. The multivariable linear control system design method, LQG/LTR, is described based on a Model-Based Compensator (MBC) structure. Some of the command following, disturbance rejection and robustness properties of the LQG/LTR compensators are also presented.

At this stage it is pertinent to remark that even though the LQG/LTR technique is for MIMO systems, it is used to design Single Input-Single Output (SISO) compensators for voltage regulation of the SNPS system, primarily for the following reasons:

1.) There are several desirable *guaranteed* properties of the LQG/LTR compensators, such as gain and phase margins, and stability robustness, and,

2.) The design of an LQG/LTR compensator is done in a *systematic* manner, allowing the designer to address issues such as system bandwidth and other frequency domain specifications in a more direct manner than what is possible using conventional SISO control design methods, while performing the design using time-domain tools.

IV.2 Mathematical Preliminaries

Some of the key results and design considerations of the LQG/LTR technique are stated in terms of *singular values* of the various system matrices. The singular values of a complex $n \times m$ matrix $\mathbf{A}$, denoted as $\sigma_i(\mathbf{A})$, are the k largest nonnegative square roots of the eigenvalues of $(\mathbf{A^H A})$, where k = $\min(n, m)$. That is :

$$\sigma_i(\mathbf{A}) = \sqrt{\lambda_i(\mathbf{A^H A})}, \quad i = 1, 2, \ldots, k, \tag{35}$$

where $\mathbf{A^H}$ is the complex conjugate transpose of $\mathbf{A}$. One representation of the matrix $\mathbf{A}$, known as the singular value decomposition (SVD), is given by:

$$\mathbf{A} = \mathbf{U \Sigma V^H} = \sum_{i=1}^{n} \sigma_i(\mathbf{A})\, u_i\, v_i^H, \tag{36}$$

where,

$$\mathbf{U} \triangleq \begin{pmatrix} \vdots & \vdots & & \vdots \\ u_1 & u_2 & \dots & u_n \\ \vdots & \vdots & & \vdots \end{pmatrix}; \quad \mathbf{U^H U} = \mathbf{I}, \tag{37}$$

$$\mathbf{V} \triangleq \begin{pmatrix} \vdots & \vdots & & \vdots \\ v_1 & v_2 & \dots & v_n \\ \vdots & \vdots & & \vdots \end{pmatrix}; \quad \mathbf{V^H V} = \mathbf{I}, \tag{38}$$

$$\Sigma = \text{diag}\,[\sigma_1, \sigma_2, \dots, \sigma_n], \tag{39}$$

where the columns of the matrices $\mathbf{V}$ and $\mathbf{U}$ are the eigenvectors of $\mathbf{A^H A}$ and $\mathbf{A A^H}$, respectively. The maximum and minimum singular values may also be defined in terms of the matrix spectral norm $\|\cdot\|$ of the matrix, as follows [17] :

$$\sigma_{max} = \max_{\mathbf{x}\neq 0} \frac{\|\mathbf{A x}\|_2}{\|\mathbf{x}\|_2} = \|\mathbf{A}\|_2, \tag{40}$$

and

$$\sigma_{min} = \min_{\mathbf{x}\neq 0} \frac{\|\mathbf{A x}\|_2}{\|\mathbf{x}\|_2} = \left\|\mathbf{A}^{-1}\right\|_2, \tag{41}$$

Also, it is true that

$$\sigma_{min} = \begin{cases} \left\|\mathbf{A}^{-1}\right\|_2^{-1}, & \text{if } \det \mathbf{A} \neq 0 \\ 0, & \text{if } \det \mathbf{A} = 0. \end{cases} \tag{42}$$

A useful property of singular values is the following inequality:

$$\sigma_{min}(\mathbf{A}) > \sigma_{max}(\mathbf{B}) \Longrightarrow \mathbf{A^H A} > \mathbf{B^H B}. \tag{43}$$

Additionally, the triangle inequality holds good for the maximum singular value. That is,

$$\sigma_{max}(\mathbf{A} + \mathbf{B}) \leq \sigma_{max}(\mathbf{A}) + \sigma_{max}(\mathbf{B}). \tag{44}$$

Also, if the inverse of the matrix **A** exists, then from Equations (40) and (42) the following is obtained:

$$\sigma_{min}(\mathbf{A}) = \frac{1}{\sigma_{max}(\mathbf{A}^{-1})}. \tag{45}$$

IV.3 Loop Shaping Concepts

Generally speaking, loop shaping refers to the design of control systems by influencing the feedback characteristics to correspond to a specific form which is known to result in systems with desired properties, such as closed loop stability, command following, disturbance rejection, and insensitivity to sensor and/or actuator noise. In the framework of SISO systems, the quantification of the characteristics of the Transfer Function Matrices (TFMs) such that the resulting closed-loop system has desired properties is fairly straightforward [18],[19]. The block diagram of a general MIMO system is shown in Figure 42. From Figure 42 it can be concluded that the closed-loop system output is given by the following expression :

$$\begin{aligned}\mathbf{y}(s) &= [\mathbf{I} + \mathbf{G}(s)\,\mathbf{K}(s)]^{-1}\,\mathbf{G}(s)\,\mathbf{K}(s)\,\mathbf{r}(s) + [\mathbf{I} + \mathbf{G}(s)\,\mathbf{K}(s)]^{-1}\,\mathbf{d_o}(s) \\ &+ [\mathbf{I} + \mathbf{G}(s)\,\mathbf{K}(s)]^{-1}\,\mathbf{G}(s)\,\mathbf{d_i}(s) - [\mathbf{I} + \mathbf{G}(s)\,\mathbf{K}(s)]^{-1}\,\mathbf{G}(s)\,\mathbf{K}(s)\,\mathbf{n}(s),\end{aligned} \tag{46}$$

where,

$\mathbf{r}(s)$: the reference input vector ($m \times 1$),

$\mathbf{d}_i(s)$: the input disturbance vector ($m \times 1$),

$\mathbf{d}_o(s)$: the output disturbance vector ($m \times 1$),

$\mathbf{y}(s)$: the output vector ($m \times 1$),

The general design requirements for a MIMO feedback loop are: a) Closed-loop stability, b) Good command following, c) Good disturbance rejection, d) Sensitivity reduction to unmodeled dynamics and e) Sensor noise insensitivity. These design requirements can be related to the system TFMs as follows:

1). Command Following

Command following is the ability of the system output $\mathbf{y}(t)$ to follow the reference input $\mathbf{r}(t)$ closely. In order to achieve good command following it is required that:

$$\mathbf{y}(s) \simeq \mathbf{r}(s) \quad \text{for all } s \in \Omega_r, \tag{47}$$

where Ω_r is the frequency range of expected references. From Equation (46), the following condition for good command following is obtained :

$$[\mathbf{I} + \mathbf{G}(s)\mathbf{K}(s)]^{-1}\, \mathbf{G}(s)\mathbf{K}(s) \simeq \mathbf{I}, \quad s \in \Omega_r, \tag{48}$$

which can be accomplished if the return difference TFM has the following property:

$$[\mathbf{I} + \mathbf{G}(s)\mathbf{K}(s)] \text{ is "large" for } s \in \Omega_r, \tag{49}$$

which implies that the forward loop TFM

$$\mathbf{G}(s)\mathbf{K}(s) \text{ is "large" for } s \in \Omega_r. \tag{50}$$

Thus, for good command following, the transfer function matrix $\mathbf{G}(s)\mathbf{K}(s)$ must be "large" for the expected range of reference input signal frequencies, provided that the closed-loop system is stable.

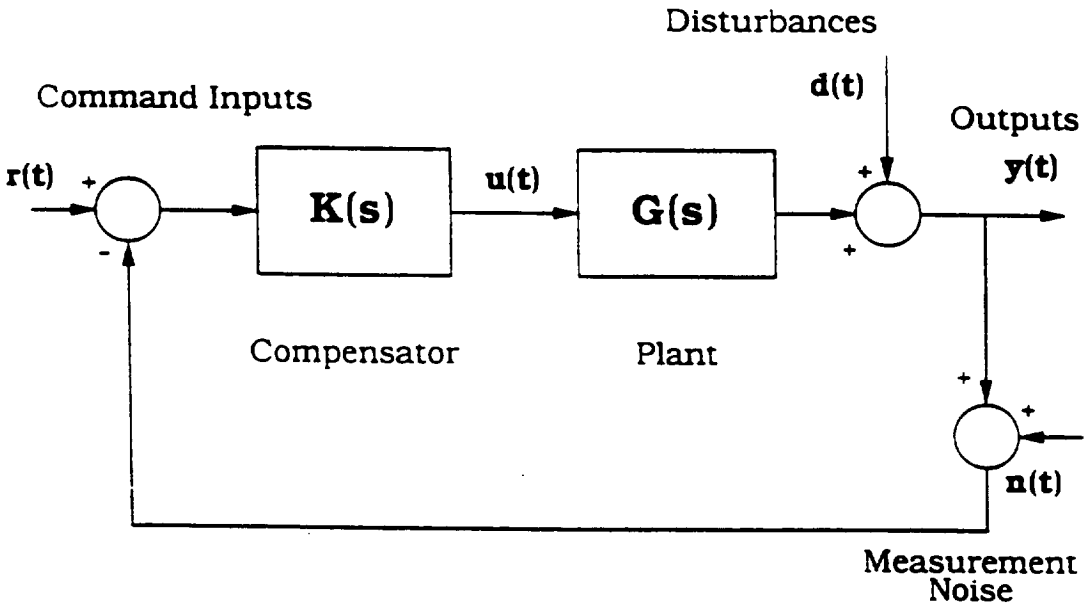

Figure 42. Schematic Diagram of a General Multiple Input-Multiple Output (MIMO) System.

$\mathbf{n}(s)$: the sensor noise vector ($m \times 1$),

and $\mathbf{G}(s)$, $\mathbf{K}(s)$ are the ($m \times m$) plant and compensator TFMs, respectively. From Equation (46), it can be inferred that:

a.) $[\mathbf{I} + \mathbf{G}(s)\,\mathbf{K}(s)]^{-1}\,\mathbf{G}(s)\,\mathbf{K}(s)$ relates the reference input to the output,

b.) $[\mathbf{I} + \mathbf{G}(s)\,\mathbf{K}(s)]^{-1}\,\mathbf{G}(s)$ relates the input disturbances to the output,

c.) $[\mathbf{I} + \mathbf{G}(s)\,\mathbf{K}(s)]^{-1}\,\mathbf{d_i}(s)$ relates the output disturbances to the output, and,

d.) $[\mathbf{I} + \mathbf{G}(s)\,\mathbf{K}(s)]^{-1}\,\mathbf{G}(s)\,\mathbf{K}(s)$ relates the sensor noise to the output.

2.) Disturbance Rejection

Disturbance rejection is the insensitivity of the closed-loop system to input disturbance signals, $\mathbf{d_i}(s), \mathbf{d_o}(s)$. In view of the discussion on good command following properties of the system, and from Equation 46, it can be observed that the output $\mathbf{y}(s)$ is influenced by disturbance signals which could force it to deviate from the reference, $\mathbf{r}(s)$. In a manner similar to the development above, it can be shown that disturbance rejection is accomplished if:

$$[\mathbf{I} + \mathbf{G}(s)\,\mathbf{K}(s)] \text{ is "large" for } s \in \Omega_{d_i},\ s \in \Omega_{d_o}, \tag{51}$$

where Ω_{d_i} and Ω_{d_o} are the frequency ranges of the expected disturbances, or, equivalently

$$\mathbf{G}(s)\,\mathbf{K}(s) \text{ is "large" for } s \in \Omega_{d_i},\ s \in \Omega_{d_o}. \tag{52}$$

Equations (51) and (52) require that the forward loop TFM must be large in the frequency range where the disturbances have most of their energy.

3.) Sensitivity Reduction to Unmodeled Dynamics

Sensitivity reduction of a control system refers to its ability to attenuate the effects of deviations of the plant from its nominal values as well as the effects of unmodeled dynamics. Consider the nominal output $\mathbf{y}^*(s)$ of a MIMO system to a reference input $\mathbf{r}(s)$:

$$\mathbf{y}^*(s) = [\mathbf{I} + \mathbf{G}^*(s)\,\mathbf{K}(s)]^{-1}\ \mathbf{G}^*(s)\,\mathbf{K}(s)\,\mathbf{r}(s), \tag{53}$$

where $\mathbf{G}^*(s)$ refers to the nominal open-loop system. Let the actual open-loop system be given by:

$$\mathbf{G}(s) = \mathbf{G}^*(s) + \delta\mathbf{G}(s), \tag{54}$$

and the actual output by:

$$\mathbf{y}(s) = \mathbf{y}^*(s) + \delta\mathbf{y}(s). \tag{55}$$

Now, from the above equations,

$$\mathbf{y}^*(s) + \delta\mathbf{y}(s) = [\mathbf{I} + [\mathbf{G}^*(s) + \delta\mathbf{G}(s)]\,\mathbf{K}(s)]^{-1}\,[\mathbf{G}^*(s) + \delta\mathbf{G}(s)]\,\mathbf{K}(s)\,\mathbf{r}(s). \tag{56}$$

From the above equations, it can be shown that:

$$\delta\mathbf{y}(s) = [\mathbf{I} + \mathbf{G}(s)\,\mathbf{K}(s)]^{-1}\,\delta\mathbf{G}(s)\,\mathbf{G}^*(s)^{-1}\,\mathbf{y}^*(s). \tag{57}$$

From Equation (57) it is observed that if the loop TFM, $\mathbf{G}(s)\,\mathbf{K}(s)$, is chosen to be large (and provided that the system is stable) the effects of $\delta\mathbf{G}(s)$ on $\delta\mathbf{y}(s)$ can be reduced to a great extent.

4.) Sensor Noise Insensitivity

From Equation (46) and from the above arguments it can be easily seen that the system will be insensitive to sensor noise by ensuring that the loop TFM, $\mathbf{G}(s)\,\mathbf{K}(s)$, is *small* in the frequency range where most of the sensor and actuator noise exists i.e. at high frequencies.

IV.4 The Role of Singular Values in Loop Shaping

Most of the loop shaping concepts, as discussed above, can be reduced to specifying the magnitude of the forward loop TFM, $\mathbf{G}(s)\,\mathbf{K}(s)$, or the return difference

TFM, $[\mathbf{I} + \mathbf{G}(s)\,\mathbf{K}(s)]$, in the specific frequency ranges of interest. It is in this context that the concept of singular values plays a role. The relations between the maximum and minimum matrix spectral norm and singular values (σ) are as follows :

$$\max_{\mathbf{u}(s)\neq 0} \frac{\|\mathbf{G}(s)\,\mathbf{u}(s)\|_2}{\|\mathbf{u}(s)\|_2} = \sigma_{max}(\mathbf{G}(s)), \tag{58}$$

and,

$$\min_{\mathbf{u}(s)\neq 0} \frac{\|\mathbf{G}(s)\,\mathbf{u}(s)\|_2}{\|\mathbf{u}(s)\|_2} = \sigma_{min}(\mathbf{G}(s)). \tag{59}$$

Thus, the transfer function matrix $\mathbf{G}(s)$ is said to be "large", if $\sigma_{min}(\mathbf{G}(s))$ is large. Similarly, $\mathbf{G}(s)$ is said to be "small", if $\sigma_{max}(\mathbf{G}(s))$ is small.

Therefore, MIMO loop shaping concepts can be restated in terms of the singular values of the loop TFM and the return difference TFM That is for good command following, disturbance rejection, sensitivity reduction, and noise insensitivity $\sigma_{min}(\mathbf{G}(s)\,\mathbf{K}(s))$ should be large in the low frequency region, and $\sigma_{max}(\mathbf{G}(s)\,\mathbf{K}(s))$ should be small in the high frequency range.

In addition to the above relations in which the system performance specifications are stated in terms of singular values of the appropriate TFMs, it can be shown that the singular values of the appropriate transfer function matrices are good measure of robustness to modeling errors [20]. This is explained as follows: if $\mathbf{E}(s)$ is the error between the actual system denoted as $\tilde{\mathbf{G}}(s)$ and a model of the system, $\mathbf{G}(s)$, then there are relations in terms of singular values of the system that guarantee closed-loop stability of the actual system when the compensator is designed using the model $\mathbf{G}(s)$. As the error $\mathbf{E}(s)$ is not known exactly, a conservative bound is used.

Define a matrix $\mathbf{L}(s)$, as a measure of uncertainty of the model, $\mathbf{G}(s)$, of the system. Therefore, the relation between the actual plant, $\tilde{\mathbf{G}}(s)$, and the model, $\mathbf{G}(s)$, is:

$$\tilde{\mathbf{G}}(s) = \mathbf{L}(s)\,\mathbf{G}(s). \tag{60}$$

Define $\mathbf{E}(s)$ such that the following relation is satisfied:

$$\mathbf{L}(s) = \mathbf{E}(s) + \mathbf{I}. \tag{61}$$

From Equations (60) and (61) the following expression for $\mathbf{E}(s)$ can be derived:

$$\mathbf{E}(s) = [\tilde{\mathbf{G}}(s) - \mathbf{G}(s)]\,\mathbf{G}^{-1}(s). \tag{62}$$

It has been shown by Lehtomaki [20] that a compensator $\mathbf{K}(s)$ which stabilizes the closed-loop based on the model $\mathbf{G}$, will also stabilize the closed-loop with of actual plant $\tilde{\mathbf{G}}$, if the following relation is true:

$$\sigma_{max}\left[\mathbf{L}(j\omega) - \mathbf{I}\right] < \sigma_{min}\left[\mathbf{I} + (\mathbf{K}(j\omega)\,\mathbf{G}(j\omega))^{-1}\right]. \tag{63}$$

It can be shown that at high frequencies (when most of the modeling errors are apparent), if $|\mathbf{L}(j\omega)| \gg 1$ and $|\,[\mathbf{G}(j\omega)\,\mathbf{K}(j\omega)]\,| \gg 1$, then Equation (63) becomes

$$\sigma_{max}\left[\mathbf{L}(j\omega)\right] < \sigma_{min}\left[(\mathbf{K}(j\omega)\,\mathbf{G}(j\omega))^{-1}\right] = \frac{1}{\sigma_{max}\left[\mathbf{K}(j\omega)\,\mathbf{G}(j\omega)\right]}. \tag{64}$$

Thus, by using Equation (64) and the high frequency noise rejection specification that $\sigma_{max}(\mathbf{G}(s)\,\mathbf{K}(s))$ is "small" in the high frequency range, the high frequency uncertainity requirements for the system model can be defined.

Thus, the above discussion summarizes the relation between the MIMO loop shaping concepts and the singular values of the system TFMs.

IV.5 Model-Based Compensation

Dynamic compensators are required for plants which must exhibit different behavior at high and low frequencies. Model-Based Compensators (MBCs) are a special class of dynamic compensators used in feedback control when only part of the state is measured. Use of MBCs allows the indirect estimation of all the unobservable states for use in the feedback control. A block diagram of an MBC in a closed-loop is shown in Figure 43.

The state-space representation of the plant is given by:

$$\dot{\mathbf{x}}(t) = \mathbf{A}\,\mathbf{x}(t) + \mathbf{B}\,\mathbf{u}(t) + \mathbf{L}\,\mathbf{w}(t) \quad ; \quad \mathbf{x}(t) \in \Re^n, \mathbf{u}(t) \in \Re^m, \mathbf{w}(t) \in \Re^p, \tag{65}$$

$$\mathbf{y}(t) = \mathbf{C}\,\mathbf{x}(t) \quad ; \quad \mathbf{y}(t) \in \Re^m, \tag{66}$$

whereas the state-space representation of the MBC is given by:

$$\dot{\mathbf{z}}(t) = \mathbf{A}\,\mathbf{z}(t) + \mathbf{B}\,\mathbf{u}(t) + \mathbf{H}\,[-\mathbf{e}(t) - \mathbf{C}\,\mathbf{z}(t)] \quad ; \mathbf{z}(t) \in \Re^n, \mathbf{e}(t) \in \Re^m, \tag{67}$$

$$\mathbf{u}(t) = -\,\mathbf{G}\,\mathbf{z}(\iota), \tag{68}$$

or, by,

$$\dot{\mathbf{z}}(t) = [\mathbf{A} - \mathbf{B}\,\mathbf{G} - \mathbf{H}\,\mathbf{C}]\,\mathbf{z}(t) - \mathbf{H}\,\mathbf{e}(t), \tag{69}$$

$$\mathbf{u}(t) = -\,\mathbf{G}\,\mathbf{z}(t), \tag{70}$$

where $\mathbf{z}(t)$ represents the MBC state vector. The feedback interconnection relation is given by:

$$\mathbf{e}(t) = \mathbf{r}(t) - \mathbf{y}(t) \quad ; \quad \mathbf{r}(t) \in \Re^m, \tag{71}$$

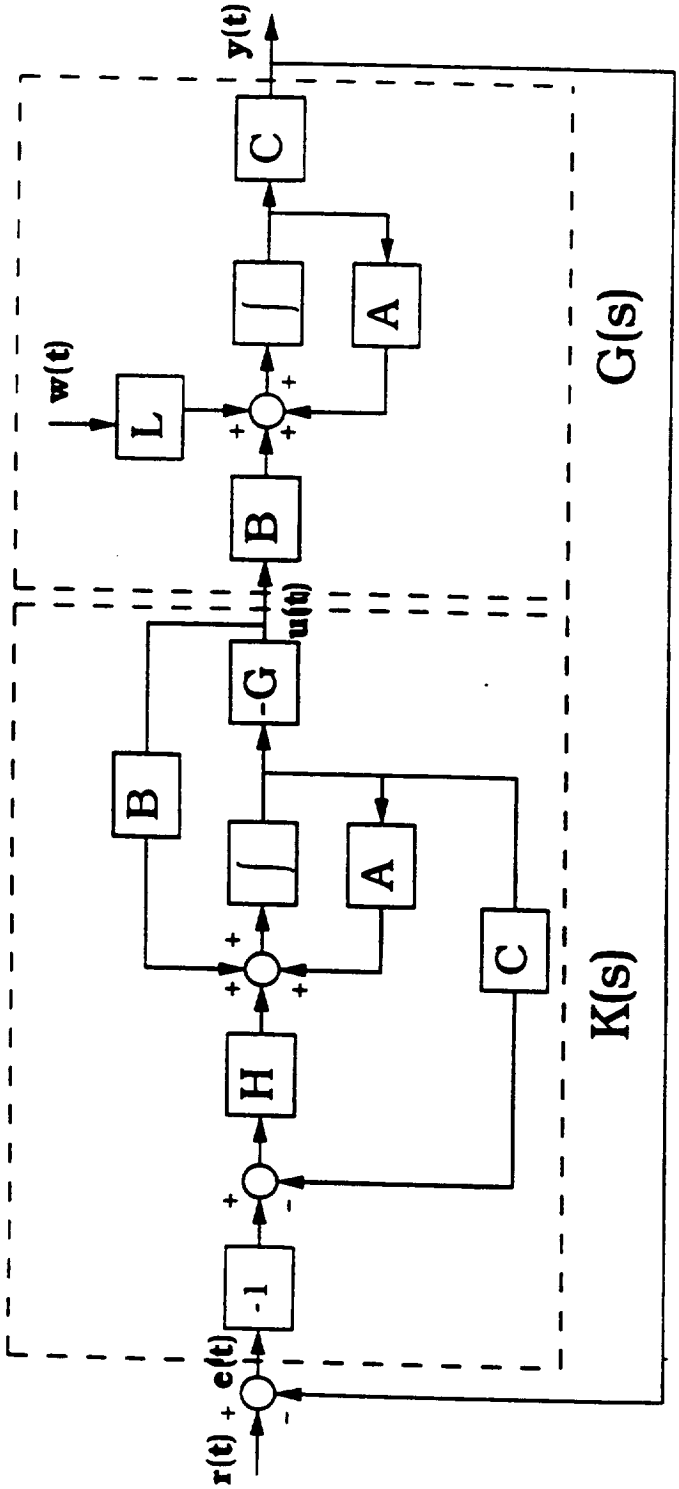

Figure 43. Model-Based Compensator in a Feedback Configuration.

where $\mathbf{r}(t)$ represents the reference vector. The state vector for the closed-loop system is defined as:

$$\mathbf{x_{cl}}(t) = [\mathbf{x}(t) \quad \tilde{\mathbf{x}}(t)]' \quad ; \quad \mathbf{x_{cl}}(t) \in \Re^{2n}, \tag{72}$$

where

$$\tilde{\mathbf{x}}(t) \equiv \mathbf{x}(t) - \mathbf{z}(t). \tag{73}$$

The state-space representation of the closed-loop system can now be expressed as :

$$\begin{bmatrix} \dot{\mathbf{x}}(t) \\ \dot{\tilde{\mathbf{x}}}(t) \end{bmatrix} = \underbrace{\begin{bmatrix} \mathbf{A} - \mathbf{B}\,\mathbf{G} & -\mathbf{B}\,\mathbf{G} \\ 0 & \mathbf{A} - \mathbf{H}\,\mathbf{C} \end{bmatrix}}_{\mathbf{A_{cl}}} \begin{bmatrix} \mathbf{x}(t) \\ \tilde{\mathbf{x}}(t) \end{bmatrix} + \begin{bmatrix} 0 \\ -\mathbf{H} \end{bmatrix} \mathbf{r}(t) + \begin{bmatrix} 0 \\ -\mathbf{L} \end{bmatrix} \mathbf{w}(t), \tag{74}$$

$$\mathbf{y}(t) = [\mathbf{C} \quad 0] \begin{bmatrix} \mathbf{x}(t) \\ \tilde{\mathbf{x}}(t) \end{bmatrix}. \tag{75}$$

Additionally, it can be shown that:

$$\det(\lambda\,\mathbf{I} - \mathbf{A_{cl}}) = \det(\lambda\,\mathbf{I} - \mathbf{A} + \mathbf{B}\,\mathbf{G})\,.\,\det(\lambda\,\mathbf{I} - \mathbf{A} + \mathbf{H}\,\mathbf{C}). \tag{76}$$

From the above representation of the MBC, **H** and **G** are the design matrices which must be chosen such that the following conditions for nominal stability of the closed-loop system are satisfied:

$$\mathrm{Re}\,\lambda_i(\mathbf{A} - \mathbf{B}\,\mathbf{G}) < 0 \quad ; i = 1, 2, \ldots, n, \tag{77}$$

$$\mathrm{Re}\,\lambda_i(\mathbf{A} - \mathbf{H}\,\mathbf{C}) < 0 \quad ; i = 1, 2, \ldots, n. \tag{78}$$

In addition to ensuring nominal plant stability, the MBC yields systems with special properties; the design matrix **G** controls n poles while the design matrix **H** controls

the other n poles. By virtue of this separability of the closed-loop poles, the poles of $(\mathbf{A} - \mathbf{B}\,\mathbf{G})$, can be placed using full-state feedback designs such as the Linear Quadratic Regulator (LQR) or even pole placement techniques [21]. This is known as the control loop design and its state-space representation (the full-state regulator problem) is:

$$\dot{\mathbf{x}}(t) = \mathbf{A}\,\mathbf{x}(t) + \mathbf{B}\,\mathbf{u}(t), \tag{79}$$

$$\mathbf{u}(t) = -\mathbf{G}\,\mathbf{x}(t). \tag{80}$$

The state-space representation of the closed-loop system is given by:

$$\dot{\mathbf{x}}(t) = [\mathbf{A} - \mathbf{B}\,\mathbf{G}]\,\mathbf{x}(t). \tag{81}$$

The other half of the closed-loop poles are the poles of $(\mathbf{A} - \mathbf{H}\,\mathbf{C})$, and they can be placed using the Kalman Filter (KF) algorithm to guarantee nominal stability. This is known as the filter loop design and its state-space representation (an output feedback problem with no external control) is:

$$\dot{\mathbf{x}}(t) = \mathbf{A}\,\mathbf{x}(t) + \mathbf{v}(t), \tag{82}$$

$$\mathbf{y}(t) = \mathbf{C}\,\mathbf{x}(t), \tag{83}$$

where $\mathbf{v}(t)$ represents the innovations term. This term is related to the sensed output as follows:

$$\mathbf{v}(t) = -\mathbf{H}\,\mathbf{y}(t) = -\mathbf{H}\,\mathbf{C}\,\mathbf{x}(t). \tag{84}$$

The state-space representation of the closed-loop system is then given by:

$$\dot{\mathbf{x}}(t) = [\mathbf{A} - \mathbf{H}\,\mathbf{C}]\,\mathbf{x}(t). \tag{85}$$

Therefore, observing that nominal plant stability can easily be achieved, the next goal is to determine a systematic manner for choosing the design matrices **H** and **G** such that the frequency domain specifications on stability robustness and nominal performance (command-following, disturbance-rejection, insensitivity to sensor noise etc.) can be achieved. The next section shows how MBCs can be designed in a systematic manner so as to meet several frequency domain specifications, in addition to nominal closed-loop stability.

IV.6 Linear Quadratic Gaussian/Loop Transfer Recovery (LQG/LTR)

The LQG/LTR design method was first developed by Doyle and Stein [16]. It is a systematic procedure by which stability and certain frequency domain specifications can be met in the design of multivariable feedback control systems [15]. As discussed in the previous section, the LQG/LTR compensator belongs to the class of MBCs. The first step in the design process is design of the Target Feedback Loop (TFL).

IV.6.1 Target Feedback Loop Design

The TFL is designed by solving an artificial KF problem. The KF was developed by Kalman and Bucy, and it has found extensive use in several diverse fields [22]. The KF is a method by which real-time "optimal" state estimates, $\hat{\mathbf{x}}(t)$, and outputs, $\hat{\mathbf{y}}(t)$, are calculated based on past sensor measurements and applied controls actions. To perform this function the KF contains a model of the plant/sensor system, and

thus it is called a model-based observer or estimator. The mathematical form of the stochastic state dynamics (without control) is given by:

$$\dot{\mathbf{x}}(t) = \mathbf{A}\,\mathbf{x}(t) + \mathbf{L}\,\boldsymbol{\xi}(t); \quad \mathbf{x}(t) \in \Re^n, \boldsymbol{\xi}(t) \in \Re^m, \tag{86}$$

where $\boldsymbol{\xi}(t)$ is a fictitious Gaussian, zero-mean, white noise (process noise) with identity intensity matrix I. That is :

$$E\,[\boldsymbol{\xi}(t)] = 0, \quad \forall t, \tag{87}$$

$$\mathrm{cov}\,[\boldsymbol{\xi}(t); \boldsymbol{\xi}(\tau)] = E\,\left[\boldsymbol{\xi}(t)\,\boldsymbol{\xi}'(\tau)\right] = \mathbf{I}\,\delta(t-\tau). \tag{88}$$

In the measurement equation, sensor errors are modeled by additive white noise:

$$\mathbf{y}(t) = \mathbf{C}\,\mathbf{x}(t) + \boldsymbol{\theta}(t) \quad ; \quad \mathbf{y}(t) \in \Re^p, \boldsymbol{\theta}(t) \in \Re^n, \tag{89}$$

where θ(t) is Gaussian, zero-mean, white noise (sensor noise) with constant intensity matrix $\mu\,\mathbf{I}$, $\mu > 0$, independent of the process noise. That is :

$$E\,[\boldsymbol{\theta}(t)] = 0, \quad \forall t, \tag{90}$$

$$\mathrm{cov}\,[\boldsymbol{\theta}(t); \boldsymbol{\theta}(\tau)] = E\,\left[\boldsymbol{\theta}(t)\,\boldsymbol{\theta}'(\tau)\right] = \mu\,\mathbf{I}\,\delta(t-\tau), \tag{91}$$

and

$$\mathrm{cov}\,[\boldsymbol{\xi}(t); \boldsymbol{\theta}(\tau)] = E\,\left[\boldsymbol{\xi}(t)\,\boldsymbol{\theta}'(\tau)\right] = 0. \tag{92}$$

A KF is driven by the control vector, $\mathbf{u}(t)$, and the noisy measurement vector, $\mathbf{y}(t)$, and generates in real-time a state estimate vector, $\hat{\mathbf{x}}(t) \in \Re^n$, and an output estimate vector, $\hat{\mathbf{y}}(t) \in \Re^p$. The KF equations are :

$$\dot{\hat{\mathbf{x}}}(t) = \mathbf{A}\,\hat{\mathbf{x}}(t) + \mathbf{B}\,\mathbf{u}(t) + \mathbf{H}\,[\mathbf{y}(t) - \mathbf{C}\,\hat{\mathbf{x}}(t)] \tag{93}$$

$$\hat{\mathbf{y}}(t) = \mathbf{C}\,\hat{\mathbf{x}}(t), \tag{94}$$

or

$$\dot{\hat{\mathbf{x}}}(t) = [\mathbf{A} - \mathbf{H}\,\mathbf{C}]\,\hat{\mathbf{x}}(t) + \mathbf{H}\,\mathbf{y}(t) + \mathbf{B}\,\mathbf{u}(t), \tag{95}$$

$$\hat{\mathbf{y}}(t) = \mathbf{C}\,\hat{\mathbf{x}}(t), \tag{96}$$

where $\mathbf{H}$ is the KF gain matrix, which is given by:

$$\mathbf{H} = (\frac{1}{\mu})\,\mathbf{\Sigma}\,\mathbf{C}', \tag{97}$$

where $\mathbf{\Sigma}$, the error covariance matrix, is determined by solving the Filter Algebraic Riccati Equation (FARE) given by:

$$\mathbf{0} = \mathbf{A}\,\mathbf{\Sigma} + \mathbf{\Sigma}\,\mathbf{A}' + \mathbf{L}\,\mathbf{L}' - (\frac{1}{\mu})\mathbf{\Sigma}\,\mathbf{C}'\,\mathbf{C}\,\mathbf{\Sigma}. \tag{98}$$

If $[\mathbf{A}, \mathbf{L}]$ is stabilizable and if $[\mathbf{A}, \mathbf{C}]$ is detectable, then it can be shown that there exists a unique n×n solution matrix $\mathbf{\Sigma}$ to FARE, such that $\mathbf{\Sigma}$ is positive definite.

In the above equations μ and $\mathbf{L}$ are the design parameters of the KF problem. These design parameters are chosen iteratively such that the KF loop (the target loop) satisfies certain frequency domain specifications. Specifically, the singular values for the TFM, $\mathbf{G}(s)\,\mathbf{K}(s)$, are to be large at low frequencies and low at high frequencies. Also, the bandwidth of the system can be set at particular values by adjusting μ.

The process of designing the KF loop such that its maximum and minimum singular values (σ_{max} and σ_{min}) have a predetermined "character" is termed as "loop shaping". In this manner, frequency domain specifications like good command following, disturbance rejection and insensitivity to noise can be met [20]. Qualitatively speaking the singular values of the KF loop should have the following characteristics:

$$\sigma_{min}(\mathbf{G_{KF}}(s)) \gg 1, \tag{99}$$

in the low frequency range, and,

$$\sigma_{max}(\mathbf{S_{KF}}(s)) \ll 1, \tag{100}$$

in the low frequency range, where,

Loop TFM: $\mathbf{G_{KF}}(s) = \mathbf{C}(s\mathbf{I} - \mathbf{A})^{-1}\mathbf{H}$,

Sensitivity TFM : $\mathbf{S_{KF}}(s) = [\mathbf{I} + \mathbf{G_{KF}}(s)]^{-1}$, and,

Closed-Loop TFM : $\mathbf{C_{KF}}(s) = [\mathbf{I} + \mathbf{G_{KF}}(s)]^{-1}\,\mathbf{G_{KF}}(s)$.

Also, for certain performance specifications to be met the plant model may have to be augmented with additional dynamics (integrators etc.) at the plant input. The filter gain matrix $\mathbf{H}$ is then determined using the augmented plant model.

IV.6.2 Actual Loop Robustness Recovery

Having determined the KF gain matrix, $\mathbf{H}$, the next step is in determining the control gain matrix, $\mathbf{G}$, such that the properties of the KF loop, such as command following, disturbance rejection and insensitivity to sensor noise are preserved when using the actual loop $\mathbf{G}(s)\,\mathbf{K}(s)$. A family of control gain matrices $\mathbf{G}_\rho$ is determined by solving the cheap-control LQR problem for minimum phase plants, as follows [15]:

$$\mathbf{G}_\rho = (\frac{1}{\rho})\,\mathbf{B}'\mathbf{K}_\rho, \qquad \text{as } \rho \to 0, \tag{101}$$

where, the matrix $\mathbf{K}_\rho$ is the solution to the following Control Algebraic Riccati Equation (CARE), and ρ is a design parameter

$$\mathbf{0} = -\mathbf{K}_\rho\mathbf{A} - \mathbf{A}'\mathbf{K}_\rho - \mathbf{C}'\mathbf{C} + (\frac{1}{\rho})\mathbf{K}_\rho\mathbf{B}\,\mathbf{B}'\mathbf{K}_\rho. \tag{102}$$

It can be shown that $\mathbf{G}_\rho$ will always be such that :

$$\mathrm{Re}\,\lambda_i(\mathbf{A} - \mathbf{B}\,\mathbf{G}_\rho) < 0, \quad \forall\, \rho > 0 \quad ; i = 1, 2, \ldots, n, \tag{103}$$

and,

$$\lim_{\rho \to 0} \sqrt{\rho}\,\mathbf{G}_\rho \to \mathbf{W}\,\mathbf{C} \qquad \mathbf{W}'\mathbf{W} = \mathbf{I}.$$

Now, the forward loop transfer function matrix of the actual loop is:

$$\mathbf{T}(s) = \mathbf{G}(s)\,\mathbf{K}_\rho(s) = \mathbf{C}\,\mathbf{\Phi}(s)\,\mathbf{B}\,\mathbf{G}_\rho\left[\mathbf{\Phi}^{-1}(s) + \mathbf{B}\,\mathbf{G}_\rho + \mathbf{H}\,\mathbf{C}\right]^{-1}\mathbf{H}, \tag{104}$$

where

$$\mathbf{\Phi}(s) = (s\mathbf{I} - \mathbf{A})^{-1}.$$

From Equation (104), the implication is that as $\rho \to 0$:

$$\mathbf{C}\,\mathbf{\Phi}(s)\,\mathbf{B}\,\mathbf{G}_\rho\left[\mathbf{\Phi}^{-1}(s) + \mathbf{B}\,\mathbf{G}_\rho + \mathbf{H}\,\mathbf{C}\right]^{-1}\mathbf{H} \longrightarrow \mathbf{C}\,\mathbf{\Phi}(s)\,\mathbf{H}.$$

This implies that as $\rho \to 0$, the MBC loop will approximate the behavior of the designed target loop with the assumption that the plant is minimum phase [23]. Therefore, if the filter loop meets the required performance specifications, then the MBC loop will also meet the same specifications. Hence, for minimum phase plants, the intuitive explanation for the operation of the LQG/LTR compensator is that it produces an approximate inverse of the plant $\mathbf{G}(s)$, and it substitutes the plant dynamics with the desirable dynamics of the KF loop, $\mathbf{G_{KF}}(s)$. That is,

$$\mathbf{K}_\rho(s) \cong \mathbf{G}^{-1}(s)\,\mathbf{G_{KF}}(s). \tag{105}$$

IV.7 Guaranteed Properties of LQG/LTR Compensators

The principal advantage of designing compensators for linear MIMO systems using systematic procedures lies in the fact that, for minimum phase systems, several good properties of the designed compensators are *guaranteed.* This enables the designer to have greater flexibility in the compensator design as several of the nominal properties of the LQG/LTR compensator are assured. In addition to nominal stability some of the guaranteed properties of the LQG/LTR compensator for minimum phase systems are as follows [20] :

1.) There is a guaranteed minimum gain margin (GM), in each loop of the general MIMO system, given by

$$GM = \left[\frac{1}{2}, +\infty\ \right), \tag{106}$$

2.) There is a guaranteed minimum phase margin (PM), in each loop of the general MIMO system, the range of which is given by:

$$-60^\circ \leq PM \leq +60^\circ. \tag{107}$$

The above properties offer an advantage over other design methods, such as pole placement or LQG, for which stability robustness is not guaranteed [21]. At this point it is important to emphasize that the above guaranteed properties are true only for *minimum* phase systems, and they cannot be ensured for systems with non-minimum phase behavior.

CHAPTER V

GAIN-SCHEDULED CONTROLLER DESIGN FOR VOLTAGE REGULATION

V.1 Introduction

This chapter discusses the actual LQG/LTR compensator design for the SNPS using the linearized reference models. The LQG/LTR compensators thus designed are analyzed, via investigating the singular values of the appropriate TFMs (as was discussed in the previous chapter), to determine if the LQG/LTR guaranteed properties are achieved. Finally, the gain-scheduling of the linear compensators to obtain a single nonlinear external controller is described.

V.2 Design and Analysis of External Controllers for the Static Space Nuclear Power System

This section describes the design sequence of an LQG/LTR compensator for the SNPS system. For this system, the design specifications are the following:

1.) The designed compensator should exhibit stability robustness to system parameter variations and unmodeled dynamics,

2.) The compensator should be capable of rejecting disturbances and regulate the load voltage with zero steady-state error by appropriately manipulating the external core reactivity,

3.) The compensator should be capable of slowing down the load voltage response of the system, thus allowing sufficient time for the movement of the control drums, and,

4.) The initial reactivity rate should not exceed 80 cents.

The third design specification sets an upper limit on the bandwidth of the system. The singular values for the open-loop system models linearized at 80% and 110% of full power are shown in Figures 44, 45, respectively. From Figures 44 and 45, it is apparent that the cross-over frequencies (or the system bandwidth) are too high to allow for sufficient time for the movement of control drums. Furthermore, the figures indicate the existence of finite D.C. gain, causing non-zero steady-state error. Therefore, the linearized reference model is augmented with an integrator at the input. The last design specification is met by augmenting the compensator input by a low-pass filter which delays and reduces the magnitude of the load voltage error. The block diagram of the overall control system in series with the linearized reference model is displayed in Figure 46. In Figure 46, the reference input is set to be zero, and $e(t)$ equals to $\delta V(t)$ which is the deviation of the load voltage from 100 Volts, $e_f(t)$ is the filtered voltage error, $\rho_{ex}(t)$ is the external reactivity $\delta w(t)$ is the system disturbance which is proportional to the change in electrical load demand, and finally, $n(t)$ is the output measurement noise, which is modeled as white Gaussian noise with a certain variance. As it can be seen from this figure, the compensator, K(s) is augmented by a filter in order to filter the load voltage error, e(t), so as to prevent

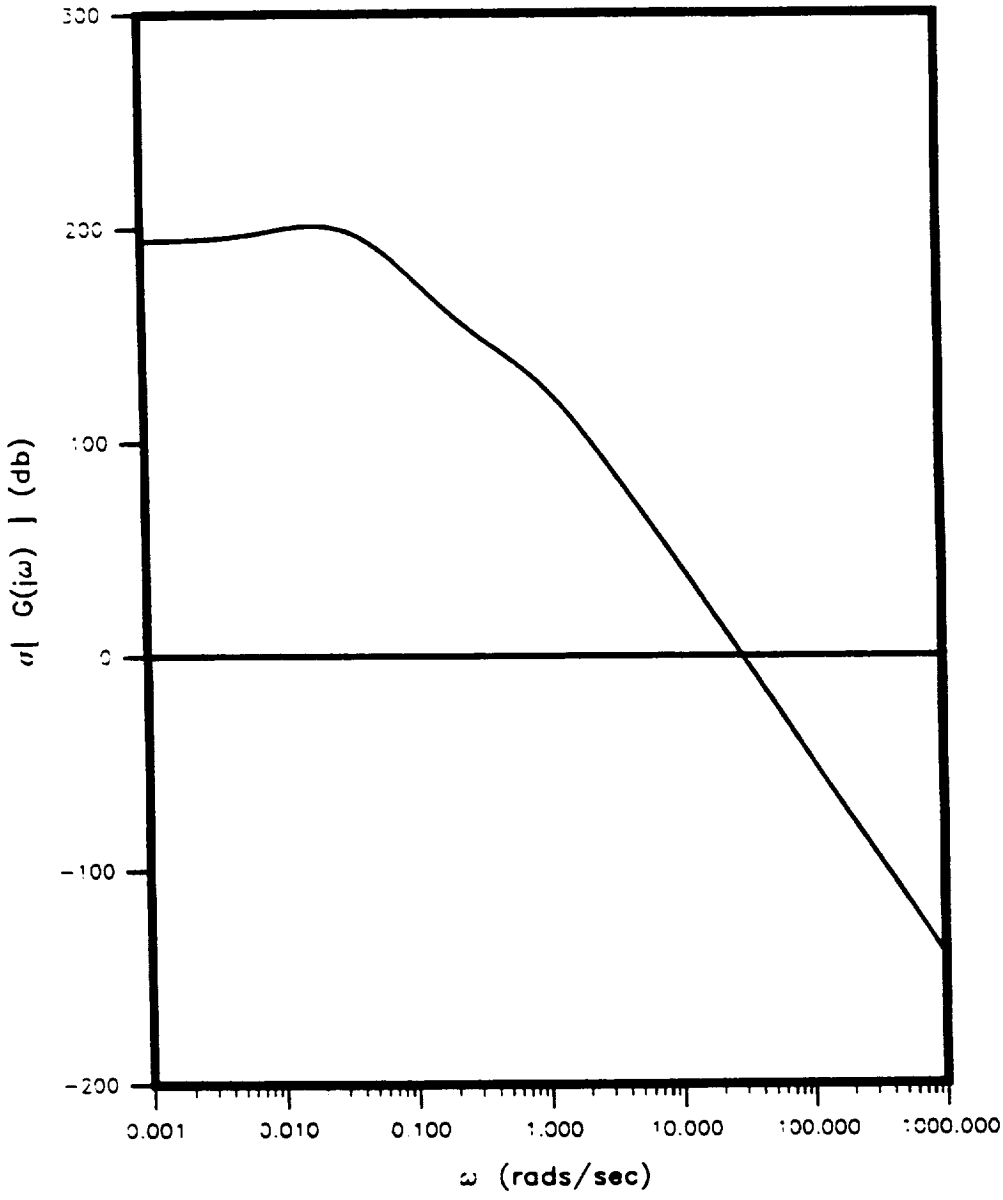

Figure 44. Singular Values of the Open-Loop SNPS Model Linearized at 80% of Full Power.

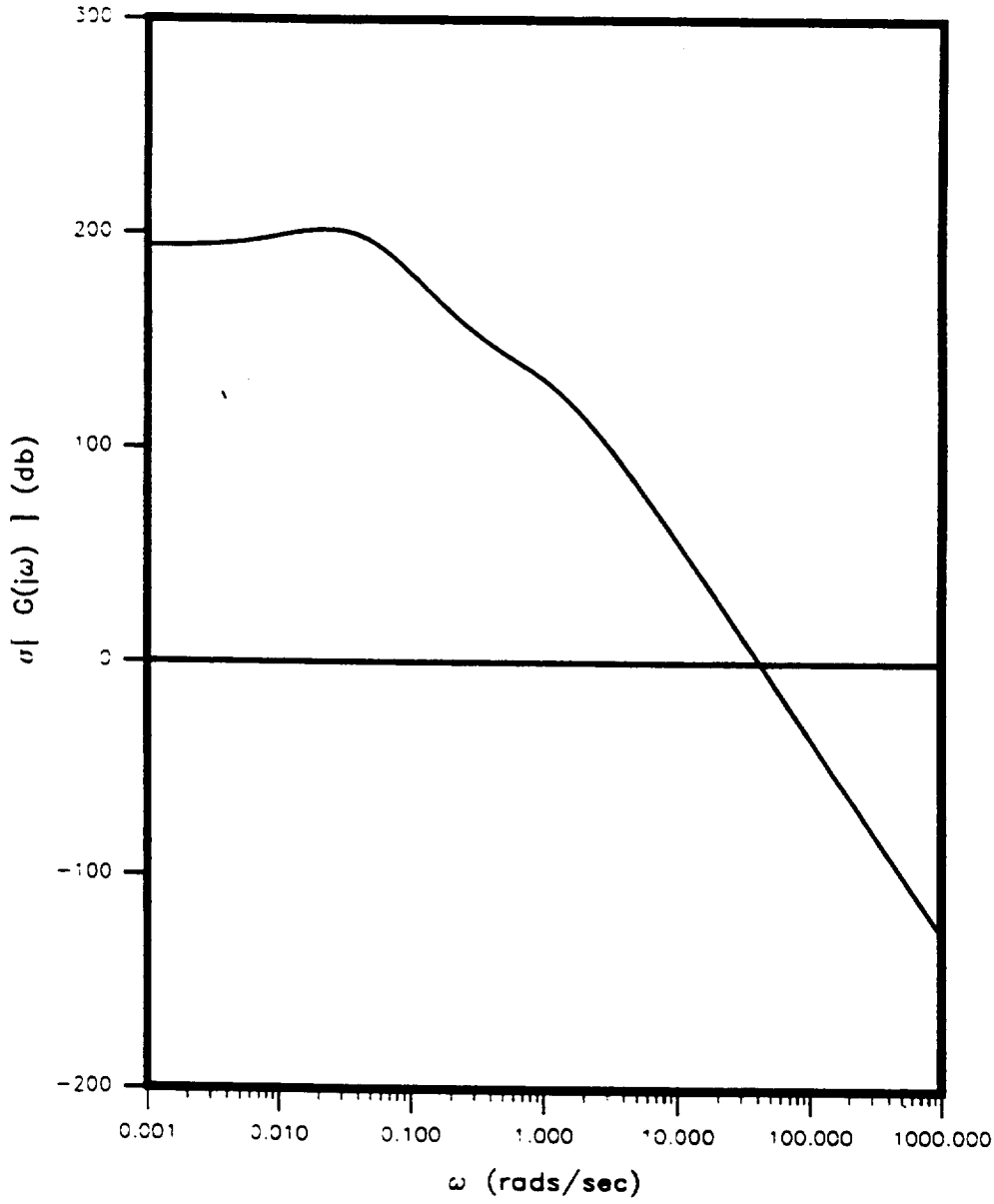

Figure 45. Singular Values of the Open-Loop SNPS Model Linearized at 110% of Full Power.

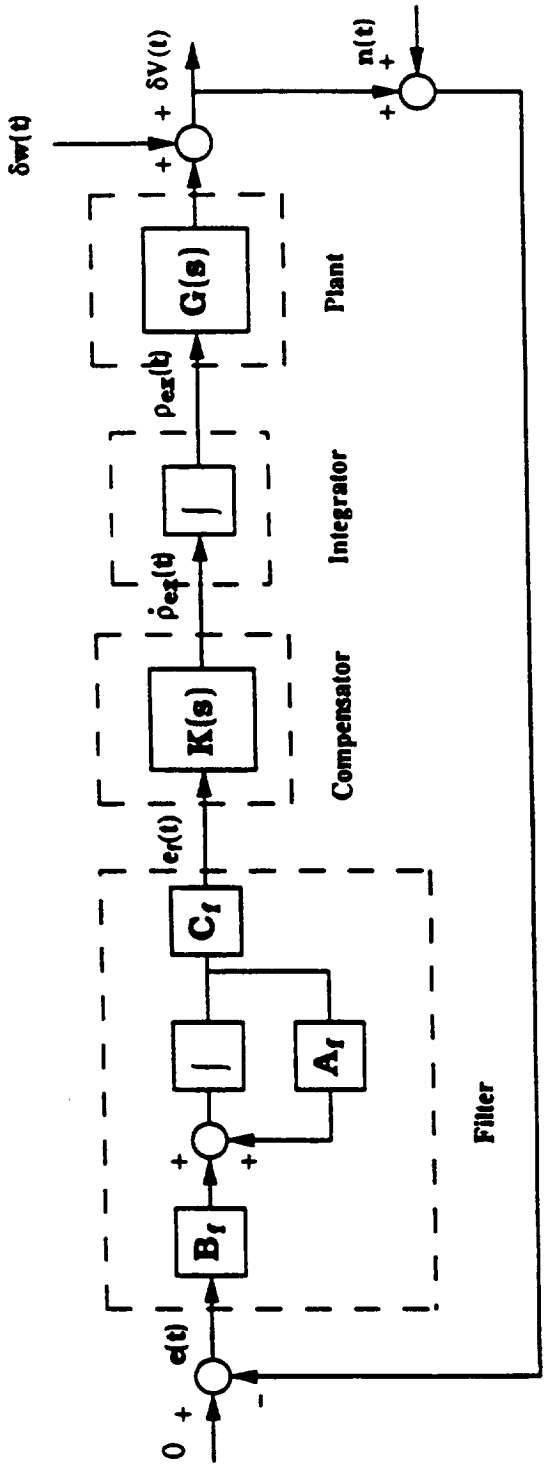

Figure 46. Block Diagram of the Overall Control System and the Linearized Reference Model.

the initial reactivity rate from exceeding 80 cents/sec. The filter transfer function, $\mathbf{G_f}(s)$ is given by:

$$\mathbf{G_f}(s) = \mathbf{C_f}(s\mathbf{I} - \mathbf{A_f})^{-1}\mathbf{B_f} \tag{108}$$

where the filter transfer function matrices, $\mathbf{A_f}$, $\mathbf{B_f}$, and $\mathbf{C_f}$ are given in Appendix C. The plant, $\mathbf{G}(s)$, is augmented with an integrator in order to minimize the load voltage steady-state error. The compensator transfer function $\mathbf{K}(s)$ is determined using the step by step LQG/LTR design method described in the previous chapter. In Figure 46, the compensator transfer function, $\mathbf{K}(s)$ is given by:

$$\mathbf{K}(s) = \mathbf{G}(s\mathbf{I} - \mathbf{A} + \mathbf{B}\,\mathbf{G} + \mathbf{H}\,\mathbf{C})^{-1}\mathbf{H}. \tag{109}$$

The two steps of the LQG/LTR design method, which uses the augmented linearized reference model of the SNPS to determine $\mathbf{K}(s)$, are as follows:

1.) The filter gain matrix $\mathbf{H}$ is fully determined by choosing a value for μ and $\mathbf{L}$, and by solving the FARE (Equation (98)). $\mathbf{L}$ is set to the input vector $\mathbf{B_{aug}}$. Initially, μ is chosen to be 10^8 and the singular values of the target loop, $\sigma[\mathbf{C}(j\omega\mathbf{I} - \mathbf{A})^{-1}\mathbf{H}]$, are plotted to determine the cross-over frequency. If the resulting target loop does not exhibit the desired characteristics, μ is changed and the above calculations are repeated until the singular values have the required specifications. In the present compensator design, μ is chosen such that for each linear compensator designed to control the system at different equilibrium points, the cross-over frequency of the target loop system is about 0.16 rads/sec. This cross-over frequency corresponds to a rise time of approximately 7.0 seconds.

Table 5. Values of μ and Corresponding Bandwidths of the Recovered Loops at Different Operating Points

Model Linearized At	μ	ω_{LTR} (rads/sec)
50%	2.3700E+09	1.59872E-01
60%	2.6680E+09	1.59892E-01
70%	2.9820E+09	1.59912E-01
80%	3.3050E+09	1.59912E-01
90%	3.6000E+09	1.59912E-01
95%	3.7430E+09	1.59912E-01
100%	3.8380E+09	1.59912E-01
105%	3.9920E+09	1.59932E-01
110%	4.1820E+09	1.59912E-01
120%	4.5480E+09	1.59952E-01
130%	4.8990E+09	1.59952E-01
140%	5.2300E+09	1.59952E-01
150%	5.5590E+09	1.59932E-01

2.) Having determined the filter gain matrix **H**, the next step involves execution of the recovery procedure to satisfy the following asymptotic condition:

$$\lim_{\rho \to 0} \left[\mathbf{G_{aug}}(j\omega) \mathbf{K_{LQG/LTR}}(j\omega) \right] = \mathbf{C}(j\omega \mathbf{I} - \mathbf{A})^{-1} \mathbf{H}, \tag{110}$$

which implies that

$$\lim_{\rho \to 0} \left[\mathbf{G_{aug}}(j\omega) \mathbf{K_{LQG/LTR}}(j\omega) \right] = \mathbf{G_{KF}}(j\omega). \tag{111}$$

Hence, for $\rho \to 0$ the CARE, Equation (102), is solved to compute the control gain vector **G**.

As mentioned earlier, the bandwidths of the target loops are fixed to be about 0.16 rads/sec at all operating points. The bandwidths of the recovered loops at different operating points and the values of μ chosen for the corresponding target loops are depicted in Table 5. The final gain matrices, **H** and **G**, obtained from the above design process are presented in Appendix D.

Figures 47 and 48 show the extent to which the target characteristics can be recovered by the LTR procedure for the 80% and 110% of full power linearized reference models, respectively. Since the plant transfer function matrix, $\mathbf{G}(s)$, is minimum-phase, $\mathbf{G_{aug}}(j\omega)\,\mathbf{K_{LQG/LTR}}(j\omega)$ of the system approximates the transfer function matrix of the target loop, $\mathbf{G_{KF}}(j\omega)$, as can be observed from Figures 47 and 48. Therefore, the actual loop has the command-following and disturbance-rejection properties of the target loop. It is further observed that LQG/LTR method yields good agreement between the singular values of the actual and the target loop for frequencies well beyond crossover. The singular values of $\mathbf{G_{KF}}(j\omega)$ roll-off at -20 db/dec, while those of $\mathbf{G_{aug}}(j\omega)\,\mathbf{K_{LQG/LTR}}(j\omega)$ eventually roll-off at -40 db/dec. Thus, the actual LQG/LTR loop offers some additional robustness to high frequency unmodeled dynamics as compared to the target loop.

The singular values of the sensivity and the closed-loop tranfer function matrices can be further observed to investigate the performance and robustness properties of the system. These properties are achieved if:

$$\sigma_{max}\left[\mathbf{S}(j\omega)\right] \leq 0\,db, \tag{112}$$

$$\sigma_{max}\left[\mathbf{C}(j\omega)\right] \leq 6.02\,db, \tag{113}$$

where $\mathbf{S}(j\omega)$ and $\mathbf{C}(j\omega)$ are the sensitivity and closed-loop transfer function matrices given, respectively, by:

$$\mathbf{S}(j\omega) = \left[\mathbf{I} + \mathbf{G}(j\omega)\,\mathbf{K}(j\omega)\right]^{-1}, \tag{114}$$

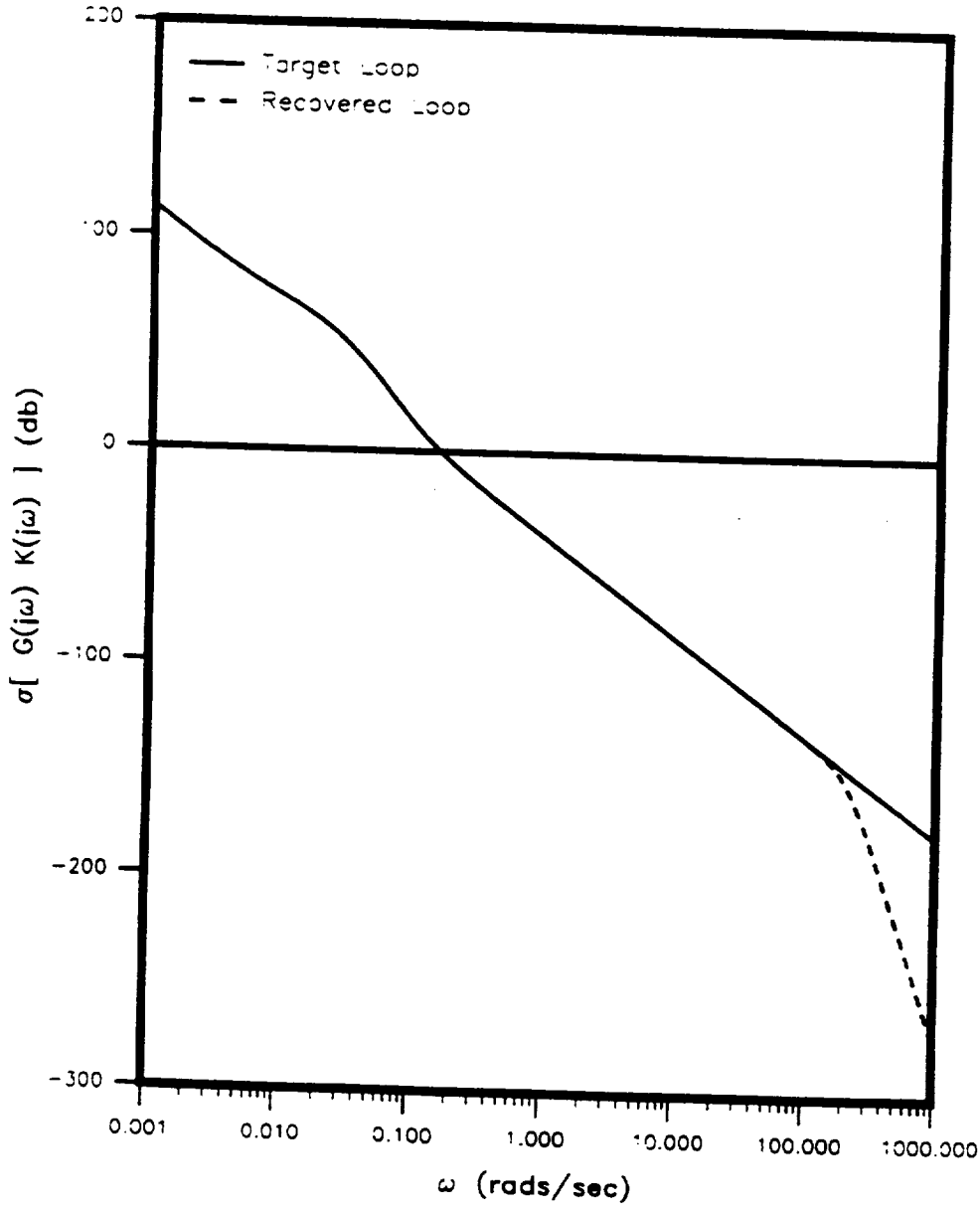

Figure 47. Singular Values of the Target Loop and the Actual Recovered Loop for the 80% of Full Power Linearized Reference Model.

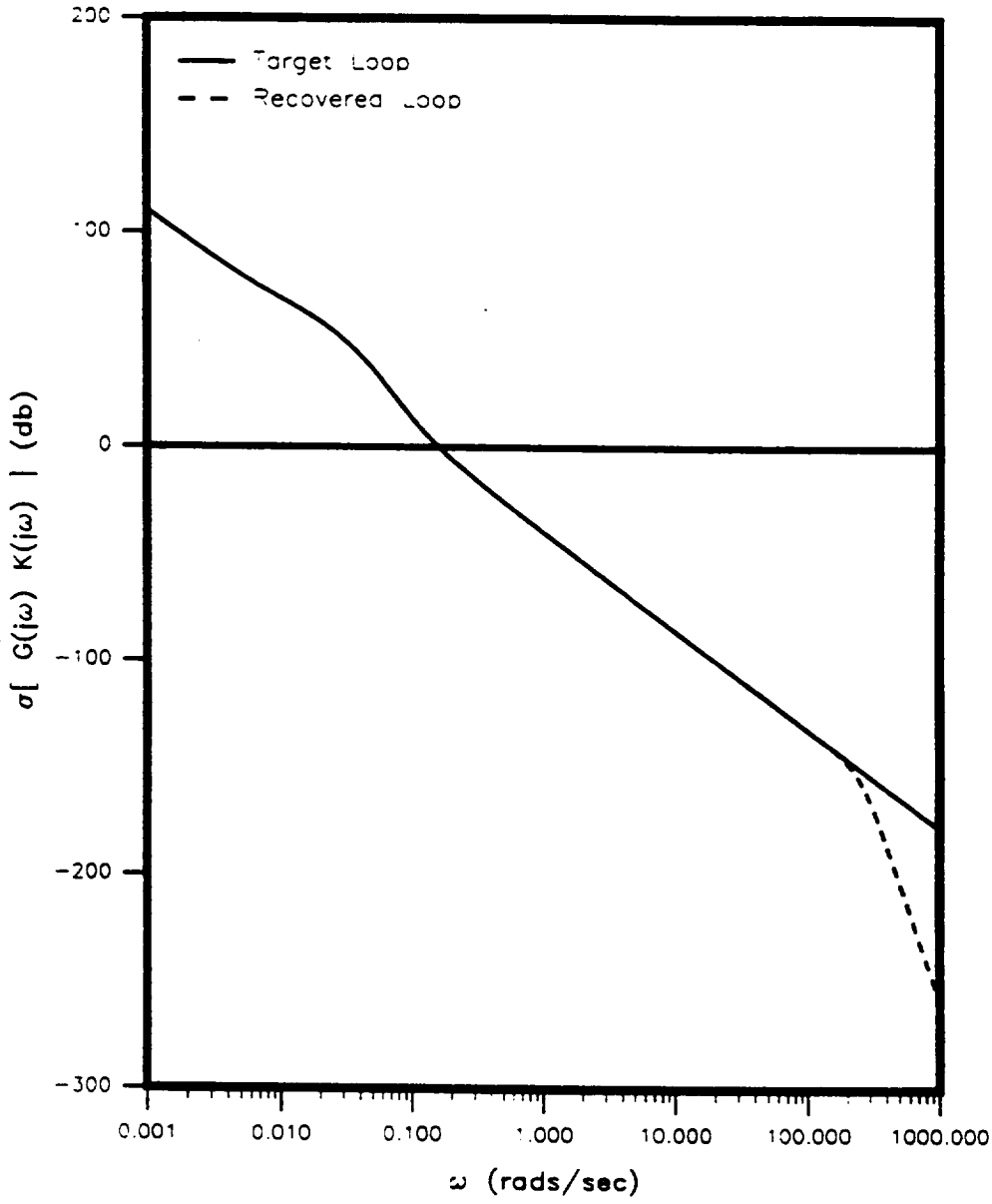

Figure 48. Singular Values of the Target Loop and the Actual Recovered Loop for the 110% of Full Power Linearized Reference Model.

and

$$\mathbf{C}(j\omega) = [\mathbf{I} + \mathbf{G}(j\omega)\,\mathbf{K}(j\omega)]^{-1}\,[\mathbf{G}(j\omega)\,\mathbf{K}(j\omega)]\,. \tag{115}$$

The singular values of the sensitivity transfer function matrix for the 80% and 110% of full power linearized reference models are plotted in Figures 49 and 50. In Figures 49 and 50, the maximum singular values of the sensitivity transfer function for the 80% and 100% of full power linearized reference models are -3.333×10^{-7} db and -6.457×10^{-6} db,respectively. Hence, the condition set by Equation (112) is satified by the actual system.

The singular values of the closed-loop transfer function matrix for the 80% and 110% of full power linearized reference models are shown in Figures 51 and 52. In Figures 51 and 52, the maximum singular values of the closed-loop transfer function for the 80% and 110% of full power linearized reference models are 3.826 db and 3.434 db, respectively. Therefore, Equation (113) is satisfied, and the designed system will not amplify the disturbances, or become unstable to multiplicative modeling errors reflected at the plant output.

Thus, from the above analysis it is observed that the linear compensators retain several of the properties guaranteed by the LQG/LTR method.

V.3 Gain-Scheduling of the External Controllers

As it was outlined in previous chapters, linearized reference models of the SNPS are obtained at several operating points covering its entire operating range. A linear compensator is designed for each linearized reference model of the SNPS, such that

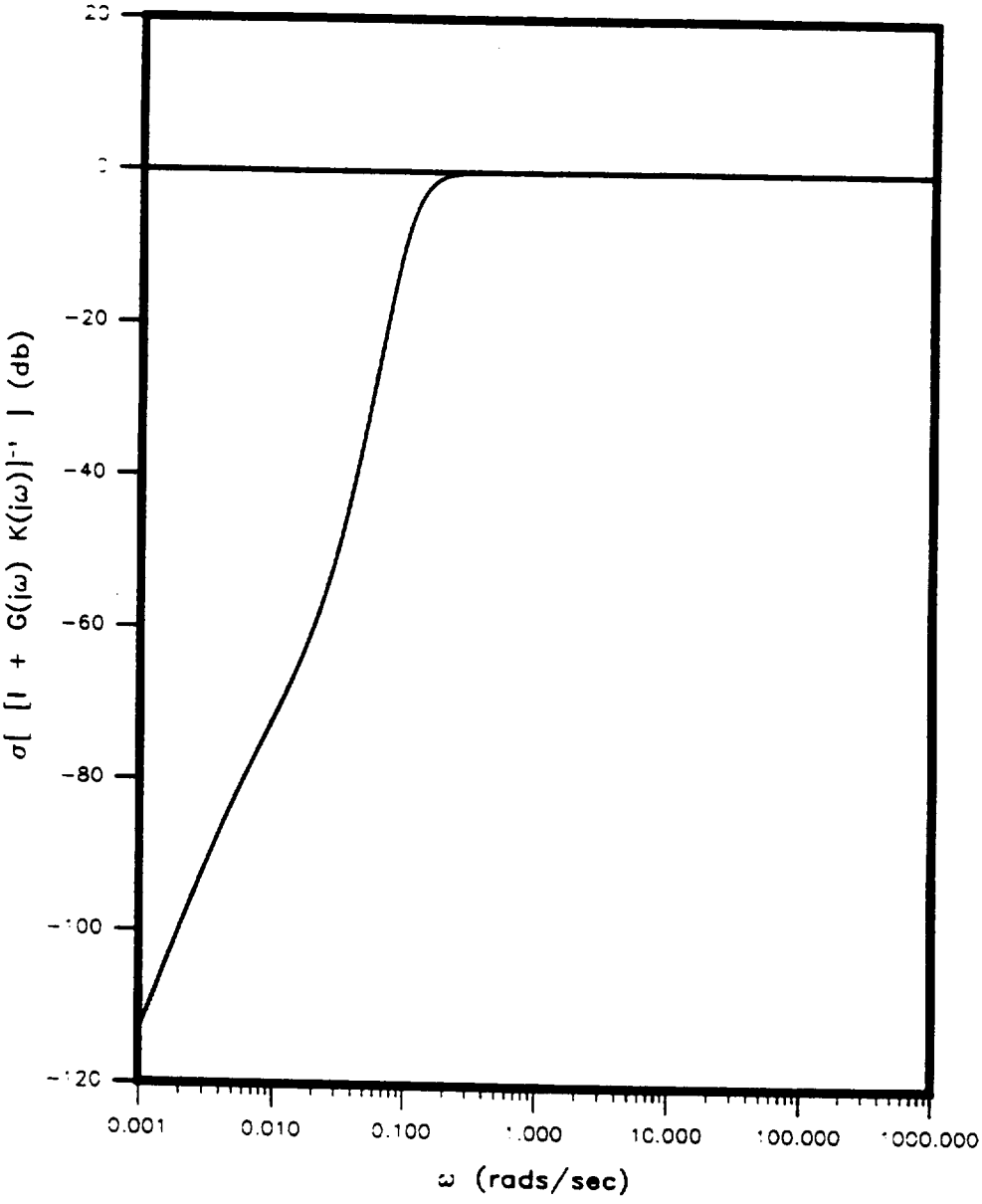

Figure 49. Singular Values of $[\mathbf{I} + \mathbf{G}(j\omega)\,\mathbf{K}(j\omega)]^{-1}$ for the 80% of Full Power Linearized Reference Model.

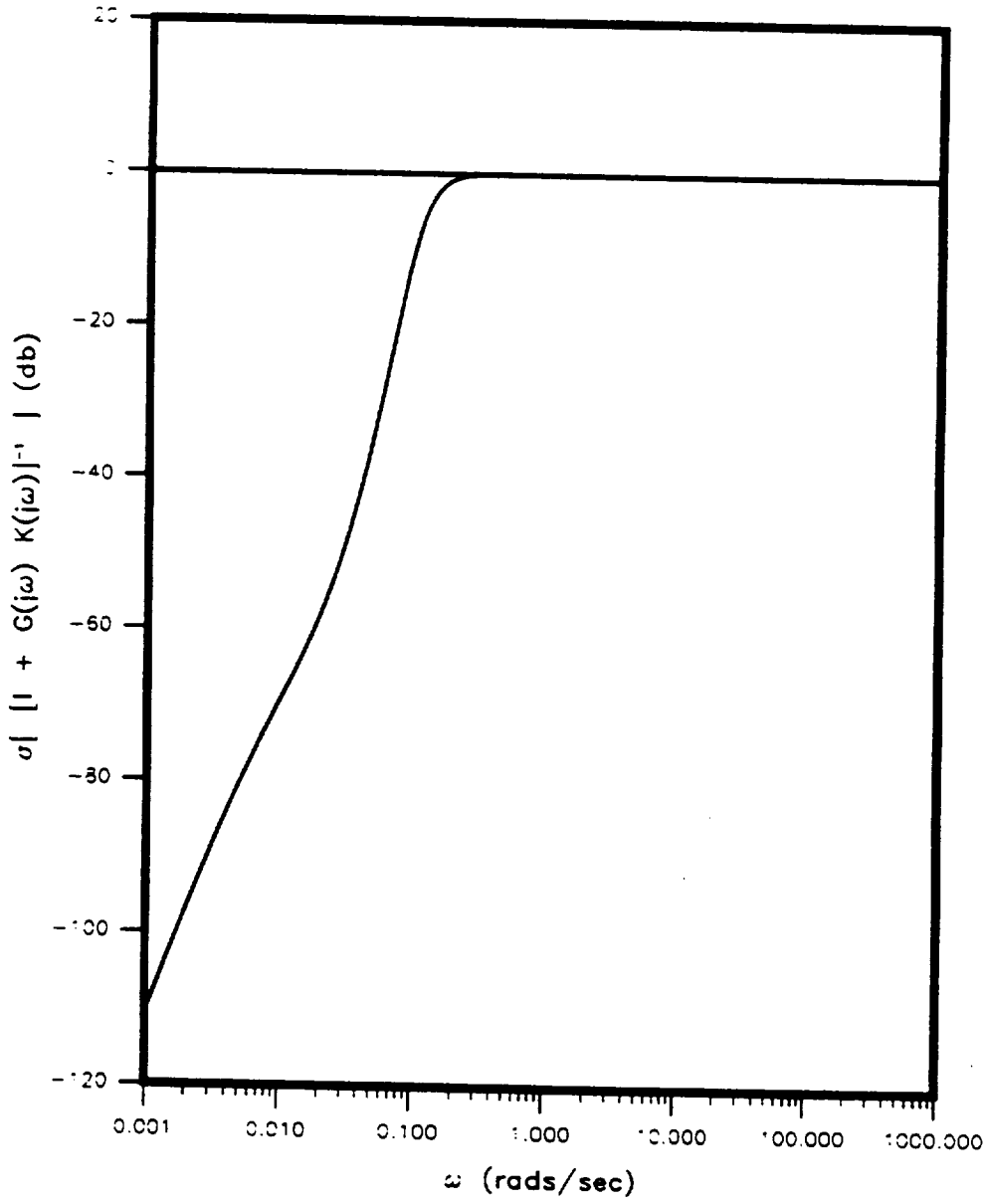

Figure 50. Singular Values of $[\mathbf{I} + \mathbf{G}(j\omega)\,\mathbf{K}(j\omega)]^{-1}$ for the 110% of Full Power Linearized Reference Model.

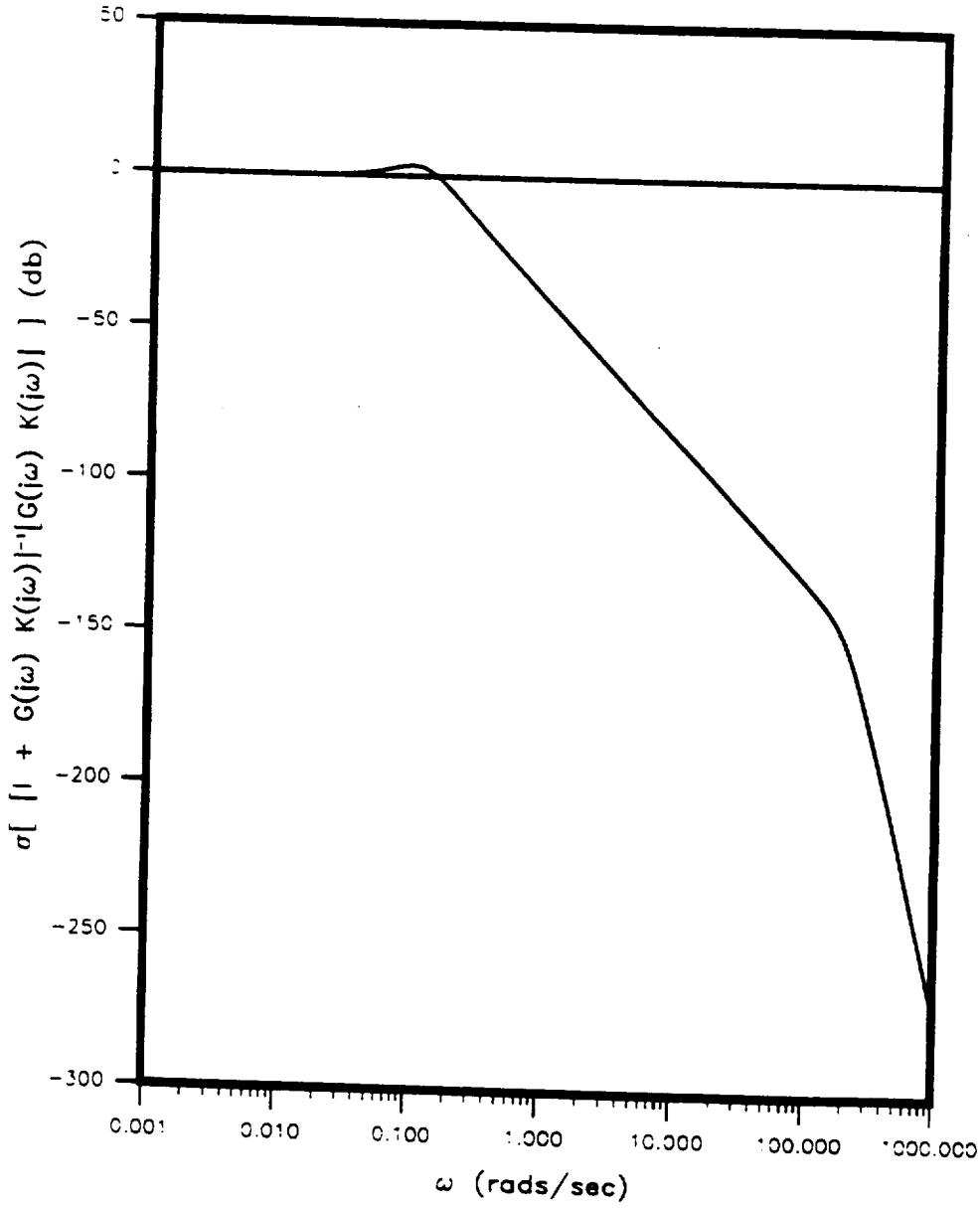

Figure 51. Singular Values of $[\mathbf{I} + \mathbf{G}(j\omega)\,\mathbf{K}(j\omega)]^{-1}\,[\mathbf{G}(j\omega)\,\mathbf{K}(j\omega)]$ for the 80% of Full Power Linearized Reference Model.

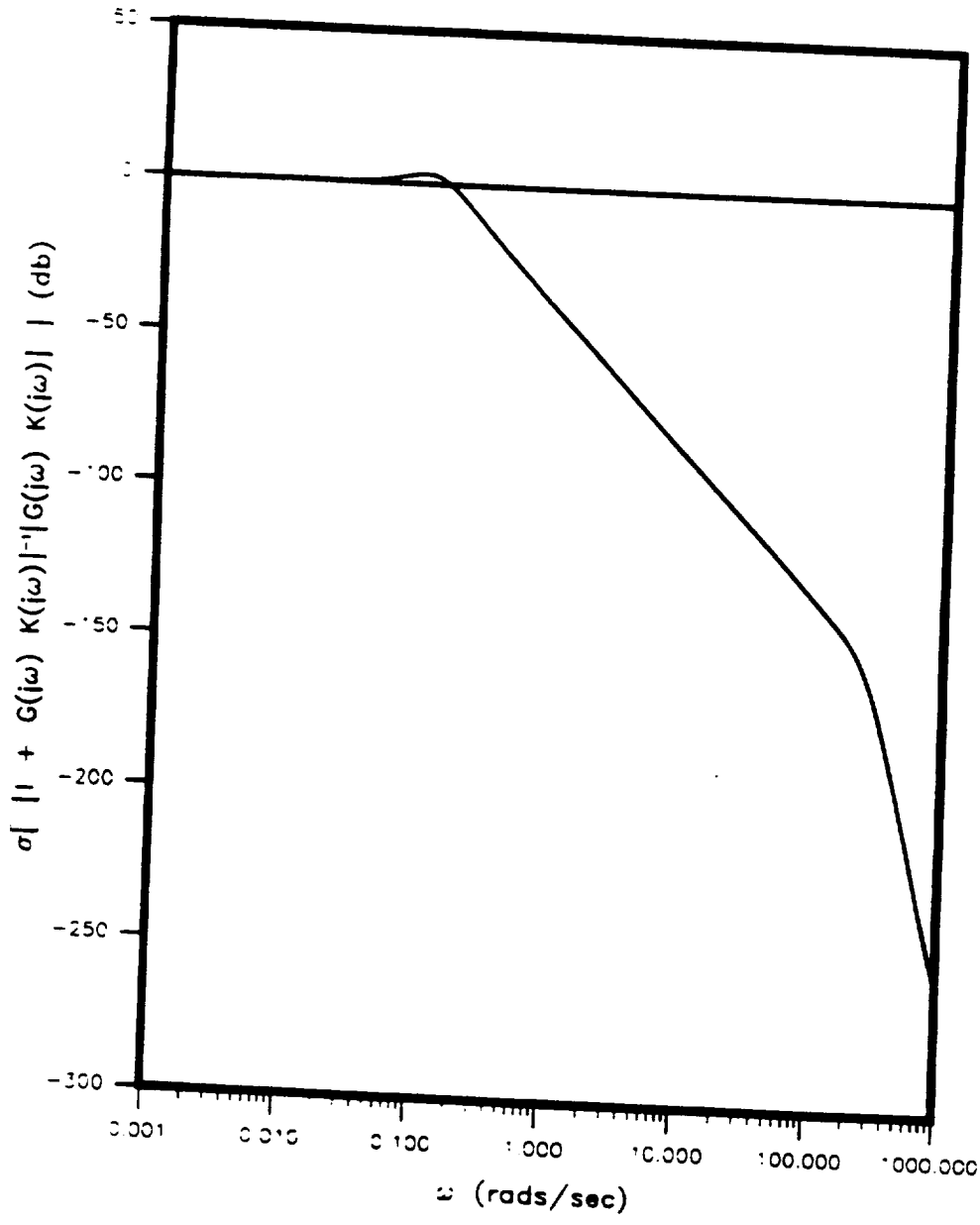

Figure 52. Singular Values of $[\mathbf{I} + \mathbf{G}(j\omega)\,\mathbf{K}(j\omega)]^{-1}\,[\mathbf{G}(j\omega)\,\mathbf{K}(j\omega)]$ for the 110% of Full Power Linearized Reference Model.

when perturbed about its operating points the feedback system is nominally stable, it exhibits desired nominal performance, and some stability robustness. The technique by which the gains of the linear compensators are interpolated (scheduled) between these operating points in order to obtain a single nonlinear compensator that is valid for the entire operating range of the SNPS is known as gain-scheduling. It can be shown that, even though the overall gain scheduled compensator need not have any of the nice properties of each of the linear time-invariant compensators, the time-varying compensator will have guaranteed robust stability and nominal performance provided that [24]: 1) the gain-scheduling variable does not vary rapidly with time, and, 2) the small nonlinearities of the system are not captured by the scheduling variable.

The gain vectors **H** and **G** obtained for each of the linear compensators (corresponding to different power levels) are valid for deviations for which the linear model is valid. In the gain-scheduling process these linear compensators, designed to control the SNPS within a finite range about its respective equilibrium points, are scheduled to arrive at a single compensator. This scheduled compensator can eliminate the transients which could result from modeling errors, while continuously regulating the load voltage of the SNPS.

As the operating point about which the nonlinear reference model was linearized was the system electrical power, the gain-scheduling variable used in this thesis is the electrical power generated by the system itself. This variable is also closely related to the reactor thermal power, which is indicative of the system's changing conditions.

In addition to gain vectors, the elements of the system matrices (i.e. $\mathbf{A}, \mathbf{B}, \mathbf{C}, \mathbf{L}$) are also fitted as a function of P_e because the compensator uses the system dynamics explicitly. Therefore, the compensator state equations can be expressed as:

$$\dot{\mathbf{z}}_c(t) = \mathbf{A}_c(P_e)\,\mathbf{z}_c(t) + \mathbf{B}_c(P_e)\,\left(y(t) - y_{ref}\right)(t) \quad ; \mathbf{z}_c(t) \in \Re^n, \tag{116}$$

$$\delta u(t) = \mathbf{C}_c(P_e)\,\mathbf{z}_c(t), \tag{117}$$

where $\mathbf{z}_c(t)$ are the states of the compensator and $\mathbf{A}_c, \mathbf{B}_c, \mathbf{C}_c$ are the compensator system matrices with elements that are functions of P_e. The input to the compensator is the filtered feedback loop error (the filtered load voltage deviation), and the compensator output is the SNPS input (the external reactivity). The compensator matrices are expressed as follows:

$$\mathbf{A}_c(P_e) = \mathbf{A}(P_e) - \mathbf{B}(P_e)\,\mathbf{G}(P_e) - \mathbf{H}(P_e)\,\mathbf{C}(P_e), \tag{118}$$

$$\mathbf{B}_c(P_e) = -\mathbf{H}(P_e), \tag{119}$$

$$\mathbf{C}_c(P_e) = -\mathbf{G}(P_e), \tag{120}$$

where, $\mathbf{A}(P_e)$, $\mathbf{B}(P_e)$, and $\mathbf{C}(P_e)$ are the scheduled reference model matrices given in Appendix B, and $\mathbf{G}(P_e)$ and $\mathbf{H}(P_e)$ are the scheduled gain matrices given in Appendix E.

CHAPTER VI

COMPUTER SIMULATION RESULTS

VI.1 Introduction

In this chapter the main computer simulation results are presented. The measurable state and output responses of the SNPS using a linear controller are presented along with the control input (external reactivity) generated by the linear compensator. In the evaluation of the gain-scheduled compensator, the simulations include the sensor (measurement) noise effects on the load voltage of the SNPS. Finally, robustness of the gain-scheduled compensator is investigated through simulations which take into account the drifts in the system's operating parameters, allowing investigation of the extent to which these variations affect the load-following capabilities of the overall system.

VI.2 Evaluation of the Linear Controllers

In this section, the performance of the linear controllers is investigated via simulations of the SNPS's measurable state and the output responses to an external reactivity input generated by the controller to meet the demanded electrical power. As mentioned earlier, the measurable states of the SNPS model are the reactor neutron power, the core coolant inlet and exit temperatures and the total core coolant mass flow rate. The SNPS's controlled output is the load voltage.

Table 6. Description of the Controllers Used in the Simulations

Controller I	Uses the 100% of Full Power Linear Compensator
Controller II	Uses the 100% of Full Power Linear Compensator up to 120% of Full Power, then Switches to the 120% of Full Power Linear Compensator.
Controller III	Uses the 100% of Full Power Linear Compensator untill 80% of Full Power, then Switches to the 80% of Full Power Linear Compensator.

Figures 53 through 58 show the responses of the measured states and output of the integrated nonlinear SNPS model to a change in the reactivity generated by Controller I and Controller II corresponding to a step load change from 100% to 120% and from 120% to 150% of the full electrical power level. A description of the controllers used in the simulations are shown in Table 6.

Figure 53 compares the load voltage responses of the SNPS using Controller I and Controller II to a step load change from 100% to 120% and from 120% to 150% of full power and it demonstrates that the 100% of full power linear compensator alone is capable of regulating the load voltage at 100 Volts with less than 0.1% relative error.

Additionally, Figures 53 through 58 show that using Controller II instead of Controller I improves the voltage regulation and the state responses of the SNPS only slightly, therefore, it can be concluded that the validity range of Controller I (100% of full power linear compensator) extends up to and beyond 120% of the full power level.

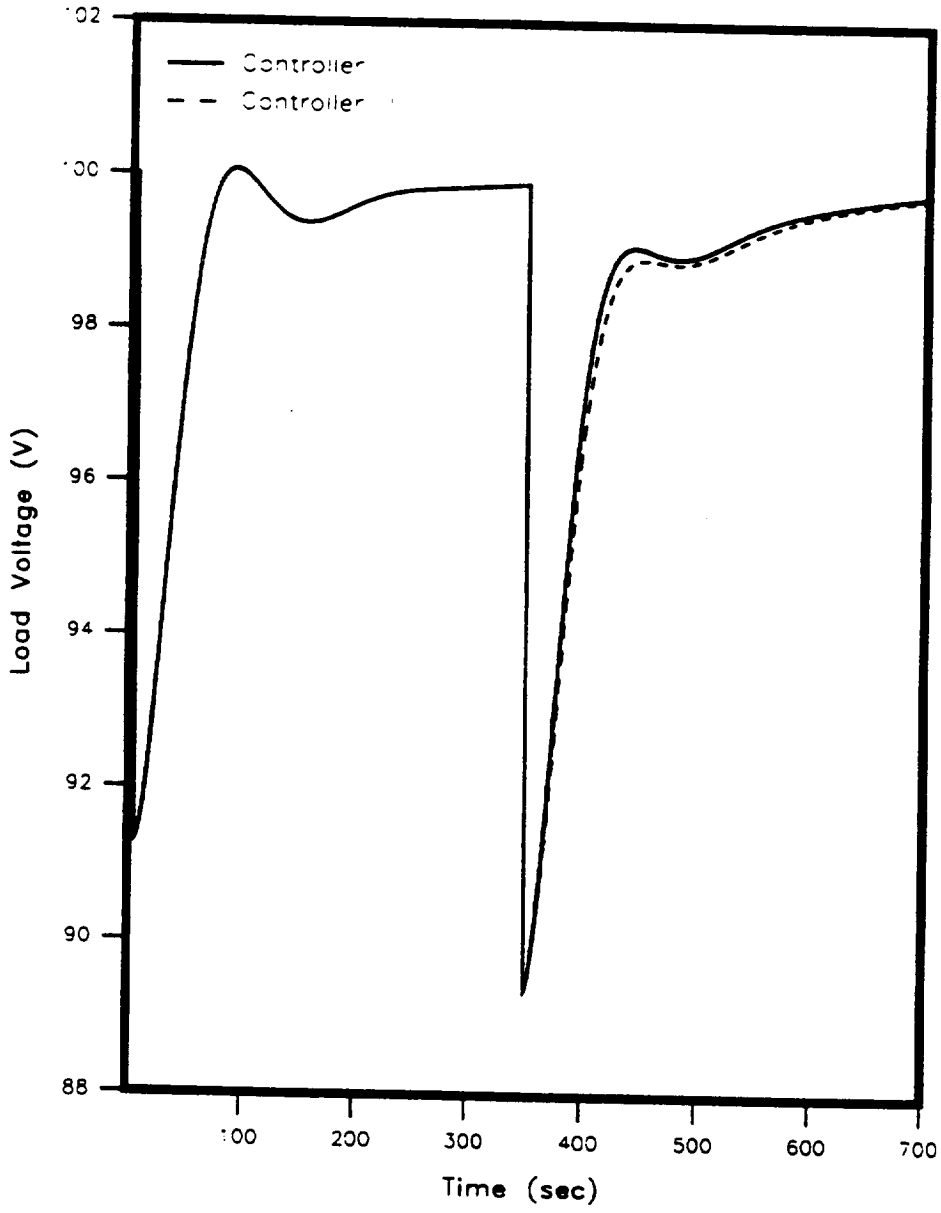

Figure 53. Load Voltage Responses for Controller I and Controller II Corresponding to a Load Change from 100% to 120% and from 120% to 150% of Full Power.

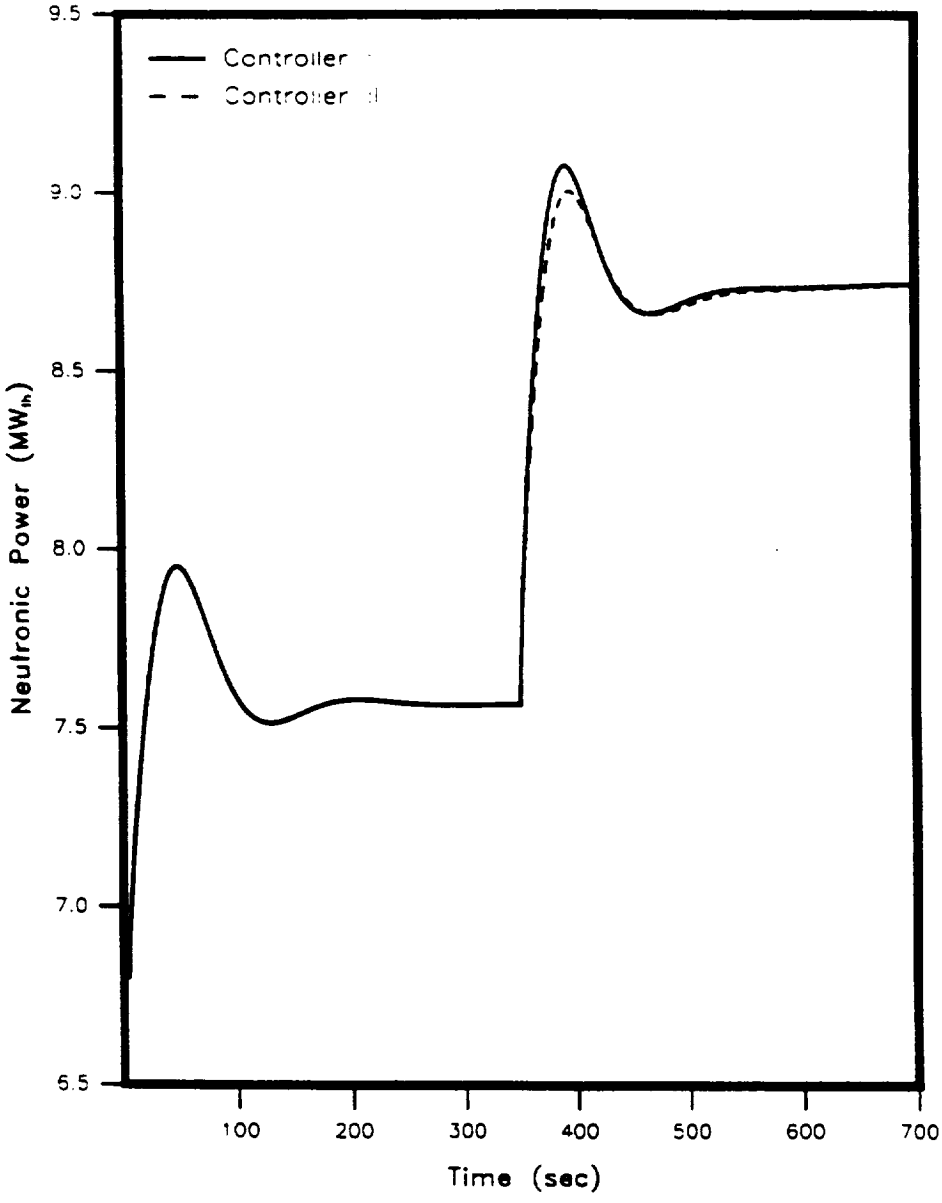

Figure 54. Neutronic Power Responses for Controller I and Controller II Corresponding to a Load Change from 100% to 120% and from 120% to 150% of Full Power.

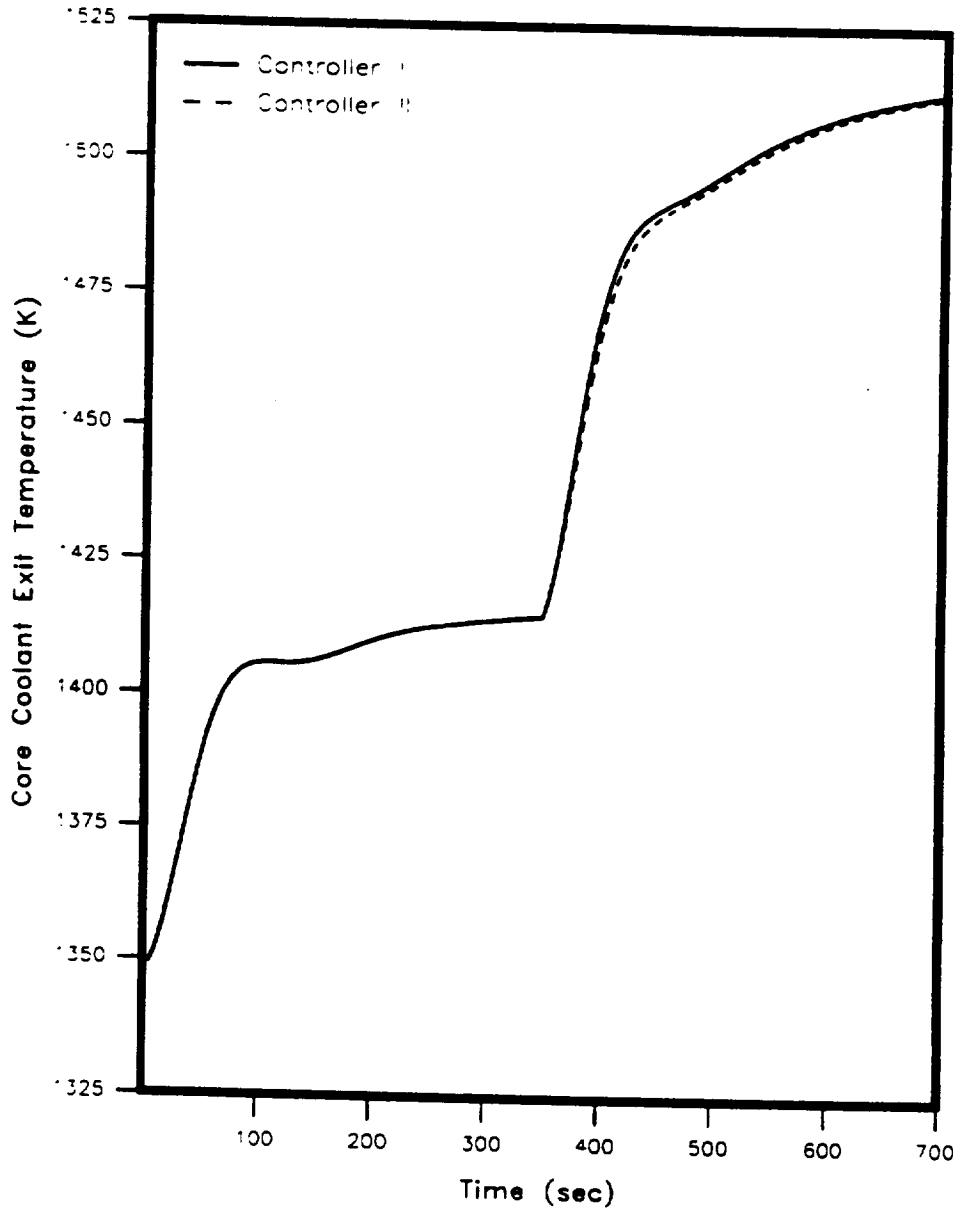

Figure 55. Core Coolant Exit Temperature Responses for Controller I and Controller II Corresponding to a Load Change from 100% to 120% and from 120% to 150% of Full Power.

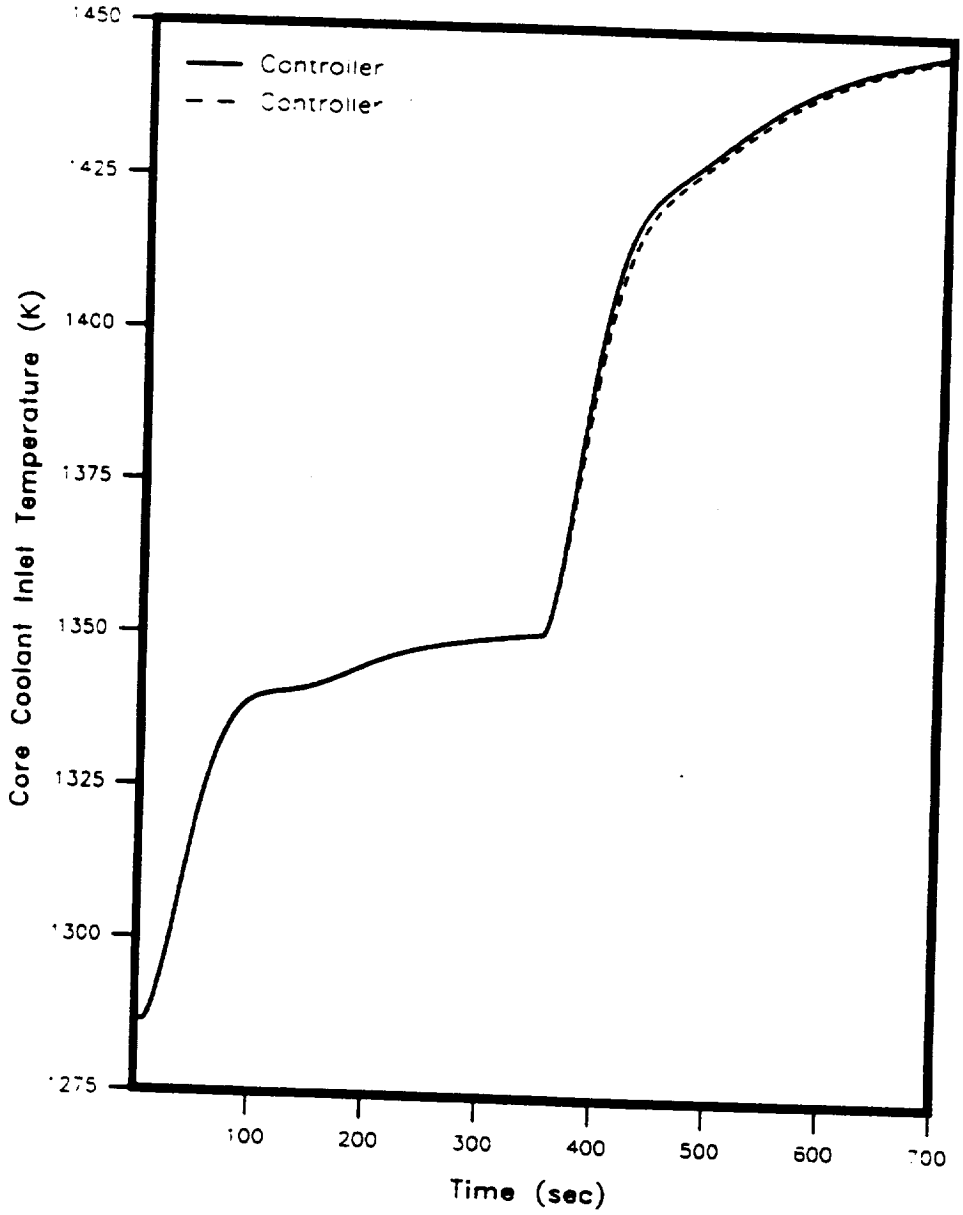

Figure 56. Core Coolant Inlet Temperature Responses for Controller I and Controller II Corresponding to a Load Change from 100% to 120% and from 120% to 150% of Full Power.

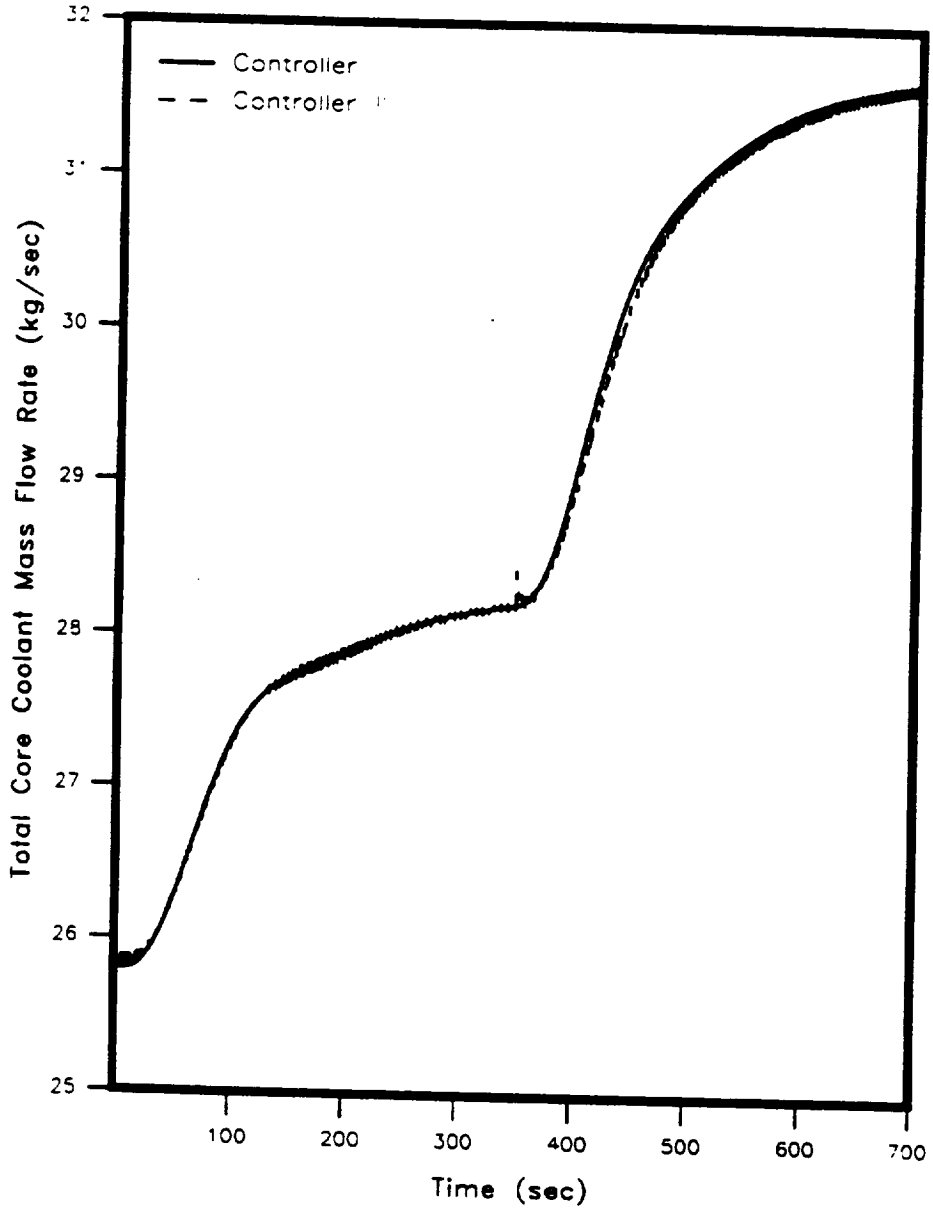

Figure 57. Total Core Coolant Mass Flow Rate Responses for Controller I and Controller II Corresponding to a Load Change from 100% to 120% and from 120% to 150% of Full Power.

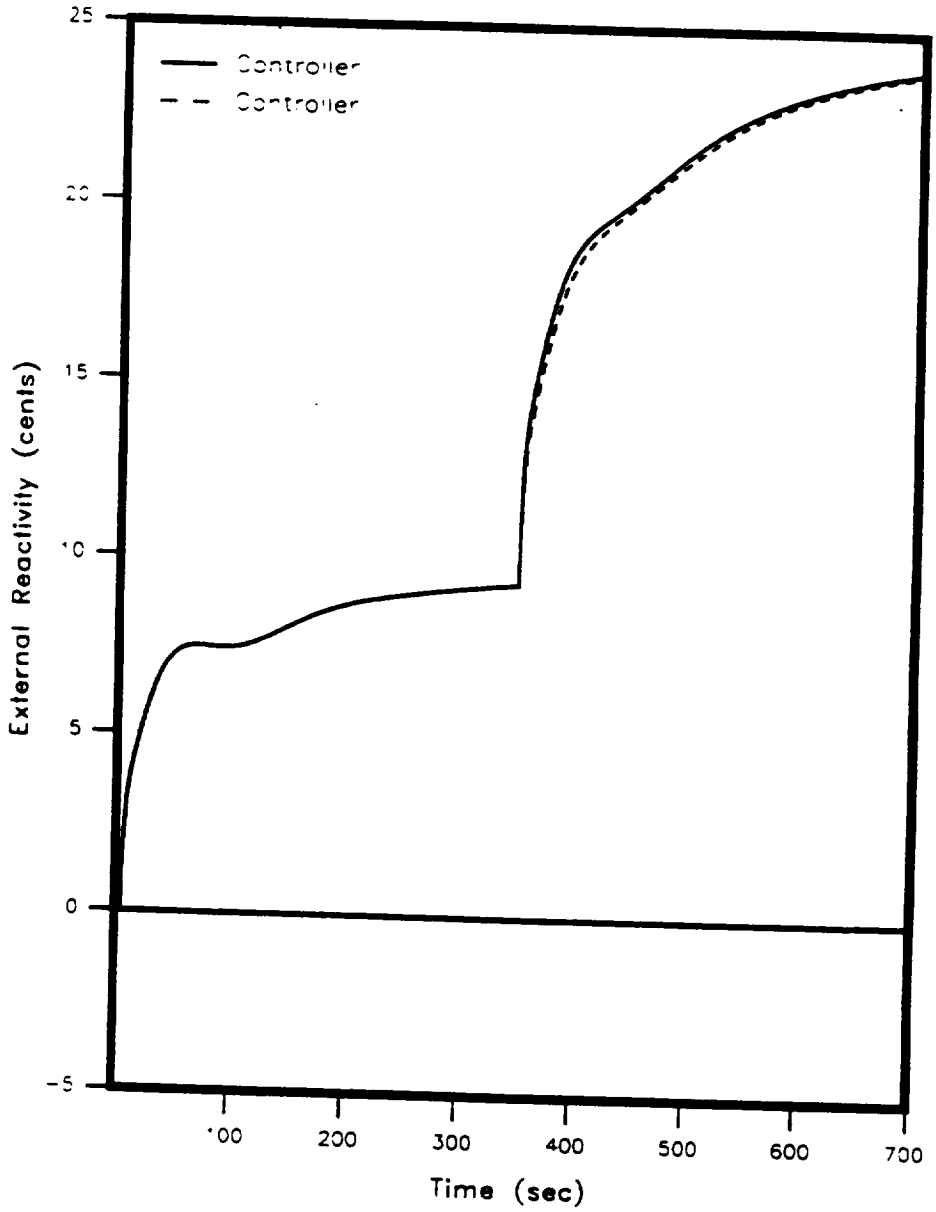

Figure 58. External Reactivity Generated by Controller I and Controller II Corresponding to a Load Change from 100% to 120% and from 120% to 150% of Full Power.

Figures 59 through 64 show the responses of the measured outputs of the integrated nonlinear SNPS model controlled by Controller I and Controller III for a step load change from 100% to 80% and from 80% to 50% of the full electrical power level. From Figure 59 it can be seen from this figure that both Controller I and Controller II are capable of regulating the voltage at about 100 Volts. It is apperant from Figures 59 through 64 that using Controller III does not improve the responses of SNPS over using Controller I. However, in the presence of sensor noise incorporated to the load voltage output of the SNPS, a gain-scheduled compensator can be needed for voltage regulation.

The above simulations show that the linear compensators can successfully regulate the load voltage at about 100 Volts.

VI.3 Performance Evaluation of the Gain-Scheduled Controller

This section investigates the performance of the gain-scheduled compensator in the presence of sensor noise which is modeled as white Gaussian noise with a variance of 0.1. Figures 65 through 71 show the responses of the measured states and output of the nonlinear SNPS model controlled by the gain-scheduled compensator to a load change from 100% to 150% of the full electrical power level. The noisy measured load voltage output of the system in Figure 65, does not give any implications of the load-following of the SNPS using the gain-scheduled compensator, therefore, this measured load voltage is smoothened out by a filter augmented to the input of the compensator as mentioned in the earlier chapters, to obtain a filtered load voltage

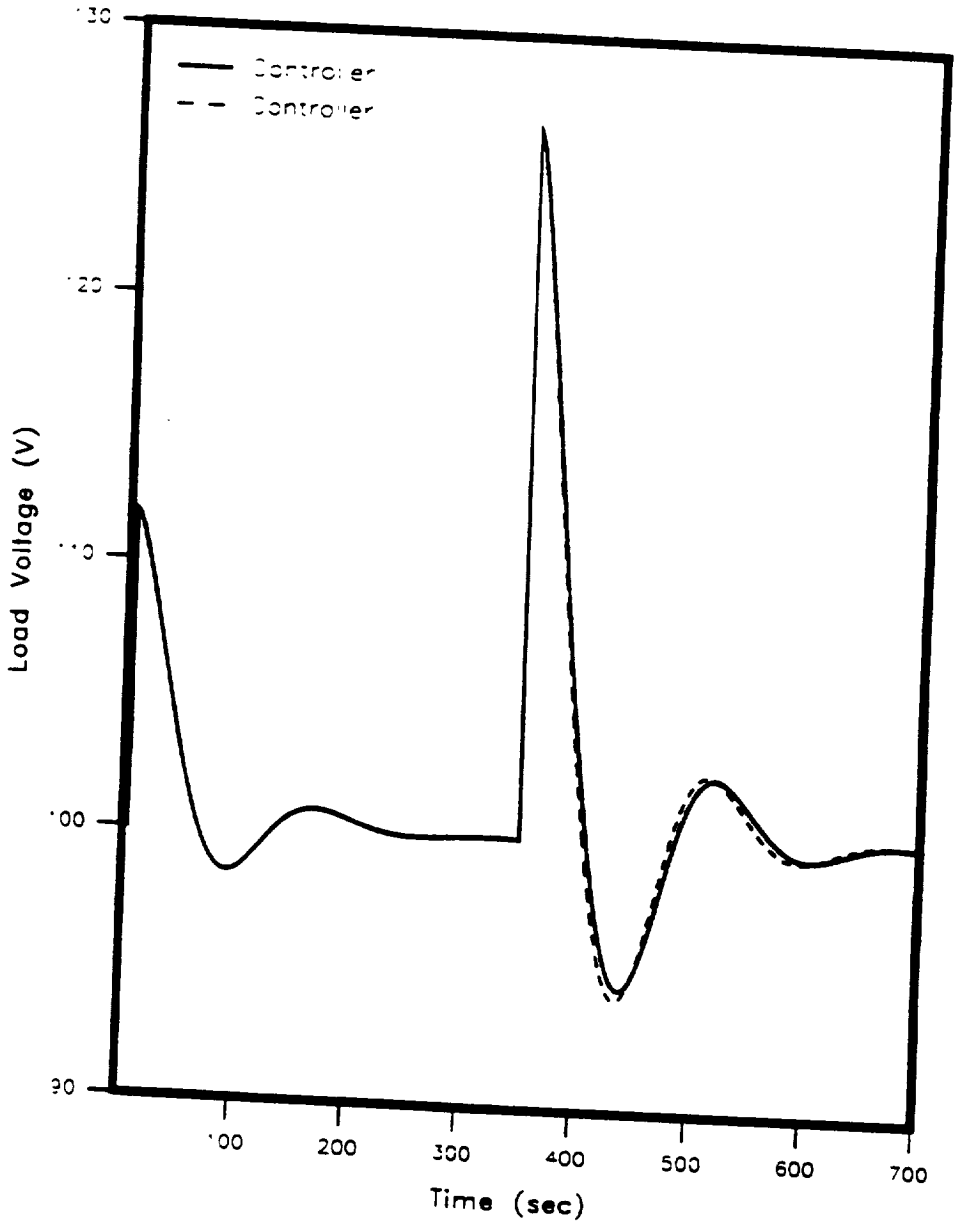

Figure 59. Load Voltage Responses for Controller I and Controller III Corresponding to a Load Change from 100% to 80% and from 80% to 50% of Full Power.

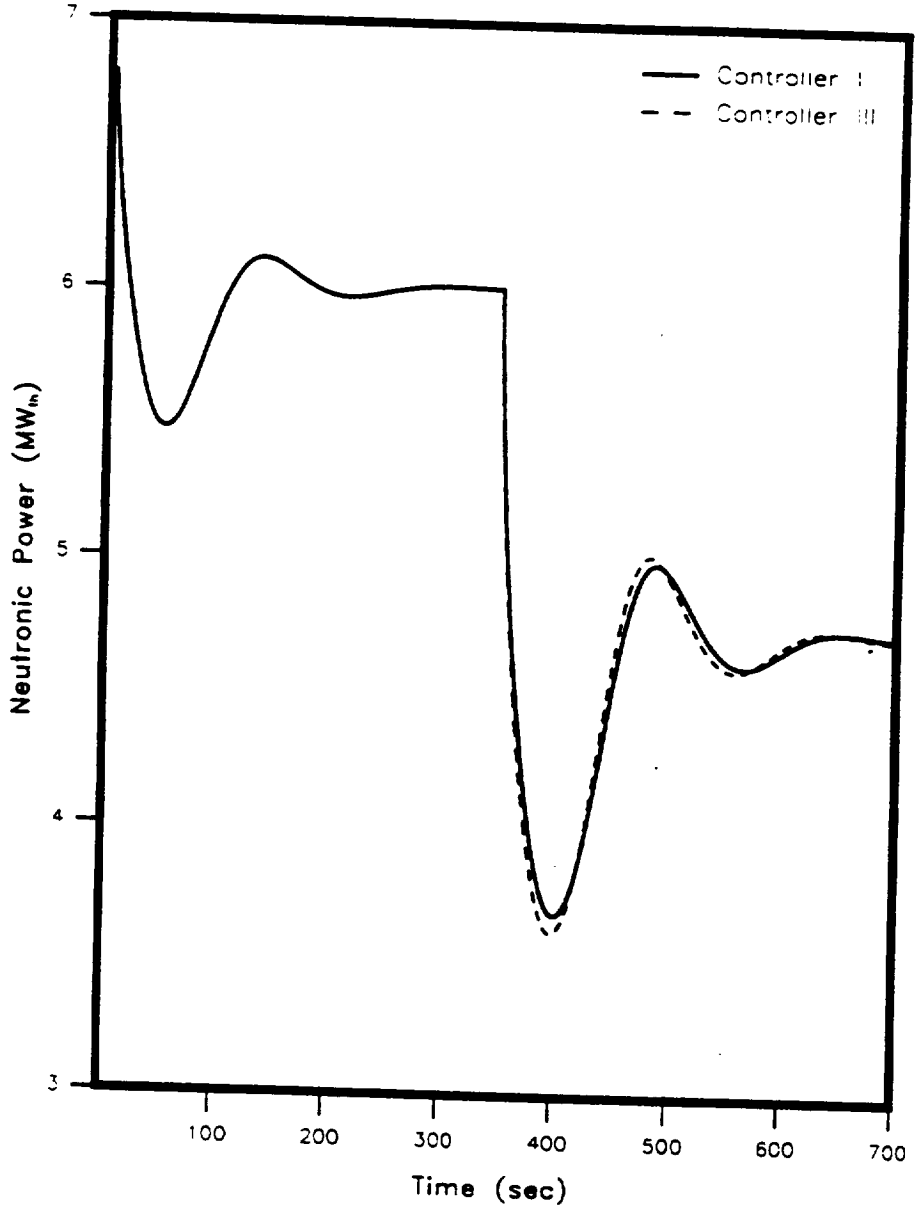

Figure 60. Neutronic Power Responses for Controller I and Controller III Corresponding to a Load Change from 100% to 80% and from 80% to 50% of Full Power.

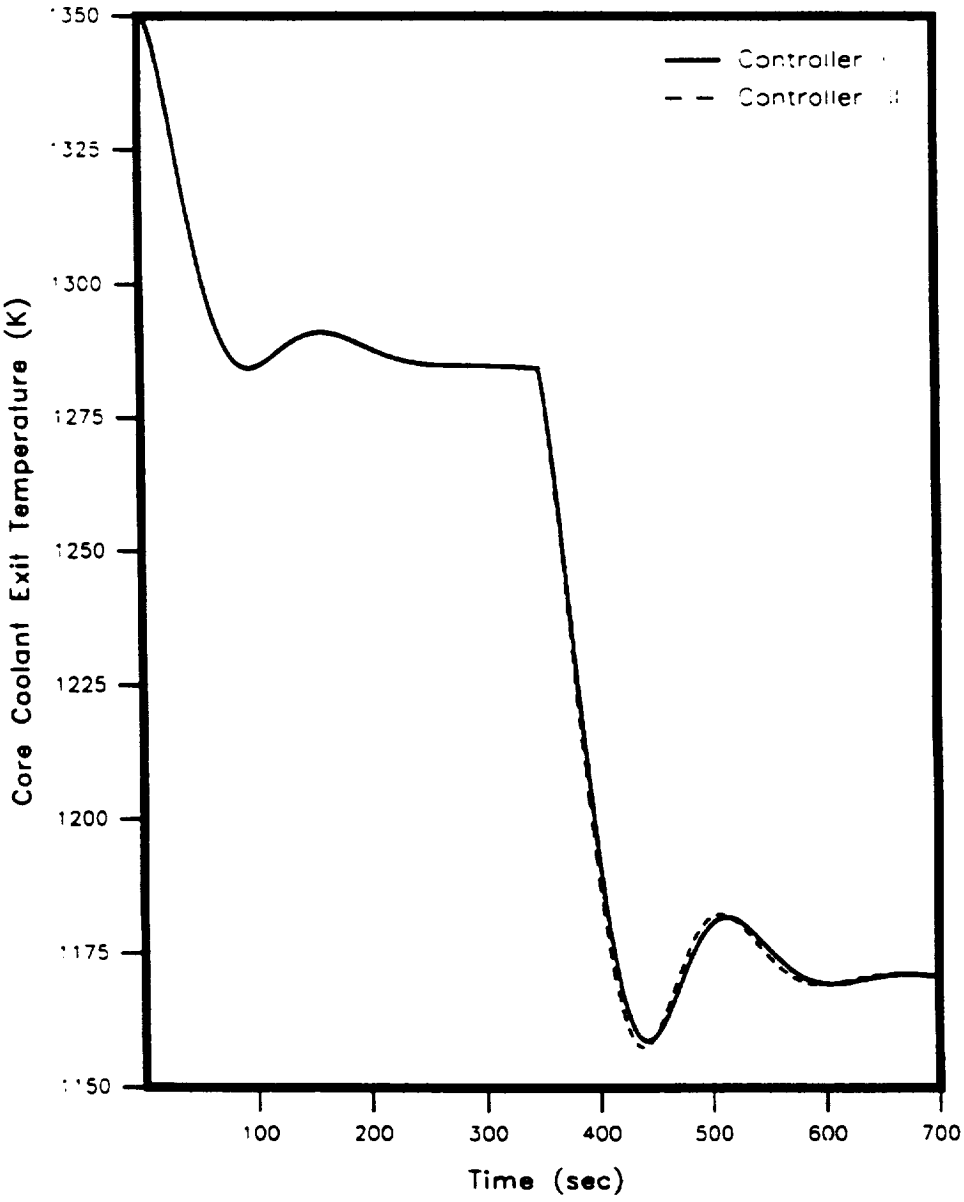

Figure 61. Core Coolant Exit Temperature Responses for Controller I and Controller III Corresponding to a Load Change from 100% to 80% and from 80% to 50% of Full Power.

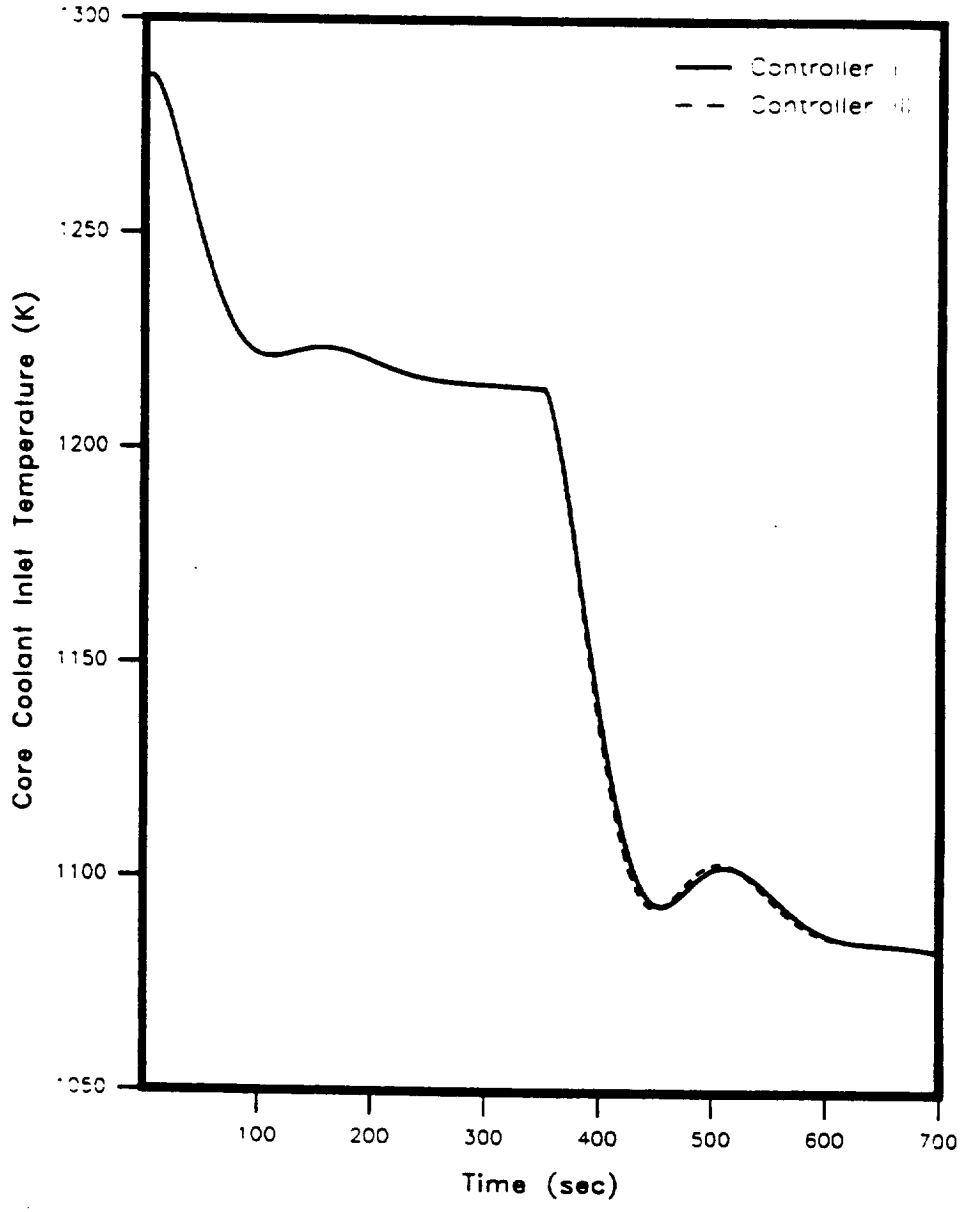

Figure 62. Core Coolant Inlet Temperature Responses Controller I and Controller III Corresponding to a Load Change from 100% to 80% and from 80% to 50% of Full Power.

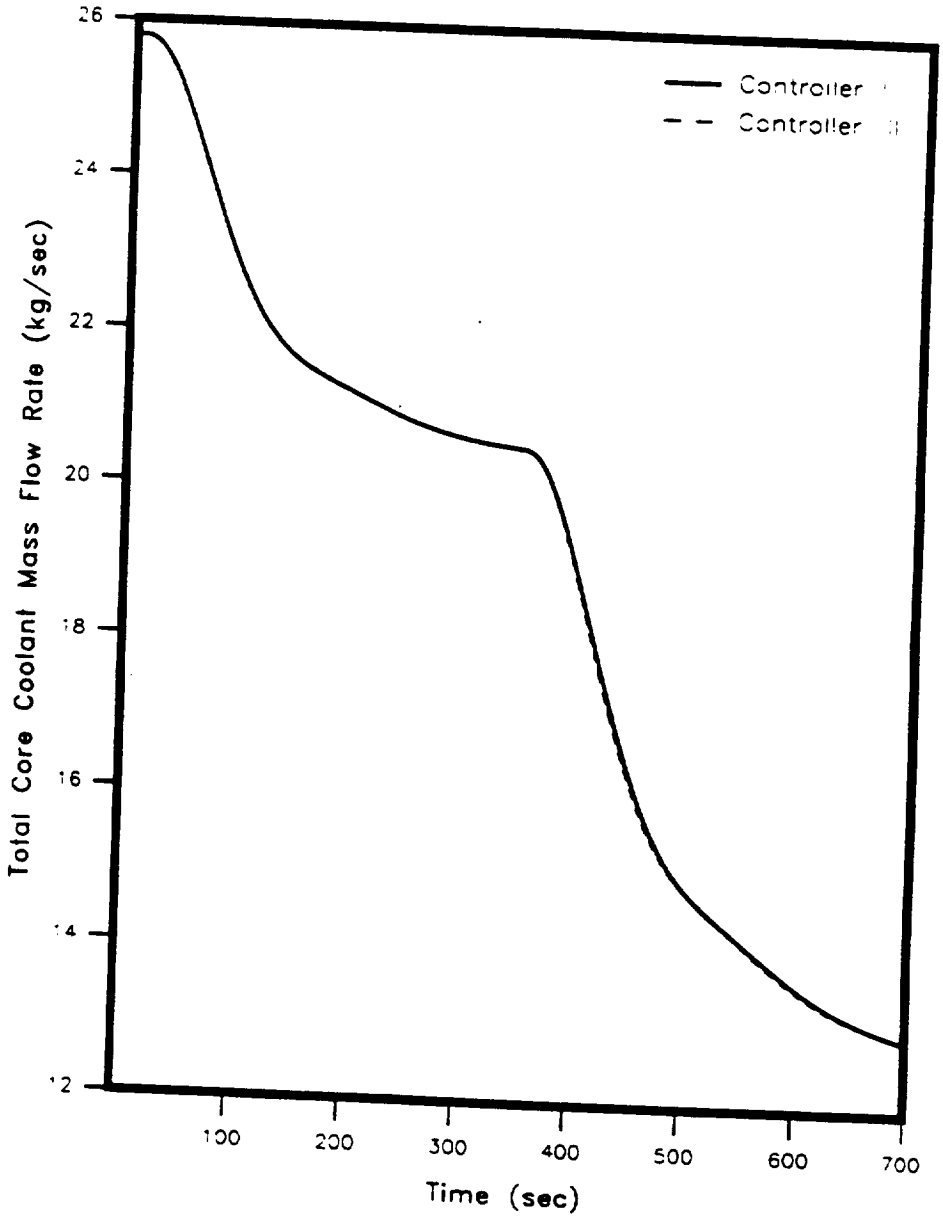

Figure 63. Total Core Coolant Mass Flow Rate Responses for Controller I and Controller III to a Load Change from 100% to 80% and from 80% to 50% of Full Power.

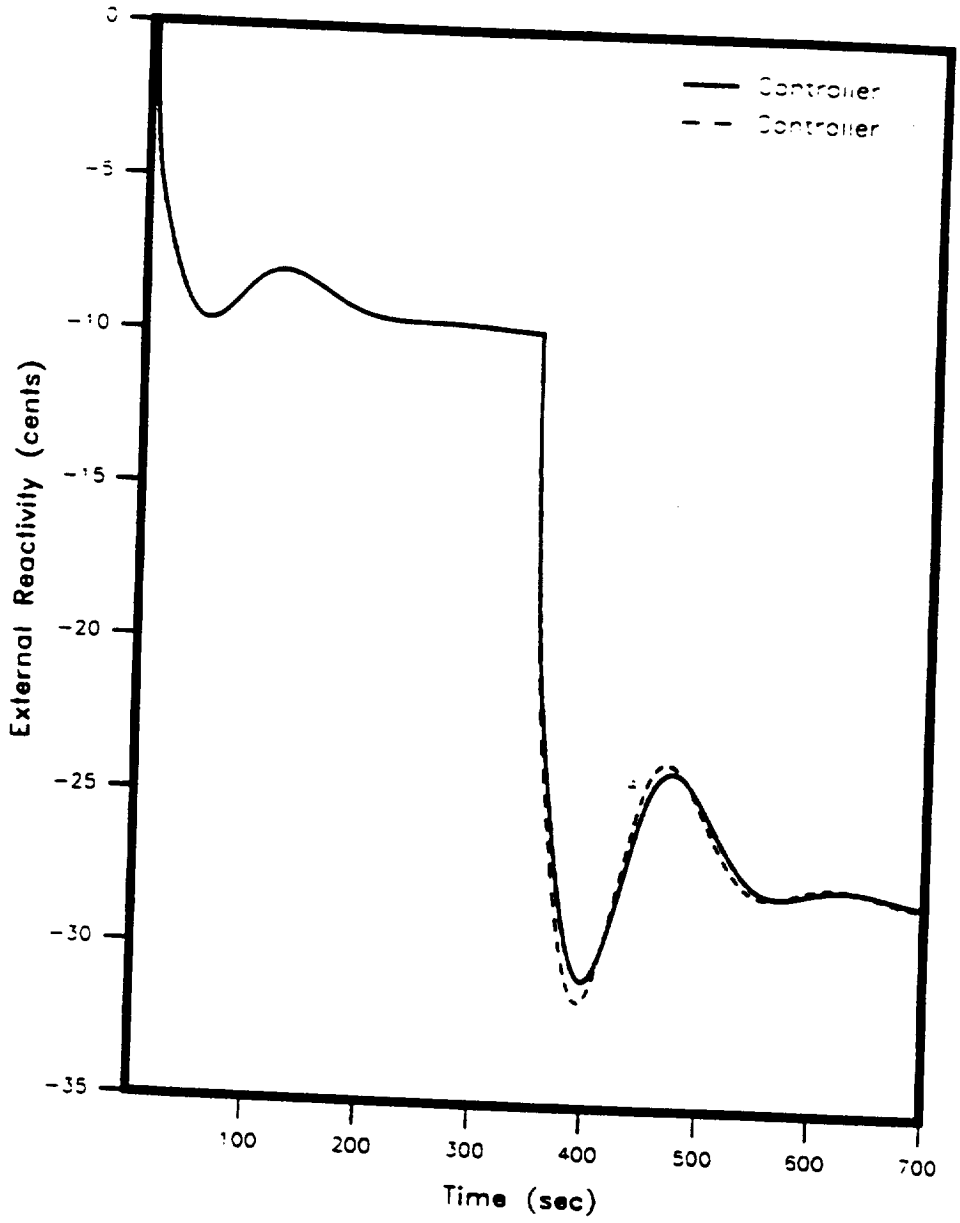

Figure 64. External Reactivity Generated by Controller I and Controller III Corresponding to a Load Change from 100% to 80% and from 80% to 50% of Full Power.

regulation error. Figure 66 shows the filtered load voltage regulation error response of the SNPS to a change in the reactivity generated by the Gain-Scheduled Compensator Corresponding to a load change from 100% to 120%, and from 120% to 150% of full power. It can be seen from this figure that the gain-scheduled compensator can regulate the load voltage with almost zero filtered load voltage regulation error despite noisy sensor readings.

Figures 72 through 77 show the responses of the measured states and output of the nonlinear SNPS model to an external reactivity change generated by the gain-scheduled compensator which corresponds to a load change from 100% to 80% and from 80% to 50% of the full electrical power level. Figure 72 shows that the filtered load voltage regulation error is stabilized at about zero by the gain-scheduled Compensator for a load change from 100% to 80% and from 80% 50% of full power.

It can be concluded from the simulations that the gain-scheduled compensator can regulate the load voltage at 100 Volts in the presence of sensor noise with zero steady-state regulation error.

VI.4 Robustness of the Gain-Scheduled Controller

Figures 78 through 89 show the responses of the measured states and output of the integrated nonlinear SNPS model to a change in reactivity generated by the gain-scheduled compensator corresponding to a step load change from 100% to 120% and from 120% to 150% of the full electrical power level for various cases of variations in the fuel feedback reactivity coefficient. In these figures three cases are investigated:

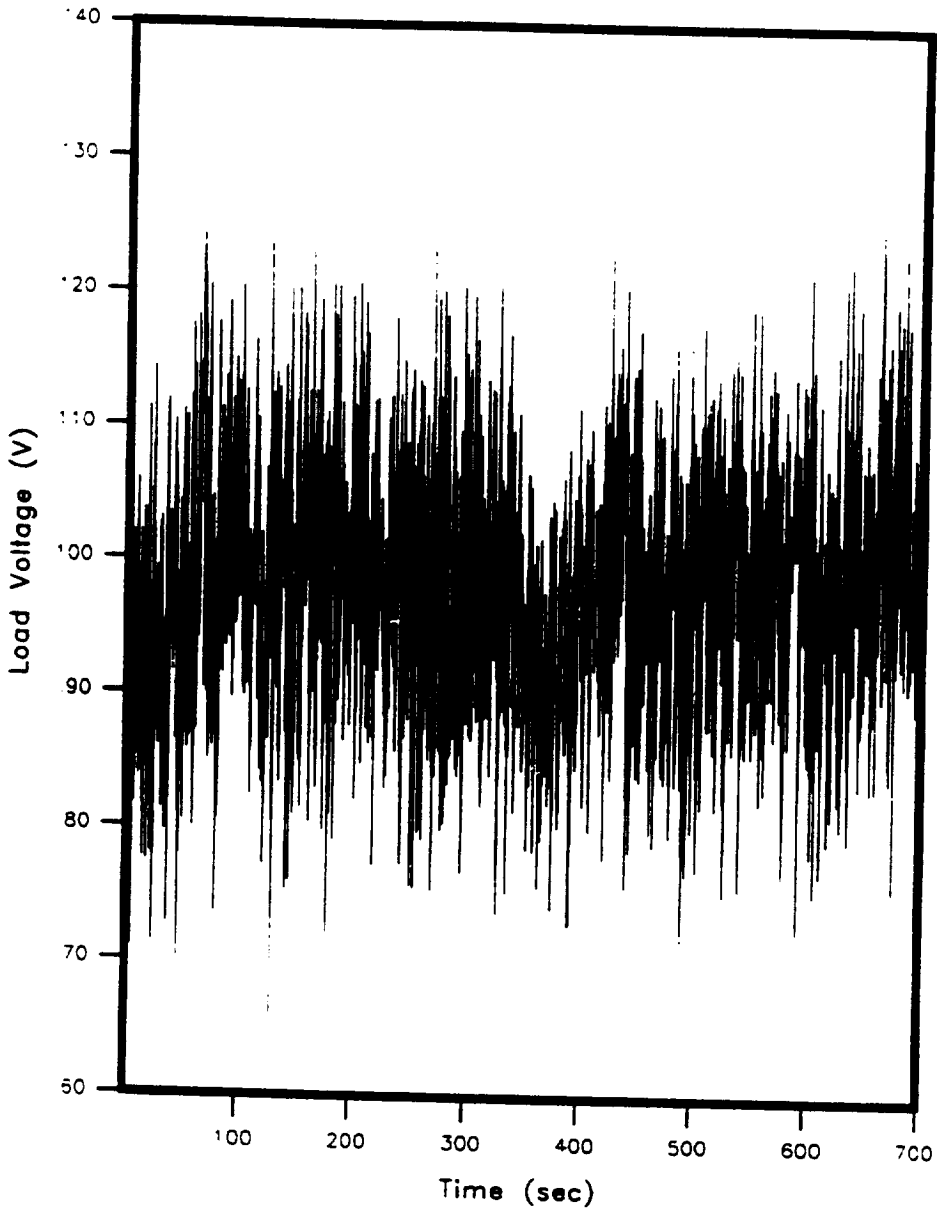

Figure 65. Load Voltage Response for the Gain-Scheduled Compensator Corresponding to to a Load Change from 100% to 120% and from 120% to 150% of Full Power.

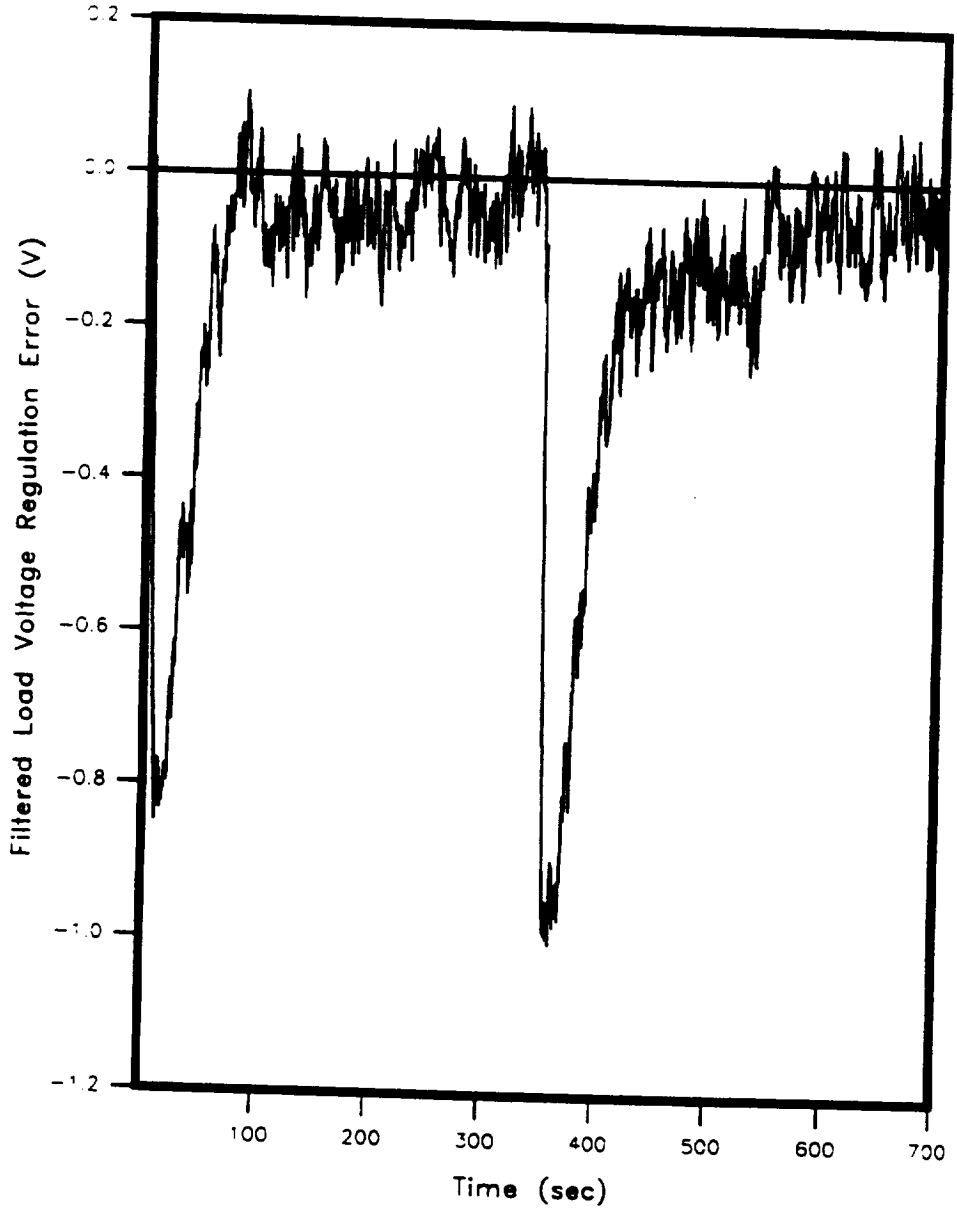

Figure 66. Filtered Load Voltage Regulation Error for the Gain-Scheduled Compensator Corresponding to to a Load Change from 100% to 120% and from 120% to 150% of Full Power.

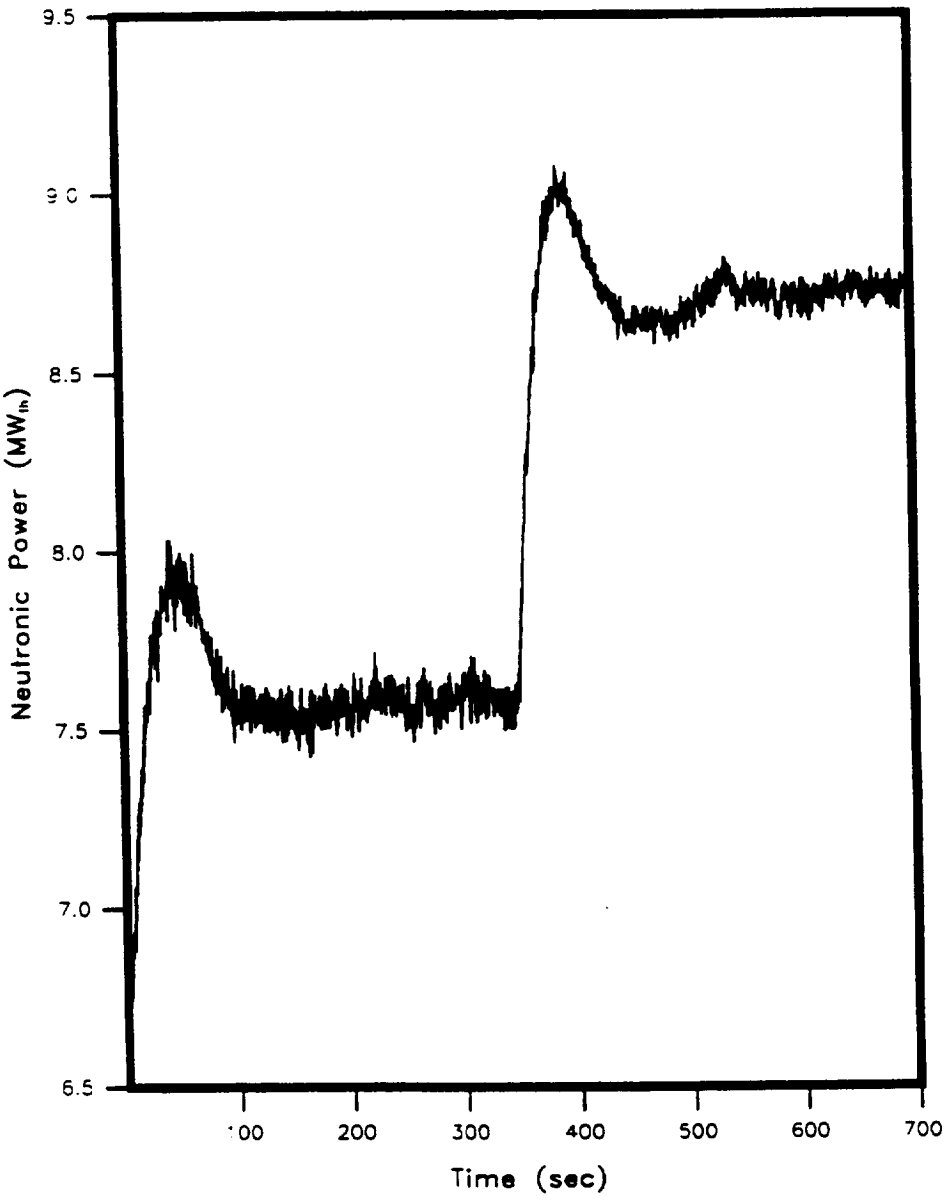

Figure 67. Neutronic Power Response for the Gain-Scheduled Compensator Corresponding to a Load Change from 100% to 120% and from 120% to 150% of Full Power.

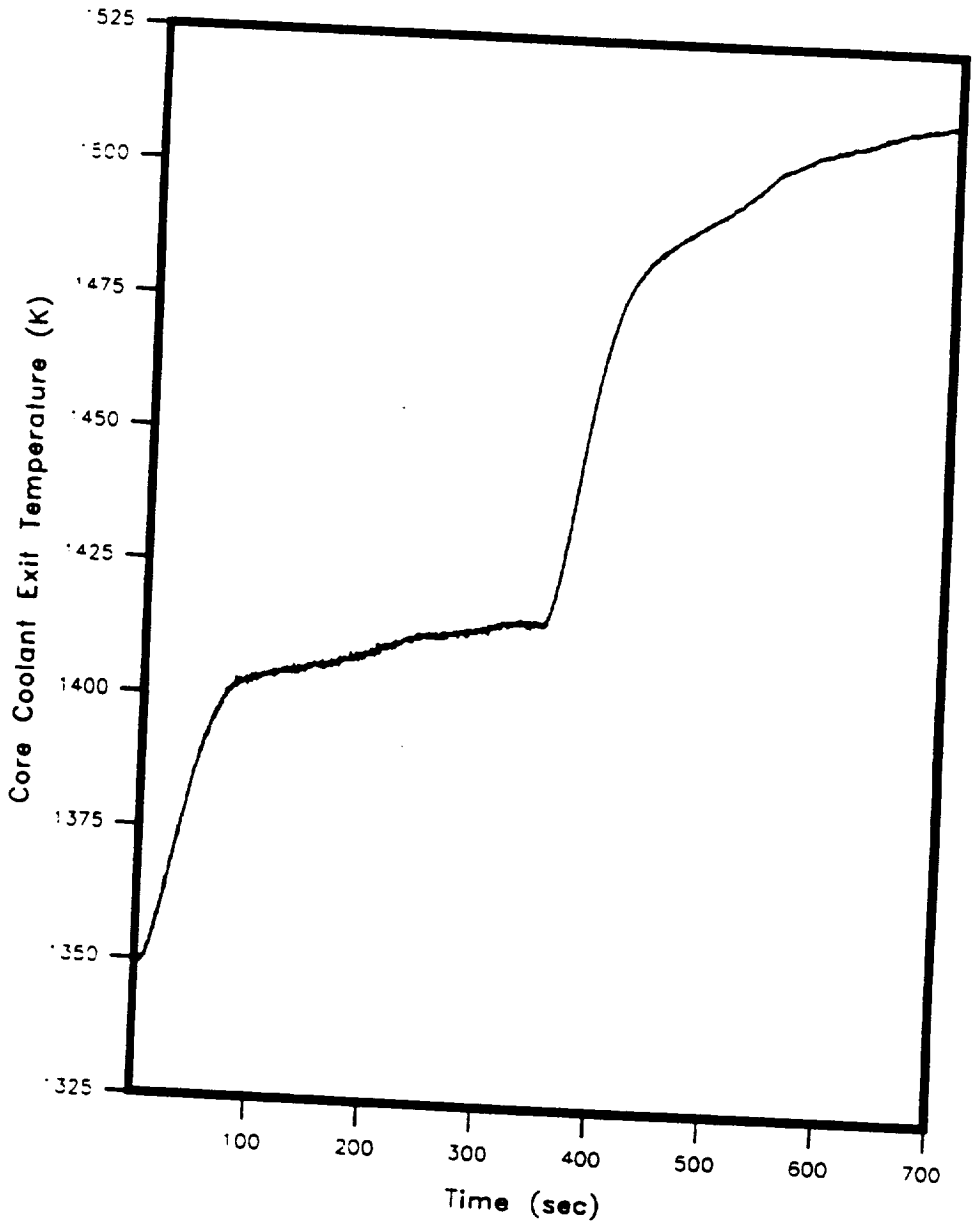

Figure 68. Core Coolant Exit Temperature Response for the Gain-Scheduled Compensator Corresponding to a Load Change from 100% to 120% and from 120% to 150% of Full Power.

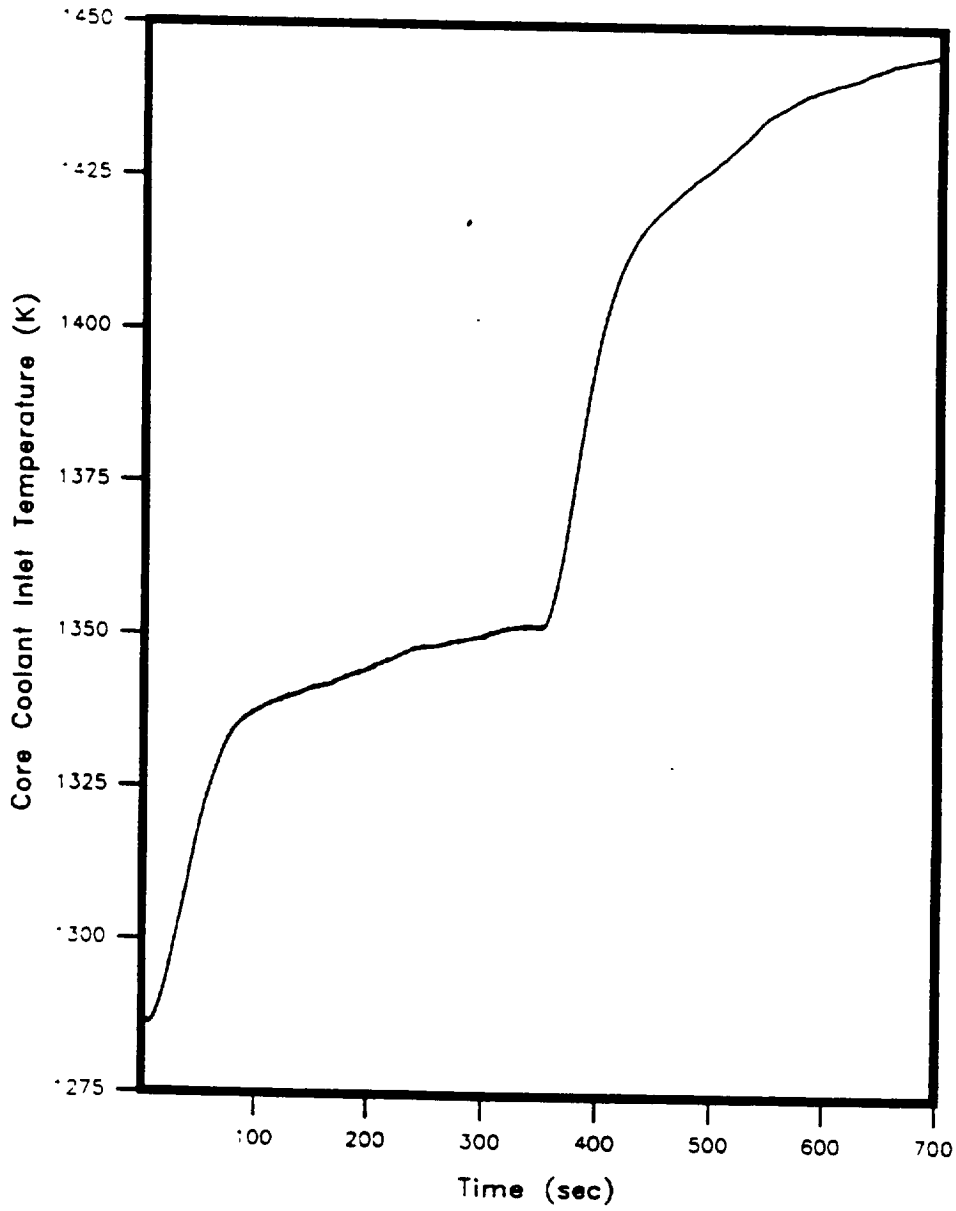

Figure 69. Core Coolant Inlet Temperature Response for the Gain-Scheduled Compensator Corresponding to a Load Change from 100% to 120% and from 120% to 150% of Full Power.

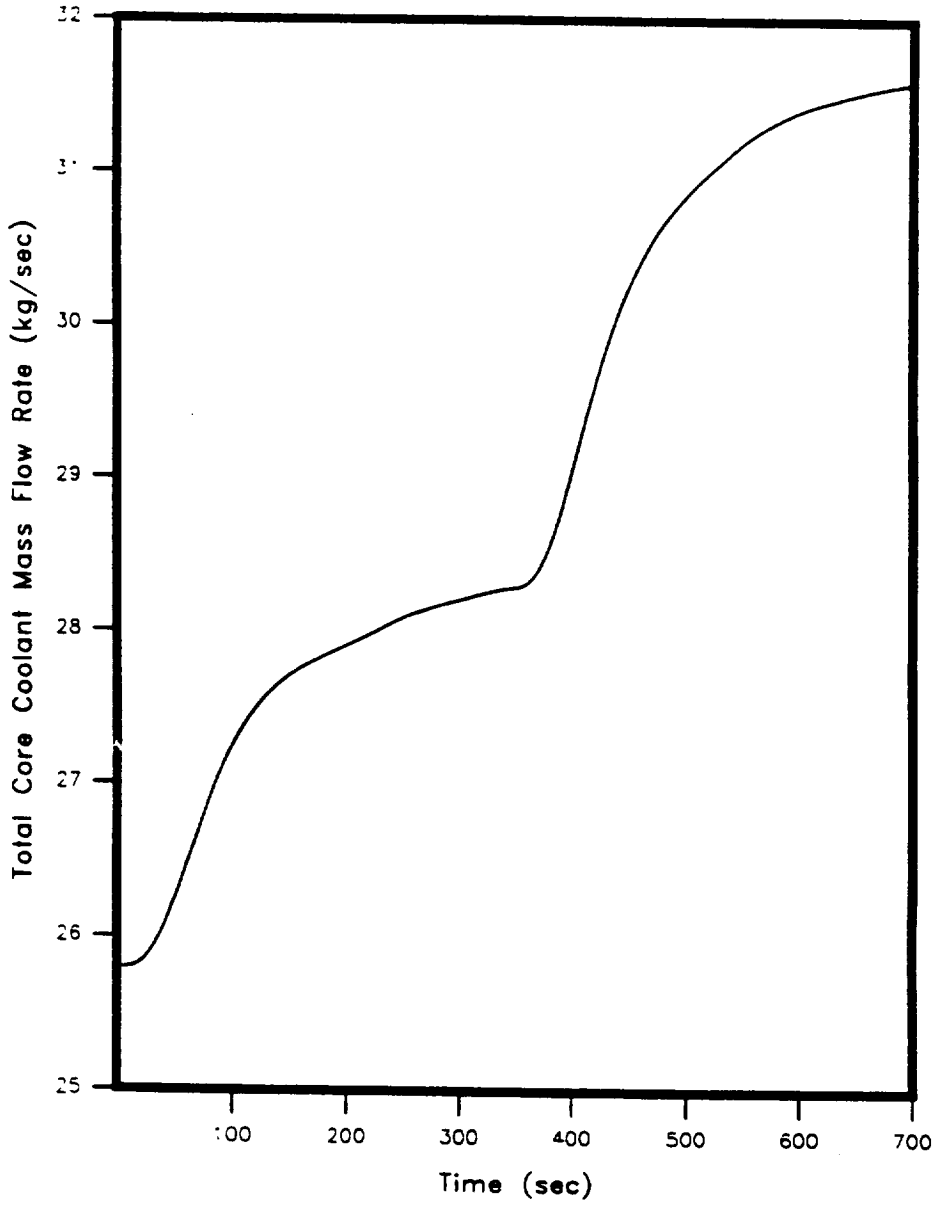

Figure 70. Total Core Coolant Mass Flow Rate Response for the Gain-Scheduled Compensator Corresponding to a Load Change from 100% to 120% and from 120% to 150% of Full Power.

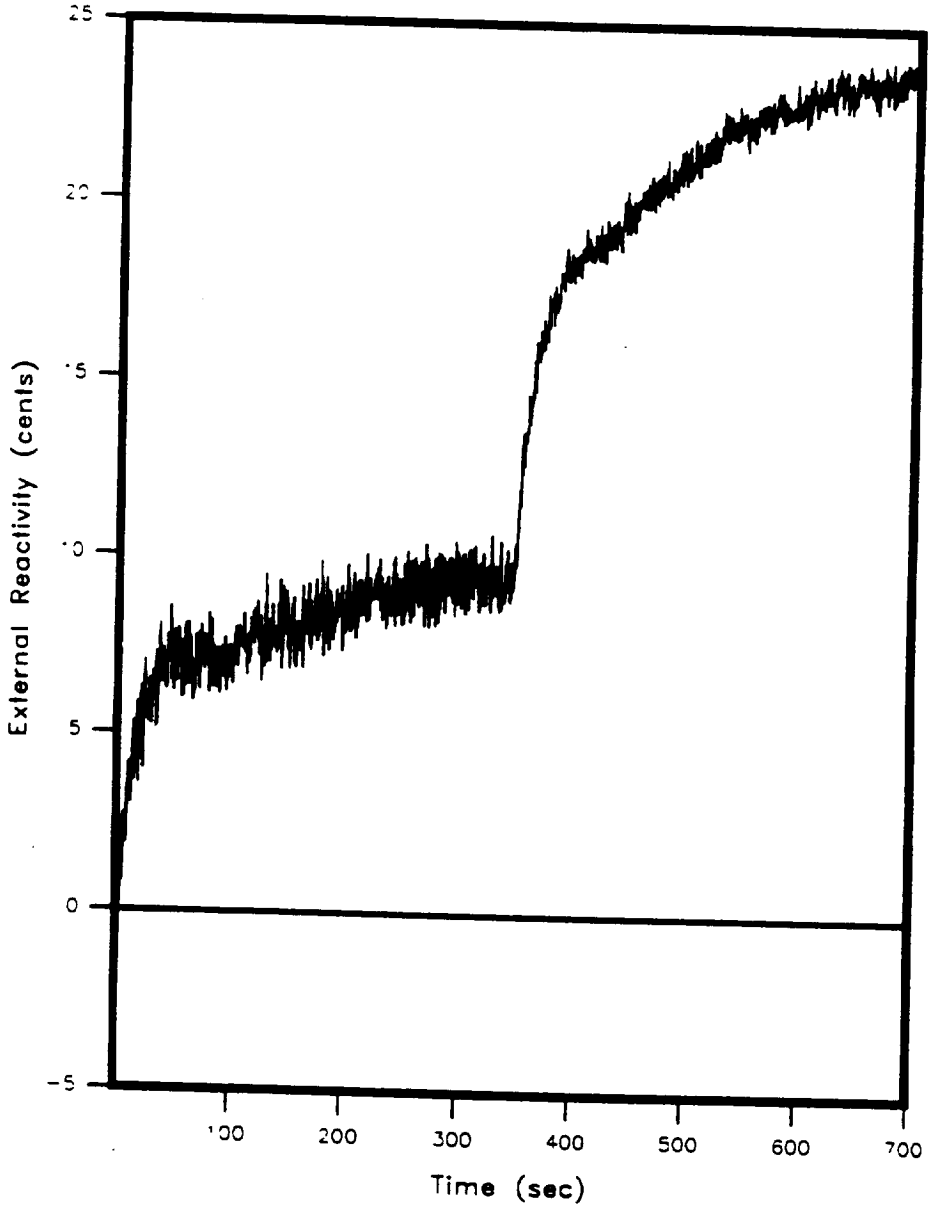

Figure 71. External Reactivity Generated by the Gain-Scheduled Compensator Corresponding to a Load Change from 100% to 120% and from 120% to 150% of Full Power.

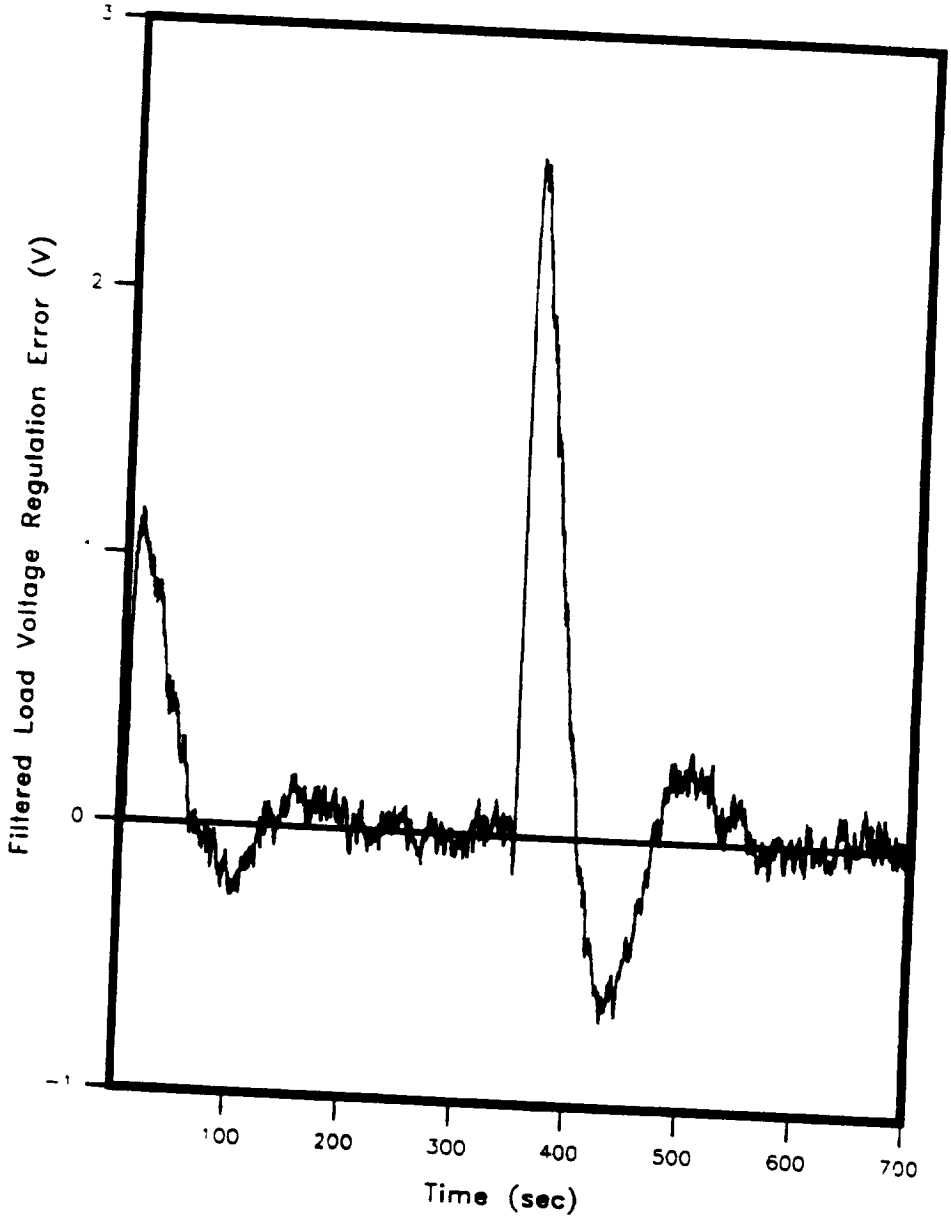

Figure 72. Filtered Load Voltage Regulation Error Response for the Gain-Scheduled Compensator Corresponding to a Load Change from 100% to 80% and from 80% to 50% of Full Power.

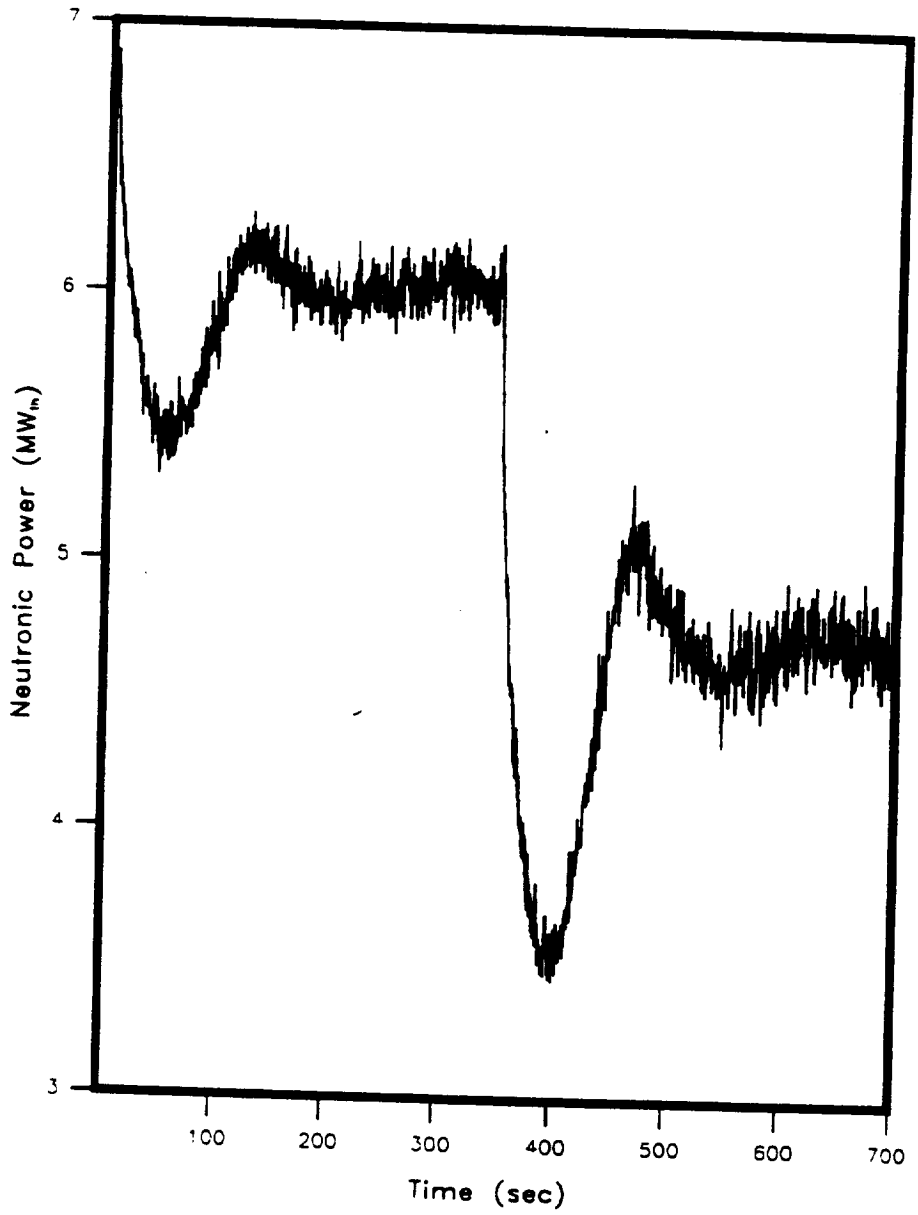

Figure 73. Neutronic Power Response for the Gain-Scheduled Compensator Corresponding to a Load Change from 100% to 80% and from 80% to 50% of Full Power.

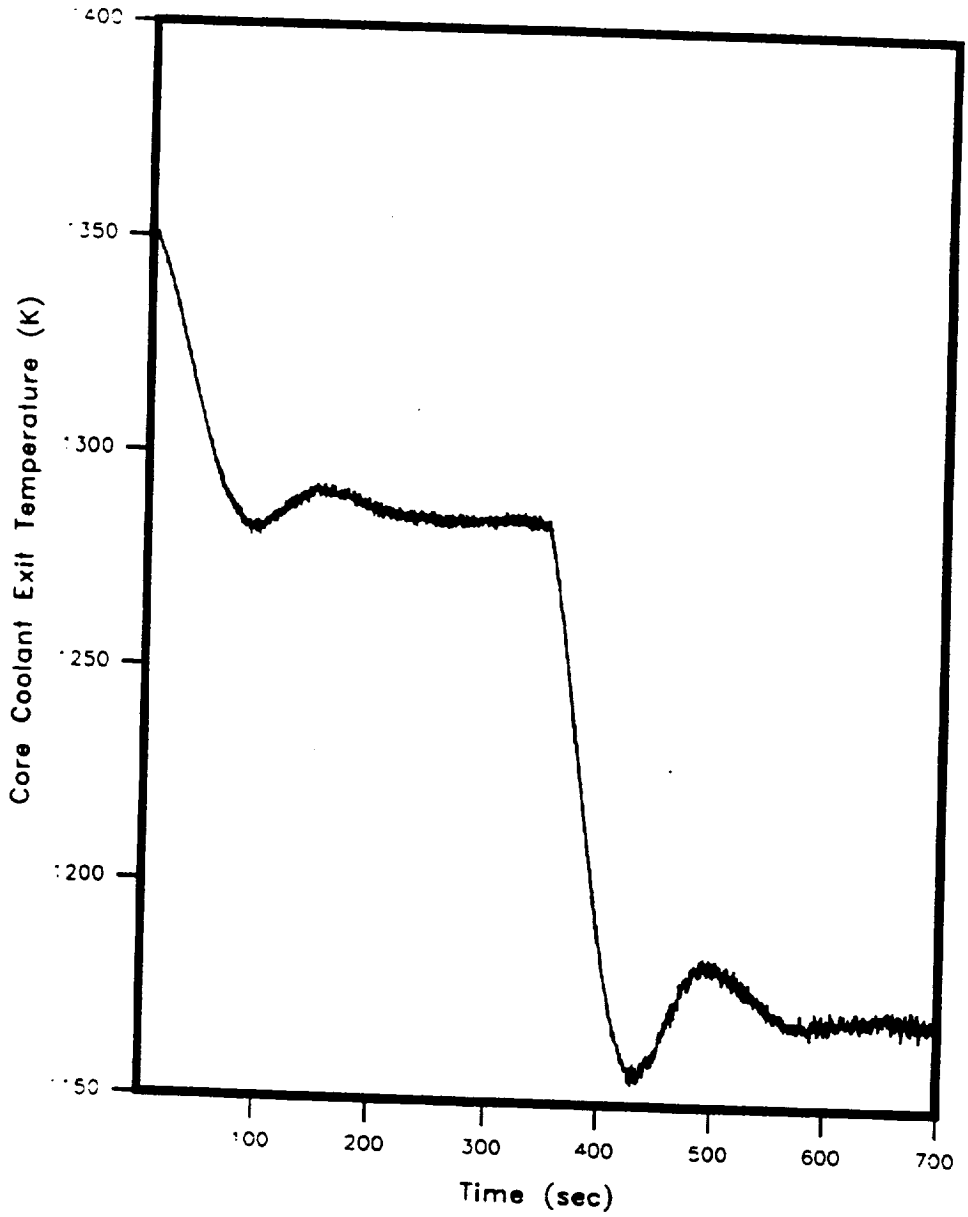

Figure 74. Core Coolant Exit Temperature Response for the Gain-Scheduled Compensator Corresponding to a Load Change from 100% to 80% and from 80% to 50% of Full Power.

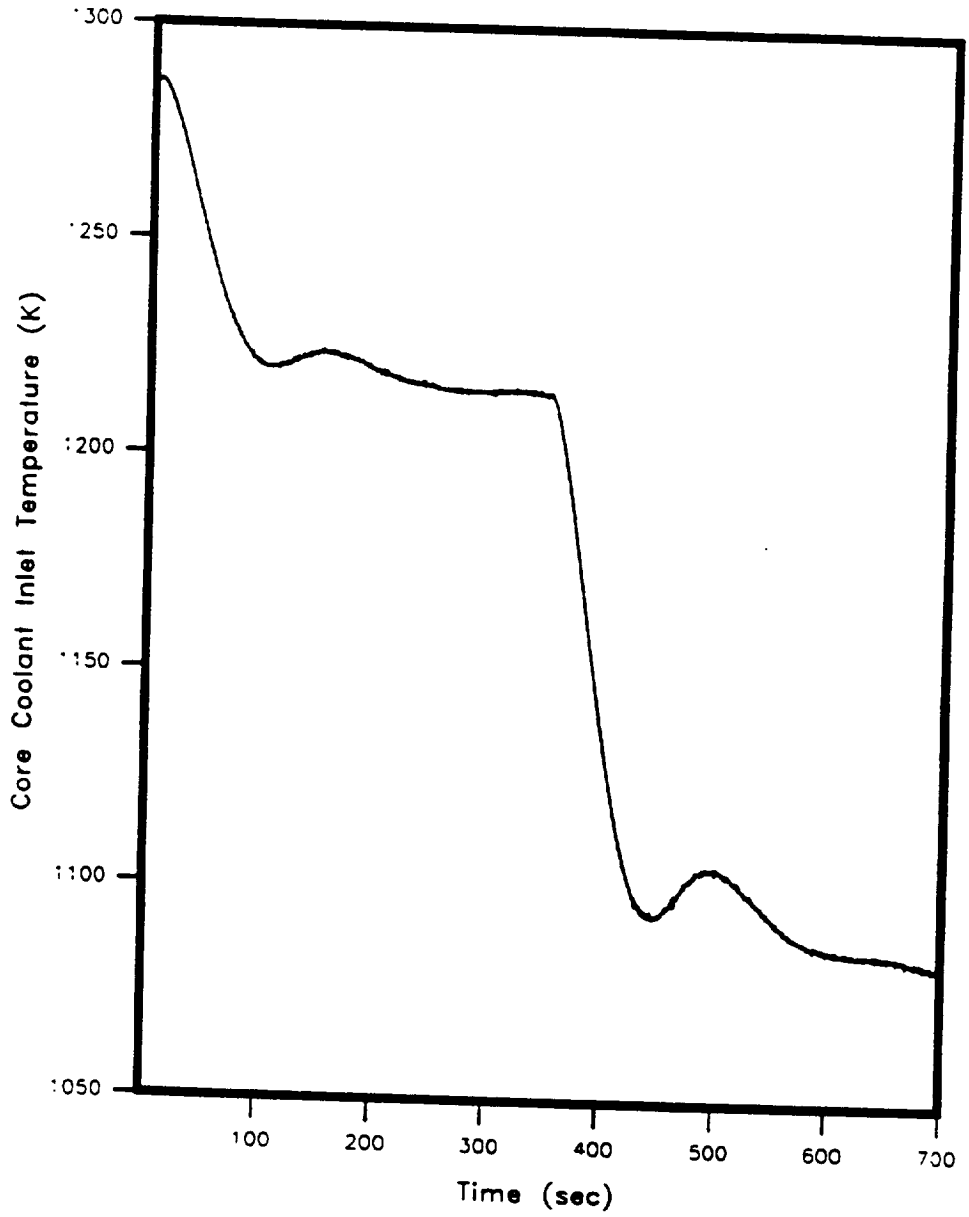

Figure 75. Core Coolant Inlet Temperature Response for the Gain-Scheduled Compensator Corresponding to a Load Change from 100% to 80% and from 80% to 50% of Full Power.

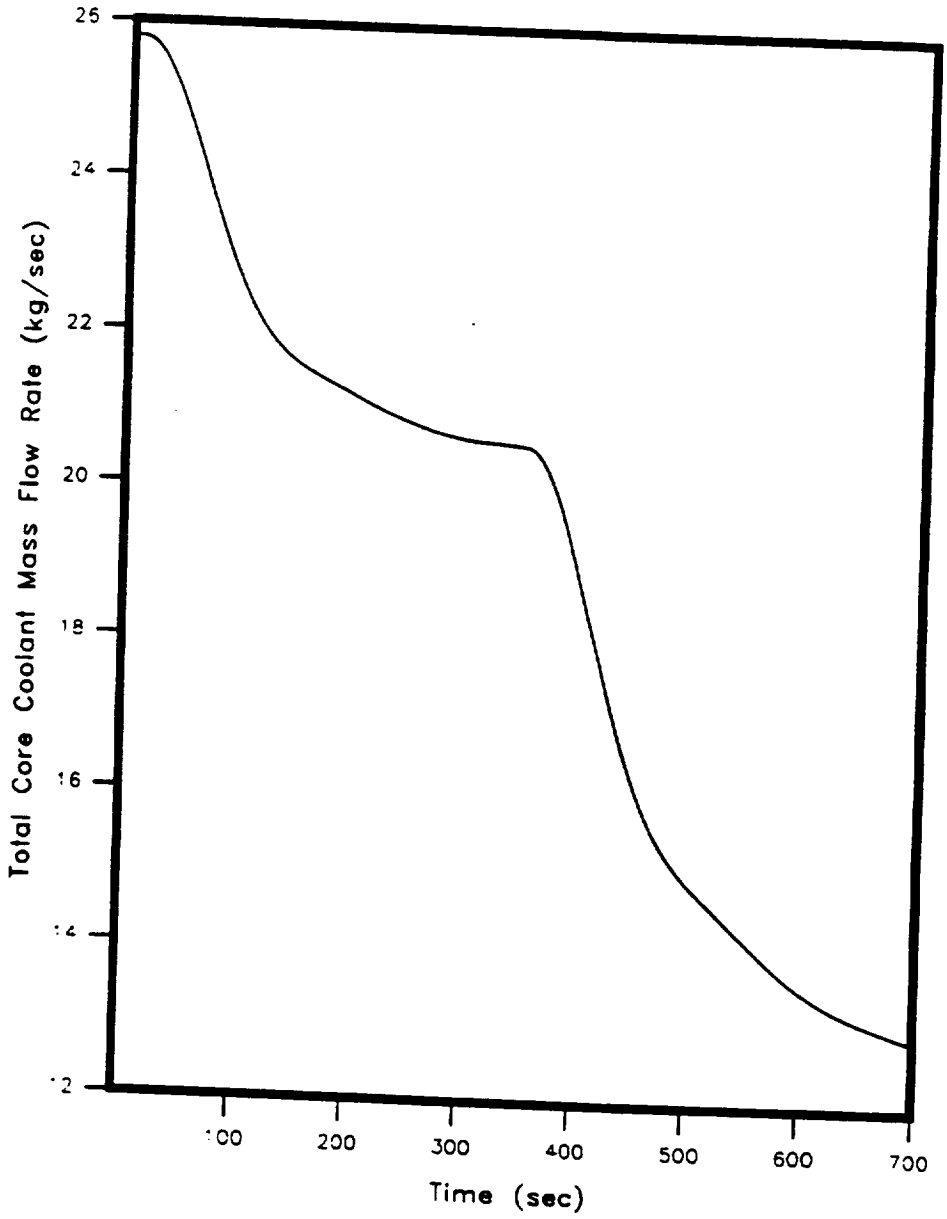

Figure 76. Total Core Coolant Mass Flow Rate Response for the Gain-Scheduled Compensator Corresponding to a Load Change from 100% to 80% and from 80% to 50% of Full Power.

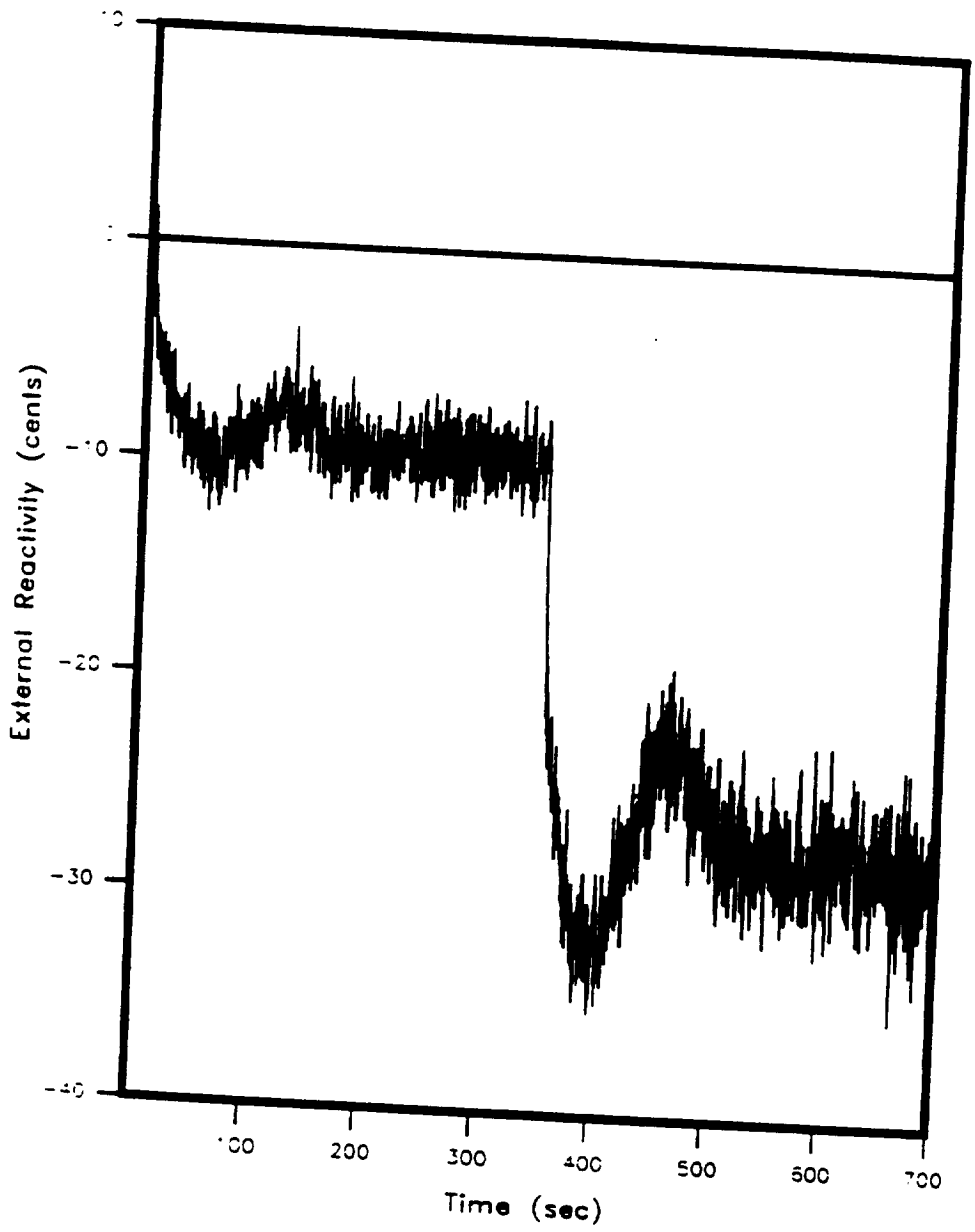

Figure 77. External Reactivity Generated by the Gain-Scheduled Compensator Corresponding to a Load Change from 100% to 80% and from 80% to 50% of Full Power.

1) Constant fuel temperature coefficient ($\alpha_f = -1.0 \times 10^{-5}$) , 2) A negative ramp which changes the α_f from -1.0×10^{-5} to -3.0×10^{-5} (Negative Ramp) in 1200 seconds, 3) A positive ramp which changes the α_f from -1.0×10^{-5} to zero (Positive Ramp) in 1200 seconds. For each of these three cases, the electrical load demand is increased from 100% to 150% of full power in two steps. In the first step, the load demand changes from 100% to 120% of full power, in the next step it changes from 120% to 150% of full power. As seen from Figures 78 and Figure 79 the case which considers a negative ramp change in the α_f, the load voltage is stabilized around 98 Volts with a 2% error from 100 Volts, whereas for the positive ramp case in which the α_f increases linearly to zero, the load voltage becomes unstable after a certain value of the α_f (-2.5×10^{-6}).

The effects of ramp variations in the α_f on the external reactivity generated by the gain-scheduled compensator can be seen in Figure 89. For the constant α_f case, the external reactivity reaches a steady-state value of 23 cents, whereas the external reactivity generated in the negative ramp case increases in order to overcome the high negative fuel feedback reactivity resulting from a ramp decrease in the α_f. The external reactivity generated by the controller for the positive ramp case approaches zero, as the α_f varies linearly approaching zero.

Figures 90 through 95 show the responses of the measured states and output of the nonlinear SNPS model to a change in reactivity generated by the gain-scheduled compensator to a load change from 120% to 150% of the full electrical power level for various cases of variations in the fuel temperature feedback reactivity coefficient.

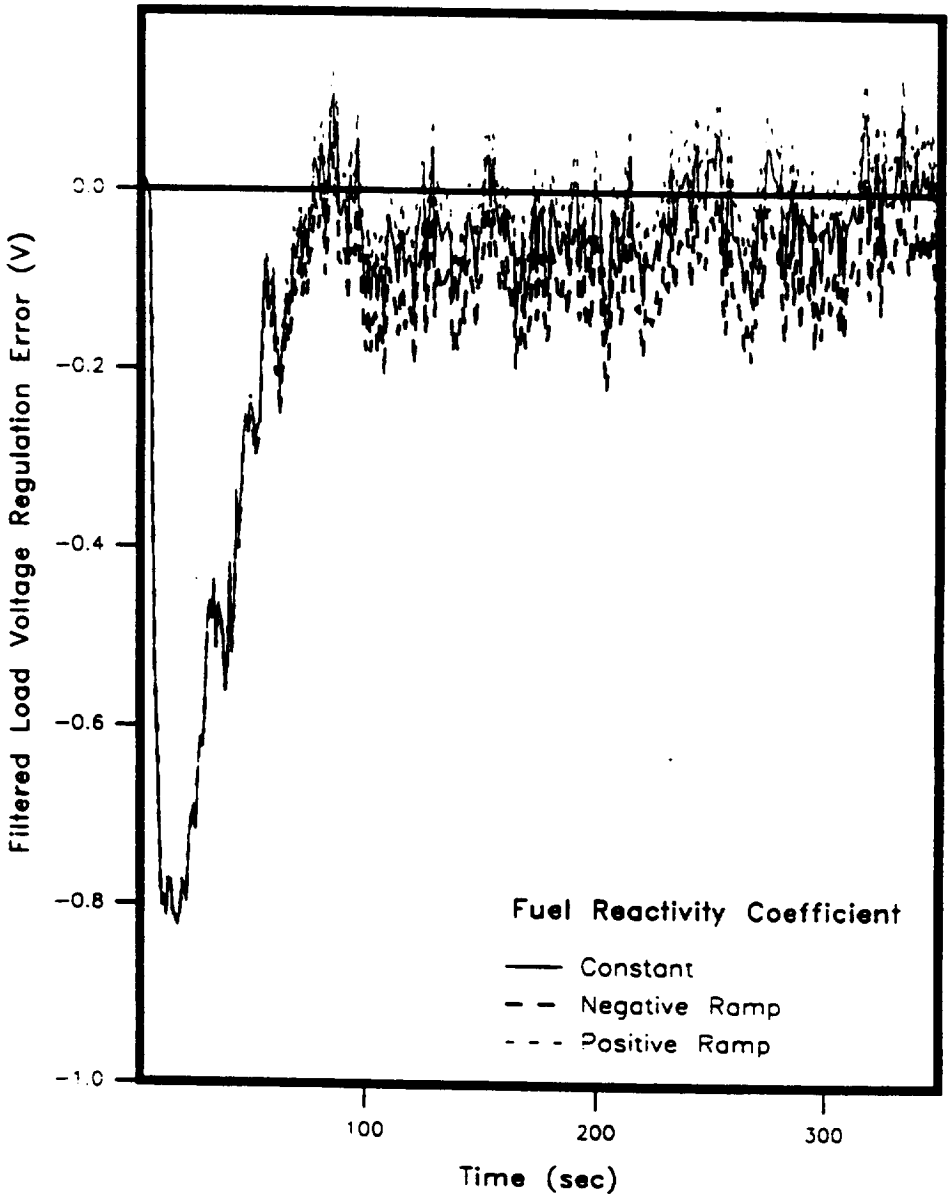

Figure 78. Filtered Load Voltage Regulation Error Responses for Various Changes in the Fuel Temperature Feedback Reactivity Coefficient to a Load Change from 100% to 120% of Full Power.

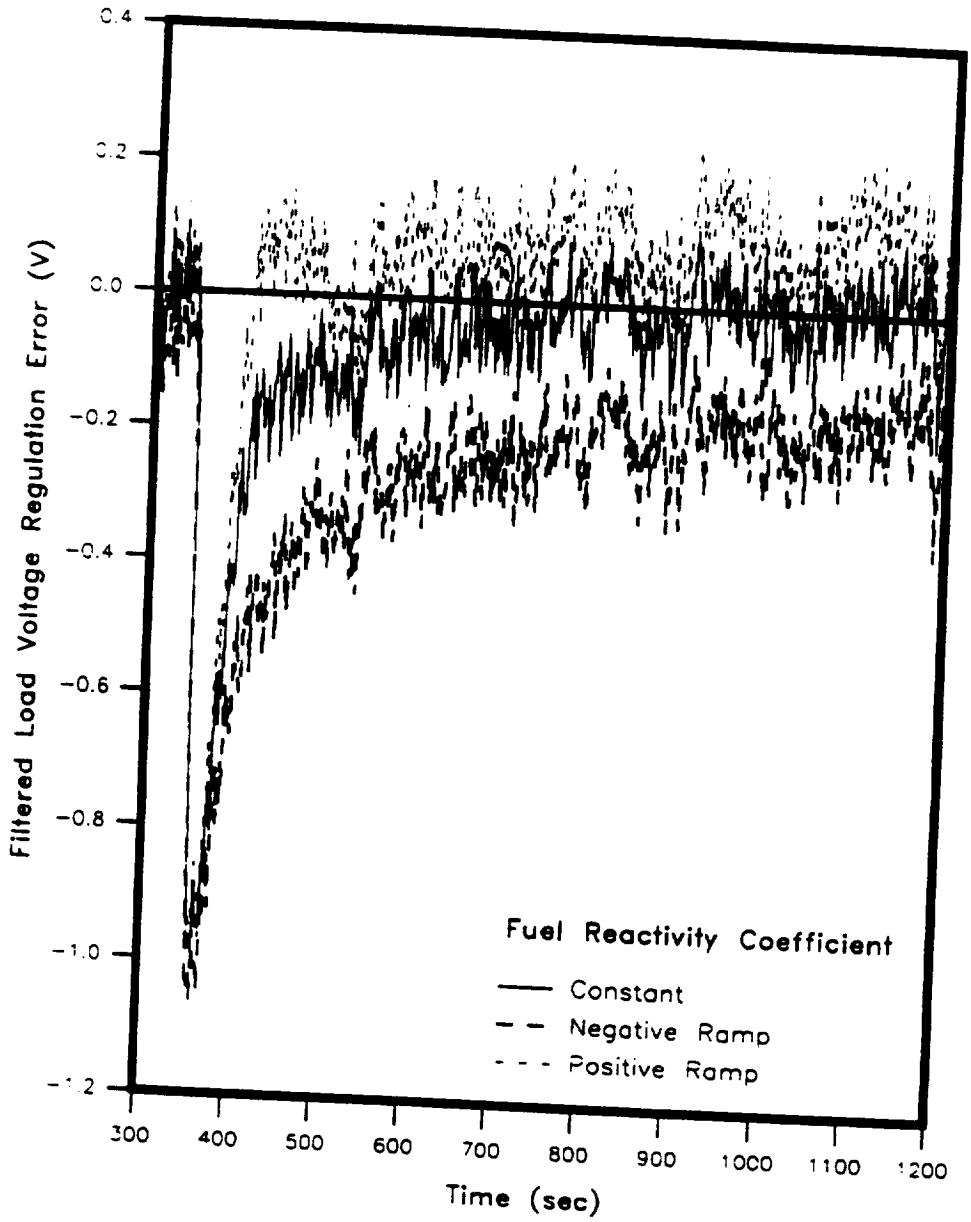

Figure 79. Filtered Load Voltage Regulation Error Responses for Various Changes in the Fuel Temperature Feedback Reactivity Coefficient to a Load Change from 120% to 150% of Full Power.

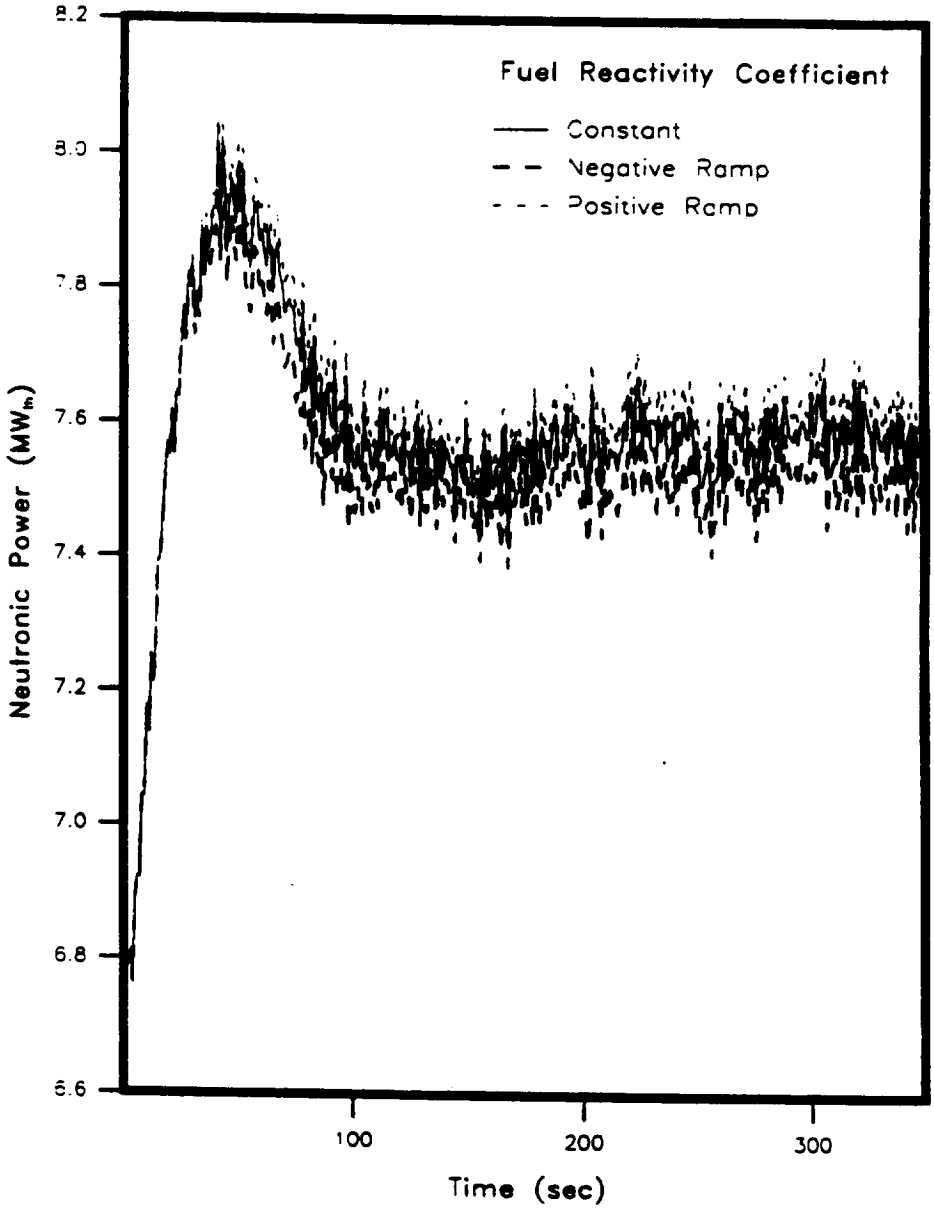

Figure 80. Neutronic Power Responses for Various Changes in the Fuel Temperature Feedback Reactivity Coefficient to a Load Change from 100% to 120% of Full Power.

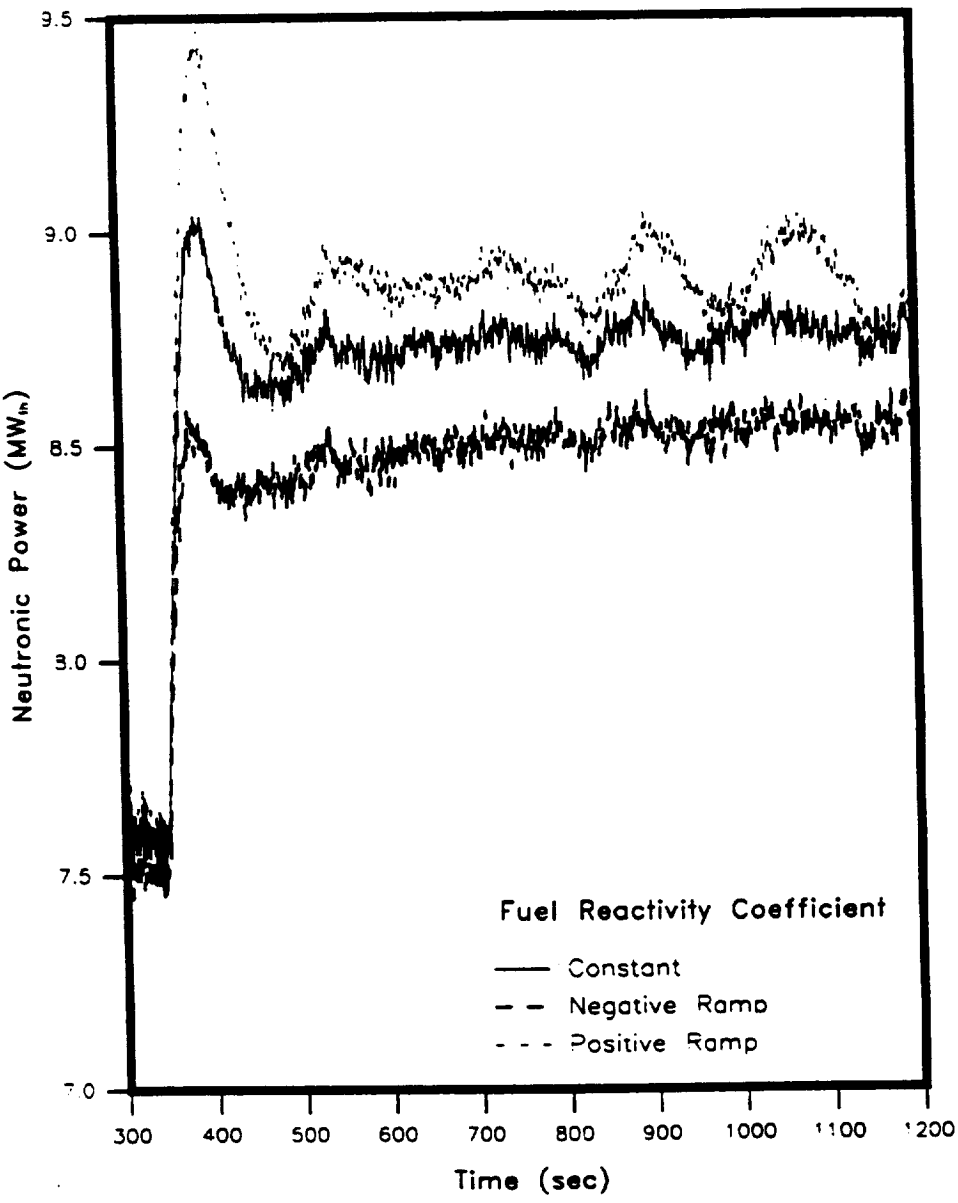

Figure 81. Neutronic Power Responses for Various Changes in Fuel Temperature Feedback Reactivity Coefficient to a Load Change from 120% to 150% of Full Power.

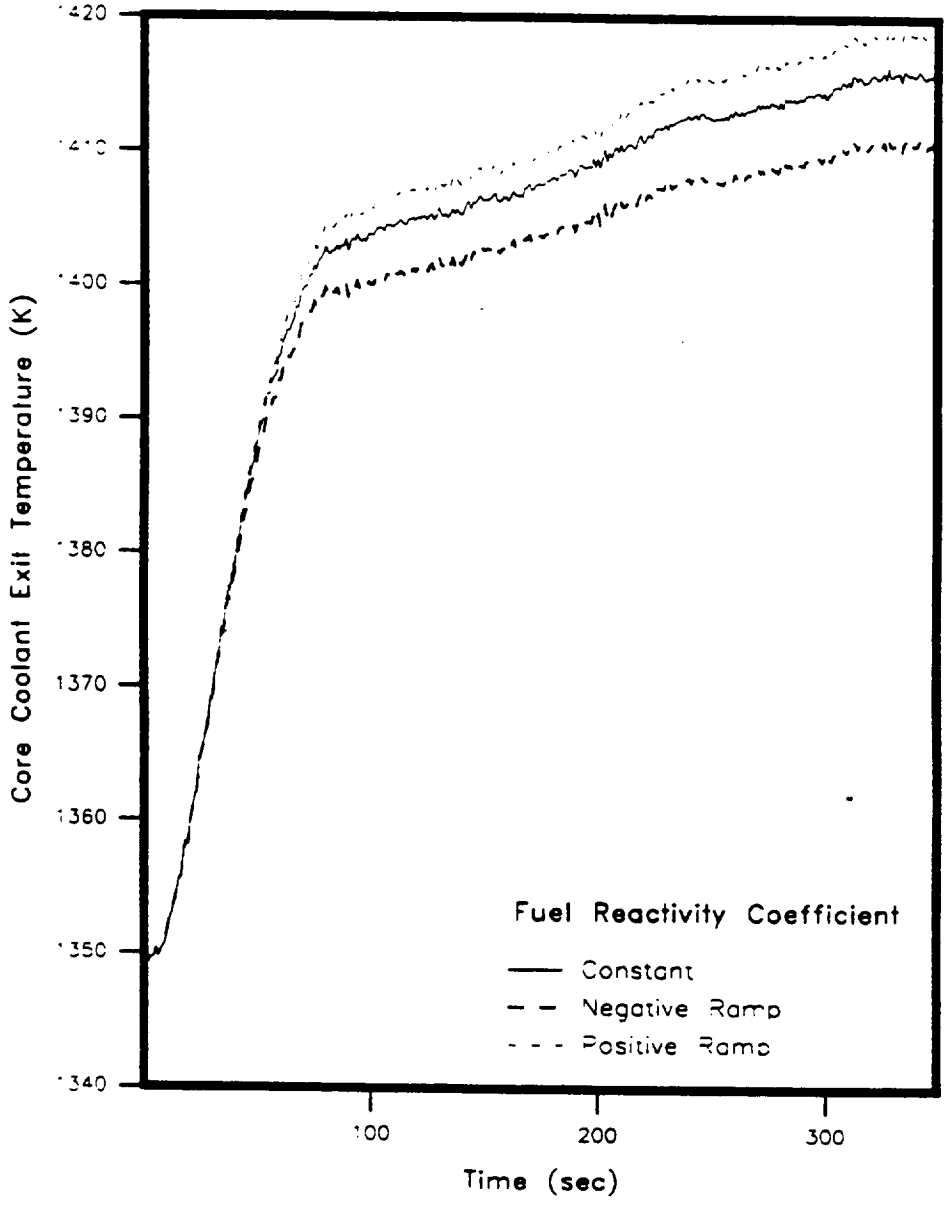

Figure 82. Core Coolant Exit Temperature Responses for Various Changes in the Fuel Temperature Feedback Reactivity Coefficient to a Load Change from 100% to 120% of Full Power.

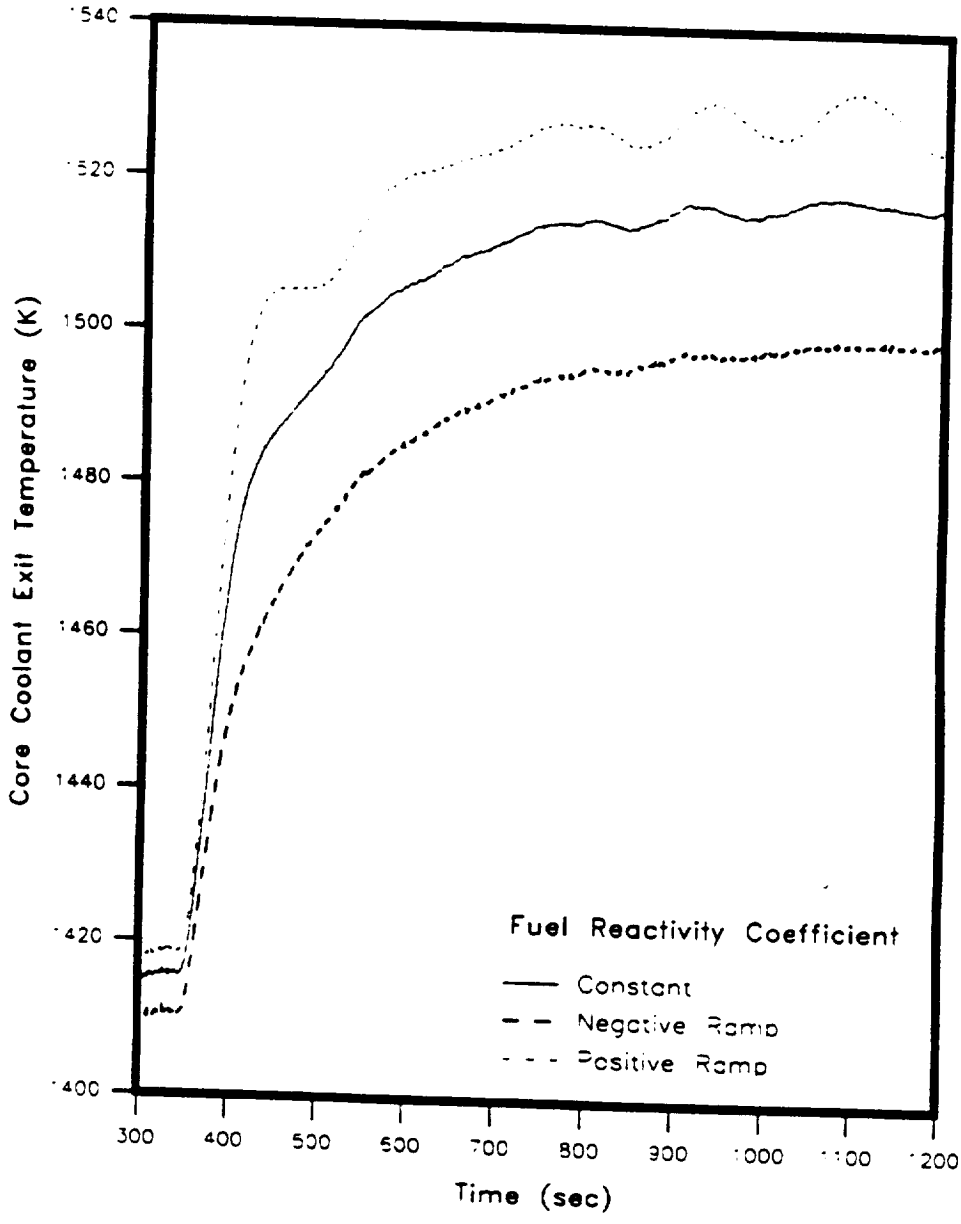

Figure 83. Core Coolant Exit Temperature Responses for Various Changes in the Fuel Temperature Feedback Reactivity Coefficient to a Load Change from 120% to 150% of Full Power.

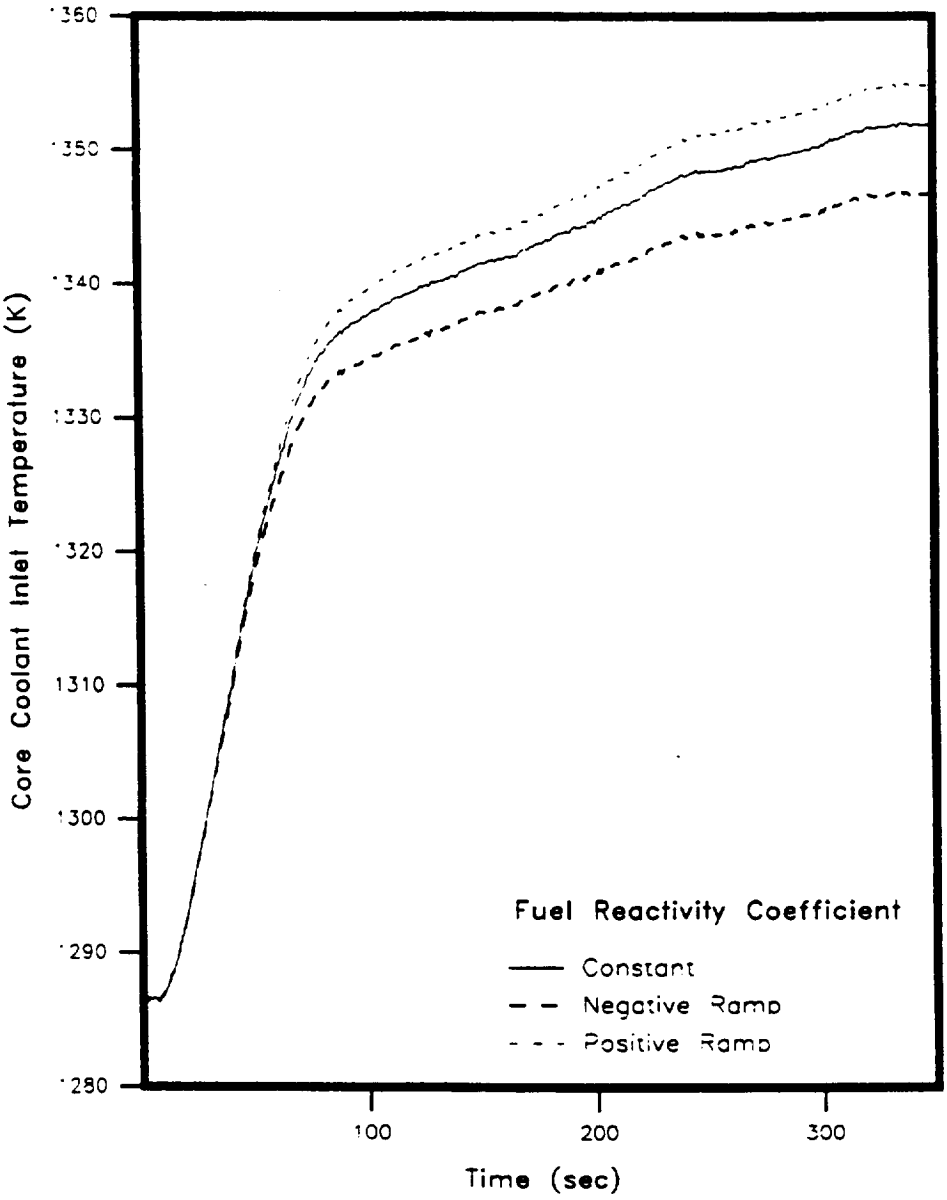

Figure 84. Core Coolant Inlet Temperature Responses for Various Changes in the Fuel Temperature Feedback Reactivity Coefficient to a Load Change from 100% to 120% of Full Power.

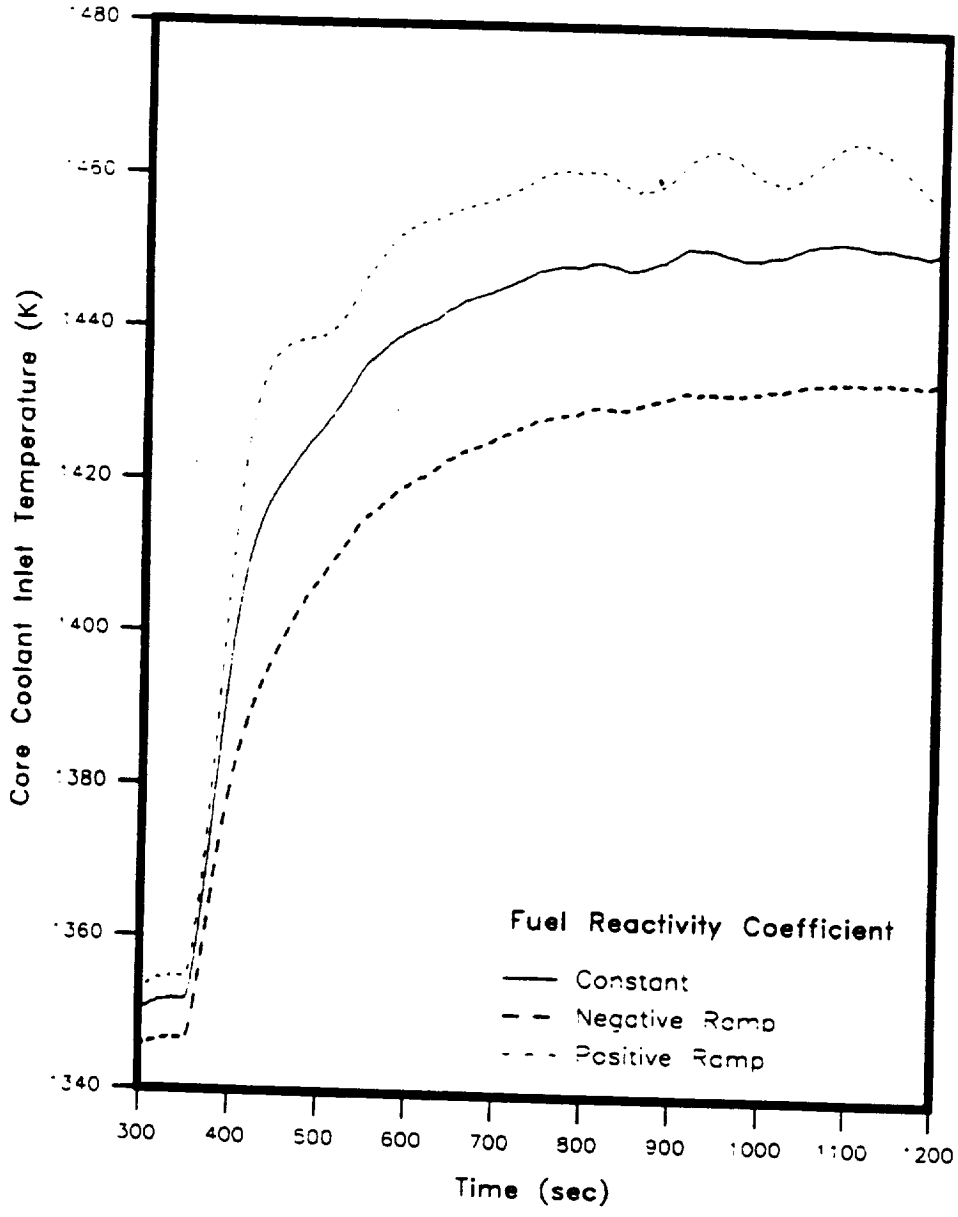

Figure 85. Core Coolant Inlet Temperature Responses for Various Changes in the Fuel Temperature Feedback Reactivity Coefficient to a Load Change from 120% to 150% of Full Power.

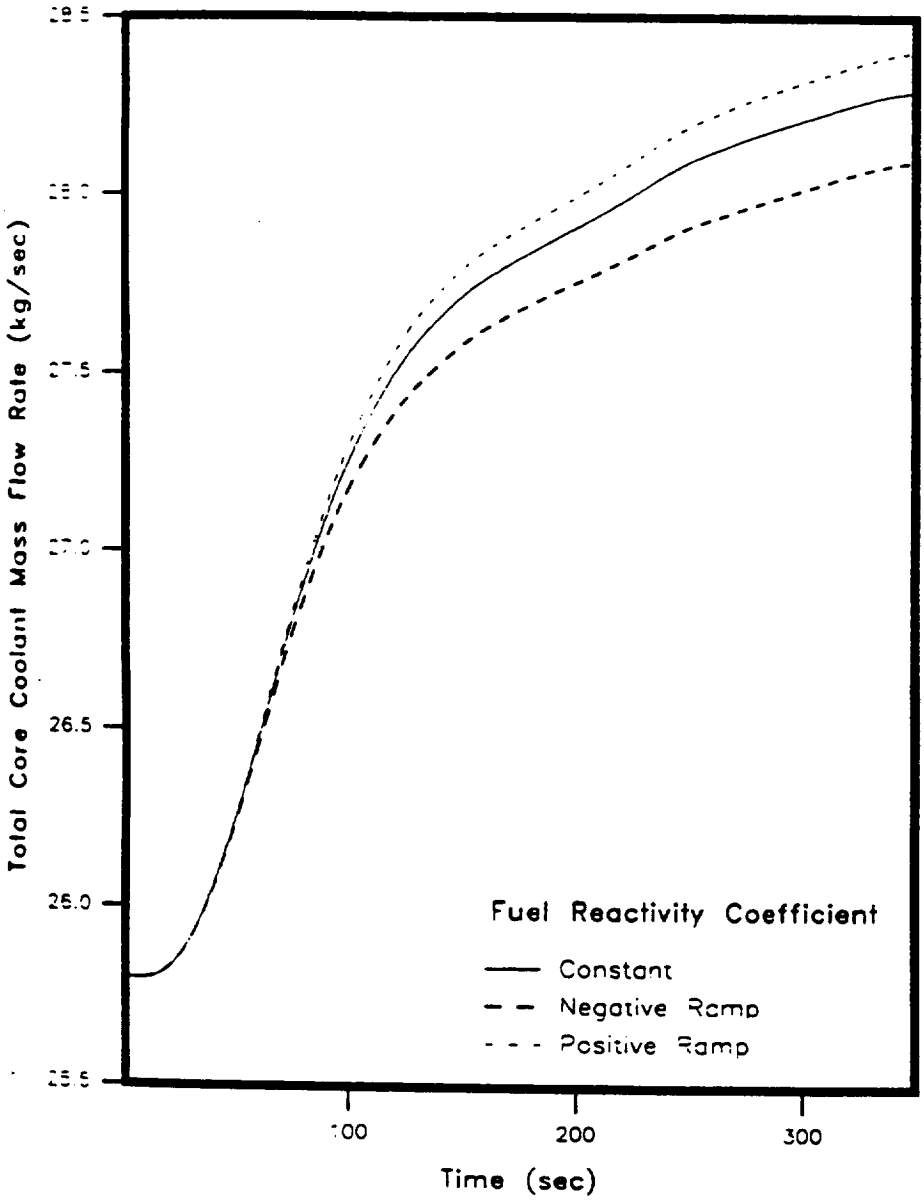

gure 86. Total Core Coolant Mass Flow Rate Responses for Various Changes in the Fuel Temperature Feedback Reactivity Coefficient to a Load Change from 100% to 120% of Full Power.

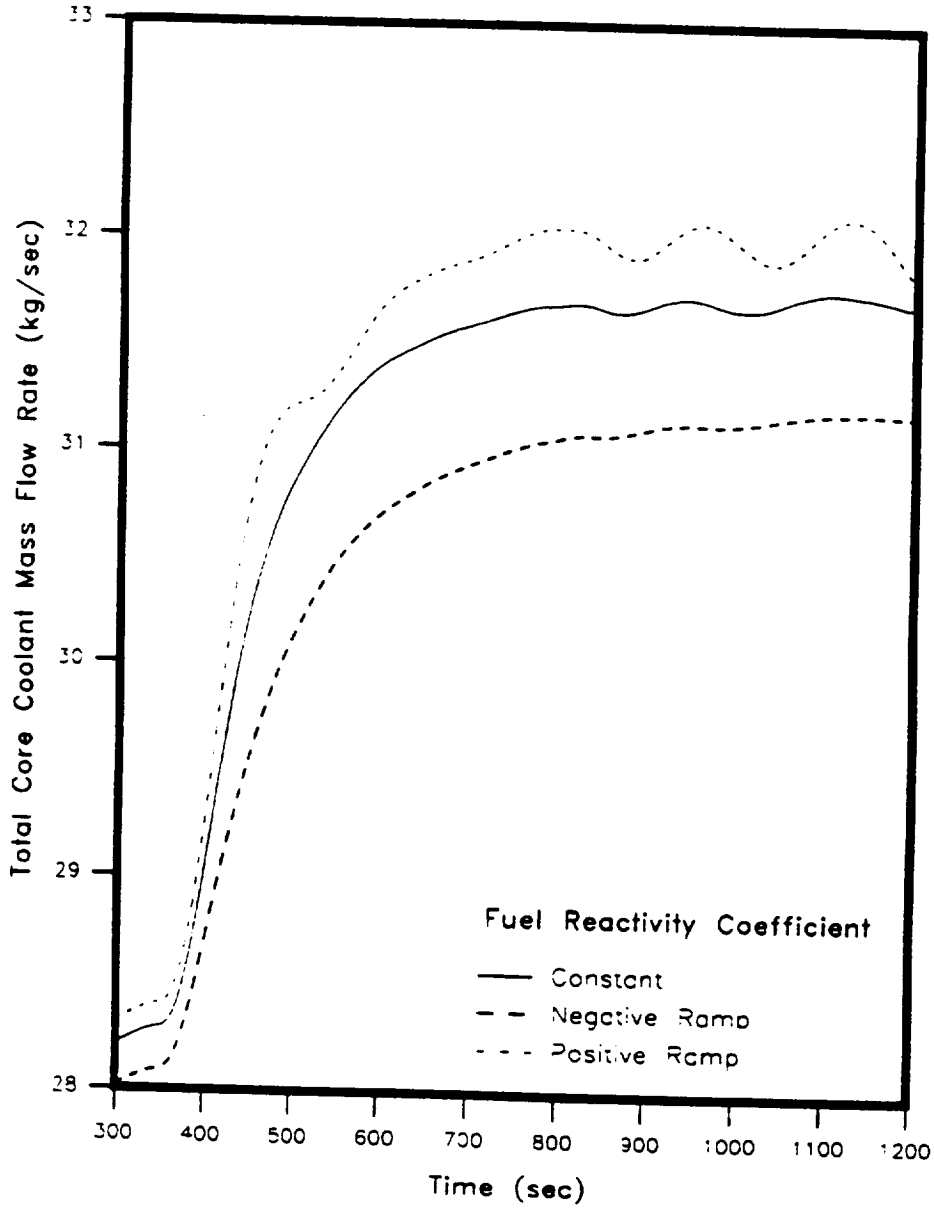

Figure 87. Total Core Coolant Mass Flow Rate Responses for Various Changes in the Fuel Temperature Feedback Reactivity Coefficient to a Load Change from 120% to 150% of Full Power.

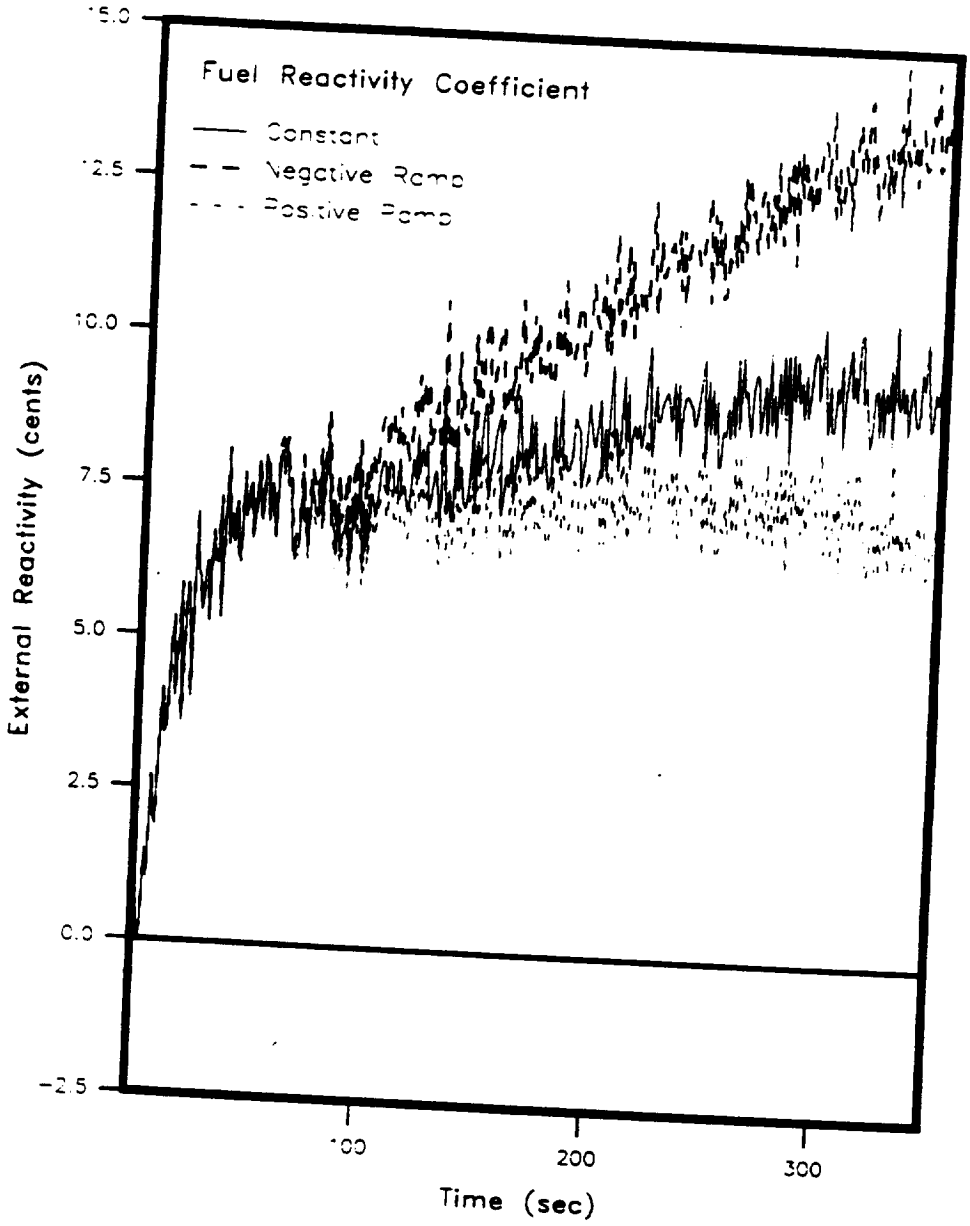

Figure 88. External Reactivity Generated by the Gain-Scheduled Compensator for Various Changes in the Fuel Temperature Feedback Reactivity Coefficient Corresponding to a Load Change from 100% to 120%.

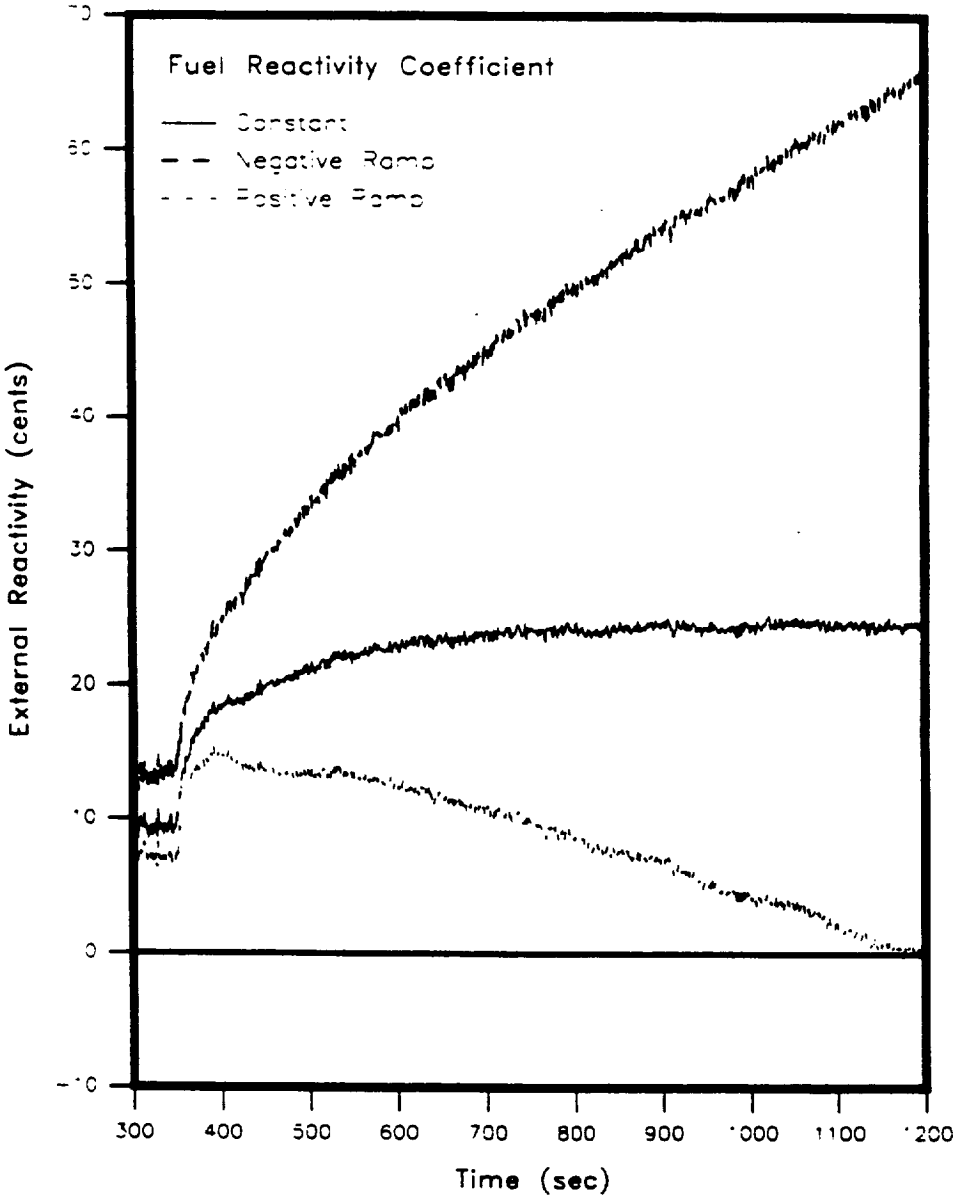

Figure 89. External Reactivity Generated by the Gain-Scheduled Compensator for Various Changes in the Fuel Temperature Feedback Reactivity Coefficient Corresponding to a Load Change from 120% to 150%.

These cases include: 1) constant α_f (constant α_f), and, 2) a negative step change in α_f from its original value of -1.0×10^{-5} to -2×10^{-5} (Negative Step).

Figure 90 shows a comparison of the load voltage response of the SNPS for the constant α_f case and negative step case. The negative step change in α_f causes the load voltage to drop initially by about 2%, however, the system response recovers and finally stabilizes at about 100 Volts. The effect of a negative step change in α_f is apparent in the neutronic power response as shown in Figure 91 where the neutronic power initially experiences a significant drop (-8%) from its steady-state value at 120% of full power level, because of high negative feedback reactivity resulting from changing the α_f by 100%. This effect can be explained by examining the external reactivity generated by the compensator as shown in Figure 95. It can be seen from this figure that the controller responds to a negative step change in α_f by increasing the external reactivity to overcome the high negative feedback reactivity in order to meet the demanded electrical power. The external reactivity generated for the constant α_f case reaches a steady-state value of about 23 cents whereas for the negative step case, the external reactivity reaches a steady-state value of 45.9 cents, which approximately twice of that for the constant α_f case.

From the robustness evaluation analysis of the gain-scheduled compensator, it can be concluded that the gain-scheduled compensator can handle variations in the fuel temperature feedback coefficient up to a certain value. The maximum value of negative step change in the α_f which the gain-scheduled compensator can handle in the presence of sensor noise has been determined to be a negative step change of 240%

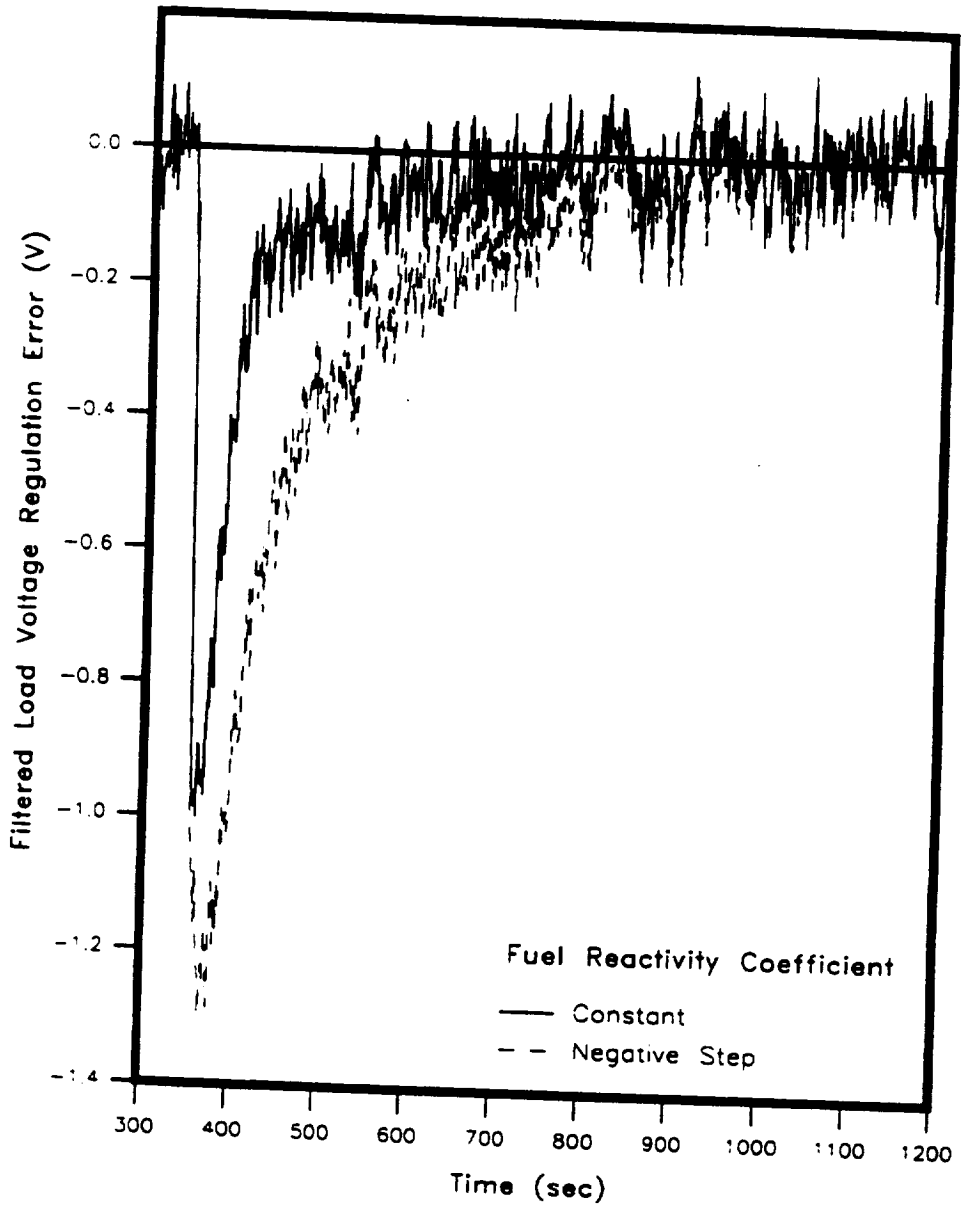

Figure 90. Filtered Load Voltage Regulation Error Responses for Various Changes in the Fuel Temperature Feedback Reactivity Coefficient to a Load Change from 120% to 150% of Full Power.

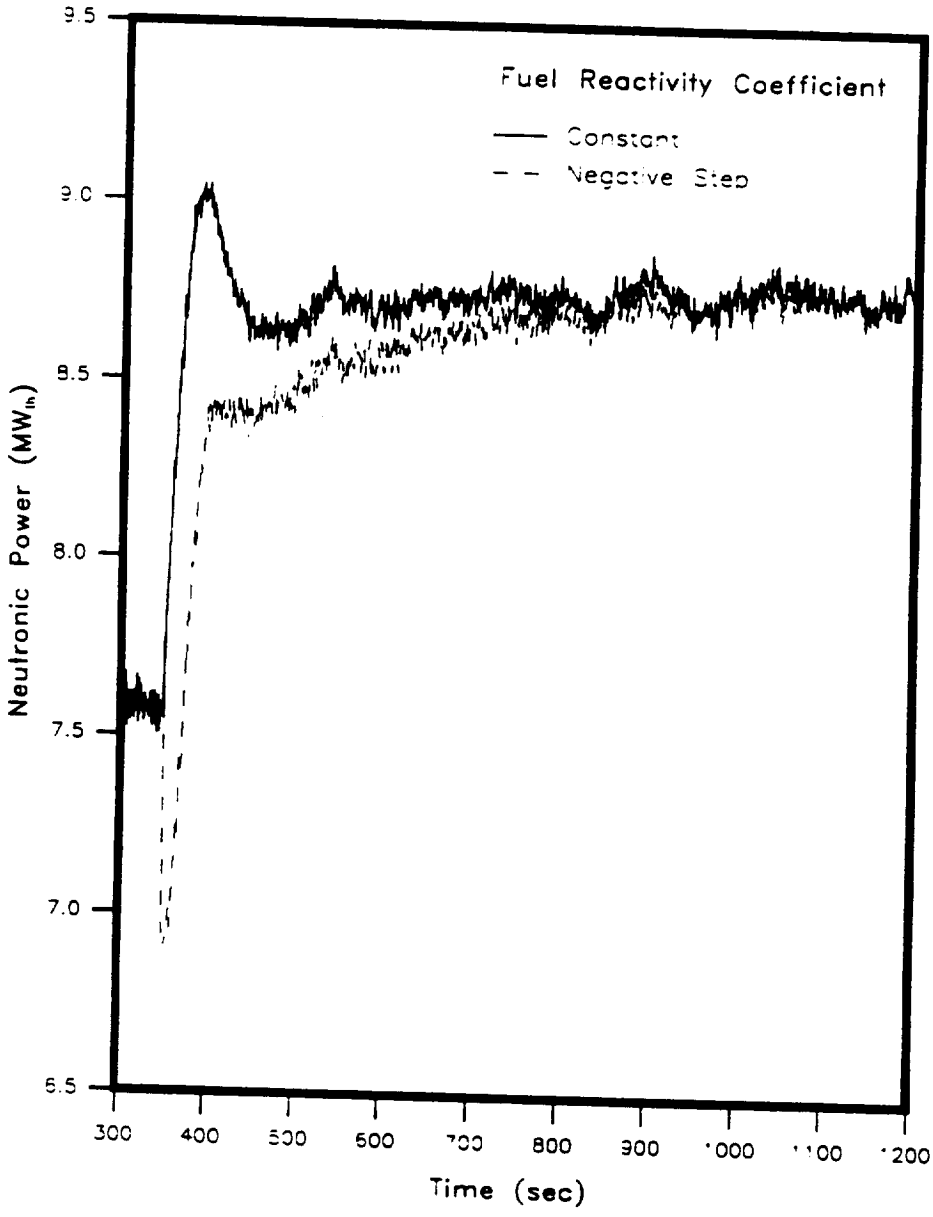

Figure 91. Neutronic Power Responses for Various Changes in the Fuel Temperature Feedback Reactivity Coefficient to a Load Change from 120% to 150% of Full Power.

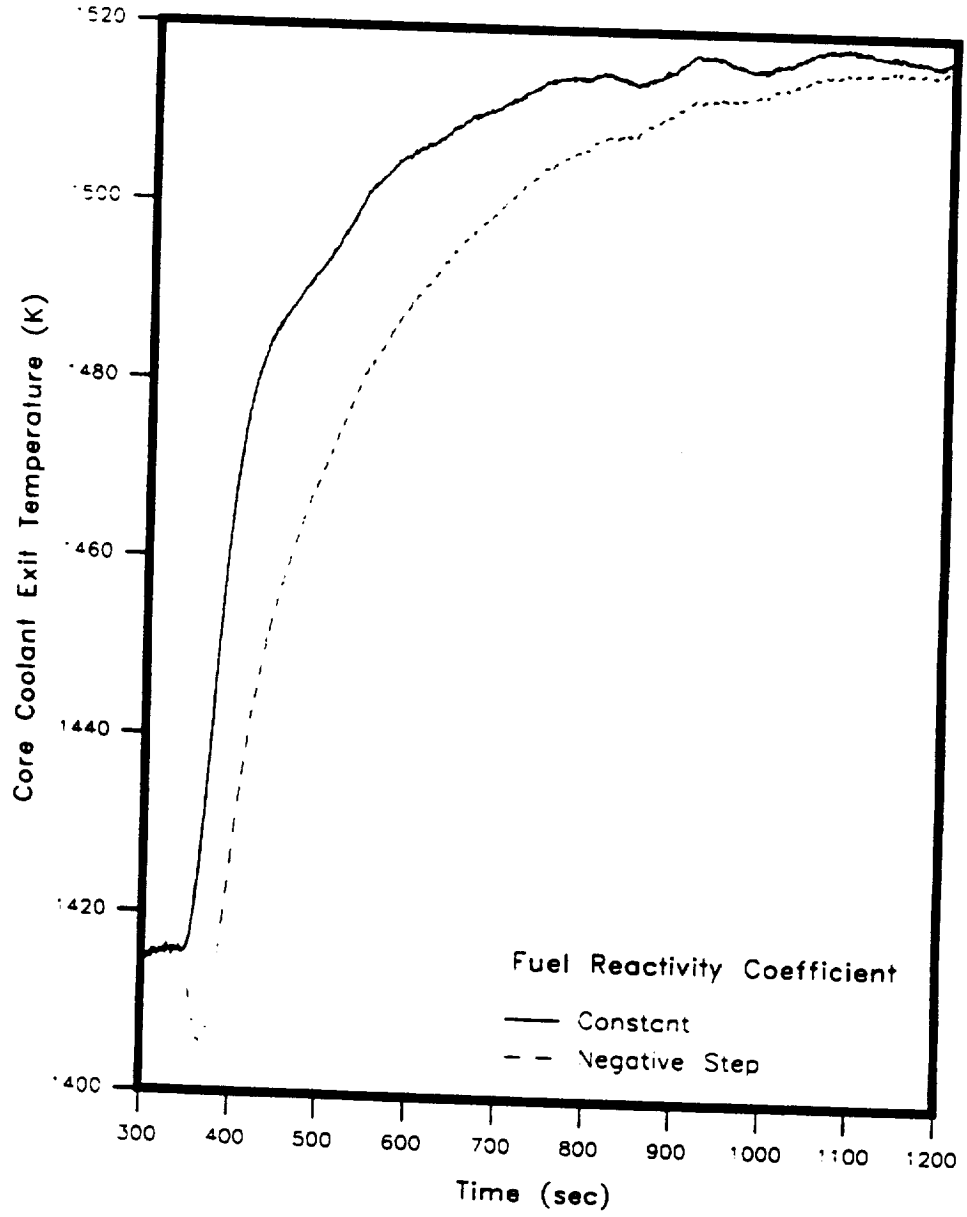

Figure 92. Core Coolant Exit Temperature Responses for Various Changes in the Fuel Temperature Feedback Reactivity Coefficient to a Load Change from 120% to 150% of Full Power.

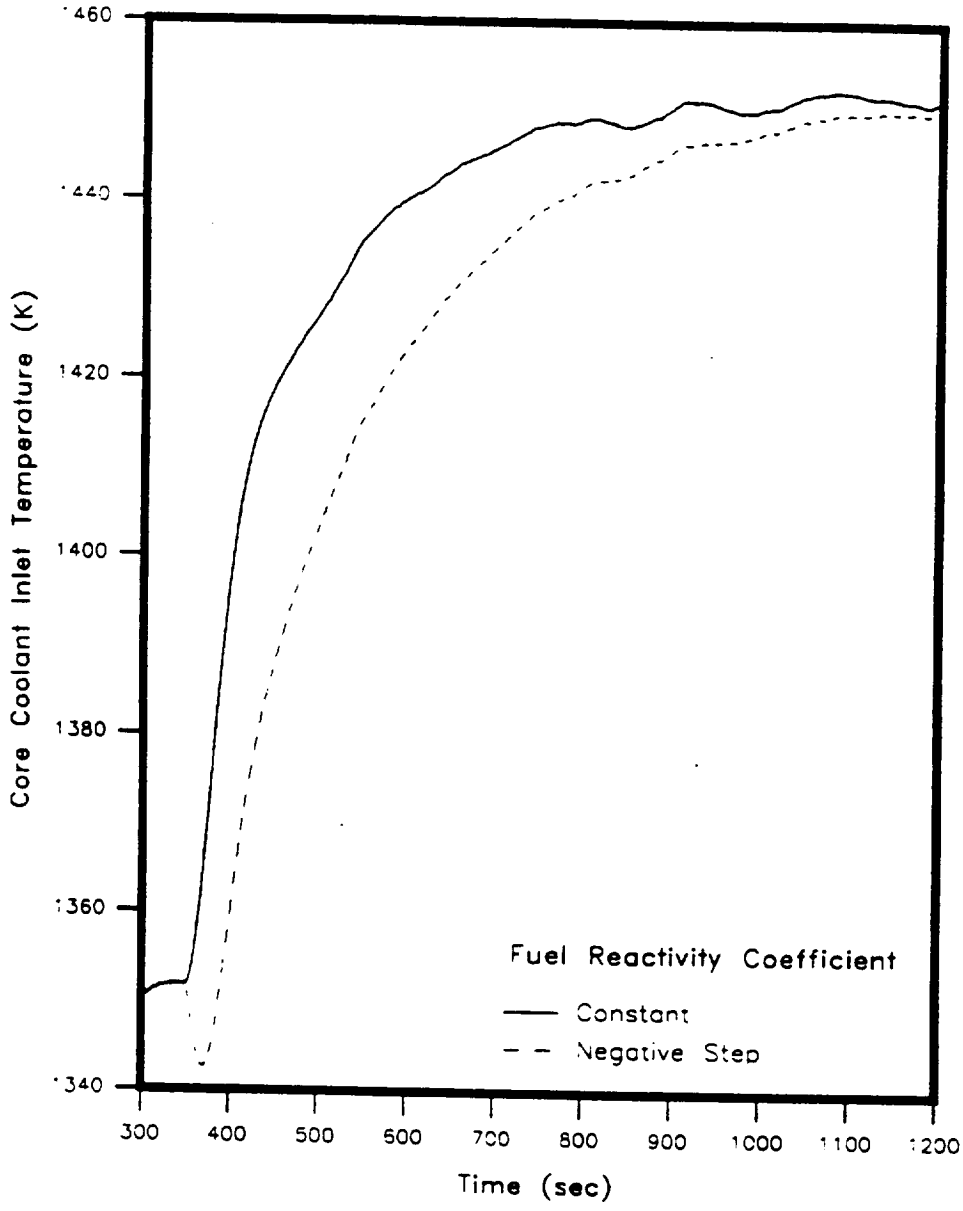

Figure 93. Core Coolant Inlet Temperature Responses for Various Changes in the Fuel Temperature Feedback Reactivity Coefficient to a Load Change from 120% to 150% of Full Power.

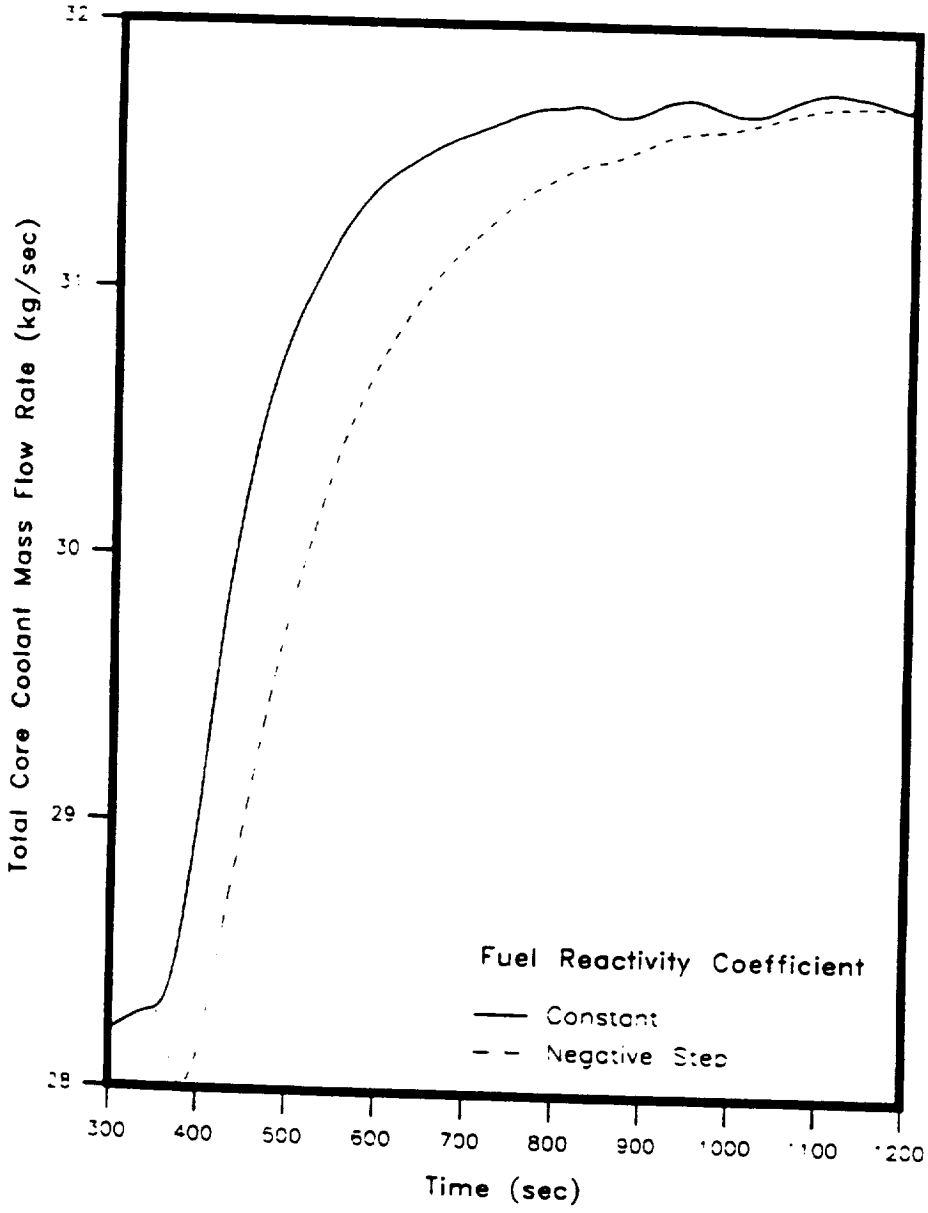

Figure 94. Total Core Coolant Mass Flow Rate Responses for Various Changes in the Fuel Temperature Feedback Reactivity Coefficient Corresponding to a Load Change from 120% to 150% of Full Power.

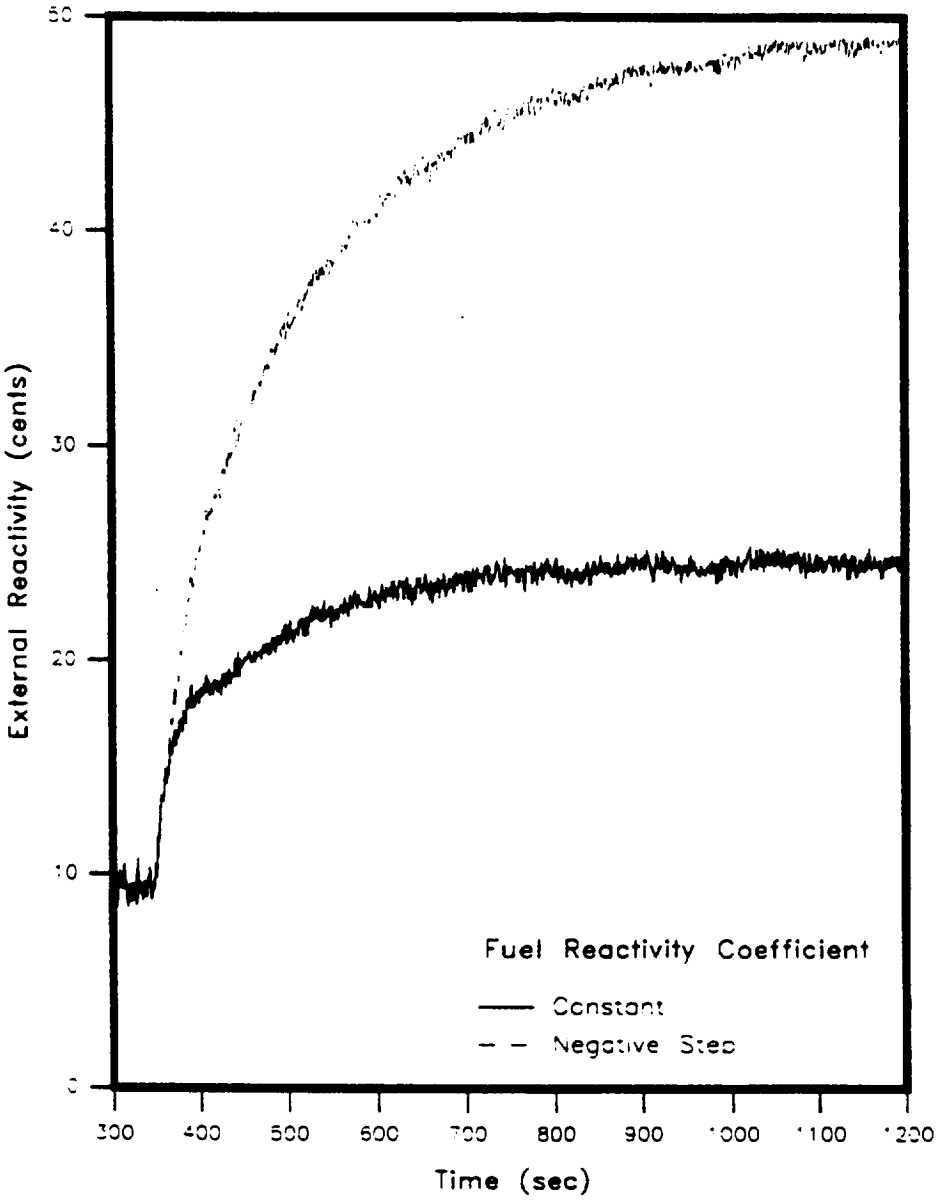

Figure 95. External Reactivity Generated by the Gain-Scheduled Compensator for Various Changes in the Fuel Temperature Feedback Reactivity Coefficient Corresponding to a Load Change from 120% to 150% of Full Power.

of the initial α_f. The limitations are set by the fact that the maximum reactivity insertion into the core can not exceed 80 cents. The gain-scheduled compensator can handle negative ramp changes in α_f more successfully than positive ramp changes. As the α_f approaches zero, as expected the system's load voltage becomes unstable.

CHAPTER VII

SUMMARY AND CONCLUSIONS

VII.1 Summary

The use of shunt regulators for the load-following of the static SNPSs raises a number of concerns, such as the possibility of a single-point failure in the shunt regulators requiring reactor shutdown, or the need to deliver somewhat higher power than originally expected due to changing mission needs. Therefore, a back-up system is needed in static SNPSs to eliminate the possibility of a single-point failure in the shunt regulators and to improve the overall system reliability despite changes in the system's operating parameters.

Specifically, in this thesis the LQG/LTR technique, which utilizes an MBC structure, is used to design a compensator. LQG/LTR is a systemic MIMO control design methodology, which eliminates the large number of tunning parameters in ad-hoc methods, thus simplifying the design process. Furthermore, the LQG/LTR design method results in linear compensators with desirable properties, such as nominal stability, command following, disturbance rejection, noise insensitivity and certain amount of stability robustness, which though not guaranteed to carry over in the nonlinear domain, they appear to provide some improvements.

The success in using the LQG/LTR method depends on the accuracy of the linearized models used to design it. The integrated, nonlinear SNPS model was

simplified to obtain a reference model which was linearized to be used in the design of the linear compensators.

The LQG/LTR method is used to design linear compensators for each of the linearized reference models. The specifications for the compensator design are in terms of the singular values of the appropriate TFMs. Therefore, the resulting compensator design can be determined to be satisfactory by inspection of the appropriate singular values. The bandwidth of the open-loop system being the tuning variable in the compensator design is fixed at a particular value so to allow enough time for control drum movements. The actual performance of the linear compensators is then determined subjecting the integrated nonlinear SNPS model to a disturbance. This disturbance is a change in the demanded electric power. If the LQG/LTR compensator performs sufficiently well with respect to certain system specifications, such as stability of the system, load-following capabilities of the power system, the limitations on the initial reactivity insertion rate, then a satisfactory LQG/LTR compensator has been obtained. Otherwise, the design procedure is repeated so as to influence the singular values of the appropriate system TFMs. At this stage the bandwidth of the system can be altered if so desired. Also, if the situation demands, additional dynamics such as integrators etc. can be augmented to the compensator input and/or output. This is usually the case when there is a physical limitation on the system and/or there is a steady-state error in the output of the system. It should be pointed out that it is easy to determine the direction in which the design tuning parameters are to be changed. The lack of a large number of tuning parameters is one of the main advantages of the LQG/LTR design technique. It has determined that a single linear compensator

designed using 100% of full power linearized model was capable of regulating the load voltage at the desired level.

Once the LQG/LTR compensators are designed for each of the linearized reference models, the gain matrices of the compensator designs are fitted to the scheduling variable, the electric power output, P_e. These gain matrices combined with the scheduled model of the SNPS developed from the linearized reference models form the gain-scheduled compensator. The motivation for developing a gain-scheduling compensator is to be able to control the power system continuously within its entire operating regime. The performance limits of the gain-scheduled compensator were determined for step and ramp variations in the fuel feedback temperature coefficient. The cases demonstrated include **1)** a negative ramp change in the fuel feedback reactivity coefficient, **2)** a positive ramp change upto zero, and **3)** a negative step change of 100% of the initial value of the fuel temperature feedback reactivity coefficient. The second case resulted in an unstable behaviour in the load voltage as the fuel temperature feedback coefficient approached zero. In the other two cases investigated, the load voltage of the SNPS has been stabilized at the desired power level with small relative error. Thus, the gain-scheduled compensator demonstrated robustness and high performance in overcoming the drifts in the system's operating parameters.

VII.2 Conclusions

From the performance analysis of the gain-scheduled compensator the following conclusions can be drawn:

1.) The linearized reference models have been found to be highly accurate and valid for large variations from their respective equilibrium points. Therefore, the 100% of full power linear compensator alone could regulate the load voltage at the desired level for the entire operating regime of the power system.

2.) The gain-scheduled compensator handled large step and ramp changes in the fuel temperature reactivity coefficient, in the presence of sensor noise incorporated to the load voltage of the SNPS under consideration.

3.) The robustness and performance analysis of the gain-scheduled compensator showed that the dual-loop control concept, which incorporates an adaptive controller with the gain-scheduled compensator as proposed earlier, can be replaced by the gain-scheduled compensator itself, hence eliminating the need for a hardware or software intensive, complex adaptive controller.

VII.3 Implemantation Issues

For the actual implementation of LQG/LTR compensators on small-scale digital systems, the finite memory, relatively slow speeds, and the expense of the hardware must be considered in the overall design process. Further details of these important considerations have been dealt with by Moroney [25]. However, some of these considerations can still be incorporated in the systematic LQG/LTR design procedure.

VII.4 Recommendations

The following are recommandations for further work on the voltage regulation problem in static SNPSs :

1.) The integrated nonlinear SNPS model can be made more amenable to investigating variations in the system's operating conditions, besides changes that can occur in the fuel temperature feedback coefficients. Such effect could include failures in the TE-EM pumps, and loss of radiator's surface area.

2.) In this research, only sensor noise has been incorporated on the load voltage measurements. The performance of the gain-scheduled compensator could also be investigated by incorporating process and actuator noise.

3.) Different linear control system design techniques, such the LQ-servo, can be considered for the load-following of the static SNPSs.

4.) Since the gain-scheduled compensator is designed for an inherently stable system, another controller designed for an inherently unstable system can be designed and used for voltage regulation in cases where the fuel temperature feedback reactivity coefficient is positive.

REFERENCES

[1] El-Genk, M. S. and Hoover M. D., 1984, *Space Nuclear Power Systems*, eds., vol. 1, p. 16-17, Orbit Book Co., Malabar, FL.

[2] J. D. Metzger, M. S. El-Genk and A. G. Parlos, "Model Reference Adaptive Control with Selective State Variable Weighting Applied to a Space Nuclear Power System," *Nuclear Science and Engineering*, vol. 109, pp. 171-187, October 1991.

[3] El-Genk, M. S., J. T. Seo, and J. J. Buksa, 1986b, "Load Following and Reliability Studies of Thermoelectric SP-100 Systems," in *Trans. 21st Intersociety Energy Conversion Engineering Conference*, held in San Diego, CA, 25-29 August 1986.

[4] M. S. El-Genk, and J. T. Seo, "SNPSAM -Space Nuclear Power System Analysis Model," *Transaction 3rd symposium on Space Nuclear Power Systems*, Albuquerque, NM, January 13-16, 1986

[5] J. D. Metzger, "Development of Model-Reference Adaptive Control with Application to a Space Nuclear Power System," PhD Dissertation, University of New Mexico, Albuquerque, NM, (Dec. 1989).

[6] Metzger, J. D., and M. S. El-Genk, 1991, "A High-Efficiency Thermoelectric Converter for Space Applications," in *Trans. 26th Intersociety Energy Conversion Conference*, held in Boston, MA, 4-9 August 1991, vol. 3, pp. 218-223.

[7] Lamp, T., and B. Donnovan, 1991, "The Advanced Thermoionics Initiative Program," in *Trans. 26th Intersociety Energy Conversion Conference*, held in Boston, MA, 4-9 August 1991, vol. 3, pp. 218-223.

[8] Begg, L., and Lt. D. Verrill, W. Otting, 1991, "STAR-C Thermionic Space Nuclear Power System," in *Trans. 26th Intersociety Energy Conversion Conference*, held in Boston, MA, 4-9 August 1991, vol. 1, pp. 446-451.

[9] Jacox, M. G., R. G. Bennett, L. B. Lundberg, B. G. Miller, and R. L. Drexler, 1991, "Small Ex-Core Heat Pipe Thermoionic Reactor Concept (SEHPTR)," in *Trans. 26th Intersociety Energy Conversion Conference*, held in Boston, MA, 4-9 August 1991, vol. 1, pp. 440-445.

[10] Nassersharif, B., M. J. Gaeta, and F. Berge, 1991, "Extension of the CENTAR System Simulation Code to Thermoionic Space Nuclear Reactors," in *Trans. 26th Intersociety Energy Conversion Conference*, held in Boston, MA, 4-9 August 1991, vol. 3, pp. 160-170.

[11] Atomic Industrial Forum (Committee on the Nuclear Space Program), 1969, *Guidebook for the Application of Space Nuclear Power Systems; Report,* Sec. 3, Atomic Industrial Forum, New York.

[12] Zarghami, F. M., J. C. Atwell, S. A. Salamah, and U. N. Sinha, 1989, "Thermoelectric Electro-Magnetic Pump Design for the SP-100 Reference Flight System," in *Trans. 24th Intersociety Energy Conversion Engineering Conference,* held in Arlington, VA, August 6-11, 1989, vol. 2, pp. 1227-1228.

[13] Rider, W. J., and M. S. El-Genk, 1989, "Reliability and Vulnerability Studies of the SP-100 System," in *Trans. 24th Intersociety Energy Conversion Engineering Conference,* held in Arlington, VA, August 6-11, 1989, vol. 2, pp. 1237-1243.

[14] Buksa, J. J., and D. B. McColl, 1989, "STEPAC-An SP-100 Thermoelectric-Electromagnetic Pump Analysis Code," in *Trans. 24th Intersociety Energy Conversion Engineering Conference,* held in Arlington, VA, August 6-11, 1989, vol. 1, pp. 81-85.

[15] M. Athans, " A Tutorial on the LQG/LTR Method," in *Proc. American Control Conference*, Seattle, WA, June 1986.

[16] J. Doyle and G. Stein, " Multivariable Feedback Design: Concepts for a Classical/Modern Synthesis,"*IEEE Transactions on Automatic Control*, vol. AC-26, pp.4-16, 1981.

[17] G. Strang, *Linear Algebra and its Applications*, Academic Press Inc., New York, 1985.

[18] K. Ogata, *Modern Control Engineering*, Prentice-Hall, Englewood Cliffs, NJ, 1987.

[19] I.J. Nagrath and M. Gopal, *Control Systems Engineering*, Wiley Eastern, New Delhi, India, 1982.

[20] N.A. Lehtomaki, N.R. Sandell, Jr., and M. Athans, "Robustness Results in Linear-Quadratic Gaussian Based Multivariable Control Designs," *IEEE Transactions on Automatic Control*, Vol. AC-26, pp. 75-92, 1981.

[21] T. Kailath, *Linear Systems*, Prentice-Hall, Englewood Cliffs, NJ, 1980.

[22] R.E. Kalman and R.S. Bucy, " New Results in Linear Filtering and Prediction Theory," *Trans. ASME D.J. Basic Eng.*, Vol. 83, pp. 95-107, Dec. 1961.

[23] H. Kwakernaak and R. Sivan, *Linear Optimal Control Systems*, Wiley-Interscience, New York, 1972.

[24] J. S. Shamma and M. Athans, "Analysis of Gain Scheduled Control for Nonlinear Plants," *IEEE Transactions on Automatic Control*, Vol. AC-35, pp. 898-907, 1990.

[25] P. Moroney, 1983, *Issues in the Implementation of the Digital Feedback Compensators*, The MIT Press. Cambridge, MA.

APPENDIX A

LINEARIZED REFERENCE SNPS MODELS

This appendix describes the linearized reference models of the SNPS about twentyone operating points.

A.1 Scaling of the Linearized Reference Model States

Scaling of the system states is done to improve the numerical characteristics of the **A** matrix, such as its condition number which is related to stiffness of the state equations. Three of the linearized reference model states, namely, the neutronic power, and the two delay-neutron precursor concentrations are scaled by the steady-state value of the neutronic power at each equilibrium point.

A.2 The Linearized Reference Model Descriptions

The linearized reference models are described by the operating power level (steady state) about which the nonlinear reference model was linearized. For example: 150% model means that the model was obtained by linearizing the nonlinear reference model while operating at 150% of full power. The **B**, and **L** vectors are constant for all the linearized reference models, given by:

$$\mathbf{B} = [2.5e6 \quad 0 \quad 0 \quad 0 \quad 0 \quad 0 \quad 0 \quad 0 \quad 0], \tag{121}$$

and,

$$\mathbf{L} = [0 \quad 0 \quad 0 \quad 0 \quad 0 \quad 0 \quad 0 \quad -4.067e-6 \quad 0], \tag{122}$$

and **D** is the zero vector. The **A**, **C** and **F** matrices for all the linearized models are given in Tables 7 through 27.

Table 7. The System Matrices (A, C, and F) of the 50% of Full Power Linearized Model

A[i,j]	1	2	3	4	5	6	7	8	9
1	-1.606E+04	2.585E-02	2.461E-01	-2.500E+01	0.000E+00	0.000E+00	0.000E+00	0.000E+00	0.000E+00
2	4.035E+03	-2.585E-02	0.000E+00	0.000E+00	0.000E+00	0.000E+00	0.000E+00	0.000E+00	0.000E+00
3	1.202E+04	0.000E+00	-2.461E-01	0.000E+00	0.000E+00	0.000E+00	0.000E+00	0.000E+00	0.000E+00
4	3.649E+01	0.000E+00	0.000E+00	-6.141E-01	3.070E-01	0.000E+00	3.070E-01	0.000E+00	0.000E+00
5	0.000E+00	0.000E+00	0.000E+00	2.704E-01	-3.145E-01	0.000E+00	4.409E-01	0.000E+00	0.000E+00
6	0.000E+00	0.000E+00	0.000E+00	0.000E+00	2.303E-01	-3.813E-01	0.000E+00	1.510E-01	0.000E+00
7	0.000E+00	0.000E+00	0.000E+00	0.000E+00	0.000E+00	1.000E+00	-1.000E+00	0.000E+00	0.000E+00
8	0.000E+00	0.000E+00	0.000E+00	0.000E+00	5.358E-02	5.358E-02	0.000E+00	-2.068E-01	9.964E-02
9	0.000E+00	0.000E+00	0.000E+00	0.000E+00	0.000E+00	0.000E+00	0.000E+00	1.384E-02	-1.837E-02

C[i,j]	1
1	0.000E+00
2	0.000E+00
3	0.000E+00
4	0.000E+00
5	2.985E-01
6	0.000E+00
7	0.000E+00
8	-1.813E-01
9	0.000E+00

F = [-1.423E-04]

Table 8. The System Matrices (**A**, **C**, and **F**) of the 55% of Full Power Linearized Model

A[ ]	1	2	3	4	5	6	7	8	9
1	-1.606E+04	2.585E-02	2.461E-01	-2.500E+01	0.000E+00	0.000E+00	0.000E+00	0.000E+00	0.000E+00
2	4.035E+03	-2.585E-02	0.000E+00	0.000E+00	0.000E+00	0.000E+00	0.000E+00	0.000E+00	0.000E+00
3	1.202E+04	0.000E+00	-2.461E-01	0.000E+00	0.000E+00	0.000E+00	0.000E+00	0.000E+00	0.000E+00
4	3.823E+01	0.000E+00	0.000E+00	-6.480E-01	3.240E-01	0.000E+00	3.240E-01	0.000E+00	0.000E+00
5	0.000E+00	0.000E+00	0.000E+00	2.854E-01	-3.390E-01	0.000E+00	5.360E-02	0.000E+00	0.000E+00
6	0.000E+00	0.000E+00	0.000E+00	0.000E+00	2.590E-01	-4.105E-01	0.000E+00	1.514E-01	0.000E+00
7	0.000E+00	0.000E+00	0.000E+00	0.000E+00	0.000E+00	1.000E+00	-1.000E+00	0.000E+00	0.000E+00
8	0.000E+00	0.000E+00	0.000E+00	0.000E+00	5.376E-02	5.376E-02	0.000E+00	-2.077E-01	1.002E-01
9	0.000E+00	0.000E+00	0.000E+00	0.000E+00	0.000E+00	0.000E+00	0.000E+00	1.391E-02	-1.859E-02

C[ ]'	1
1	0.000E+00
2	0.000E+00
3	0.000E+00
4	0.000E+00
5	3.023E-01
6	0.000E+00
7	0.000E+00
8	-1.835E-01
9	0.000E+00

F = [-1.357E-04]

Table 9. The System Matrices (A, C, and F) of the 60% of Full Power Linearized Model

A[ ]	1	2	3	4	5	6	7	8	9
1	-1.606E+04	2.585E-02	2.461E-01	-2.500E+01	0.000E+00	0.000E+00	0.000E+00	0.000E+00	0.000E+00
2	4.035E+03	-2.585E-02	0.000E+00	0.000E+00	0.000E+00	0.000E+00	0.000E+00	0.000E+00	0.000E+00
3	1.202E+04	0.000E+00	-2.461E-01	0.000E+00	0.000E+00	0.000E+00	0.000E+00	0.000E+00	0.000E+00
4	3.992E+01	0.000E+00	0.000E+00	-6.874E-01	3.437E-01	0.000E+00	0.000E+00	0.000E+00	0.000E+00
5	0.000E+00	0.000E+00	0.000E+00	3.028E-01	-3.653E-01	0.000E+00	6.254E-02	0.000E+00	0.000E+00
6	0.000E+00	0.000E+00	0.000E+00	0.000E+00	2.889E-01	-4.408E-01	0.000E+00	1.519E-01	0.000E+00
7	0.000E+00	0.000E+00	0.000E+00	0.000E+00	0.000E+00	1.000E+00	-1.000E+00	0.000E+00	0.000E+00
8	0.000E+00	0.000E+00	0.000E+00	0.000E+00	5.393E-02	5.393E-02	0.000E+00	-2.085E-01	1.007E-01
9	0.000E+00	0.000E+00	0.000E+00	0.000E+00	0.000E+00	0.000E+00	0.000E+00	1.398E-02	-1.879E-02

C[ ]'	1
1	0.000E+00
2	0.000E+00
3	0.000E+00
4	0.000E+00
5	3.057E-01
6	0.000E+00
7	0.000E+00
8	-1.857E-01
9	0.000E+00

F = [-1.284E-04]

Table 10. The System Matrices (**A**, **C**, and **F**) of the 65% of Full Power Linearized Model

A[ ]	1	2	3	4	5	6	7	8	9
1	-1.606E+04	2.585E-02	2.461E-01	-2.500E+01	0.000E+00	0.000E+00	0.000E+00	0.000E+00	0.000E+00
2	4.035E+03	-2.585E-02	0.000E+00	0.000E+00	0.000E+00	0.000E+00	0.000E+00	0.000E+00	0.000E+00
3	1.202E+04	0.000E+00	-2.461E-01	0.000E+00	0.000E+00	0.000E+00	0.000E+00	0.000E+00	0.000E+00
4	4.156E+01	0.000E+00	0.000E+00	-7.325E-01	3.662E-01	0.000E+00	3.662E-01	0.000E+00	0.000E+00
5	0.000E+00	0.000E+00	0.000E+00	3.227E-01	-3.933E-01	0.000E+00	7.067E-02	0.000E+00	0.000E+00
6	0.000E+00	0.000E+00	0.000E+00	0.000E+00	3.194E-01	-4.718E-01	0.000E+00	1.524E-01	0.000E+00
7	0.000E+00	0.000E+00	0.000E+00	0.000E+00	0.000E+00	1.000E+00	-1.000E+00	0.000E+00	0.000E+00
8	0.000E+00	0.000E+00	0.000E+00	0.000E+00	5.411E-02	5.411E-02	0.000E+00	-2.094E-01	1.012E-01
9	0.000E+00	0.000E+00	0.000E+00	0.000E+00	0.000E+00	0.000E+00	0.000E+00	1.405E-02	-1.898E-02

C[ ]'	1
1	0.000E+00
2	0.000E+00
3	0.000E+00
4	0.000E+00
5	3.124E-01
6	0.000E+00
7	0.000E+00
8	-1.880E-01
9	0.000E+00

F = [-1.210E-04]

Table 11. The System Matrices (A, C, and F) of the 70% of Full Power Linearized Model

A[i,j]	1	2	3	4	5	6	7	8	9
1	-1.606E+04	2.585E-02	2.461E-01	-2.500E+01	0.000E+00	0.000E+00	0.000E+00	0.000E+00	0.000E+00
2	4.035E+03	-2.585E-02	0.000E+00	0.000E+00	0.000E+00	0.000E+00	0.000E+00	0.000E+00	0.000E+00
3	1.202E+04	0.000E+00	-2.461E-01	0.000E+00	0.000E+00	0.000E+00	0.000E+00	0.000E+00	0.000E+00
4	4.316E+01	0.000E+00	0.000E+00	-7.836E-01	3.918E-01	0.000E+00	3.918E-01	0.000E+00	0.000E+00
5	0.000E+00	0.000E+00	0.000E+00	3.452E-01	-4.231E-01	0.000E+00	7.789E-02	0.000E+00	0.000E+00
6	0.000E+00	0.000E+00	0.000E+00	0.000E+00	3.507E-01	-5.036E-01	0.000E+00	1.529E-01	0.000E+00
7	0.000E+00	0.000E+00	0.000E+00	0.000E+00	0.000E+00	1.000E+00	-1.000E+00	0.000E+00	0.000E+00
8	0.000E+00	0.000E+00	0.000E+00	0.000E+00	5.428E-02	5.428E-02	0.000E+00	-2.102E-01	1.016E-01
9	0.000E+00	0.000E+00	0.000E+00	0.000E+00	0.000E+00	0.000E+00	0.000E+00	1.411E-02	-1.917E-02

C'[i]	1
1	0.000E+00
2	0.000E+00
3	0.000E+00
4	0.000E+00
5	3.124E-01
6	0.000E+00
7	0.000E+00
8	-1.904E-01
9	0.000E+00

F = [-1.142E-04]

Table 12. The System Matrices (A, C, and F) of the 75% of Full Power Linearized Model

A[i,j]	1	2	3	4	5	6	7	8	9
1	-1.606E+04	2.585E-02	2.461E-01	-2.500E+01	0.000E+00	0.000E+00	0.000E+00	0.000E+00	0.000E+00
2	4.035E+03	-2.585E-02	0.000E+00	0.000E+00	0.000E+00	0.000E+00	0.000E+00	0.000E+00	0.000E+00
3	1.202E+04	0.000E+00	-2.461E-01	0.000E+00	0.000E+00	0.000E+00	0.000E+00	0.000E+00	0.000E+00
4	4.472E+01	0.000E+00	0.000E+00	-8.406E-01	4.203E-01	0.000E+00	4.203E-01	0.000E+00	0.000E+00
5	0.000E+00	0.000E+00	0.000E+00	3.703E-01	-4.543E-01	0.000E+00	8.402E-02	0.000E+00	0.000E+00
6	0.000E+00	0.000E+00	0.000E+00	0.000E+00	3.823E-01	-5.358E-01	0.000E+00	1.534E-01	0.000E+00
7	0.000E+00	0.000E+00	0.000E+00	0.000E+00	0.000E+00	1.000E+00	-1.000E+00	0.000E+00	0.000E+00
8	0.000E+00	0.000E+00	0.000E+00	0.000E+00	5.445E-02	5.445E-02	0.000E+00	-2.110E-01	1.021E-01
9	0.000E+00	0.000E+00	0.000E+00	0.000E+00	0.000E+00	0.000E+00	0.000E+00	1.418E-02	-1.934E-02

C'[i]	1
1	0.000E+00
2	0.000E+00
3	0.000E+00
4	0.000E+00
5	3.153E-01
6	0.000E+00
7	0.000E+00
8	-1.928E-01
9	0.000E+00

F = [-1.086E-04]

Table 13. The System Matrices (A, C, and F) of the 80% of Full Power Linearized Model

A[i,j]	1	2	3	4	5	6	7	8	9
1	-1.606E+04	2.585E-02	2.461E-01	-2.500E+01	0.000E+00	0.000E+00	0.000E+00	0.000E+00	0.000E+00
2	4.035E+03	-2.585E-02	0.000E+00	0.000E+00	0.000E+00	0.000E+00	0.000E+00	0.000E+00	0.000E+00
3	1.202E+04	0.000E+00	-2.461E-01	0.000E+00	0.000E+00	0.000E+00	0.000E+00	0.000E+00	0.000E+00
4	4.627E+01	0.000E+00	0.000E+00	-9.043E-01	4.521E-01	0.000E+00	4.521E-01	0.000E+00	0.000E+00
5	0.000E+00	0.000E+00	0.000E+00	3.984E-01	-4.874E-01	0.000E+00	8.907E-02	0.000E+00	0.000E+00
6	0.000E+00	0.000E+00	0.000E+00	0.000E+00	4.146E-01	-5.685E-01	0.000E+00	1.539E-01	0.000E+00
7	0.000E+00	0.000E+00	0.000E+00	0.000E+00	0.000E+00	1.000E+00	-1.000E+00	0.000E+00	0.000E+00
8	0.000E+00	0.000E+00	0.000E+00	0.000E+00	5.462E-02	5.462E-02	0.000E+00	-2.118E-01	1.025E-01
9	0.000E+00	0.000E+00	0.000E+00	0.000E+00	0.000E+00	0.000E+00	0.000E+00	1.424E-02	-1.952E-02

C'[i]	1
1	0.000E+00
2	0.000E+00
3	0.000E+00
4	0.000E+00
5	3.183E-01
6	0.000E+00
7	0.000E+00
8	-1.953E-01
9	0.000E+00

F = [-1.036E-04]

Table 11. The System Matrices (**A**, **C**, and **F**) of the 85% of Full Power Linearized Model

A[i,j]	1	2	3	4	5	6	7	8	9
1	-1.606E+04	2.585E-02	2.461E-01	-2.500E+01	0.000E+00	0.000E+00	0.000E+00	0.000E+00	0.000E+00
2	4.035E+03	-2.585E-02	0.000E+00	0.000E+00	0.000E+00	0.000E+00	0.000E+00	0.000E+00	0.000E+00
3	1.202E+04	0.000E+00	-2.461E-01	0.000E+00	0.000E+00	0.000E+00	0.000E+00	0.000E+00	0.000E+00
4	4.779E+01	0.000E+00	0.000E+00	-9.737E-01	4.869E-01	0.000E+00	4.869E-01	0.000E+00	0.000E+00
5	0.000E+00	0.000E+00	0.000E+00	4.290E-01	-5.219E-01	0.000E+00	9.290E-02	0.000E+00	0.000E+00
6	0.000E+00	0.000E+00	0.000E+00	0.000E+00	4.470E-01	-6.014E-01	0.000E+00	1.544E-01	0.000E+00
7	0.000E+00	0.000E+00	0.000E+00	0.000E+00	0.000E+00	1.000E+00	-1.000E+00	0.000E+00	0.000E+00
8	0.000E+00	0.000E+00	0.000E+00	0.000E+00	5.479E-02	5.479E-02	0.000E+00	-2.125E-01	1.030E-01
9	0.000E+00	0.000E+00	0.000E+00	0.000E+00	0.000E+00	0.000E+00	0.000E+00	1.430E-02	-1.969E-02

C'[i]	1
1	0.000E+00
2	0.000E+00
3	0.000E+00
4	0.000E+00
5	3.201E-01
6	0.000E+00
7	0.000E+00
8	-1.979E-01
9	0.000E+00

F = [-9.890E-05]

Table 15. The System Matrices (A, C, and F) of the 90% of Full Power Linearized Model

A[i,j]	1	2	3	4	5	6	7	8	9
1	-1.606E+04	2.585E-02	2.461E-01	-2.500E+01	0.000E+00	0.000E+00	0.000E+00	0.000E+00	0.000E+00
2	4.035E+03	-2.585E-02	0.000E+00	0.000E+00	0.000E+00	0.000E+00	0.000E+00	0.000E+00	0.000E+00
3	1.202E+04	0.000E+00	-2.461E-01	0.000E+00	0.000E+00	0.000E+00	0.000E+00	0.000E+00	0.000E+00
4	4.929E+01	0.000E+00	0.000E+00	-1.049E+00	5.247E-01	0.000E+00	5.247E-01	0.000E+00	0.000E+00
5	0.000E+00	0.000E+00	0.000E+00	4.623E-01	-5.579E-01	0.000E+00	9.553E-02	0.000E+00	0.000E+00
6	0.000E+00	0.000E+00	0.000E+00	0.000E+00	4.797E-01	-6.345E-01	0.000E+00	1.548E-01	0.000E+00
7	0.000E+00	0.000E+00	0.000E+00	0.000E+00	0.000E+00	1.000E+00	-1.000E+00	0.000E+00	0.000E+00
8	0.000E+00	0.000E+00	0.000E+00	0.000E+00	5.496E-02	5.496E-02	0.000E+00	-2.133E-01	1.034E-01
9	0.000E+00	0.000E+00	0.000E+00	0.000E+00	0.000E+00	0.000E+00	0.000E+00	1.436E-02	-1.986E-02

C'[i]	1
1	0.000E+00
2	0.000E+00
3	0.000E+00
4	0.000E+00
5	3.225E-01
6	0.000E+00
7	0.000E+00
8	-2.006E-01
9	0.000E+00

F = [-9.480E-05]

Table 16. The System Matrices (**A**, **C**, and **F**) of the 95% of Full Power Linearized Model

A[i,j]	1	2	3	4	5	6	7	8	9
1	-1.606E+04	2.585E-02	2.461E-01	-2.500E+01	0.000E+00	0.000E+00	0.000E+00	0.000E+00	0.000E+00
2	4.035E+03	-2.585E-02	0.000E+00	0.000E+00	0.000E+00	0.000E+00	0.000E+00	0.000E+00	0.000E+00
3	1.202E+04	0.000E+00	-2.461E-01	0.000E+00	0.000E+00	0.000E+00	0.000E+00	0.000E+00	0.000E+00
4	5.078E+01	0.000E+00	0.000E+00	-1.131E+00	5.653E-01	0.000E+00	5.653E-01	0.000E+00	0.000E+00
5	0.000E+00	0.000E+00	0.000E+00	4.981E-01	-5.950E-01	0.000E+00	9.696E-02	0.000E+00	0.000E+00
6	0.000E+00	0.000E+00	0.000E+00	0.000E+00	5.124E-01	-6.677E-01	0.000E+00	1.553E-01	0.000E+00
7	0.000E+00	0.000E+00	0.000E+00	0.000E+00	0.000E+00	1.000E+00	-1.000E+00	0.000E+00	0.000E+00
8	0.000E+00	0.000E+00	0.000E+00	0.000E+00	5.513E-02	5.513E-02	0.000E+00	-2.141E-01	1.038E-01
9	0.000E+00	0.000E+00	0.000E+00	0.000E+00	0.000E+00	0.000E+00	0.000E+00	1.442E-02	-2.002E-02

C[i]	1
1	0.000E+00
2	0.000E+00
3	0.000E+00
4	0.000E+00
5	3.243E-01
6	0.000E+00
7	0.000E+00
8	-2.033E-01
9	0.000E+00

F = [-9.080E-05]

Table 17. The System Matrices (A, C, and F) of the 100% of Full Power Linearized Model

A[i,j]	1	2	3	4	5	6	7	8	9
1	-1.606E+04	2.585E-02	2.461E-01	-2.500E+01	0.000E+00	0.000E+00	0.000E+00	0.000E+00	0.000E+00
2	4.035E+03	-2.585E-02	0.000E+00	0.000E+00	0.000E+00	0.000E+00	0.000E+00	0.000E+00	0.000E+00
3	1.202E+04	0.000E+00	-2.461E-01	0.000E+00	0.000E+00	0.000E+00	0.000E+00	0.000E+00	0.000E+00
4	5.225E+01	0.000E+00	0.000E+00	-1.217E+00	6.087E-01	0.000E+00	6.087E-01	0.000E+00	0.000E+00
5	0.000E+00	0.000E+00	0.000E+00	5.364E-01	-6.336E-01	0.000E+00	9.726E-02	0.000E+00	0.000E+00
6	0.000E+00	0.000E+00	0.000E+00	0.000E+00	5.453E-01	-7.011E-01	0.000E+00	1.558E-01	0.000E+00
7	0.000E+00	0.000E+00	0.000E+00	0.000E+00	0.000E+00	1.000E+00	-1.000E+00	0.000E+00	0.000E+00
8	0.000E+00	0.000E+00	0.000E+00	0.000E+00	5.529E-02	5.529E-02	0.000E+00	-2.148E-01	1.042E-01
9	0.000E+00	0.000E+00	0.000E+00	0.000E+00	0.000E+00	0.000E+00	0.000E+00	1.447E-02	-2.018E-02

C'[i]	1
1	0.000E+00
2	0.000E+00
3	0.000E+00
4	0.000E+00
5	3.247E-01
6	0.000E+00
7	0.000E+00
8	-2.062E-01
9	0.000E+00

F = [-8.350E-05]

Table 18. The System Matrices (**A**, **C**, and **F**) of the 105% of Full Power Linearized Model

A[i,j]	1	2	3	4	5	6	7	8	9
1	-1.606E+04	2.585E-02	2.461E-01	-2.500E+01	0.000E+00	0.000E+00	0.000E+00	0.000E+00	0.000E+00
2	4.035E+03	-2.585E-02	0.000E+00	0.000E+00	0.000E+00	0.000E+00	0.000E+00	0.000E+00	0.000E+00
3	1.202E+04	0.000E+00	-2.461E-01	0.000E+00	0.000E+00	0.000E+00	0.000E+00	0.000E+00	0.000E+00
4	5.372E+01	0.000E+00	0.000E+00	-1.310E+00	6.552E-01	0.000E+00	6.552E-01	0.000E+00	0.000E+00
5	0.000E+00	0.000E+00	0.000E+00	5.773E-01	-6.608E-01	0.000E+00	8.349E-02	0.000E+00	0.000E+00
6	0.000E+00	0.000E+00	0.000E+00	0.000E+00	5.566E-01	-7.128E-01	0.000E+00	1.562E-01	0.000E+00
7	0.000E+00	0.000E+00	0.000E+00	0.000E+00	0.000E+00	1.000E+00	-1.000E+00	0.000E+00	0.000E+00
8	0.000E+00	0.000E+00	0.000E+00	0.000E+00	5.544E-02	5.544E-02	0.000E+00	-2.155E-01	1.046E-01
9	0.000E+00	0.000E+00	0.000E+00	0.000E+00	0.000E+00	0.000E+00	0.000E+00	1.452E-02	-2.033E-02

C'[i]	1
1	0.000E+00
2	0.000E+00
3	0.000E+00
4	0.000E+00
5	3.250E-01
6	0.000E+00
7	0.000E+00
8	-2.092E-01
9	0.000E+00

F = [-8.500E-05]

Table 19. The System Matrices (A, C, and F) of the 110% of Full Power Linearized Model

A[i,j]	1	2	3	4	5	6	7	8	9
1	-1.606E+04	2.585E-02	2.461E-01	-2.500E+01	0.000E+00	0.000E+00	0.000E+00	0.000E+00	0.000E+00
2	4.035E+03	-2.585E-02	0.000E+00	0.000E+00	0.000E+00	0.000E+00	0.000E+00	0.000E+00	0.000E+00
3	1.202E+04	0.000E+00	-2.461E-01	0.000E+00	0.000E+00	0.000E+00	0.000E+00	0.000E+00	0.000E+00
4	5.520E+01	0.000E+00	0.000E+00	-1.410E+00	7.050E-01	0.000E+00	7.050E-01	0.000E+00	0.000E+00
5	0.000E+00	0.000E+00	0.000E+00	6.213E-01	-6.892E-01	0.000E+00	6.799E-02	0.000E+00	0.000E+00
6	0.000E+00	0.000E+00	0.000E+00	0.000E+00	5.673E-01	-7.240E-01	0.000E+00	1.566E-01	0.000E+00
7	0.000E+00	0.000E+00	0.000E+00	0.000E+00	0.000E+00	1.000E+00	-1.000E+00	0.000E+00	0.000E+00
8	0.000E+00	0.000E+00	0.000E+00	0.000E+00	5.559E-02	5.559E-02	0.000E+00	-2.161E-01	1.050E-01
9	0.000E+00	0.000E+00	0.000E+00	0.000E+00	0.000E+00	0.000E+00	0.000E+00	1.457E-02	-2.049E-02

C'[i]	1
1	0.000E+00
2	0.000E+00
3	0.000E+00
4	0.000E+00
5	3.263E-01
6	0.000E+00
7	0.000E+00
8	-2.124E-01
9	0.000E+00

F = [-8.200E-04]

Table 20. The System Matrices (A, C, and F) of the 115% of Full Power Linearized Model

A[i,j]	1	2	3	4	5	6	7	8	9
1	-1.606E+04	2.585E-02	2.461E-01	-2.500E+01	0.000E+00	0.000E+00	0.000E+00	0.000E+00	0.000E+00
2	4.035E+03	-2.585E-02	0.000E+00	0.000E+00	0.000E+00	0.000E+00	0.000E+00	0.000E+00	0.000E+00
3	1.202E+04	0.000E+00	-2.461E-01	0.000E+00	0.000E+00	0.000E+00	0.000E+00	0.000E+00	0.000E+00
4	5.667E+01	0.000E+00	0.000E+00	-1.513E+00	7.564E-01	0.000E+00	7.564E-01	0.000E+00	0.000E+00
5	0.000E+00	0.000E+00	0.000E+00	6.665E-01	-7.178E-01	0.000E+00	5.133E-02	0.000E+00	0.000E+00
6	0.000E+00	0.000E+00	0.000E+00	0.000E+00	5.773E-01	-7.343E-01	0.000E+00	1.570E-01	0.000E+00
7	0.000E+00	0.000E+00	0.000E+00	0.000E+00	0.000E+00	1.000E+00	-1.000E+00	0.000E+00	0.000E+00
8	0.000E+00	0.000E+00	0.000E+00	0.000E+00	5.574E-02	5.574E-02	0.000E+00	-2.168E-01	1.053E-01
9	0.000E+00	0.000E+00	0.000E+00	0.000E+00	0.000E+00	0.000E+00	0.000E+00	1.462E-02	-2.064E-02

C'[i]	1
1	0.000E+00
2	0.000E+00
3	0.000E+00
4	0.000E+00
5	3.276E-01
6	0.000E+00
7	0.000E+00
8	-2.157E-01
9	0.000E+00

F = [-7.917E-05]

Table 21. The System Matrices (A, C, and F) of the 120% of Full Power Linearized Model

A[i,j]	1	2	3	4	5	6	7	8	9
1	-1.606E+04	2.585E-02	2.461E-01	-2.500E+01	0.000E+00	0.000E+00	0.000E+00	0.000E+00	0.000E+00
2	4.035E+03	-2.585E-02	0.000E+00	0.000E+00	0.000E+00	0.000E+00	0.000E+00	0.000E+00	0.000E+00
3	1.202E+04	0.000E+00	-2.461E-01	0.000E+00	0.000E+00	0.000E+00	0.000E+00	0.000E+00	0.000E+00
4	5.814E+01	0.000E+00	0.000E+00	-1.619E+00	8.094E-01	0.000E+00	8.094E-01	0.000E+00	0.000E+00
5	0.000E+00	0.000E+00	0.000E+00	7.132E-01	-7.467E-01	0.000E+00	3.356E-02	0.000E+00	0.000E+00
6	0.000E+00	0.000E+00	0.000E+00	0.000E+00	5.866E-01	-7.440E-01	0.000E+00	1.575E-01	0.000E+00
7	0.000E+00	0.000E+00	0.000E+00	0.000E+00	0.000E+00	1.000E+00	-1.000E+00	0.000E+00	0.000E+00
8	0.000E+00	0.000E+00	0.000E+00	0.000E+00	5.589E-02	5.589E-02	0.000E+00	-2.175E-01	1.057E-01
9	0.000E+00	0.000E+00	0.000E+00	0.000E+00	0.000E+00	0.000E+00	0.000E+00	1.467E-02	-2.079E-02

C'[i]	1
1	0.000E+00
2	0.000E+00
3	0.000E+00
4	0.000E+00
5	3.288E-01
6	0.000E+00
7	0.000E+00
8	-2.191E-01
9	0.000E+00

F = [-7.656E-05]

Table 22. The System Matrices (**A**, **C**, and **F**) of the 125% of Full Power Linearized Model

A[i,j]	1	2	3	4	5	6	7	8	9
1	-1.606E+04	2.585E-02	2.461E-01	-2.500E+01	0.000E+00	0.000E+00	0.000E+00	0.000E+00	0.000E+00
2	4.035E+03	-2.585E-02	0.000E+00	0.000E+00	0.000E+00	0.000E+00	0.000E+00	0.000E+00	0.000E+00
3	1.202E+04	0.000E+00	-2.461E-01	0.000E+00	0.000E+00	0.000E+00	0.000E+00	0.000E+00	0.000E+00
4	5.962E+01	0.000E+00	0.000E+00	-1.727E+00	8.637E-01	0.000E+00	8.637E-01	0.000E+00	0.000E+00
5	0.000E+00	0.000E+00	0.000E+00	7.611E-01	-7.759E-01	0.000E+00	1.478E-02	0.000E+00	0.000E+00
6	0.000E+00	0.000E+00	0.000E+00	0.000E+00	5.952E-01	-7.531E-01	0.000E+00	1.579E-01	0.000E+00
7	0.000E+00	0.000E+00	0.000E+00	0.000E+00	0.000E+00	1.000E+00	-1.000E+00	0.000E+00	0.000E+00
8	0.000E+00	0.000E+00	0.000E+00	0.000E+00	5.604E-02	5.604E-02	0.000E+00	-2.181E-01	1.060E-01
9	0.000E+00	0.000E+00	0.000E+00	0.000E+00	0.000E+00	0.000E+00	0.000E+00	1.473E-02	-2.094E-02

C'[i]	1
1	0.000E+00
2	0.000E+00
3	0.000E+00
4	0.000E+00
5	3.300E-01
6	0.000E+00
7	0.000E+00
8	-2.228E-01
9	0.000E+00

F = [-7.425E-05]

Table 23. The System Matrices (A, C, and F) of the 130% of Full Power Linearized Model

A[i,j]	1	2	3	4	5	6	7	8	9
1	-1.606E+04	2.585E-02	2.461E-01	-2.500E+01	0.000E+00	0.000E+00	0.000E+00	0.000E+00	0.000E+00
2	4.035E+03	-2.585E-02	0.000E+00	0.000E+00	0.000E+00	0.000E+00	0.000E+00	0.000E+00	0.000E+00
3	1.202E+04	0.000E+00	-2.461E-01	0.000E+00	0.000E+00	0.000E+00	0.000E+00	0.000E+00	0.000E+00
4	6.112E+01	0.000E+00	0.000E+00	-1.839E+00	9.193E-01	0.000E+00	9.193E-01	0.000E+00	0.000E+00
5	0.000E+00	0.000E+00	0.000E+00	8.101E-01	-8.052E-01	0.000E+00	-4.890E-03	0.000E+00	0.000E+00
6	0.000E+00	0.000E+00	0.000E+00	0.000E+00	6.032E-01	-7.615E-01	0.000E+00	1.583E-01	0.000E+00
7	0.000E+00	0.000E+00	0.000E+00	0.000E+00	0.000E+00	1.000E+00	-1.000E+00	0.000E+00	0.000E+00
8	0.000E+00	0.000E+00	0.000E+00	0.000E+00	5.620E-02	5.620E-02	0.000E+00	-2.188E-01	1.064E-01
9	0.000E+00	0.000E+00	0.000E+00	0.000E+00	0.000E+00	0.000E+00	0.000E+00	1.478E-02	-2.109E-02

C'[i]	1
1	0.000E+00
2	0.000E+00
3	0.000E+00
4	0.000E+00
5	3.311E-01
6	0.000E+00
7	0.000E+00
8	-2.268E-01
9	0.000E+00

F = [-7.204E-05]

Table 24. The System Matrices (**A**, **C**, and **F**) of the 135% of Full Power Linearized Model

A[i,j]	1	2	3	4	5	6	7	8	9
1	-1.606E+04	2.585E-02	2.461E-01	-2.500E+01	0.000E+00	0.000E+00	0.000E+00	0.000E+00	0.000E+00
2	4.035E+03	-2.585E-02	0.000E+00	0.000E+00	0.000E+00	0.000E+00	0.000E+00	0.000E+00	0.000E+00
3	1.202E+04	0.000E+00	-2.461E-01	0.000E+00	0.000E+00	0.000E+00	0.000E+00	0.000E+00	0.000E+00
4	6.262E+01	0.000E+00	0.000E+00	-1.950E+00	9.750E-01	0.000E+00	9.750E-01	0.000E+00	0.000E+00
5	0.000E+00	0.000E+00	0.000E+00	8.592E-01	-8.341E-01	0.000E+00	-2.503E-02	0.000E+00	0.000E+00
6	0.000E+00	0.000E+00	0.000E+00	0.000E+00	6.105E-01	-7.693E-01	0.000E+00	1.588E-01	0.000E+00
7	0.000E+00	0.000E+00	0.000E+00	0.000E+00	0.000E+00	1.000E+00	-1.000E+00	0.000E+00	0.000E+00
8	0.000E+00	0.000E+00	0.000E+00	0.000E+00	5.636E-02	5.636E-02	0.000E+00	-2.195E-01	1.068E-01
9	0.000E+00	0.000E+00	0.000E+00	0.000E+00	0.000E+00	0.000E+00	0.000E+00	1.483E-02	-2.124E-02

C'[i]	1
1	0.000E+00
2	0.000E+00
3	0.000E+00
4	0.000E+00
5	3.319E-01
6	0.000E+00
7	0.000E+00
8	-2.309E-01
9	0.000E+00

F = [-7.000E-05]

Table 25. The System Matrices (A, C, and F) of the 140% of Full Power Linearized Model

A[i,j]	1	2	3	4	5	6	7	8	9
1	-1.606E+04	2.585E-02	2.461E-01	-2.500E+01	0.000E+00	0.000E+00	0.000E+00	0.000E+00	0.000E+00
2	4.035E+03	-2.585E-02	0.000E+00	0.000E+00	0.000E+00	0.000E+00	0.000E+00	0.000E+00	0.000E+00
3	1.202E+04	0.000E+00	-2.461E-01	0.000E+00	0.000E+00	0.000E+00	0.000E+00	0.000E+00	0.000E+00
4	6.417E+01	0.000E+00	0.000E+00	-2.063E+00	1.032E+00	0.000E+00	1.032E+00	0.000E+00	0.000E+00
5	0.000E+00	0.000E+00	0.000E+00	9.091E-01	-8.632E-01	0.000E+00	-4.593E-02	0.000E+00	0.000E+00
6	0.000E+00	0.000E+00	0.000E+00	0.000E+00	6.172E-01	-7.765E-01	0.000E+00	1.593E-01	0.000E+00
7	0.000E+00	0.000E+00	0.000E+00	0.000E+00	0.000E+00	1.000E+00	-1.000E+00	0.000E+00	0.000E+00
8	0.000E+00	0.000E+00	0.000E+00	0.000E+00	5.652E-02	5.652E-02	0.000E+00	-2.202E-01	1.071E-01
9	0.000E+00	0.000E+00	0.000E+00	0.000E+00	0.000E+00	0.000E+00	0.000E+00	1.488E-02	-2.139E-02

C'[i]	1
1	0.000E+00
2	0.000E+00
3	0.000E+00
4	0.000E+00
5	3.329E-01
6	0.000E+00
7	0.000E+00
8	-2.354E-01
9	0.000E+00

F = [-6.805E-05]

Table 26. The System Matrices (A, C, and F) of the 145% of Full Power Linearized Model

A[i,j]	1	2	3	4	5	6	7	8	9
1	-1.606E+04	2.585E-02	2.461E-01	-2.500E+01	0.000E+00	0.000E+00	0.000E+00	0.000E+00	0.000E+00
2	4.035E+03	-2.585E-02	0.000E+00	0.000E+00	0.000E+00	0.000E+00	0.000E+00	0.000E+00	0.000E+00
3	1.202E+04	0.000E+00	-2.461E-01	0.000E+00	0.000E+00	0.000E+00	0.000E+00	0.000E+00	0.000E+00
4	6.572E+01	0.000E+00	0.000E+00	-2.176E+00	1.088E+00	0.000E+00	1.088E+00	0.000E+00	0.000E+00
5	0.000E+00	0.000E+00	0.000E+00	9.587E-01	-8.916E-01	0.000E+00	-6.704E-02	0.000E+00	0.000E+00
6	0.000E+00	0.000E+00	0.000E+00	0.000E+00	6.232E-01	-7.829E-01	0.000E+00	1.597E-01	0.000E+00
7	0.000E+00	0.000E+00	0.000E+00	0.000E+00	0.000E+00	1.000E+00	-1.000E+00	0.000E+00	0.000E+00
8	0.000E+00	0.000E+00	0.000E+00	0.000E+00	5.669E-02	5.669E-02	0.000E+00	-2.209E-01	1.075E-01
9	0.000E+00	0.000E+00	0.000E+00	0.000E+00	0.000E+00	0.000E+00	0.000E+00	1.493E-02	-2.154E-02

C'[i]	1
1	0.000E+00
2	0.000E+00
3	0.000E+00
4	0.000E+00
5	3.338E-01
6	0.000E+00
7	0.000E+00
8	-2.403E-01
9	0.000E+00

F = [-6.623E-05]

Table 27. The System Matrices (A, C, and F) of the 150% of Full Power Linearized Model

A[i,j]	1	2	3	4	5	6	7	8	9
1	-1.606E+04	2.585E-02	2.461E-01	-2.500E+01	0.000E+00	0.000E+00	0.000E+00	0.000E+00	0.000E+00
2	4.035E+03	-2.585E-02	0.000E+00	0.000E+00	0.000E+00	0.000E+00	0.000E+00	0.000E+00	0.000E+00
3	1.202E+04	0.000E+00	-2.461E-01	0.000E+00	0.000E+00	0.000E+00	0.000E+00	0.000E+00	0.000E+00
4	6.733E+01	0.000E+00	0.000E+00	-2.288E+00	1.144E+00	0.000E+00	1.144E+00	0.000E+00	0.000E+00
5	0.000E+00	0.000E+00	0.000E+00	1.008E+00	-9.196E-01	0.000E+00	-8.855E-02	0.000E+00	0.000E+00
6	0.000E+00	0.000E+00	0.000E+00	0.000E+00	6.285E-01	-7.887E-01	0.000E+00	1.602E-01	0.000E+00
7	0.000E+00	0.000E+00	0.000E+00	0.000E+00	0.000E+00	1.000E+00	-1.000E+00	0.000E+00	0.000E+00
8	0.000E+00	0.000E+00	0.000E+00	0.000E+00	5.687E-02	5.687E-02	0.000E+00	-2.216E-01	1.079E-01
9	0.000E+00	0.000E+00	0.000E+00	0.000E+00	0.000E+00	0.000E+00	0.000E+00	1.498E-02	-2.170E-02

C'[i]	1
1	0.000E+00
2	0.000E+00
3	0.000E+00
4	0.000E+00
5	3.350E-01
6	0.000E+00
7	0.000E+00
8	-2.455E-01
9	0.000E+00

F = [-6.450E-05]

APPENDIX B

LISTING OF THE FITS FOR THE SCHEDULED REFERENCE SNPS MODEL

B.1 Fits Used for the Scheduled Reference Model

The following pages list the fits used in the scheduled reference model of the SNPS. The fits are used to model the elements of the system matrices **A**, **B**, and **C**. The scheduling variable used is the electric power produced by the SNPS, $\mathbf{P_e}$.

```
c
c THIS IS THE SEGMENT OF A FORTRAN PROGRAM THAT FITS THE ELEMENTS
c OF THE LINEARIZED REFERENCE MODELS OF SNPS AS A FUNCTION OF
c EECTRIC POWER OUTPUT OF THE SYSTEM.
c
c
c THE VARIABLES USED IN THIS SEGMENT ARE:
c am(9,9)     --- 'A' MATRIX ELEMENTS - STATE MATRIX
c bm(9)       --- 'B' VECTOR, INPUT VECTOR
c c(9)        --- 'C' VECTOR, OUTPUT VECTOR
c x           --- SCHEDULING VARIABLE SCALED BY THE
c                 NOMINAL ELECTRIC POWER PRODUCED
c rparrm(21) --- VECTOR, VECTOR OF PARAMETERS
c                 EXPRESSED IN TERMS OF THE STATES
c

c   the beta(i) - 2 group
   20 amkc=1.0d0
      rparrm(2)=0.001614d0
      rparrm(3)=0.004809d0
c   the neutron generation time
      rparrm(4)=4.0d-07
c   the lambda(i) - 2 group
      rparrm(5)=0.025853d0
      rparrm(6)=0.2461d0
c   the total beta
      rparrm(7)=rparrm(2)+rparrm(3)
c   the T-H eqn constants
      rparrm(8)=amf*cpf
      if(x.le.1.0d0)then
      rparrm(9)=2.74068196d0-2.49397632d0*x
```

```
*+0.568972018d0*x**2
 else
 rparrm(9)=2.790241234d0-2.7782255246d0*x
*+0.8072848472d0*x**2
 end if
 rparrm(10)=6.581062334d0-6.668101788d0*x
*+1.9627778d0*x**2
 if(x.le.1.0d0)then
 rparrm(11)=-0.00996d0+0.37388d0*x
 else
 rparrm(11)=0.1489629021d0+0.294024646d0*x
*-0.0775379499d0*x**2
 end if
 if(x.le.1.0d0)then
 rparrm(12)=6.8277d0-0.41033d0*x
 else
 rparrm(12)=6.69599893d0-0.225052886d0*x
*-0.0519716859d0*x**2
 end if
 if(x.le.1.0d0)then
 rparrm(13)=9.6181d0-0.57802d0*x
 else
 rparrm(13)=9.43263192d0-0.3170429624d0*x
*-0.073207497894d0*x**2
 end if
 if(x.le.1.0d0)then
 rparrm(14)=10.63032195d0-1.34773111d0*x
*+0.3128847781d0*x**2
 else
 rparrm(14)=10.242d0-0.64923d0*x
 end if
 if(x.le.1.0d0)then
 rparrm(15)=76.5558133d0-9.7058838674d0*x
*+2.25329290d0*x**2
 else
 rparrm(15)=73.761d0-4.6755d0*x
 end if
 if(x.le.1.0d0)then
 rparrm(16)=298.8763343d0-192.28559175d0*x
*+68.84927513d0*x**2
 else
 rparrm(16)=251.36611922d0-92.256681688d0*x
*+15.95455235d0*x**2
 end if
 if(x.le.1.0d0)then
 rparrm(17)=-0.016985d0+0.63759d0*x
```

```
      else
      rparrm(17)=0.2540285113d0+0.5014043415d0*x-
     *0.132226566d0*x**2
      end if
c      rparrm(18)=v*curi
c      rparrm(18)=-4.0713d5+602.28d0*x
      rparrm(18)=0.56940d6*x
      rparrm(19)=1.0d0
      rparrm(20)=tsink
      rparrm(22)=amte*cpte
c     additional rparrm for Tauin
      rparrm(23)=1.0d0
      go to 24
   24 continue
      am(1,1)=-1.0d0*(rparrm(2)+rparrm(3))/rparrm(4)
      am(1,2)=rparrm(5)
      am(1,3)=rparrm(6)
      am(1,4)=pn1*alft/rparrm(4)
      am(1,5)=0.0d0
      am(1,6)=0.0d0
      am(1,7)=0.0d0
      am(1,8)=0.0d0
      am(1,9)=0.0d0
      am(2,1)=(rparrm(2))/rparrm(4)
      am(2,2)=(-1.0d0)*rparrm(5)
      am(2,3)=0.0d0
      am(2,4)=0.0d0
      am(2,5)=0.0d0
      am(2,6)=0.0d0
      am(2,7)=0.0d0
      am(2,8)=0.0d0
      am(2,9)=0.0d0
      am(3,1)=(rparrm(3))/rparrm(4)
      am(3,2)=0.0d0
      am(3,3)=(-1.0d0)*rparrm(6)
      am(3,4)=0.0d0
      am(3,5)=0.0d0
      am(3,6)=0.0d0
      am(3,7)=0.0d0
      am(3,8)=0.0d0
      am(3,9)=0.0d0
      am(4,1)=1.0d0/rparrm(8)
      am(4,2)=0.0d0
      am(4,3)=0.0d0
      am(4,4)=-1.0d0/rparrm(9)
      am(4,5)=0.5d0/rparrm(9)
```

```
am(4,6)=0.0d0
am(4,7)=0.5d0/rparrm(9)
am(4,8)=0.0d0
am(4,9)=0.0d0
am(5,1)=0.0d0
am(5,2)=0.0d0
am(5,3)=0.0d0
am(5,4)=1.0d0/rparrm(10)
am(5,5)=(-1.0d0)*(1.0d0*rparrm(11)+0.5d0/rparrm(10))
am(5,6)=0.0d0
am(5,7)=-0.5d0/rparrm(10)+rparrm(11)
am(5,8)=0.0d0
am(5,9)=0.0d0
am(6,1)=0.0d0
am(6,2)=0.0d0
am(6,3)=0.0d0
am(6,4)=0.0d0
am(6,5)=rparrm(17)-0.5d0/rparrm(12)
am(6,6)=-1.0d0*(rparrm(17)+0.5d0/rparrm(12))
am(6,7)=0.0d0
am(6,8)=1.0d0/rparrm(12)
am(6,9)=0.0d0
am(7,1)=0.0d0
am(7,2)=0.0d0
am(7,3)=0.0d0
am(7,4)=0.0d0
am(7,5)=0.0d0
am(7,6)=1.0d0/rparrm(23)
am(7,7)=-1.0d0/rparrm(23)
am(7,8)=0.0d0
am(7,9)=0.0d0
am(8,1)=0.0d0
am(8,2)=0.0d0
am(8,3)=0.0d0
am(8,4)=0.0d0
am(8,5)=0.5d0/rparrm(13)
am(8,6)=0.5d0/rparrm(13)
am(8,7)=0.0d0
am(8,8)=-1.0d0*(1.0d0/rparrm(13)+1.0d0/rparrm(14))
am(8,9)=1.0d0/rparrm(14)
am(9,1)=0.0d0
am(9,2)=0.0d0
am(9,3)=0.0d0
am(9,4)=0.0d0
am(9,5)=0.0d0
am(9,6)=0.0d0
```

```
am(9,7)=0.0d0
am(9,8)=1.0d0/rparrm(15)
am(9,9)=-1.0d0*(1.0d0/rparrm(15)+1.0d0/rparrm(16))
bm(1)=pn/rparrm(4)
bm(2)=0.0d0
bm(3)=0.0d0
bm(4)=0.0d0
bm(5)=0.0d0
bm(6)=0.0d0
bm(7)=0.0d0
bm(8)=0.0d0
bm(9)=0.0d0
rparrm(1)=rhotem
rparrm(21)=rhoexm
c(1)=0.0d0
c(2)=0.0d0
c(3)=0.0d0
c(4)=0.0d0
if(x.le.0.95d0)then
c(5)=0.24595128d0+0.129600564d0*x-0.04953809777d0*x**2
else
end if
if((x.gt.0.95d0).and.(x.le.1.05d0))then
c(5)=0.3246625d0
else
end if
if(x.gt.1.05d0)then
c(5)=0.28725935d0+0.046055781d0*x-0.0095683919d0*x**2
else
end if
c(6)=0.0d0
c(7)=0.0d0
if(x.le.1.0d0)then
c(8)=-0.164194325d0-0.0266547088d0*x-0.0153233547d0*x**2
else
c(8)=-0.201684183d0+0.0440687154d0*x-0.0487757874d0*x**2
end if
c(9)=0.0d0
```

APPENDIX C

DESCRIPTION OF THE NOISE REJECTION FILTER

C.1 The description of the system matrices of the noise rejection filter, $\mathbf{G_f}(s)$

The filter matrices, $\mathbf{A_f}$, $\mathbf{B_f}$, and $\mathbf{C_f}$ are scalars and have the following values:

$$\mathbf{A_f} = [-0.50], \tag{123}$$

$$\mathbf{B_f} = [0.25], \tag{124}$$

and,

$$\mathbf{C_f} = [0.20]. \tag{125}$$

APPENDIX D

THE GAIN VECTORS OF THE LINEAR COMPENSATORS

D.1 The Gain Matrices of the Linear Compensators

In this appendix the numerical values of the gain vectors **H** and **G** for thirteen different linear compensators are given in Tables 28 and 29, respectively.

Table 28. Filter Gain Vector, H, Obtained for the Different Linear Compensators at Different Power Levels

H[i]	50%	60%	70%	80%	90%	95%	100%
1	2.0542E-05	1.9360E-05	1.8313E-05	1.7395E-05	1.6667E-05	1.6345E-05	1.6141E-05
2	6.9410E-03	6.4259E-03	6.0053E-03	5.6572E-03	5.3868E-03	5.2685E-03	5.1885E-03
3	2.8200E+02	2.6017E+02	2.4218E+02	2.2724E+02	2.1550E+02	2.1039E+02	2.0668E+02
4	2.9234E+02	2.7053E+02	2.5264E+02	2.3778E+02	2.2620E+02	2.2114E+02	2.1765E+02
5	7.6528E-01	7.4078E-01	7.1144E-01	6.8160E-01	6.5632E-01	6.4502E-01	6.3777E-01
6	5.6257E-01	5.5234E-01	5.4329E-01	5.3591E-01	5.3195E-01	5.3056E-01	5.3201E-01
7	3.2131E-01	3.4413E-01	3.6174E-01	3.7565E-01	3.8820E-01	3.9380E-01	4.0089E-01
8	2.9206E-01	3.1347E-01	3.3007E-01	3.4324E-01	3.5508E-01	3.6037E-01	3.6697E-01
9	1.5364E-01	1.5637E-01	1.5841E-01	1.6010E-01	1.6209E-01	1.6308E-01	1.6474E-01
10	9.3366E-03	9.7122E-03	1.0032E-02	1.0326E-02	1.0624E-02	1.0771E-02	1.0931E-02

H[i]	105%	110%	120%	130%	140%	150%
1	1.5827E-05	1.5463E-05	1.4828E-05	1.4286E-05	1.3827E-05	1.3412E-05
2	5.0695E-03	4.9346E-03	4.6939E-03	4.4812E-03	4.2926E-03	4.1146E-03
3	2.0144E+02	1.9564E+02	1.8532E+02	1.7614E+02	1.6803E+02	1.6039E+02
4	2.1254E+02	2.0678E+02	1.9653E+02	1.8747E+02	1.7946E+02	1.7190E+02
5	6.2707E-01	6.1472E-01	5.9419E-01	5.7796E-01	5.6593E-01	5.5636E-01
6	5.3284E-01	5.3160E-01	5.2990E-01	5.2889E-01	5.2908E-01	5.2946E-01
7	4.0338E-01	4.0417E-01	4.0580E-01	4.0733E-01	4.0926E-01	4.1084E-01
8	3.6928E-01	3.7003E-01	3.7155E-01	3.7293E-01	3.7466E-01	3.7604E-01
9	1.6546E-01	1.6552E-01	1.6578E-01	1.6607E-01	1.6665E-01	1.6721E-01
10	1.1052E-02	1.1120E-02	1.1280E-02	1.1419E-02	1.1571E-02	1.1728E-02

Table 29. Control Gain Vector, G, Obtained for the Different Linear Compensators at Different Power Levels

G'[i]	50%	60%	70%	80%	90%	95%	100%
1	3.3367E+02	3.5703E+02	3.8475E+02	4.1607E+02	4.4584E+02	4.6526E+02	4.7966E+02
2	2.2498E-02	2.5455E-02	2.9470E-02	3.4531E-02	3.9296E-02	4.3213E-02	4.5646E-02
3	2.4648E-04	-7.5673E-05	-1.0645E-04	-1.5702E-04	-2.3961E-04	6.9141E-05	-2.6598E-05
4	5.7874E-04	-4.5656E-05	-2.9484E-04	-1.5999E-04	-1.1235E-03	-1.9651E-04	-9.4110E-04
5	9.7451E+00	1.0315E+01	1.1116E+01	1.2110E+01	1.3167E+01	1.3804E+01	1.4342E+01
6	2.9734E+03	3.0426E+03	3.1081E+00	3.1666E+03	3.2064E+03	3.2256E+03	3.2278E+03
7	-1.1659E+00	-1.1075E+00	-1.0555E+00	-1.0092E+00	-9.6529E-01	-9.5081E-01	-9.3229E-01
8	1.6039E+00	2.1475E+00	2.5283E+00	2.7334E+00	2.7528E+00	2.7242E+00	2.6402E+00
9	-1.8092E+03	-1.8529E+03	-1.8993E+03	-1.9487E+03	-2.0008E+03	-2.0295E+03	-2.0580E+03
10	-2.1916E+00	-2.0949E+00	-2.0060E+00	-1.9241E+00	-1.8435E+00	-1.8162E+00	-1.7830E+00

G'[i]	105%	110%	120%	130%	140%	150%
1	4.9886E+02	5.1753E+02	5.5069E+02	5.8540E+02	6.2000E+02	6.5468E+02
2	4.9778E-02	5.3742E-02	6.0520E-02	6.8383E-02	7.6848E-02	8.5949E-02
3	-8.4303E-05	1.0666E-04	4.6299E-05	-1.6441E-04	-1.4420E-04	2.1364E-04
4	9.0711E-05	4.9130E-04	-2.8936E-04	-3.1311E-04	1.6952E-05	6.2912E-04
5	1.4979E+01	1.5649E+01	1.6915E+01	1.8193E+01	1.9417E+01	2.0591E+01
6	3.2317E+03	3.2454E+03	3.2692E+03	3.2909E+03	3.3088E+03	3.3313E+03
7	-9.2185E-01	-9.0880E-01	-8.8514E-01	-8.6986E-01	-8.6303E-01	-8.6304E-01
8	2.2088E+00	1.7592E+00	8.4811E-01	-5.3665E-02	-9.1916E-01	-1.7437E+00
9	-2.0882E+03	-2.1204E+03	-2.1877E+03	-2.2638E+03	-2.3508E+03	-2.4526E+03
10	-1.7597E+00	-1.7339E+00	-1.6843E+00	-1.6512E+00	-1.6334E+00	-1.6304E+00

APPENDIX E

LISTING OF THE FITS FOR THE GAIN-SCHEDULED COMPENSATOR

E.1 Fits Used for the Scheduled Reference Model

The following pages list the fits used to implement gain-scheduled compensator. The fits are used to model the elements of the system matrices **A**, **B**, and **C** of the reference model. The gain matrices **H** and **G** are also fitted. The scheduling variable used is the electric power produced by the SNPS, $\mathbf{P_e}$.

```
c
c  THIS IS THE SEGMENT OF A FORTRAN PROGRAM THAT FITS THE
c  ELEMENTS OF THE LINEAR COMPENSATORS AS A FUNCTION OF
c  THE ELECTRIC POWER PRODUCED BY THE SYSTEM.
c
c  THE VARIABLES USED IN THIS SEGMENT ARE:
c  r(132)  --- ELEMENTS OF THE LINEAR COMPENSATOR
c  h(10)   --- FILTER GAIN VECTOR EXPRESSED IN
c        TERMS OF THE r(.)'s
c  g(10)   --- CONTROL GAIN VECTOR EXPRESSED IN
c        TERMS OF THE r(.)'s
c  x       --- SCHEDULING VARIABLE SCALED WITH THE
c        NOMINAL ELECTRIC POWER OUTPUT OF
c        THE SYSTEM
c


      if(x.le.1.0d0)then
      r(1)=-241.77656423d0-125.82813557d0*x-
     *113.21292827d0*x**2
      else
      r(1)=-133.76d0-347.43d0*x
      end if
      if(x.le.1.0d0)then
      r(2)=-0.0174896478d0+8.75806245d-3*x-0.037150464d0*x**2
      else
      r(2)=8.70330778d-4-0.025337685d0*x-0.021621332d0*x**2
      end if
      r(3)=0.0d0
      r(4)=0.0d0
      if(x.le.1.0d0)then
```

```
r(5)=-8.72496835d0+1.70332824d0*x-7.36811712d0*x**2
else
r(5)=0.50195175d0-16.363583d0*x+1.53105584d0*x**2
end if
if(x.le.1.0d0)then
r(6)=-2409.4821706d0-1419.0829657d0*x+595.14332435d0*x**2
else
r(6)=-2996.263463d0-238.93897943d0*x+10.475350112d0*x**2
end if
if(x.le.1.0d0)then
r(7)=1.5441046d0-0.90103442d0*x+0.28934191d0*x**2
else
r(7)=1.58272175d0-0.98353868d0*x+0.335526696d0*x**2
end if
if(x.le.1.0d0)then
r(8)=3.64205606d0-14.711441275d0*x+8.43403914d0*x**2
else
r(8)=-11.469d0+8.8356d0*x
end if
if(x.le.1.0d0)then
r(9)=1641.9713094d0+254.15676338d0*x+161.60976489d0*x**2
else
r(9)=2017.0039659d0-450.37132179d0*x+493.12719647d0*x**2
end if
r(10)=2.8609797858d0-1.580192198d0*x+0.5035063073d0*x**2
r(11)=0.0d0
if(x.le.1.0d0)then
r(12)=2.90246324d-5-2.096244951d-5*x+8.0481963644d-6*x**2
else
r(12)=2.7155547d-5-1.46730506d-5*x+3.67507453d-6*x**2
end if
r(13)=2.5d6
r(14)=-1.60575d4
r(15)=0.025853d0
r(16)=0.2461d0
r(17)=-25.0d0
if(x.le.1.0d0)then
r(18)=-0.0027886485d0+0.0017706142d0*x-6.6748138d-4*x**2
else
r(18)=-0.0027480766d0+0.00136594377d0*x-3.02178662d-4*x**2
end if
r(19)=0.0d0
r(20)=0.0d0
if(x.le.1.0d0)then
r(21)=0.0017808008d0-0.0013775201d0*x+6.6562939d-4*x**2
else
```

```
r(21)=0.0016410608d0-8.67344804d-4*x+2.9781543d-4*x**2
end if
r(22)=0.0d0
r(23)=0.0d0
if(x.le.1.0d0)then
r(24)=0.010630065d0-0.0093263183d0*x+0.0038834858d0*x**2
else
r(24)=0.00895748175d0-0.0048373576d0*x+0.0010731668426*x**2
end if
r(25)=0.0d0
r(26)=4035.0d0
r(27)=-0.025853d0
r(28)=0.0d0
r(29)=0.0d0
if(x.le.1.0d0)then
r(30)=-114.86772685d0+75.314375616d0*x-27.599383096d0*x**2
else
r(30)=-113.64225635d0+59.835062282d0*x-13.27536245d0*x**2
end if
r(31)=0.0d0
r(32)=0.0d0
if(x.le.1.0d0)then
r(33)=73.20809844d0-57.7014691d0*x+27.081150244d0*x**2
else
r(33)=67.509081587d0-36.989723269d0*x+12.156680824d0*x**2
end if
r(34)=0.0d0
r(35)=0.0d0
if(x.le.1.0d0)then
r(36)=437.1947937d0-390.79382385d0*x+160.27328293d0*x**2
else
r(36)=370.0056601d0-210.10759902d0*x+46.938195816d0*x**2
end if
r(37)=0.0d0
r(38)=1.20225d4
r(39)=0.0d0
r(40)=-0.2461d0
r(41)=0.0d0
if(x.le.1.0d0)then
r(42)=-117.57496196d0+74.649282d0*x-27.7788018d0*x**2
else
r(42)=-116.40011835d0+58.8671043d0*x-13.118211847*x**2
end if
r(43)=0.0d0
r(44)=0.0d0
if(x.le.1.0d0)then
```

```
r(45)=75.056071961-57.99157055d0*x+27.774862583d0*x**2
else
r(45)=69.461506179d0-37.196699811d0*x+12.68228478d0*x**2
end if
r(46)=0.0d0
r(47)=0.0d0
if(x.le.1.0d0)then
r(48)=448.17466022d0-393.28013148d0*x+162.70187123d0*x**2
else
r(48)=379.2609485d0-207.8651728d0*x+46.444946921d0*x**2
end if
r(49)=0.0d0
r(50)=21.714d0+30.427d0*x
r(51)=0.0d0
r(52)=0.0d0
r(53)=-0.44626946276d0+0.16150150049d0*x-0.93686258384d0*x**2
if(x.le.1.0d0)then
r(54)=0.068628583934d0-0.29559371258d0*x+0.62931944246d0*x**2
else
r(54)=-0.72194d0+1.1175d0*x
end if
r(55)=0.0d0
if(x.le.1.0d0)then
r(56)=0.30417768093d0-0.29300248518d0*x+0.59764210265d0*x**2
else
r(56)=-0.17279099907d0+0.58101010423d0*x+0.19858729212d0*x**2
end if
if(x.le.0.95d0)then
r(57)=0.14873473368d0-0.02022433039d0*x+0.0015317469082d0*x**2
else
end if
if((x.gt.0.95d0).and.(x.le.1.05d0))then
r(57)=0.13116d0
else
end if
if(x.gt.1.05d0)then
r(57)=0.21599116507d0-0.14582842787d0*x+0.061950756343d0*x**2
else
end if
r(58)=0.0d0
r(59)=0.0d0
if(x.le.1.0d0)then
r(60)=0.93871276585d0-0.38153433085d0*x+0.077841340437d0*x**2
else
r(60)=1.0782397381d0-0.62377925728d0*x+0.18395982702d0*x**2
end if
```

```
r(61)=0.0d0
r(62)=0.0d0
r(63)=0.0d0
r(64)=0.0d0
if(x.le.1.0d0)then
r(65)=0.267676544d0-0.257528202d0*x+0.52630175255d0*x**2
else
r(65)=-0.1523653644d0+0.5121013797d0*x+0.1749441954d0*x**2
end if
if(x.le.1.0d0)then
r(66)=-0.316139159d0-0.17384025d0*x-0.316644742d0*x**2
else
r(66)=-0.22123d0-0.58386d0*x
end if
r(67)=0.0d0
if(x.le.1.0d0)then
r(68)=-0.11626056742d0+0.426381303d0*x-0.2126024288d0*x**2
else
r(68)=0.22488813863d0+0.038378732074d0*x-0.1651654236d0*x**2
end if
if(x.le.1.0d0)then
r(69)=0.109587181d0-0.029687181d0*x+0.02956891044d0*x**2
else
r(69)=0.11631705d0-0.0371580942d0*x+0.030807431323d0*x**2
end if
r(70)=0.0d0
r(71)=0.0d0
if(x.le.0.95d0)then
r(72)=0.64918377d0-0.22570807d0*x+0.1059844276d0*x**2
else
end if
if((x.gt.0.95d0).and.(x.le.1.05d0))then
r(72)=0.531d0
else
end if
if(x.gt.1.05d0)then
r(72)=0.60301764d0-0.108657998d0*x+0.0397866829d0*x**2
else
end if
r(73)=0.0d0
r(74)=0.0d0
r(75)=0.0d0
r(76)=0.0d0
r(77)=0.0d0
if(x.le.1.0d0)then
r(78)=-0.077828932d0+0.352743204d0*x+0.140932428d0*x**2
```

```
else
r(78)=0.069076382d0+0.4755497775d0*x-0.129550456d0*x**2
end if
if(x.le.1.0d0)then
r(79)=-0.102865522d0-0.51287762d0*x-0.085853237d0*x**2
else
r(79)=-0.3284062266d0-0.5042657899d0*x+0.1315858366d0*x**2
end if
r(80)=0.0d0
if(x.le.1.0d0)then
r(81)=0.17456649d0+0.0756895688d0*x-0.012086411d0*x**2
else
r(81)=0.2252048896d0-0.00738815938d0*x+0.02084031699d0*x**2
end if
r(82)=0.0d0
r(83)=0.0d0
if(x.le.0.95d0)then
r(84)=0.167800199d0+0.38669139d0*x-0.15720338d0*x**2
else
end if
if((x.gt.0.95d0).and.(x.le.1.05d0))then
r(84)=-0.61282476857d0+1.93163028d0*x-0.917917005d0*x**2
else
end if
if(x.gt.1.05d0)then
r(84)=0.3896305d0+0.0105961918d0*x+0.0023816599d0*x**2
else
end if
r(85)=0.0d0
r(86)=0.0d0
r(87)=0.0d0
r(88)=0.0d0
r(89)=0.0d0
if(x.le.1.0d0)then
r(90)=-0.030360992d0-0.13910675d0*x+0.050487252d0*x**2
else
r(90)=-0.0996051345d0-0.0236785024d0*x+0.00407918287d0*x**2
end if
r(91)=1.0d0
r(92)=-1.0d0
if(x.le.1.0d0)then
r(93)=0.0253887348d0+0.060873223d0*x-0.0108383838d0*x**2
else
r(93)=0.068620443d0-0.00979847597d0*x+0.0170355203d0*x**2
end if
r(94)=0.0d0
```

```
r(95)=0.0d0
if(x.le.0.95d0)then
r(96)=0.147999563d0+0.36246270d0*x-0.14675276d0*x**2
else
end if
if((x.gt.0.95d0).and.(x.le.1.05d0))then
r(96)=-0.579140314d0+1.803128994d0*x-0.8570189753d0*x**2
else
end if
if(x.gt.1.05d0)then
r(96)=0.354150196d0+0.01393371122d0*x+4.549830352d-4*x**2
else
end if
r(97)=0.0d0
r(98)=0.0d0
r(99)=0.0d0
r(100)=0.0d0
r(101)=0.0d0
if(x.le.1.0d0)then
r(102)=0.018010301d0-0.0250815518d0*x+0.0089096534d0*x**2
else
r(102)=0.00426963189d0-0.0029206475d0*x+4.34904379d-4*x**2
end if
if(x.le.1.0d0)then
r(103)=0.051876d0+0.0034231d0*x
else
r(103)=0.0531105105d0+0.00154143379d0*x+6.42869498d-4*x**2
end if
r(104)=0.0d0
if(x.le.0.95d0)then
r(105)=-0.174619597d0-0.0107835062d0*x+0.00435952586d0*x**2
else
end if
if((x.gt.0.95d0).and.(x.le.1.05d0))then
r(105)=-0.180875d0
else
end if
if(x.gt.1.05d0)then
r(105)=-0.1676871111d0-0.02170685834d0*x+0.00874028692d0*x**2
else
end if
if(x.le.1.0d0)then
r(106)=0.093853593d0+0.0128137098d0*x-0.0024473029d0*x**2
else
r(106)=0.096919d0+0.0073056d0*x
end if
```

```
      r(107)=0.0d0
      if(x.le.0.95d0)then
      r(108)=0.138998897d0+0.034342255d0*x-0.00959476153d0*x**2
      else
      end if
      if((x.gt.0.95d0).and.(x.le.1.05d0))then
      r(108)=-0.0466983878d0+0.399036999d0*x-0.187599509d0*x**2
      else
      end if
      if(x.gt.1.05d0)then
      r(108)=0.171449193d0-0.0124447735d0*x+0.006418066221d0*x**2
      else
      end if
      r(109)=0.0d0
      r(110)=0.0d0
      r(111)=0.0d0
      r(112)=0.0d0
      r(113)=0.0d0
      if(x.le.1.0d0)then
      r(114)=-0.001671924d0-0.00258061887d0*x+7.01570863d-4*x**2
      else
      r(114)=-0.0026799402d0-9.50021147d-4*x+7.90890137d-5*x**2
      end if
      r(115)=0.0d0
      r(116)=0.0d0
      if(x.le.1.0d0)then
      r(117)=0.014349d0+0.0023788d0*x
      else
      r(117)=0.0154564814d0+6.29356966d-4*x+6.47303304d-4*x**2
      end if
      if(x.le.1.0d0)then
      r(118)=-0.016038793312d0-0.005217989d0*x+0.00107811734d0*x**2
      else
      r(118)=-0.017152d0-0.0030301d0*x
      end if
      r(119)=0.0d0
      if(x.le.1.0d0)then
      r(120)=0.00738678741d0+0.0043190172944d0*x-7.88904557d-4*x**2
      else
      r(120)=0.00897486168d0+0.002263234d0*x-2.88498892d-4*x**2
      end if
      if(x.le.1.0d0)then
      r(121)=-241.77656423d0-125.82813557d0*x-
     *113.21292827d0*x**2
      else
      r(121)=-133.76d0-347.43d0*x
```

```
      end if
      if(x.le.1.0d0)then
      r(122)=-0.0174896478d0+8.75806245d-3*x-0.037150464d0*x**2
      else
      r(122)=8.70330778d-4-0.025337685d0*x-0.021621332d0*x**2
      end if
      r(123)=0.0d0
      r(124)=0.0d0
      if(x.le.1.0d0)then
      r(125)=-8.72496835d0+1.70332824d0*x-7.36811712d0*x**2
      else
      r(125)=0.50195175d0-16.363583d0*x+1.53105584d0*x**2
      end if
      if(x.le.1.0d0)then
      r(126)=-2409.4821706d0-1419.0829657d0*x+595.14332435d0*x**2
      else
      r(126)=-2996.263463d0-238.93897943d0*x+10.475350112d0*x**2
      end if
      if(x.le.1.0d0)then
      r(127)=1.5441046d0-0.90103442d0*x+0.28934191d0*x**2
      else
      r(127)=1.58272175d0-0.98353868d0*x+0.335526696d0*x**2
      end if
      if(x.le.1.0d0)then
      r(128)=3.64205606d0-14.711441275d0*x+8.43403914d0*x**2
      else
      r(128)=-11.469d0+8.8356d0*x
      end if
      if(x.le.1.0d0)then
      r(129)=1641.9713094d0+254.15676338d0*x+161.60976489d0*x**2
      else
      r(129)=2017.0039659d0-450.37132179d0*x+493.12719647d0*x**2
      end if
      r(130)=2.8609797858d0-1.580192198d0*x+0.5035063073d0*x**2
      r(131)=0.0d0
      r(132)=0.0d0
c
c   FILTER GAIN VECTOR
c
      h(1)=r(12)
      h(2)=r(24)
      h(3)=r(36)
      h(4)=r(48)
      h(5)=r(60)
      h(6)=r(72)
      h(7)=r(84)
```

```
      h(8)=r(96)
      h(9)=r(108)
      h(10)=r(120)
c
c     CONTROL GAIN VECTOR
c
      g(1)=r(1)
      g(2)=r(2)
      g(3)=r(3)
      g(4)=r(4)
      g(5)=r(5)
      g(6)=r(6)
      g(7)=r(7)
      g(8)=r(8)
      g(9)=r(9)
      g(10)=r(10)
```

REPORT DOCUMENTATION PAGE

Form Approved
OMB No. 0704-0188

1. AGENCY USE ONLY (*Leave blank*)	2. REPORT DATE	3. REPORT TYPE AND DATES COVERED
	May 1998	Final Contractor Report

4. TITLE AND SUBTITLE

Investigation and Feasibility Assessment of TOPAZ-II Derivatives for Space Power Applications

5. FUNDING NUMBERS

WU–506–31–3M
NAG3–1235

6. AUTHOR(S)

Alexander G. Parlos and Kenneth L. Peddicord

7. PERFORMING ORGANIZATION NAME(S) AND ADDRESS(ES)

Texas A&M University
Department of Nuclear Engineering
College Station, Texas 77843–2124

8. PERFORMING ORGANIZATION REPORT NUMBER

E–9370

9. SPONSORING/MONITORING AGENCY NAME(S) AND ADDRESS(ES)

National Aeronautics and Space Administration
Lewis Research Center
Cleveland, Ohio 44135–3191

10. SPONSORING/MONITORING AGENCY REPORT NUMBER

NASA CR–195423

11. SUPPLEMENTARY NOTES

Project Manager, Steven M. Stevenson (retired), Advanced Space Analysis Office, NASA Lewis Research Center, organization code 6840, (216) 977–7087.

12a. DISTRIBUTION/AVAILABILITY STATEMENT

Unclassified - Unlimited
Subject Categories: 20 and 44 Distribution: Nonstandard

This publication is available from the NASA Center for AeroSpace Information, (301) 621–0390.

12b. DISTRIBUTION CODE

13. ABSTRACT (***Maximum 200 words***)

The ability to provide continuous power at significant levels is of utmost importance for many space missions, from simple satellite operations to manned Mars missions. One of the main problems faced in delivering solar or chemical space power in the tens of kW range, is the increasingly massive nature of the power source and the costs associated with its launch, operation and maintenance. A national program had been initiated to study the feasibility of using certain advanced technologies in developing an efficient, lightweight space power source. The starting point for these studies has been the Russian TOPAZ-II space reactor system, with the ultimate goal to aid in the development of a TOPAZ-II derivative which will be ready for flight by the year 2000. The main objective of this project has been to perform feasibility assessment and trade studies which would allow the development of an advanced space nuclear power system based on the in-core thermionic fuel element technology currently used in the Russian TOPAZ-II reactor. Two of the important considerations in developing the concept are: (1) compliance of the current TOPAZ-II and of any advanced designs with U.S. nuclear safety expectations, and (2) compliance of the design with the seven years lifetime requirement. The project was composed of two major phases. The initial phase of the project has concentrated on understanding the TOPAZ-II thermionic reactor in sufficient detail to allow several follow-on tasks. The primary interest during this first phase has been given on identifying the potential of the TOPAZ-II design for further improvements. The second phase of the project has focused on the feasibility of a TOPAZ-II system capable of delivering 30–50 kWe. Towards the elimination of single-point failures in the load voltage regulation system, an active voltage regulator has been designed to be used in conjunction with the available shunt load voltage regulator. The possible use of a dual-loop, model-based adaptive control system for load-following in the TOPAZ-II has also been investigated. The objective of this fault-tolerant, autonomous control system is to deliver the demanded electric power at the desired voltage level, by appropriately manipulating the neutron power through the control drums. As a result, sufficient thermal power is produced to meet the required demand in the presence of dynamically changing system operating conditions and potential sensor failures. The designed controller is proposed for use in combination with the currently available shunt regulators, or as a back-up controller when other means of power system control, including some of the sensors, fail.

14. SUBJECT TERMS

TOPAZ; Thermionic systems; Space nuclear power

15. NUMBER OF PAGES

225

16. PRICE CODE

A10

17. SECURITY CLASSIFICATION OF REPORT	18. SECURITY CLASSIFICATION OF THIS PAGE	19. SECURITY CLASSIFICATION OF ABSTRACT	20. LIMITATION OF ABSTRACT
Unclassified	Unclassified	Unclassified	